# Experimental Considerations and Theoretical Treatment of Time Resolved Polarization Spectroscopy

by

Richard Thurston

A dissertation submitted in partial satisfaction of the

requirements for the degree of

Doctor of Philosophy

in

Chemistry

in the

Graduate Division

of the

University of California, Berkeley

Committee in charge:

Doctor Daniel S. Slaughter, Co-chair
Professor Richard J. Saykally, Co-chair
Professor Holger Müller
Professor Stephen R. Leone

Fall 2023

Abstract

Experimental Considerations and Theoretical Treatment of Time Resolved Polarization Spectroscopy

by

Richard Thurston

Doctor of Philosophy in Chemistry

University of California, Berkeley

Doctor Daniel S. Slaughter, Co-chair

Professor Richard J. Saykally, Co-chair

The decay dynamics in molecular systems are important to consider for a wide number of phenomena and have implications across many fields of study. One common set of methods used to study these dynamics involve measurements of the time evolution of the excited state enhancement/suppression of nonlinear spectroscopic signals. Here we develop the novel technique of ultrafast transient polarization spectroscopy which allows us to measure decay dynamics in molecular systems using a polarization sensitive technique based on the optical Kerr effect. This is a three pulse technique where an exciting-pump pulse brings a portion of a sample into an electronic excited state and a pair of probing pulses measure changes in the sample's intensity dependent refractive index as a function of time delay. We then apply this technique to the study of neat liquid nitrobenzene where we measure oscillations in the dephasing time that we associate with oscillatory wave packet motion on the $S_1$ excited state. We then develop a set of theoretical methods that can be applied to study these polarization sensitive signals starting from a foundation in quantum chemistry. We also introduce a formalism for the projected density matrix which allows for an implicit transformation of lab frame signals into a molecular frame representation given a polarization sensitive measurement. These methods are then used to simulate the electronic response from a number of polarization sensitive signals with applications discussed.

Dedicated to words

for explaining things

# Contents

# List of Figures

# List of Tables

# Acknowledgments

It has been described that the completion of a doctorate takes the efforts of a village and this is no exception. As such there are many people to thank for their contributions both large and small that have made this work possible.

For their direct contributions to this work I want to first thank my advisor Doctor Daniel Slaughter, Professor Niranjan Shivaram, Doctor Matthew Brister, and Doctor Liang Tan. Doctor Daniel Slaughter's patience and support has been extremely appreciated throughout this project and is the primary reason this work has been able to reach its current conclusion. While he was a postdoctoral researcher in our group, Professor Niranjan Shivaram trained me on the laser system, introduced me to the field of ultrafast laser spectroscopy, and together we made our first ultrafast transient polarization spectroscopy measurements. Doctor Matthew Brister made many contributions to the experimental work in this dissertation. His reliable and diligent approach to laser lab work was always appreciated. Doctor Liang Tan provided many contributions to the theoretical work presented in this thesis. I especially appreciate his many critical insights and honest critique of this work.

For their indirect contributions I want to start by thanking the AMOS group members I've had a chance to interact with. I especially want to thank Doctor Thorsten Weber whose feedback throughout my time in the group challenged my understanding and helped me grow as a researcher. I also want to thank all the graduate students and postdoctoral researchers I've had the privilege of interacting with during my time in the AMOS group. In particular I want to thank Kirk Larsen, Ashley Fidler, Catherine Saladrigas, Felix Brausse, Benjamin Toulson, James Gaynor, Zachary Streeter, and Jordan Dudley for their enthusiasm and insightful discussions.

Lastly, I want to thank my family and friends for their support through out this process. I especially want to thank my wife Margaret Sy. Much of this work would not have been possible without your vehement insistence on code quality. Your love, support, and guidance throughout my studies has been invaluable.

# Chapter 1

# Motivation

This work is focused on the development of a novel time resolved spectroscopic technique dubbed ultrafast transient polarization spectroscopy (UTPS). The aim of this technique is to provide an additional means by which the time evolution of electronic excited states in atomic and molecular systems on femtosecond time scales can be studied. Our overarching goal is to develop a set of tools to experimentally measure, analyze, and simulate nonlinear signals that are sensitive to electronic relaxation dynamics of molecular systems. The technique is polarization sensitive, and employs three pulses separated by variable time delays. Therefore, UTPS is a multidimensional technique that is potentially sensitive to electronic structural dynamics that wouldn't be accessible through other methods.

## 1.1 A Brief Introduction to Decay Dynamics in Molecular Systems

The study of decay dynamics after the electronic excitation is of fundamental interest in the field of atomic and molecular physics and has impacts across a wide range of disciplines including materials science, biochemistry, atmospheric chemistry, and others [1, 2, 3, 4]. As an illustrative example of the importance of studying these decay dynamics, we can consider the stability of DNA/RNA nucleobases after UV excitation. As measured through time-resolved photoelectron spectroscopy [5] and photo-ionization spectroscopy [6], after a UV pulse populates the $S_2(\pi\pi*)$ excited state, the DNA/RNA nucleobases of cytosine, thymine, and uracil show evidence for a rapid internal conversion (<50 fs) [5] populating the $S_1(n\pi*)$ state which further decays to the ground state at a time scale >100 fs [5, 6]. Additional experimental evidence [5] suggests that this decay process dominates over a separate dissociative decay process in which the populated $S_2(\pi\pi*)$ state relaxes via the dissociative $S_3(\pi\sigma*)$ state. Furthermore, a detailed quantum chemical treatment using the surface hopping method, which was further bounded by the previous experimental measurements [7], suggests that the rapid internal conversion is mediated by a conical intersection (CI) between the $S_2(\pi\pi*)$ state and the $S_1(n\pi*)$ state. Recently, proposals to measure the passage of the $S_2$ population through the $S_2/S_1$ conical intersection in uracil, have been given that may uti-

lize x-ray transient absorption [8] and/or stimulated x-ray Raman measurements [9] of uracil to measure these effects. Such measurements could be performed by potentially exploiting the few to sub-femtosecond time resolution of the x-ray pulses generated at free electron lasers [10, 8].

This example demonstrates some general themes when studying the decay dynamics of molecular systems. First is the importance of the interplay of both experimental and theoretical methods in understanding these decay mechanisms. In the previous example, time-resolved photoelectron and photo-ionization spectroscopic methods were used to measure the decay rates associated with the relaxation process [5, 6]. However the interpretation and mechanism of the experiment was enabled by developments in quantum chemistry that allowed for the detailed treatment of non-adiabatic decay processes in molecular systems [3, 7].

Second is the role that conical intersections play in the decay processes in these molecular systems. One way to understand conical intersections is as a generalization of avoided crossings when there are 2 or more vibrational degrees of freedom [3, 4]. Under these conditions, two electronic potential energy surfaces can have a point (or a seam) where the system experiences energy degeneracy between these surfaces [3, 4, 11]. These conical intersections are generally accepted as being the dominant mediator of non-adiabatic energy flow between electronic and vibrational degrees of freedom [3, 4, 11]. Additionally, in a review by Schuurman and Stolow [3], the authors suggests that these conical intersections can be interpreted in the lens of transition state theory of chemical reactions, as the transition state in reactions mediated by electronic transitions.

From a theoretical perspective, conical intersections represent molecular configurations where the Born-Oppenheimer approximation no longer applies [12, 11, 3, 4, 13]. In these regimes, the contribution of nuclear kinetic energy to the molecular Hamiltonian is comparable to that of the electronic motion and the Coulombic interactions [12] and can no longer be treated using perturbation theory, which was allowed under the Born-Oppenheimer approximation [12, 11, 3]. This has necessitated the development of a variety of ab initio theoretical methods capable of treating the dynamics at conical intersections [3, 11].

While a full review of the ab initio methods used to treat the nonadiabatic dynamics that occur near conical intersections in molecular systems is beyond the scope of this work, we acknowledge some of the methods currently employed when treating these problems. In general there are two broad classes of approaches used to treat these dynamics, full quantum dynamics approaches that aim to solve the full molecular Schrödinger equation [3, 11, 13] and semi-classical methods that treat the nuclear wavepacket using an ensemble of classical trajectories but keeps some quantum effects [11, 13]. Broadly speaking methods like multiconfigurational time-dependent Hartree (MCTDH) [11, 14, 13] and multilayer multiconfigurational time-dependent Hartree (ML-MCTDH) [13] methods are techniques capable of treating the full quantum dynamics of molecular systems. These techniques allow for exact treatments of the quantum dynamics of a system of interest but such exact treatments involve expensive calculations that may not be feasible for systems with a large number of degrees of freedom [13]. Semiclassical methods, like the surface hopping techniques of Tully's fewest switching surface hopping (FSSH) algorithm and ab initio multiple spawning (AIMS) [13, 4, 3] as well as the multiconfigurational Ehrenfest (MCE) dynamics method [14, 13], allow for the treatment of a wider class of systems by considering the motion of the nuclei to be primarily classically driven while explicitly treating the electronic portion quantum mechan-

ically [13, 4].

From an experimental perspective, advances in experimental methods have allowed for greater sensitivity to a wide range of dynamical processes. Pump-probe spectroscopy, which can trace a history back to the birth of high speed photography in Eadweard Muybridge's racetrack images of a horse in gallop [1], is a technique where a dynamical process in a target of interest is initiated by a pump pulse, and whose dynamics are sampled by a probing pulse [1, 15, 16]. By measuring how the probe pulse is modified after interacting with the time evolving system as a function of the time-delay between the pump and probe pulses, information about the time evolution of the system of interest can be recovered [1, 15, 16]. The conceptual simplicity of this technique and it's applicability over a wide range of frequencies have made this technique particularly productive with dynamical information being recovered for a wide range of samples [1] including biomolecules, nanostructures, and solids, with some results giving site-specific information[16] in the case of XUV/X-ray probe schemes.

One common way to extend these types of measurements is by including a second pumping pulse [1]. The inclusion of this additional pulse allows for a number of different spectroscopic methods including 2D electronic spectroscopy (2DES) [17, 18], variants of Raman spectroscopy like time-resolved coherent stokes Raman Spectroscopy (CSRS) and coherent anti-stokes Raman spectroscopy (CARS) [19], and other spectroscopies based on four-wave mixing [20, 21]. The techniques mentioned here are all third order spectroscopic methods that can be described using a four wave mixing formalism [17, 19, 22]. In 2DES for example, three pulses interact with a sample of interest with the first two pulses acting as a pair of pump pulses that prepare the state of the sample, and the third pulse acts as a probing pulse that samples this time evolution [17, 1, 18]. Using this technique, the evolution of coherences in photochemical processes can be observed [17, 23]. Similar information can be obtained from other four wave mixing spectroscopic techniques such as non-collinear four wave mixing [18] where, because of the additional control over the excitation pathway, information about dark states [18, 24] can be measured, that would not be accessible through 1-photon transitions.

For some atomic or molecular systems, especially dilute gas phase samples, traditional pump-probe absorption spectroscopy might not be sensitive enough to recover the dynamics of interest [25]. In these cases, the technique of time-resolved photoelectron spectroscopy, where in a probing pulse ionizes a sample of interest after excitation from a pump pulse and the kinetic energy distribution of the ionized electrons are then recovered [26, 25], can be more be sensitive to some of these dynamics. By effectively probing occupied orbital binding energies with femtosecond time resolution one can obtain information on dynamics in atomic and molecular systems. Additionally, by measuring the angle-resolved photoelectron distribution and looking at the appropriate asymmetry parameter [26], one can recover molecular frame information about the dynamics of the system.

Analogously, some forms of polarization sensitive 2D spectroscopy have also been shown to be sensitive to molecular frame quantities [27, 28, 29, 30, 31]. Utilizing asymmetry parameters derived from the $n^{th}$ order orientational correlation function [29], 2D spectroscopic methods have been able to determine the evolution of relative angles between coupled transition dipoles [31], reorientation-induced spectral diffusion in deuterated methanol [32], and even map measured elec-

tronic dynamics onto specific vibrational degrees of freedom [33].

All of this showcases an array of experimental methods that are sensitive to a variety of decay dynamics mediated by conical intersections. Here, our aim is to develop the technique of Ultrafast Transient Polarization spectroscopy (UTPS). This technique is based on the measurement technique of time-resolved Optical Kerr Effect (OKE) spectroscopy in which a Kerr gating pulse sets up a transient birefringence in a sample and the polarization of the probing pulse is modified by this birefringence. With the addition of an electronic excitation pulse prior to the Kerr gating pulse, we may be sensitive to dynamics that haven't been observed previously [34].

This thesis is laid out as follows. After providing a brief introduction, we first demonstrate the experimental method while also providing a framework for the analysis of these experimental signals. We then discuss some experimental UTPS measurements in neat liquid nitrobenzene. This is followed by a description of novel methods to simulate these signals using a semi-empirical approach with partial ab initio parameterization, to calculate a measured polarization signal. We finally conclude by discussing some of the implications and potential future directions of this work.

## 1.2 A Brief Introduction to N-Wave Mixing

While a complete description of nonlinear spectroscopy using an n-wave mixing formalism is beyond the scope of this text, in this section we aim to briefly go over some of the fundamentals of classical n-wave mixing with an eye towards later discussions of optical Kerr effect spectroscopy and ultrafast transient polarization spectroscopy using this formalism. Our goal is to provide a general framework that we can use later on to understand some of our experimental and theoretical results in the context of $3^{\text{rd}}$ and $5^{\text{th}}$ order perturbative signals. However for a more thorough introduction to nonlinear spectroscopy and some additional implications/applications of the n-wave mixing formalism, we encourage the reader to consider the following review articles from Gelin et. al. [35] and Biswas et. al. [17] as well as the textbooks of Prof. Boyd [36], Prof. Mukamel [37], and of professors Hamm and Zanni [38].

When studying spectroscopic signals from a macroscopic sample of interest, the measured response from the sample can be described by considering how the polarization ($\vec{P}$) of a sample varies as a function of the incident electric field ($\vec{E}_{\text{in}}$) [36, 37]. This relationship between the measured signal electric field ($\vec{E_{\text{sig}}}$) and the polarization as derived from Maxwell's equations [36] can be expressed as follows

$$\nabla^2 \vec{E}_{\text{sig}} - \frac{1}{c^2}\frac{\partial^2}{\partial t^2}\vec{E}_{\text{sig}} = \frac{1}{\varepsilon_0 c^2}\frac{\partial^2}{\partial t^2}\vec{P}(\vec{E}_{\text{in}}) \tag{1.1}$$

Here the sample's varying polarization acts as a driving term in the second order wave equation that results in a nonzero measurable signal field ($\vec{E}_{\text{sig}}$). As the the form of the function describing how the polarization varies as a function of the incident electric field depends on intrinsic properties of the sample, such a spectroscopic measurement can provide insight into the chemical physics of the sample under study.

In the n-wave mixing formalism, one way to systematize the types of interactions that can occur is to consider the series expansion of the polarization with respect to the incident field [36, 37] where each term ($\vec{P}^{(n)}$) represents the resultant polarization from an n$^{\text{th}}$ order interaction with the incident fields. We can write this formally as follows

$$\vec{P}(\vec{E}_{\text{in}}) = \vec{P}^{(0)} + \vec{P}^{(1)}(\vec{E}_{\text{in}}) + \vec{P}^{(2)}(\vec{E}_{\text{in}}, \vec{E}_{\text{in}}) + \vec{P}^{(3)}(\vec{E}_{\text{in}}, \vec{E}_{\text{in}}, \vec{E}_{\text{in}}) + ... + \vec{P}^{(n)}(\vec{E}_{\text{in}}, ..., \vec{E}_{\text{in}}) + ... \quad (1.2)$$

In the frequency domain [36, 37], the n$^{\text{th}}$ order polarization can be expressed explicitly as an n$^{\text{th}}$ order integral of a tensor product between the fields and a frequency dependent n$^{\text{th}}$ order susceptibility ($\chi^{(n)}$). This n$^{\text{th}}$ order susceptibility is intrinsic to the sample of interest and is determined in part by the fundamental quantum mechanics of the sample of interest [36, 37]. Thus if we can measure information about the n$^{\text{th}}$ order susceptibility we can access intrinsic information about a sample of interest. Using index notation, we can write the expression for the n$^{\text{th}}$ order polarization as follows

$$P_i^{(n)}(\omega_{\text{sig}}) = \int_{-\infty}^{\infty} ... \int_{-\infty}^{\infty} d\omega_1 ... d\omega_n \, \chi^{(n)}_{ij_1...j_n}(\omega_{\text{out}}; \omega_1, ..., \omega_n) E^{\text{in}}_{j_1}(\omega_1) ... E^{\text{in}}_{j_n}(\omega_n) \quad (1.3)$$

To represent the n$^{\text{th}}$ order polarization in the time domain, first we consider the result of equation 1.4 after taking the Fourier transform [36, 37]. In performing such a transformation we can represent the frequency domain n$^{\text{th}}$ order susceptibility in terms of a time dependent n$^{\text{th}}$ order intrinsic response function ($R^{(n)}$), which are related to $\chi^{(n)}$ through a Fourier transform. This response function allows us to express the time dependent n$^{\text{th}}$ order polarization as convolutions between the response function and the interacting time dependent incident fields. We can write this relationship explicitly as

$$P_i^{(n)}(t) = \int_{-\infty}^{\infty} ... \int_{-\infty}^{\infty} d\tau_1 ... d\tau_n \, R^{(n)}_{ij_1...j_n}(\tau_1, ..., \tau_n) E^{\text{in}}_{j_1}(t - \tau_1) ... E^{\text{in}}_{j_n}(t - \tau_1 ... - \tau_n) \quad (1.4)$$

We note here that, due to phase matching considerations [36, 37], the output signal frequency ($\omega_{\text{sig}}$) and output signal wave vector ($\vec{k}_{\text{sig}}$) are related to the input frequencies ($\omega_n$) and input wave vectors ($\vec{k}_n$) by the following relations

$$\omega_{\text{sig}} = \omega_1 + \omega_2 + ... + \omega_n \quad (1.5a)$$

$$\vec{k}_{\text{sig}} = \vec{k}_1 + \vec{k}_2 + ... + \vec{k}_n \quad (1.5b)$$

At this point we have outlined some of the key expressions describing classical n-wave mixing. These expressions can be used to describe a number of nonlinear optical phenomena but of particular interest in this work is that of the intensity dependent refractive index also known as the optical Kerr effect [36, 39, 40]. This phenomenon can be represented by the third order susceptibility ($\chi^{(3)}$), which is in general a rank 4 tensor with 81 separate elements. Later in chapter 2, we will present a more complete discussion of the intensity dependent refractive index along with how this n-wave mixing framework relates to optical Kerr effect measurements and the related UTPS measurements.

## 1.3 Excited state enhancements of Non-linear Optical Signals

For a number of reasons, nonlinear spectroscopic signals from molecular systems can be expected to be enhanced after the molecule is brought into an excited electronic state. First, as population moves from the ground state into the excited state, the energy gap between a large number of other excited states gets reduced. This reduction in the transition frequencies between these states can lead to an enhancement of a higher order response [41, 42]. Secondly, transition dipole moments between excited states can be larger than those between the ground state and an excited state [41, 42], which can again lead to an enhancement.

The previous two points suggest that excited state enhancement of the third order signal is a general phenomena but may depend on the specifics of the accessible dipole transition moments from the excited state. These theoretical justifications help to explain the experimentally observed excited state enhancement and suppression of nonlinear optical signals.

Pump-degenerate four-wave mixing experiments [43, 44, 45, 46] have a particularly rich history in both demonstrating and using excited state enhanced nonlinear signals to study nuclear and electronic dynamics in atomic and molecular systems. In degenerate four-wave mixing experiments, a target sample interacts with three photons of the same frequency such that the resulting signal photon is the same frequency as the incident fields but with a separate k-vector [36]. The interaction of the three incident fields that generates the resulting signal is well described through the target's third order susceptibility [36, 47]. As in other pumped methods, in pump-degenerate four-wave mixing, an additional excitation pulse brings the target out of equilibrium wherein the degenerate four-wave mixing process can track the dynamics of interest in the system by sampling the third order susceptibility as a function of time-delay of the exciting pulse [43].

An early demonstration of the enhancement of nonlinear optical signals was in a degenerate four-wave mixing experiment studying organic linear conjugated molecules where the authors noted an enhancement of 37 times as compared to the ground state response [48, 49]. Later studies looking at a set of organic dyes also showed significant enhancement of excited state signals [50]. In atomic systems, this technique showed that while the absolute signal was lower without pumping, the authors note a significant signal-to-noise enhancement in the pumped case when studying flame atomized gold [20]. More recently, this technique has been used to study both the electronic relaxation and the subsequent vibrational relaxation of $\beta$-carotene and lycopene [51] as well as in several retinal derivatives [45].

Pumped optical Kerr effect measurements and multi-gate Kerr effect measurement have also been shown to result in modified, delay dependent nonlinear optical signals. In optical Kerr effect measurements, due to the 45° offset relative orientation of the polarization between a Kerr gate and probing pulse, as well as the use of a crossed polarizer along the probe axis, these experiments are able to probe the $\chi^{(3)}_{yxxx}$, $\chi^{(3)}_{yxxy}$, $\chi^{(3)}_{yxyx}$, $\chi^{(3)}_{yxyy}$, lab frame tensor elements of the third order susceptibility [36, 39, 47]. Given an isotropic sample the nonzero tensor elements reduce to $\chi^{(3)}_{yxxy}$, $\chi^{(3)}_{yxyx}$ [36, 52, 39, 40]. In prior pumped OKE experiments, an additional excitation pulse was used to measure an enhanced Kerr effect signal in several organic dyes given a fixed delay of the excitation pulse relative to the probing pulse pair [50]. Kerr effect measurements utilizing multiple

degenerate gating pulses with variable polarizations between the gating pulses, have demonstrated either enhancement or suppression of Kerr signals [53, 54] in a variety of different liquid samples by enhancing or suppressing various modes of nuclear motion by modifying the polarization of the incident gating pulses.

In pumped third harmonic generation experiments an intense NIR pulse probes a sample that has been brought into an excited state though an interaction with a resonant pumping pulse. The probing pulse then generates a third harmonic signal that can be subsequently filtered for and measured. As the polarization of the probing pulse is often the same as the polarization of the signal (especially in the case of isotropic samples), these experiments are direct probes of the $\chi^{(3)}_{xxxx}$ lab frame tensor element of the third order susceptibility [36, 47]. In these experiments, time delay dependent excited state enhancement of the third harmonic signal has been observed in fishnet metamaterials [55] (multilayered nanopatterned solid state matterials) as well as atmospheric air samples [56].

Taken together, these experiments demonstrate the power of pumped nonlinear optical techniques to observe nuclear and electronic dynamics in a wide range of time scales and sample types. It's for this reason that we might expect that UTPS may allow us to study dynamics that would not be accessible through other means.

# Chapter 2

# UTPS Experimental Technique

Ultrafast Transient Polarization Spectroscopy is a three pulse technique consisting of an excitation pump pulse, a Kerr gate pulse, and a probing pulse (see Figure 2.1). Similar to optical Kerr effect (OKE) measurements, the gate pulse initiates a transient birefringence in a sample and the probing pulse samples this birefringence after excitation. This transient birefringence modifies the polarization of the probing pulse (by rotating the polarization or by introducing ellipticity into the pulse) which introduces a nonzero signal component to the polarization of the probing pulse that is orthogonal to the input probe polarization. This signal can be measured using an analyzing polarizer that is crossed relative to the incident probe pulse's polarization [40, 57, 58, 59]. This signal is maximized by setting the polarization of the gate pulse to 45° relative to the probe pulse [40, 39]. These signals are sensitive to the sample's effective third order susceptibility ($\chi^{(3)}_{\text{eff}}$) which can be modified or even enhanced after a sufficient fraction of the targets within a sample are brought into an electronic excited state [36, 48, 49, 41, 60]. For this reason we introduce an excitation pulse that brings a fraction of our sample into an excited state whose modified third order susceptibility is measured through an optical Kerr effect measurement [61, 34]. By scanning the time delay between the excitation pulse and the OKE gate-probe pair, we can use the measurement of $\chi^{(3)}_{\text{eff}}$ as a means to extract information about the time evolution of a system after electronic excitation [34, 61].

One key assumption typically made in ultrafast transient polarization spectroscopy is that the excitation process is independent from the probing mechanism. This assumption can be justified when the time scale of the excitation is short relative to the probing mechanism, [34, 61, 60]. Given this non-equilibrium state, 4WM techniques that target these states can be analyzed using the same order of perturbation theory used when studying the same process that begins with the target near it's ground state equilibrium [60]. In essence this allows us to linearly separate the sample's effective third order susceptibility into a ground state response and an excited state response weighted by the fraction of the sample left in the non-equilibrium state after excitation. This simplifying assumption allows us to leverage existing techniques of analysis developed for time-resolved optical Kerr effect measurements. For this reason we will aim to provide a framework for analyzing of UTPS by extending the techniques used to study OKE spectroscopy.

This chapter is laid out as follows. After giving an overview of our experimental implementation of UTPS, we will then derive the expressions used when analyzing time resolved OKE spectra by performing a Jones matrix analysis of the Kerr effect signal. After providing the relevant expressions for a correlation analysis of the homodyne and heterodyne OKE signals, we will then extend these relations to the case of UTPS measurements. With the experimental and analysis framework in place, in chapter 3 we will then apply this technique to study the excited state electronic dynamics of nitrobenzene. More specifically, with this technique we aim to demonstrate excited state wave packet motion on the $S_1$ state.

## 2.1 Ultrafast Transient Polarization Spectroscopy Experimental Set-Up

In our implementation of a UTPS experiment we relied on a commercial KMlabs laser system as our light source. This system was used to generate optical pulses with a FWHM of 40 fs and a central wavelength at 780 nm with a repetition rate of 1 kHz. To generate the used optical pulses, first, a Kerr-Lens mode locked Griffin oscillator by KMLabs, was used to supply a pulse train with approximately 300 mW of average power at 88 MHz repetition rate. This oscillator utilized a Titanium Sapphire gain medium pumped using a 532 nm CW laser with 4.5 W of power. This pulse train was then sent to a KMLabs Wyvern regenerative amplifier that reduced the repetition rate but increased the pulse energy. This was achieved using a Pockels cell to send the selected pulse into a cryo cooled cavity, pumped using a coherent Evo-30 laser that supplied around 10 W of pulsed 527 nm light. The selected fundamental IR pulse was contained in this cavity until saturation which typically resulted in per pulse energy of approximately 1 mJ at a repetition rate of to 1 kHz. We further amplified the pulses using the KMLabs Komodo two stage multipass amplifier with each stage of amplification using cryo cooled amplifiers pumped by a pair of coherent Evo-HE lasers that supplied roughly 30 W of pulsed 527 nm light. After the two stages of amplification we could achieve per pulse energies of > 20 mJ with a 1 kHz repetition rate however we would typically operate the laser system so that it would supply < 5 mJ of per pulse energy in the fundamental pulse train.

This pulse train was then split twice with a pair of beam splitters to generate an excitation pulse and the OKE measurement pulse pair labeled pulse A and pulse B. In our experiments, the OKE measuring pulses have the same intensity, duration, and central wavelength. Given the symmetry of these pulses, this labeling is chosen since pulse A can exchange roles as a gate or probe pulse, depending on the sign of the time delay between the two pulses, and whether the signal that is colinear with pulse A or pulse B is the one being measured. Our samples were contained in a Spectrosil quartz cuvette with a path length of 1 mm and a wall thickness of 1 mm.

The time delay between the excitation pulse and the OKE pulses ($T$) as well as the time delay between the OKE measurement pulses ($\tau$) was set using two optical delay stages. At positive time ($T$), the excitation pulse arrives before pulse A, whereas for positive time $\tau$ pulse A arrives before pulse B. The polarization and power of each of the beam lines was set using a half-wave

plate followed by a polarizer for the excitation pulse and for pulse B. In the case of pulse A, the polarization was set using a half-wave plate and the power was set using a variable neutral density filter. These pulses were then focused onto our sample using 30 cm lenses and would intersect the sample with a non-colinear geometry where the angles between each pulse would measure less than 3°. Spatial and temporal overlap at the sample was achieved before each experiment and checked periodically during and after each experiment, by optimizing sum frequency generation with each pulse pair in a beta-barium borate (BBO) crystal at the sample position. After the pulses interact with the sample, separate polarization measurements along pulse A and pulse B propagation directions were done using an analyzing polarizer that's crossed relative to the incident pulse polarization. The light that passes through the analyzer is detected using a photodiode. As the polarization between pulse A and pulse B differ by 45°, the pair of polarization measurements let us measure differences in the signal due to polarization of the excitation pulse relative to the probing pulses. Additionally, the transmission signal of pulse B was collected using a small portion of the output beam and a photodiode [61].

The pump pulse train was modulated with a mechanical chopper at a frequency of 137 Hz, with a duty cycle of 50%, for use with a lock-in amplifier. This frequency was chosen to avoid harmonics of the line frequency noise at 60 Hz while still allowing for several pulses within the 1 kHz pulse train to be incident on the sample during each chopper duty cycle [62, 63]. By chopping the pump beam line and using lock-in detection along the probe beamline, we ensure that the detected signal included pump interaction with the probe. Specifically, the detected total signal includes the pump-probe (2-pulse) interaction with the media and the pump-gate-probe (3-pulse) interaction with the media. The 2-pulse signal is measured with the gate pulse blocked and the 3-pulse interaction is determined by subtracting the 2-pulse signal from the total signal.

In principle this lock-in detection scheme could be extended with the addition of a $2^{nd}$ chopper on the gate beam path and using a difference frequency reference to detect 3 pulse signal on detectors along the probe beam path but there are challenges associated with this scheme. First, these two choppers are inherently noisy where the true frequency and relative phases would need to be measured for an accurate measurement. To do this would require a specialized nonlinear circuit that can both mix the low frequency chopper pulse trains to generate a frequency difference pulse train and then filter out the frequency difference pulse train into a usable reference for a lock-in. Additionally, a correlation analysis of these UTPS signals suggests such a 3-pulse only interaction measurement may not be desirable. In particular, we will show that the correlation analysis of UTPS experimental signals in the homodyne and the heterodyne out-of-phase configurations can be nonlinear with respect to the excited state response function. This correlation analysis suggests that to properly deconvolve the response function from the measurement, that several two pulse measurements may be needed.

With the use of a quarter-wave plate after the polarizer in the probe beam line, the apparatus was configured to perform either a homodyne or heterodyne UTPS measurement. In the homodyne configuration, the probe pulse is polarized in the y-direction before interacting with the sample and the analyzer is aligned to the orthogonal x-direction. A heterodyne measurement can be made using either an in-phase or out-of-phase local oscillator. For the in-phase heterodyne measurement, the input polarization of the probe B pulse has no ellipticity and the analyzer is rotated by a small angle

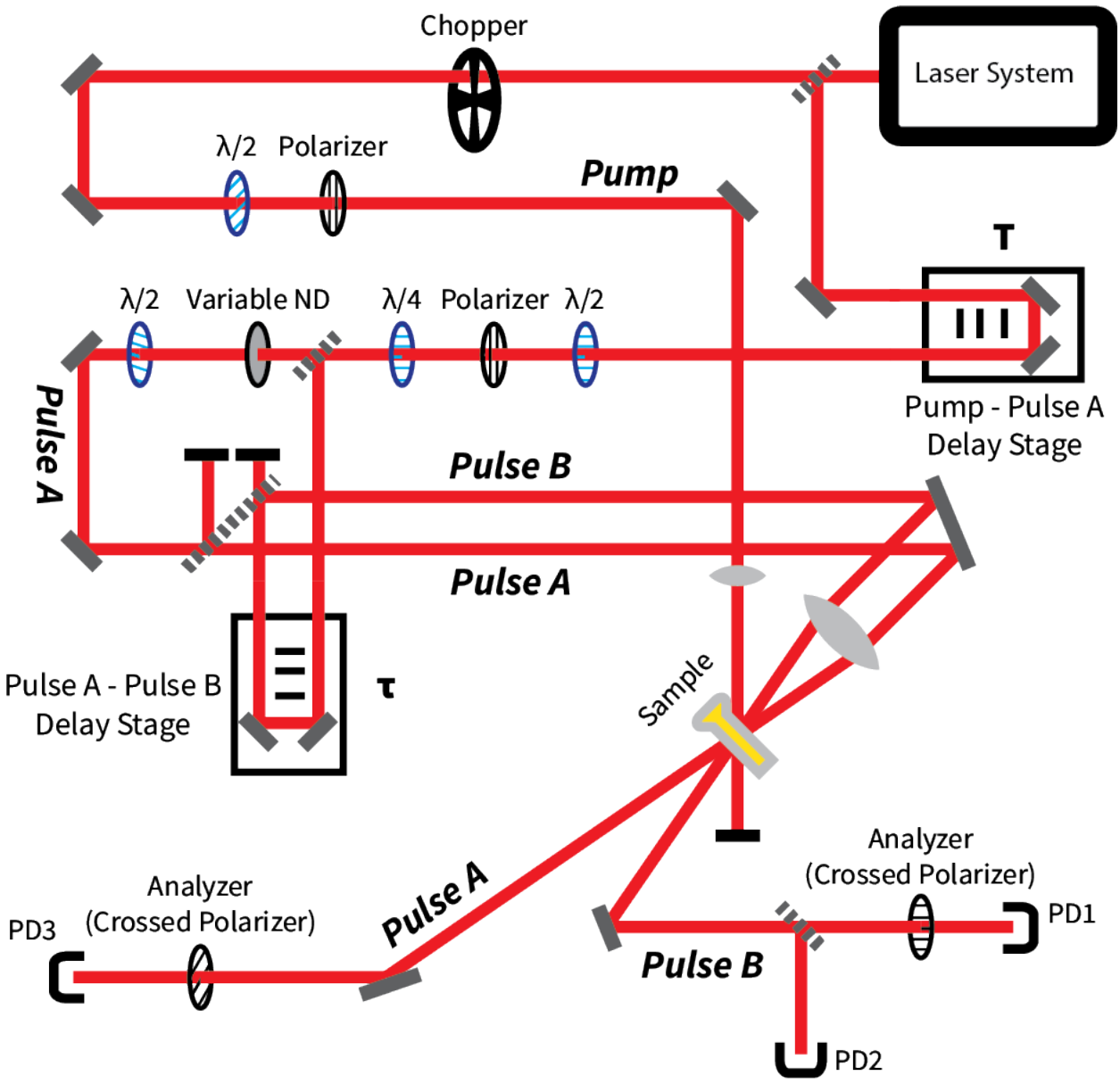


Figure 2.1: Schematic of a UTPS set-up. An amplified pulsed laser source is split into 3 pulses: an excitation pump pulse, a Kerr gating pulse, and a probing pulse. Changes in polarization due to the transient birefringence are measured using a pair of high contrast polarizers with the output coupled onto sensitive photodiodes. The quarter-wave plate in the probe beam path allows for out-of-phase heterodyne measurements to be performed by introducing a small amount of ellipticity. For homodyne and in-phase heterodyne measurements the fast axis of the quarter-wave plate is aligned parallel to the probe polarization.

$\pm\varepsilon$ to sample a portion of the probe pulse along the y-axis. This portion is the local oscillator and it is in-phase with the signal along the x-axis. The out-of-phase heterodyne measurement involves introducing a small amount of ellipticity into the probe pulse by rotating the polarizer away from the y-axis by a small angle $\pm\varepsilon$. A quarter-wave plate (fast axis aligned to the y-direction) introduces a small ellipticity to the probe B polarization. This out-of-phase component of the input polarization along the direction of the analyzer is the local oscillator.

As summarized in figure 2.2, in the case of the heterodyne experiment, a small in-phase or out-of-phase local oscillator is introduced onto the detector. For the in-phase case, we can rotate the analyzer polarizer by a small amount off axis to introduce the local oscillator. For the out-of-phase case, we can use a polarizer in-line with a quarter-wave plate to introduce a small amount of ellipticity into the probe before the sample interaction giving us a local oscillator that's out-of-phase with the generated signal [39, 52, 40].

## Validation of Kerr Effect Probe

To check that our probing pulse pair accurately samples the intensity dependent refractive index, we measured the ground state OKE spectra of neat liquid nitrobenzene in homodyne, heterodyne in-phase, and heterodyne out-of-phase configurations. These measurements were made using the same set-up in figure 2.1 with the excitation pulse blocked and the reference frequency of the lock-in detector set to the laser repetition rate of 1 kHz. Nitrobenzene was chosen as a sample for its large ground state third order susceptibility and its history as a target in published homodyne and heterodyne OKE experiments [64, 65, 66, 36]. Additionally, later in chapter 3, we will use this ground state information as a basis for analyzing and interpreting the excited state response of this system.

For the homodyne measurement, as seen in figure 2.3, each lock-in measurement at a given time delay was allowed integrate for 1500 ms before a value was recorded, with the lock-in time constant being 100 ms. The delay stage was scanned from $-453$ fs of probe delay relative to the gate, to $+1881$ fs of delay with time steps of 6.7 fs. Each time step was sampled in a random order for each scan, with the resulting spectrum being an average of 6 scans.

In the heterodyne measurement, as seen in figure 2.4, a similar set of measurement parameters was used as compared with the homodyne measurments. In this case the time allowed for the lock-in to settle was 1500 ms, and the lock-in time constant was again 100 ms. For each of the heterodyne measurements, the delay stage was scanned from $-620$ fs of probe delay relative to the gate, to $+1547$ fs of delay with time steps of 6.7 fs. Each time step was again sampled in a random order for each scan, with the resulting spectrum being an average of 7 to 9 scans.

For the in-phase measurement, a set of 8 scans were taken with the analyzing polarizer rotated by $+2^\circ$ relative to the homodyne configuration, and a set of 9 scans were taken with the analyzing polarizer rotated by $-2^\circ$. After averaging, these two raw heterodyne data sets were subtracted against each other yielding the resulting heterodyne in-phase OKE spectrum for neat nitrobenzene.

For the out-of-phase measurement, a set of 8 scans were taken with the input probe polarization before the $\frac{\lambda}{4}$ waveplate, was rotated by $+2^\circ$ relative to the homodyne configuration which corresponded to shift in the ellipticity of the probe of $3.4^\circ$ as measured through a stokes vector

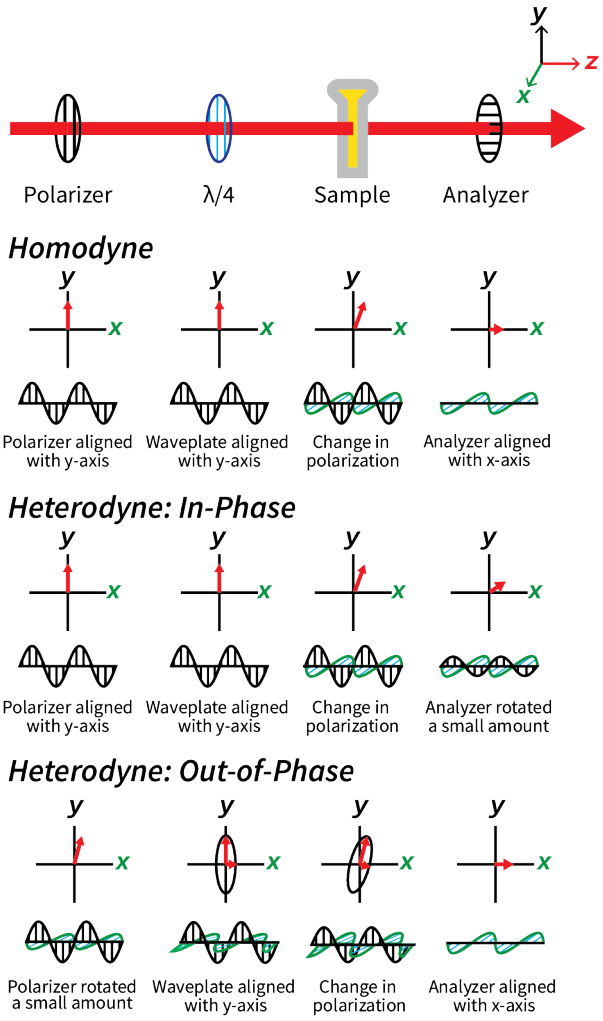


Figure 2.2: This figure shows the three different probe polarization schemes that are used for homodyne, in-phase heterodyne, and out-of-phase heterodyne OKE/UTPS experiments. In the homodyne case, the first polarizer aligns the measured pulse along the lab-frame y-axis and the quarter-wave plate doesn't change the polarization of input pulse. The polarization of the measured pulse is modified due to interaction with the sample and an analyzer is aligned to the x-axis to reject light with polarization along the y-axis. In the in-phase heterodyne case, the analyzer is rotated by $\pm\varepsilon$ so that a small in-phase component along the y axis is transmitted to the detector. For the heterodyne out-of-phase measurement, the first polarizer is rotated by $\pm\varepsilon$ which introduces a small off-axis component into the pulse. This off axis polarization in conjunction with the quarter-wave plate, introduces ellipticity in the probe pulse. When performing a heterodyne measurement, the resultant signal can be determined by taking the difference between $+\varepsilon$ and $-\varepsilon$ heterodyne measurements.

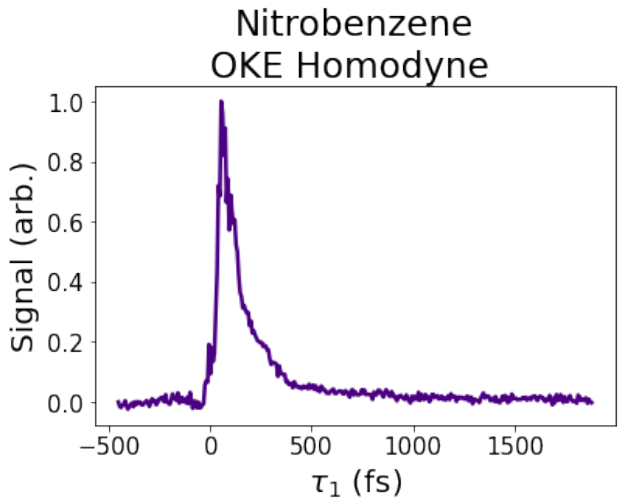


Figure 2.3: Time resolved homodyne optical Kerr effect spectrum of neat liquid nitrobenzene. Positive time delays represent the gating pulse arriving before the probing pulse.

measurement [67]. In the case where the input probe polarization was rotated by $-2^\circ$ before the $\frac{\lambda}{4}$ waveplate, a set of 7 scans were averaged to give the raw $-2^\circ$ out-of-phase spectrum. After averaging, these two raw heterodyne data sets were subtracted from each other yielding the net heterodyne out-of-phase OKE spectrum for neat nitrobenzene.

Previous studies have used time resolved optical Kerr effect spectroscopy to make measurements of nitrobenzene and other benzene derivatives as a means of studying ultrafast and orientational dynamics in these systems [65, 64, 66, 68]. These studies have found evidence that reorientational dynamics in nitrobenzene can be well described using two decay time constants that range in time scale from 0.5 to 20 ps in addition to ultrafast dynamics that occur on the time scale of 80 fs.

Lotshaw et al. [65], using pulses with autocorrelations of 100 fs centered at 633 nm, fit heterodyne detected OKE measurements of nitrobenzene using a sum of exponentials model for the intrinsic response function using 3 time constants of 32 ps attributed to molecular reorientations, 0.51 ps attributed to some intermolecular interaction, and 80 fs attributed to ultrafast electronic dynamics. The rise time of the electronic response was modeled as instantaneous at t=0. They found that in order to properly fit the data, they needed to introduce an additional delay of 100 fs to the non-electronic components which they attribute to inertial effects.

Smith and Meech [64] performed similar heterodyne OKE measurements on nitrobenzene using 50 fs pulses generated from a titanium sapphire oscillator. In these experiments, the researchers measured the temperature and viscosity dependence of nitrobeznene and found that, over the range of parameters tested, the two slowest relaxation components had a relaxation times between 16 - 35 ps and 1 - 2 ps. The researchers then modeled the temperature dependence of the slow picosecond dynamics using a hydrodynamic Debye model that incorporated the effects of viscosity, molecu-

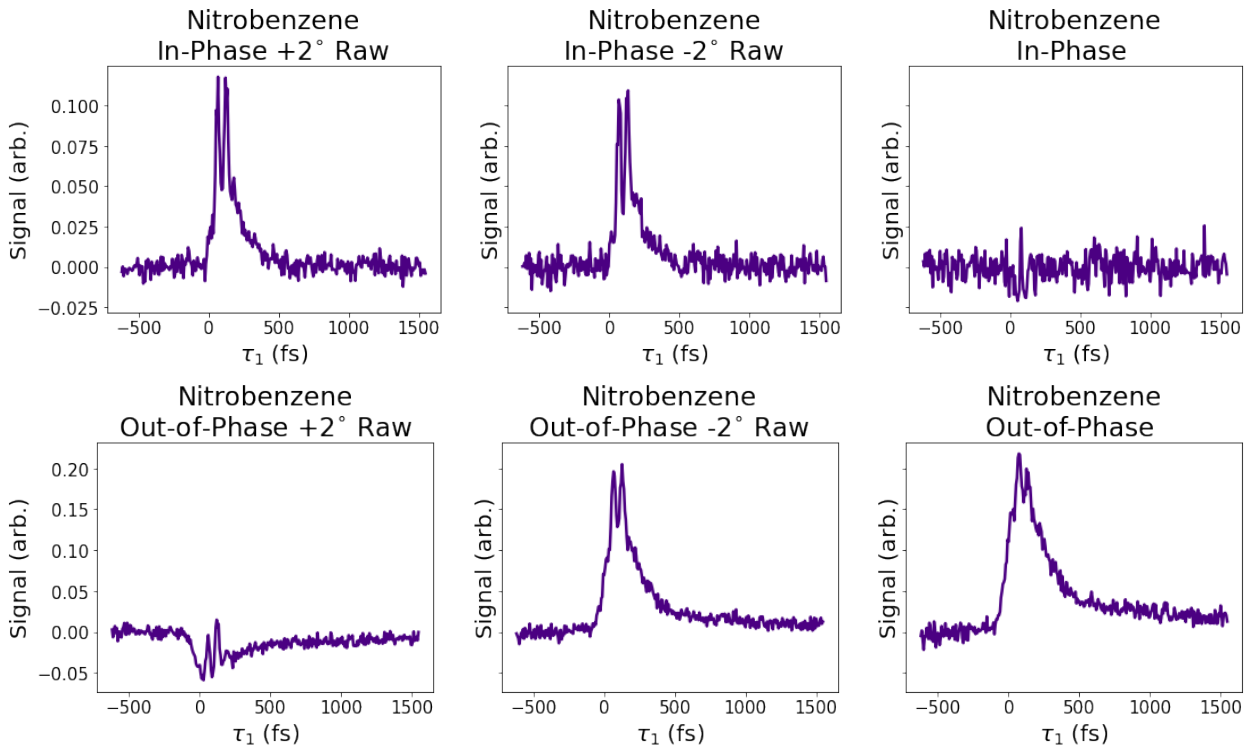


Figure 2.4: Time resolved heterodyne optical Kerr effect spectra of neat liquid nitrobenzene. Raw measurements represent the raw + or - $\varepsilon$ spectra. The raw spectra are then subtracted against each other to yield the net in-phase or net out-of-phase heterodyne OKE spectrum. Positive time delays represent the gating pulse arriving before the probing pulse.

lar size, molecular shape, temperature, moments of inertia, and the polarizability of the molecule. Using this model they were able to model the slower picosecond relaxation times previously associated with reorientational dynamics as well as the intermolecular interaction. They found that, while a simple hydrodynamic model is able to qualitatively model the trends seen as a function of temperature and viscosity, the model consistently underestimated the longest relaxation time and overestimated the shorter relaxation time. The authors [66] suggest that, this discrepancy shows that the picosecond relaxation dynamics can't be ascribed to simple reoriational dynamics and that a Brownian oscillator model might be better able to describe these dynamics.

Nikiforov et al. [66] using 45 fs pulses with a central wavelength of 790 nm, also performed heterodyne OKE measurements of nitrobenzene, however in this case, they modeled the orientational response of the system using a pair of exponential rise terms coupled to their own exponential decay factors. Using this fit function and by assuming correlations between the librational and orientational dynamics, they use the fit decay and rise time constants to extract a librational time constant for nitrobenzene. They found decay time constants of 20 ps and 0.9 ps, rise time constants of 54 fs and 180 fs, with the extracted librational time constant being 320 fs.

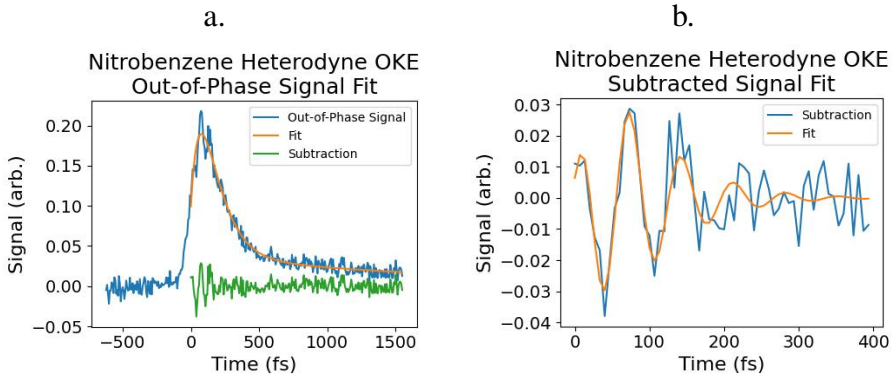


| Fit Terms $R_1$ | $A$ | $\tau_1$ | $\tau_2$ | $\gamma_1$ | $\gamma_2$ | $\Delta$ |
|---|---|---|---|---|---|---|
| Fit Values $R_1$ | 0.0395 arb. | 1.93 ps | 121 fs | 79.0 fs | 204 fs | -24.6 fs |
| Fit Terms $R_2$ | $B$ | $\tau_3$ | $\gamma_3$ | $T$ | $\phi$ | |
| Fit Values $R_2$ | 52.5 arb. | 51.2 fs | 32.5 ps | 70.2 fs | -0.679 rad. | |

Figure 2.5: Fits of the Out-of-phase time resolved heterodyne optical Kerr effect spectra of neat liquid nitrobenzene with the fit parameters tabulated. Based on the fitting procedure used by Nikiforov et. al. [66], we first fit our OKE data using the response function shown in equation 2.1a which represented the sum of two decaying and rising exponentials. This fit resulted in rise constants of 79 fs and 200 fs with the fit shown in panel a. After subtracting the fit from the data we then fit the early time response using a cosine function multiplied by a rising and decaying exponential to capture the apparent oscillatory behavior between 0 fs and 200 fs of time delay as shown in in equation 2.1b. This resulted in a rise constant of 32 ps, a decay constant of 51 fs, and a fit oscillatory period of 70 fs with the fit shown in panel b.

$$R_1 = (1-A)e^{(t-\Delta)/\tau_1}\left(1-e^{(t-\Delta)/\gamma_1}\right) + Ae^{(t-\Delta)/\tau_2}\left(1-e^{(t-\Delta)/\gamma_2}\right) \tag{2.1a}$$

$$R_2 = Be^{(t-\Delta)/\tau_3}\left(1-e^{(t-\Delta)/\gamma_3}\right)\cos\left(2\pi\frac{t}{T}+\phi\right) \tag{2.1b}$$

Overall, our measurements give reasonably good agreement with the OKE nitrobenzene spectra reported in the literature. As depicted in figure 2.5, we used a fitting approach based on the approach from Nikiforov et. al. [66]. We recovered decay rate constants of 1.9 ps and 120 fs which according to the previously discussed literature [66, 64, 65] may correspond to reorientational and electronic dynamics respectively. Additionally, after fitting the early time component to a cosine function multiplied by rising and decaying exponentials, we recovered rise and decay constants of 32 ps and 51 fs respectively, with an oscillatory period of 70 fs. While this behavior has not been reported in previous OKE measurements of nitrobenzene, such structures have been seen in OKE measurements of $CS_2$ [69, 70]. In reporting those measurements, the authors attributed those structures to competing ultrafast electronic and/or librational phenomena. In addition to validating

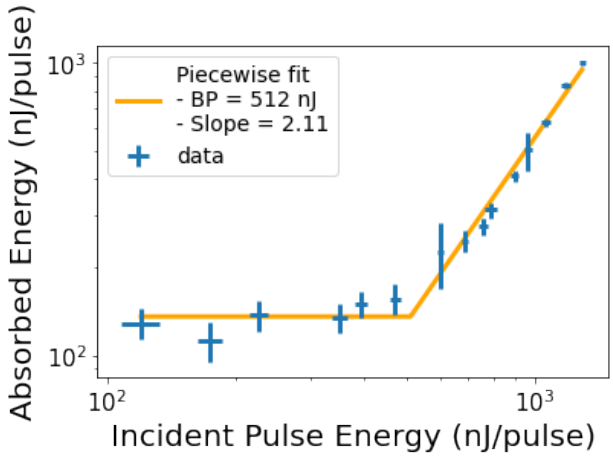


Figure 2.6: Piecewise least-squares fit of two photon absorption of 780 nm light of neat nitrobenzene on a log-log scale. The optimal fit parameters were found by scanning the break point and optimizing the least-squares loss function.

our ability to measure third order optical responses, measurements from a sample of neat nitrobenzene these measurements of the ground state OKE signal will allow us to distinguish between the excited state signal given three pulse polarization sensitive measurements.

## Validation of excited state preparation

As the first step in a UTPS measurement is preparing a system in an excited state, we utilized a two-photon absorption scheme using a 780 nm excitation pulse to bring nitrobenzene into the S1 state. Theoretical studies of nitrobenzene using both time dependent density functional theory as well as wavefunction methods suggest that the $S_0$ to $S_1$ transition is of $n\pi^*$ character and has a resonant energy separation between 3.32 eV - 3.73 eV [71, 72, 73]. Experimentally, this transition has been observed to be relatively weak with the absorption band associated with this transition occurring between 3.1 eV - 4.1 eV [74].

To ensure our excitation pulse was in the two-photon regime, we performed an absorption measurement where we compared the transmitted energy of the excitation pulse through a sample of nitrobenzene to a blank empty cuvette. As seen in figure 2.6 we then plotted the resultant absorption vs incident energy on a log-log scale and fit the graph to a piecewise linear fit. This allowed us to prepare a sample of nitrobenzene in a non-equilibrium electronic state prior to the Kerr effect measurement [61, 34].

## 2.2 Analysis of Optical Kerr Effect Experimental Signals

In an OKE experiment, information about a sample of interest is accessed through a measurement that is dependent on the intensity dependent refractive index of the sample as well as the characteristics of the incident pulses where intrinsic information about a sample is contained in the intensity dependent refractive index [39, 40]. When considering the experiment in the time domain, this intensity dependent refractive index can be represented by considering the sample's intrinsic response function $\mathscr{R}(t)$. Under this framework, extracting information about about a sample of interest requires accounting for how the pulse characteristic of the gate and probe pulses impact the measured signal [39, 52, 57, 70, 75, 76].

In the case of the homodyne experiment, a typical correlation analysis results in the following nonlinear relationship between the response function and the measured signal [39, 52, 57, 70]

$$\mathrm{V}_{\mathrm{homo}}(T) \propto \int_{-\infty}^{\infty} dt\, I_{\mathrm{probe}}(T-t) \left| \int_{-\infty}^{\infty} d\tau\, \mathscr{R}(t-\tau) I_{\mathrm{gate}}(\tau) \right|^2 \tag{2.2}$$

In the heterodyne OKE experiment, a standard correlation analysis shows that the relationship between the response function and the signal is a linear correlation between the intensity cross correlation of the gate and probe pulses and either the real or imaginary components of the response function given an out-of-phase or in-phase local-oscillator respectively [39, 52, 57, 70, 75].

$$\frac{\mathscr{F}\left[\mathrm{V}_{\text{in-phase / out-of-phase}}\right]}{\mathscr{F}\left[\mathrm{G}\right]} \propto \mathscr{F}\left[\mathscr{R}_{\text{imaginary / real}}\right] \tag{2.3}$$

A typical argument when deriving the relationship between the heterodyne in-phase/out-of-phase signals to the intrinsic response function is based off of the introduction of a small local oscillator with a polarization that's orthogonal to the polarization of the signal. In this analysis, the measured signal given a specific phase of the local oscillator is decomposed as follows [39, 52, 57, 70, 75, 59]

$$I_{\mathrm{det}} = I_{\mathrm{signal}} + I_{\mathrm{LO}} + I_{\mathrm{background}} + \frac{nc}{8\pi}(E^*_{\mathrm{LO}} E_{\mathrm{signal}} + E_{LO} E^*_{\mathrm{signal}}) \tag{2.4}$$

In this analysis, the resulting contribution of the local oscillator can be removed by considering two separate in-phase/out-of-phase measurements where the phase of the local oscillator has been shifted by 180°, which is denoted with a $+$ or $-$ depending on the convention being used [39, 52, 57, 70, 75, 76].

Experimentally, these local oscillators are derived from the probe pulse by either rotating the analyzing polarizer by a small amount or by introducing a small amount of ellipticity into the probe. As the effects of these changes in the experimental set up primarily impact the net polarization of the fields, the resulting signal can be modeled using a Jones calculus. By following Jones vector analysis we can more directly represent the heterodyne OKE signal without explicitly invoking a local oscillator that is treated separately from the probing field.

In the following sections, we will present a Jones vector analysis of the homodyne and heterodyne OKE signals using a minimal set of assumptions. To the best of our knowledge such an

analysis has not been presented before in the OKE literature. With this analysis, we will recover the typical OKE correlation expressions as shown in equations 2.3 and 2.2 and show the conditions under which those expressions are valid. Furthermore, we will provide a more general expression in the case where the typical heterodyne expression is not complete. Lastly, in deriving these expressions we will show that the heterodyne signal is maximized when using purely circularly polarized light in the case of the out-of-phase experiment, or by rotating the analyzing polarizer such that it is 45° off axis relative to the input probe pulse's polarization in the case of the in-phase experiment.

## Jones Matrix Analysis of Homodyne and Heterodyne Optical Kerr Effect Measurements

Time resolved optical Kerr effect spectroscopy is a technique that is based on the observation that for many materials the refractive index can be described with the following expression [36, 39, 40].

$$n = n_0 + n_2 I_{\text{gate}} \tag{2.5}$$

Due to the polarization of an optical pulse, the refractive index of the medium along the polarization axis of the field can be significantly different than that of the off axis refractive index leading to a transient birefringence that can be sampled by a separate probing pulse. For a birefringent sample whose fast and slow axes are orthogonal to each other and aligned perpendicular to propagation axis of the sampling optical pulse, the Jones matrix of that sample can be described as

$$\mathbf{B}_{\text{sample}} = \begin{pmatrix} \exp\left(-i2\pi\frac{d}{\lambda}n_{\parallel}\right) & 0 \\ 0 & \exp\left(-i2\pi\frac{d}{\lambda}n_{\perp}\right) \end{pmatrix} \tag{2.6}$$

with the parameters $n_{\parallel}$, $n_{\perp}$, $d$, $\lambda$, and $\theta_{\text{probe}}$ representing the refractive index of the medium along the axis parallel to the polarization of a Kerr gating pulse, the refractive index of the medium perpendicular to the polarization of that same Kerr gating pulse (and is thus not being modified through the intensity dependent refractive index), and the interaction length between the pulse and the sample, the center frequency of the pulse, respectively [77].

### OKE Homodyne Jones Matrix Analysis

In typical homodyne optical Kerr effect measurements, a separate linearly polarized probing pulse samples the transient birefringence that was initiated through the initial Kerr effect pulse. This transient birefringence modifies the polarization of the probing pulse, which can be detected by introducing an analyzing polarizer whose transmission axis is set orthogonal to the polarization of the linearly polarized probe [67, 40, 78]. This allows us to represent the Jones vector for the resultant probe field $\vec{E}_{\text{sample}}$ after the linearly polarized probe interacts with the sample as

$$\vec{E}_{\text{sample}} = |\vec{E}(t)| \begin{pmatrix} \exp\left(-i2\pi\frac{d}{\lambda}n_{\parallel}\right)\cos\theta_{\text{probe}} \\ \exp\left(-i2\pi\frac{d}{\lambda}n_{\perp}\right)\sin\theta_{\text{probe}} \end{pmatrix} \tag{2.7}$$

as well as the Jones matrix for the analyzing polarizer in terms of the polarization axis of the probe [67, 77].

$$\mathbf{P} = \begin{pmatrix} \sin^2(\theta_{\text{probe}}) & -\sin(\theta_{\text{probe}})\cos(\theta_{\text{probe}}) \\ -\sin(\theta_{\text{probe}})\cos(\theta_{\text{probe}}) & \cos^2(\theta_{\text{probe}}) \end{pmatrix} \tag{2.8}$$

We can then combine expressions 2.9 and 2.8 to solve for the resulting signal field.

$$\mathbf{P}\vec{E}_{\text{sample}} = |\vec{E}_{\text{probe}}(t)|e^{-i(a+b)} \begin{pmatrix} -\left(e^{ia}-e^{ib}\right)\sin^2\left(\theta_{\text{probe}}\right)\cos\left(\theta_{\text{probe}}\right) \\ \left(e^{ia}-e^{ib}\right)\sin\left(\theta_{\text{probe}}\right)\cos^2\left(\theta_{\text{probe}}\right) \end{pmatrix} \tag{2.9}$$

where the phase factors $a$ and $b$ have been defined as

$$a = 2\pi\frac{d}{\lambda}n_{\parallel} \tag{2.10a}$$

$$b = 2\pi\frac{d}{\lambda}n_{\perp} \tag{2.10b}$$

Furthermore we can solve for the resulting signal, by taking the magnitude of expression 2.9 and integrating over the time representing a time averaging detector. This gives us an expression for the measured voltage up to a proportionality yielding

$$\mathrm{V}_{\text{homo}} \propto \int_{-\infty}^{\infty} dt\ |\vec{E}_{\text{probe}}(t)|^2 \frac{1-\cos\left(4\theta_{\text{probe}}\right)}{8}\left|e^{ia}-e^{ib}\right|^2 \tag{2.11}$$

Note that, since the factor $1-\cos\left(4\theta_{\text{probe}}\right)$ is maximal at $\theta_{\text{probe}} = \pi/4$, this provides one justification for the common choice of the probe polarization being $45^\circ$ offset from the polarization of the Kerr gating pulse.

In the limit of small phase shifts, we can make the assumption that $e^{ia}-e^{ib} \approx i(a-b)$. Subtracting the phase terms as defined in 2.10 and by expressing the difference between the parallel and perpendicular refractive indices in terms of the intensity dependent refractive index lets us write the following

$$\Delta\phi = a-b = 2\pi\frac{d}{\lambda}n_2 I_{\text{gate}} \tag{2.12}$$

By factoring out the terms that don't depend on time in equation 2.11, we arrive at the homodyne signal expression for a time integrated detector as expressed in terms of phase shifts [39, 79].

$$\mathrm{V}_{\text{homo}}(T) \propto \int_{-\infty}^{\infty} dt\ I_{\text{probe}}(T-t)\,|\Delta\phi|^2 \tag{2.13}$$

At this point it's important to note that the refractive index is in general a complex quantity and thus the phase shifts $a$, $b$, $\Delta\phi$ are themselves complex [37, 67]. We therefore represent those quantities as follows

$$a = a' + ia'' \tag{2.14a}$$
$$b = b' + ib'' \tag{2.14b}$$
$$\Delta\phi = \Delta\phi' + i\Delta\phi'' \tag{2.14c}$$

While the contribution to the real and imaginary components of the phase shifts are combined in the typical homodyne optical Kerr effect measurement, the heterodyned experiment gives us a way of disentangling that information using modified experimental parameters.

### OKE Heterodyne In-Phase Jones Matrix Analysis

We will now consider the Jones matrix analysis of the heterodyne in-phase experiment. In this case, the only modification required to represent the heterodyne in-phase experiment as compared to the homodyne case would be to add an additional rotation term $\pm\varepsilon_\theta$ onto the Jones matrix of the analyzing polarizer. This allows us to easily represent the positive/negative rotation of the transmission axis of the analyzer symmetrically about the crossed orientation. With the assumption that the probe polarization is orientated at a 45° angle relative to the Kerr gate polarization, we can represent the analyzing polarizer used in the heterodyne in-phase experiment with the following Jones matrix.

$$\mathbf{P}^{(\pm)}_{\text{in-phase}} = \begin{pmatrix} \sin^2(\frac{\pi}{4} \pm \varepsilon_\theta) & -\frac{1}{2}\cos(\pm 2\varepsilon_\theta) \\ -\frac{1}{2}\cos(\pm 2\varepsilon_\theta) & \cos^2(\frac{\pi}{4} \pm \varepsilon_\theta) \end{pmatrix} \tag{2.15}$$

Combining equations 2.7 and 2.15 gives us the resulting detectable field. By then taking the square magnitude of that resultant field we can compute the detected in-phase homodyne signal for the positive and negative in-phase experiment. Following this procedure yields the following expression for the in-phase signals

$$\begin{aligned} \mathrm{V}^{(\pm)}_{\text{in-phase}} \propto \int_{-\infty}^{\infty} dt \frac{|\vec{E}_{\text{probe}}(t)|^2}{4} \Big[ & (e^{2a''} + e^{2b''}) \\ & + e^{a''+b''}(e^{i\Delta\phi'} - e^{-i\Delta\phi'})\cos(2\varepsilon_\theta) \\ & \pm (e^{2a''} - e^{2b''})\sin(2\varepsilon_\theta) \Big] \end{aligned} \tag{2.16}$$

Taking the difference between the positive and negative in-phase signals to remove the contribution of the local oscillator terms and simplifying the resulting expression allows us to express the heterodyne in-phase signal as follows

$$\begin{aligned} &\mathrm{V}^{(+)}_{\text{in-phase}} - \mathrm{V}^{(-)}_{\text{in-phase}} = \\ &\qquad \mathrm{V}_{\text{in-phase}} \propto \int_{-\infty}^{\infty} dt \frac{|\vec{E}_{\text{probe}}(t)|^2}{2} e^{2b''} \sin(2\varepsilon_\theta) \left[\sinh(2\Delta\phi'') + \cosh(2\Delta\phi'') - 1\right] \end{aligned} \tag{2.17}$$

in the limit of small $\Delta\phi$ equation 2.17 simplifies even further to give us the following

$$\mathrm{V}_{\text{in-phase}} \propto e^{2b''} \sin(2\varepsilon_\theta) \int_{-\infty}^{\infty} dt I_{\text{probe}}(t) \Delta\phi'' \tag{2.18}$$

Expression 2.18 allows us to make the following observations. First is that by introducing an in-phase local oscillator, we can obtain a signal that is linear with respect to the imaginary component of the Kerr phase shift greatly simplifying the analysis, which is consistent with previous analysis on these signals [39, 40, 52]. Second is that this linearity is preserved regardless of the magnitude chosen for the perturbing angle $\varepsilon_\theta$. Whatsmore this analysis suggests that the in-phase OKE signal will peak when the perturbing angle of the analyzer is chosen to be $\pm 45^\circ$ off axis from the homodyne condition. Physically, equation 2.18 also implies that the dynamics of the in-phase signal are encoded in the imaginary component of the Kerr phase shift and thus the absorption of the probing pulse due to the intensity dependent refractive index.

### OKE Heterodyne Out-of-Phase Jones Matrix Analysis

We will now consider the heterodyne out-of-phase case, which in comparison to the homodyne case, the probing pulse is modified by adding a small amount of either right or left handed ellipticity to add an out-of-phase local oscillator onto the detected signal. Taking the difference between the two out of phase signals allows us to removed the contribution of the local oscillator and recover the out-of-phase heterodyned Kerr effect signal. To represent a Jones vector of the out-of-phase probing pulse we can add a phase factor $\pm\delta_E$ onto the $y$-component of the incident pulse allowing us to add or subtract a given amount of ellipticity from the pulse [**?**, 67]. The resulting Jones vector for the probing pulse is thus

$$\vec{E}^{(\pm)}_{\text{probe}} = |\vec{E}(t)| \begin{pmatrix} \cos\theta_{\text{probe}} \\ e^{\mp i\delta_E} \sin\theta_{\text{probe}} \end{pmatrix} \tag{2.19}$$

We can then combine the matrix representations of the out-of-phase probe in equation 2.19 with the representations of the transient birefringent sample and the polarizer in equations 2.6 and 2.8 to represent the signal field. Following the previous analysis we can again take the square magnitude of this resulting field to give us expressions representing the out-of-phase signal given a positive or negative elliptical phase shift. Under the assumption of a probe polarization oriented $45^\circ$ relative to the Kerr effect pulse, We obtain the following expression for the positive or negative out-of-phase signal

$$\mathrm{V}^{(\pm)}_{\text{out-of-phase}} \propto \int_{-\infty}^{\infty} dt \frac{|\vec{E}_{\text{probe}}(t)|^2}{4} \left[(e^{2a''} + e^{2b''}) - e^{2b''} e^{\delta\phi''} \left(e^{-i\Delta\phi'} e^{\pm i\delta_E} + e^{i\Delta\phi'} e^{\mp i\delta_E}\right)\right] \tag{2.20}$$

Taking the difference between the positively and negatively shifted out-of-phase signals and simplifying, gives us the following expression for the resulting out-of-phase heterodyne signal

$$\begin{aligned} \mathrm{V}^{(+)}_{\text{out-of-phase}} - \mathrm{V}^{(-)}_{\text{out-of-phase}} = \\ \mathrm{V}_{\text{out-of-phase}} \propto \int_{-\infty}^{\infty} dt |\vec{E}_{\text{probe}}(t)|^2 e^{2b''} e^{\delta\phi''} \sin(\delta_E) \sin(\Delta\phi') \end{aligned} \tag{2.21}$$

and again, under the limit of small $\Delta\phi$ expression 2.21 simplifies even further to

$$\mathrm{V}_{\text{out-of-phase}} \propto \sin(\delta_E) e^{2b''} \int_{-\infty}^{\infty} dt I_{\text{probe}}(t) e^{\Delta\phi''} \Delta\phi' \tag{2.22}$$

For the case of purely real phase shifts, expressions 2.21 and 2.22 recover previously derived expressions for the out-of-phase heterodyne signal and the Kerr effect signal difference from right and left handed circularly polarized light [80, 40, 39]. This analysis also suggests that, given expression 2.22, this signal both doesn't depend on the ellipticity of the probe and that the signal is maximized when $\delta_E$ obtains a value of $\frac{\pi}{2}$. This suggests that the peak signal for the out-of-phase heterodyne signal would be obtained when using purely right and left circularly polarized light. Additionally, equation 2.22 allows us to interpret the out-of-phase signal as being approximately linear with respect to the real component of the Kerr phase shift and but exponentially dependent on the Kerr absorption.

## Correlation Analysis of Homodyne and Heterodyne Optical Kerr Effect Measurements

Thus far we have derived expressions relating the phase shifts from a Kerr medium to the expected signals from a time resolved homodyne and heterodyne optical Kerr effect experimental measurement. We will now use these expressions to extract information about the intrinsic response function of the medium using a general model describing these phase shifts and Fourier analysis of the time resolved OKE spectrum, dubbed the correlation analysis [39, 40].

The model for these phase shifts as described in equation 2.12, that we'll be using is as follows

$$\Delta\phi(t) = \int_{-\infty}^{\infty} d\tau \, \mathscr{R}(t-\tau) I_{\text{gate}}(\tau) \tag{2.23}$$

Additionally, since the intensity of the gate pulse is a real quantity any imaginary component in the phase shift $\Delta\phi$ must come from the intrinsic response function $\mathscr{R}$. Thus we can break up equation 2.23 into real and imaginary components allowing us to identify the following expressions for $\Delta\phi'$ and $\Delta\phi''$

$$\Delta\phi'(t) = \int_{-\infty}^{\infty} d\tau \, \mathscr{R}'(t-\tau) I_{\text{gate}}(\tau) \tag{2.24a}$$

$$\Delta\phi''(t) = \int_{-\infty}^{\infty} d\tau \, \mathscr{R}''(t-\tau) I_{\text{gate}}(\tau) \tag{2.24b}$$

One interpretation for equations 2.23 and 2.24 is that it is the Fourier transform of the frequency domain expression in equation 2.12. This interpretation allows us to directly map the measured response function onto the intensity dependent refractive index as show in equation 2.5 through Fourier analysis. This allows us to write the following

$$\mathscr{F}^{-1}\left[\Delta\phi(\omega)\right] \propto \mathscr{F}^{-1}\left[\omega n_2(\omega) I_{\text{gate}}(\omega)\right] \tag{2.25}$$

$$\propto \left(-i\frac{d}{dt}\mathscr{F}^{-1}\left[n_2\right](t)\right) * I_{\text{gate}}(t) \tag{2.26}$$

By comparing equations 2.23 and 2.25, we can therefore identify the general response function ($\mathscr{R}$) as the following

$$\mathscr{R} \propto -i\frac{d}{dt}\mathscr{F}^{-1}\left[n_2\right](t) \tag{2.27}$$

Given information about the intensity profile of the incident probe and gating pulses, the model as written in equation 2.23 has been successfully used to recover the intrinsic response functions from many liquid systems including a variety of benzene derivatives, water, $CS_2$, among many others [65, 64, 66, 40, 52, 78, 81, 68, 69]. This analysis has been used to study nuclear dynamics such as reorientational effects and molecular librations which tend to occur on picosecond time scales, as well as electronic dynamics which tend to occur on femtosecond time scales [**??**, 65].

When considering the homodyne OKE experiment, expression 2.23 in combination with equation 2.13, allows us to write the following standard expression for the signal of the homodyne experimental configuration given a time averaging detector [39, 78].

$$\mathrm{V}_{\text{homo}}(T) \propto \int_{-\infty}^{\infty} dt\, I_{\text{probe}}(T-t)\left|\int_{-\infty}^{\infty} d\tau\, \mathscr{R}(t-\tau) I_{\text{gate}}(\tau)\right|^2 \tag{2.28}$$

Using equations 2.24, 2.18, and 2.22 we can similarly write expressions relating the heterodyne signals to the intrinsic response function of the sample. For the heterodyne in-phase case, the resulting expression is

$$\mathrm{V}_{\text{in-phase}}(T) \propto \int_{-\infty}^{\infty}\int_{-\infty}^{\infty} dt\, d\tau\, I_{\text{probe}}(T-t) I_{\text{gate}}(\tau) \mathscr{R}''(t-\tau) \tag{2.29}$$

and for the heterodyne out-of-phase case

$$\mathrm{V}_{\text{out-of-phase}}(T) \propto \int_{-\infty}^{\infty}\int_{-\infty}^{\infty} d\tau_1\, dt\, I_{\text{probe}}(T-t) I_{\text{gate}}(\tau_1) \mathscr{R}'(t-\tau_1) e^{\int_{-\infty}^{\infty} d\tau_2\, \mathscr{R}''(t-\tau_2) I_{\text{gate}}(\tau_2)} \tag{2.30}$$

Equation 2.29 can be simplified even further through the use of the cross-correlation function $\mathscr{G}$ which represents the intensity cross-correlation between the Kerr gate and probing pulses. Given the distributive property of convolutions, Equation 2.29 can be rewritten as [39, 52]

$$\mathrm{V}_{\text{in-phase}}(T) \propto \int_{-\infty}^{\infty} dt\, d\tau\, \mathscr{G}(T-t)\mathscr{R}''(t) \tag{2.31}$$

This allows us to directly recover the imaginary component of the intrinsic response function $\mathscr{R}''$ through an in-phase heterodyne experiment and a measurement of the intensity cross-correlation function of the incident fields [39, 40, 52]. We can thus re-write expression 2.31 into the following simple expression.

$$\frac{\mathscr{F}\left[\mathrm{V}_{\text{in-phase}}\right]}{\mathscr{F}\left[\mathrm{G}\right]} \propto \mathscr{F}\left[\mathscr{R}''\right] \tag{2.32}$$

For the case of the out-of-phase measurement, in the limit of constant $\mathscr{R}''$, the term $e^{\mathscr{R}''*I_{\text{gate}}}$, reduces to a constant. This allows us to use the same analysis as was used for the in-phase case yielding the standard out-of-phase heterodyne expression [39, 52]

$$\frac{\mathscr{F}\left[\mathrm{V}^{\text{const-}\mathscr{R}''}_{\text{out-of-phase}}\right]}{\mathscr{F}\left[\mathrm{G}\right]} \propto \mathscr{F}\left[\mathscr{R}'\right] \tag{2.33}$$

However in the more general case, Fourier analysis of equation 2.30 yields the following expression

$$\mathscr{F}\left[\frac{\mathscr{F}^{-1}\left[\frac{\mathscr{F}\left[\mathrm{V}_{\text{out-of-phase}}\right]}{\mathscr{F}\left[I_{\text{probe}}\right]}\right]}{e^{\mathscr{R}''*I_{\text{gate}}}}\right] \propto \mathscr{F}\left[\mathscr{R}'\right]\mathscr{F}\left[I_{\text{gate}}\right] \tag{2.34}$$

Equation 2.34 implies that the intensity profile of the incident pulses and a measurement of the convolution between $\mathscr{R}''$ and $I_{\text{gate}}$ through an in-phase measurement, are needed recover the real component of intrinsic response function $\mathscr{R}'$. Using ultrafast pulse measurement techniques (like Frequency Resolved Optical Gating, spectral phase interferometry for direct electric-field reconstruction, or many others) one can obtain the intensity profile of an ultrashort pulse of interest [82, 83, 84, 85, 86]. Thus, through a set of pulse measurements of the probe and gate fields and results from an in-phase heterodyne OKE measurement, one can recover the real component of intrinsic response function $\mathscr{R}'$ through equation 2.34.

Thus far we have used the model of a sample being described by the intensity dependent refractive index in conjunction with an imperially driven response function to derive signal expressions that can be expressed as convolutions of experimentally measurable pulse characteristics and an imperially motivated sample response function. In the next section we will relate this response function to the effective third order susceptibility allowing us to connect a measurement of $\mathscr{R}(t)$ to fundamental properties of a system (ie. relaxation rates of a system) through the system's effective third order susceptibility.

## 4WM Analysis of Time Resolved Optical Kerr Effect Measurements

In the last section we were able to relate the intrinsic response function $\mathscr{R}$ as measured from an OKE experiment, to the intensity dependent refractive index $n_2$ through equation 2.27. Here we present a derivation of the relationship between $n_2$ and effective third order susceptibility $\chi^{(3)}_{\text{eff}}$ in the context of the full tensor nature of $\chi^{(3)}$ [36]. Through this context we will then derive $\chi^{(3)}_{\text{eff}}$ in terms of specific tensor elements of $\chi^{(3)}$.

The general expression for the third order polarization is as follows

$$\begin{aligned}\vec{P}^{(3)}_i(\omega_{\text{out}}) &= \varepsilon_0 \chi^{(3)}_{ijkl}(\omega_{\text{out}};\omega_1,\omega_2,\omega_3)\vec{E}_j(\omega_1)\vec{E}_k(\omega_2)\vec{E}_l(\omega_3) \\ &= \varepsilon_0 \left(\chi^{(3)}_{ijkl}\vec{e}_i\vec{e}_i\vec{e}_i\right) E(\omega_1)E(\omega_2)E(\omega_3) \\ &= \varepsilon_0 \chi^{(3)}_{\text{eff}} E(\omega_1)E(\omega_2)E(\omega_3)\end{aligned} \tag{2.35}$$

where in the second step, we factored out the unit polarization vector of the incident field terms and associated them with the $\chi^{(3)}$ tensor. This step gives us a path to deriving $\chi^{(3)}_{\text{eff}}$ with respect to the tensor elements of $\chi^{(3)}$ given the field orientations and the polarization axis by which the signal is measured. In the case of the intensity dependent refractive index, in order for $\chi^{(3)}$ to act as a refractive index, the input field frequency must be the same as the output field frequency. We therefore make the following simplifying assumption that $\omega_1$ and $\omega_2$ are equal in magnitude but opposite in sign and which implies that $\omega_{\text{out}}$ must equal $\omega_3$. Thus allowing us to write the following

$$\begin{aligned}\vec{P}^{(3)}(\omega) &= \varepsilon_0 \chi^{(3)}_{\text{eff}} E(\omega_1)E(-\omega_1)E(\omega) \\ &= \varepsilon_0 \chi^{(3)}_{\text{eff}} |E(\omega_1)|^2 E(\omega)\end{aligned} \tag{2.36}$$

Under fairly general circumstances, the first electric field driven nonliterary for isotropic media is $P^{(3)}$ [87, 36]. We can then write the following approximation for the total polarization of an isotropic media as

$$\begin{aligned}\vec{P}^{(\text{tot})}(\omega) &= \varepsilon_0 \chi^{(1)} E(\omega) + \varepsilon_0 \chi^{(3)}_{\text{eff}} |E(\omega_1)|^2 E(\omega) \\ &= \varepsilon_0 \left(\chi^{(1)} + \chi^{(3)}_{\text{eff}} |E(\omega_1)|^2\right) E(\omega) \\ &= \varepsilon_0 \chi E(\omega)\end{aligned} \tag{2.37}$$

where in the last step we identified the term $\left(\chi^{(1)} + \chi^{(3)}_{\text{eff}} |E(\omega_1)|^2\right)$ as the total susceptibility $\chi$. Using the following general expression relating the refractive index to the susceptibility

$$n^2 = 1 + \chi \tag{2.38}$$

allows us to relate the intensity dependent refractive index of equation 2.5 to the total susceptibility as identified in equation 2.37 [36]. After noting the following relationship between intensity and field strength

$$I = 2cn_0\varepsilon_0 |E|^2 \tag{2.39}$$

and in combination with equation 2.5 we can expand equation 2.40 up to first order in intensity into the following form

$$n_0^2 + 2n_0n_2I = 1 + \chi^{(1)} + \frac{\chi^{(3)}_{\text{eff}}}{2cn_0\varepsilon_0}I \tag{2.40}$$

By equating terms equal in their order of intensity, we can solve for $n_2$ yielding

$$n_2 = \frac{\chi^{(3)}_{\text{eff}}}{4c\varepsilon_0 n_0^2} \tag{2.41}$$

which is a typical expression relating $n_2$ to $\chi^{(3)}_{\text{eff}}$ [36]. Thus a measurement of the Kerr effect response function $\mathscr{R}$ can be related to $\chi^{(3)}$ through equations 2.41 and 2.27.

As mentioned previously, equation 2.35 hints at a way relating $\chi^{(3)}_{\text{eff}}$ to specific tensor elements of $\chi^{(3)}$ given an OKE experiment. Before we proceed with the derivation, we note some relevant experimental conditions for the homodyne OKE case. First, the presence of the analyzing polarizer orthogonal to the probing pulse. Second, a typical homodyne experiment consists of two pulses a probing pulse ($E_{\text{probe}}$) and a Kerr gating pulse ($E_{\text{gate}}$) that are oriented 45° relative to each other. Taking the probe to be $\hat{x}$ aligned and the analyzing polarizer to be $\hat{y}$ aligned, we can write the third order polarization that contributes to the signal as follows

$$P_y^{(3)} = \varepsilon_0\chi^{(3)}_{yjkl}(\omega_j,\omega_k,\omega_l)\left(\vec{E}_j^{(\text{probe})} + \vec{E}_j^{(\text{gate})}\right)\left(\vec{E}_k^{(\text{probe})} + \vec{E}_k^{(\text{gate})}\right)\left(\vec{E}_l^{(\text{probe})} + \vec{E}_l^{(\text{gate})}\right) \tag{2.42}$$

Since the gate pulse drives the intensity dependent refractive index and since the signal propagates along the probe, after expanding equation 2.42, phase matching conditions allow us to ignore terms that don't include two factors of the gating pulse and 1 factor of the probing pulse. Additionally, phase matching conditions require that the two input gate frequencies must be equal and opposite from one another. These conditions allow us to rewrite equation 2.42 into the following form

$$\begin{aligned} P_y^{(3)} = \varepsilon_0 \chi_{yjkl}^{(3)}(\omega_j,\omega_k,\omega_l)\Big(&\vec{E}_j^{(\text{probe})}(\omega_p)\vec{E}_k^{(\text{gate})}(+\omega_g)\vec{E}_l^{(\text{gate})}(-\omega_g)+ \\ &\vec{E}_j^{(\text{probe})}(\omega_p)\vec{E}_k^{(\text{gate})}(-\omega_g)\vec{E}_l^{(\text{gate})}(+\omega_g)+ \\ &\vec{E}_j^{(\text{gate})}(+\omega_g)\vec{E}_k^{(\text{probe})}(\omega_p)\vec{E}_l^{(\text{gate})}(-\omega_g)+ \\ &\vec{E}_j^{(\text{gate})}(-\omega_g)\vec{E}_k^{(\text{probe})}(\omega_p)\vec{E}_l^{(\text{gate})}(+\omega_g)+ \\ &\vec{E}_j^{(\text{gate})}(+\omega_g)\vec{E}_k^{(\text{gate})}(-\omega_g)\vec{E}_l^{(\text{probe})}(\omega_p)+ \\ &\vec{E}_j^{(\text{gate})}(-\omega_g)\vec{E}_k^{(\text{gate})}(+\omega_g)\vec{E}_l^{(\text{probe})}(\omega_p)\Big) \end{aligned} \tag{2.43}$$

After noting that the gate field can be written in the following form

$$\vec{E}^{(gate)}(\omega_g) = E^{(gate)}(\omega_g)\left(\frac{1}{\sqrt{2}}\hat{x}+\frac{1}{\sqrt{2}}\hat{y}\right) \tag{2.44}$$

and that the probe field has the following form

$$\vec{E}^{(probe)}(\omega_p) = E^{(probe)}(\omega_p)\hat{x} \tag{2.45}$$

we can rewrite equation 2.43 into the follow expression

$$\begin{aligned} P_y^{(3)} = \frac{1}{2}\varepsilon_0 \chi_{yjkl}^{(3)}(\omega_j,\omega_k,\omega_l)\Big(&E^{(\text{probe})}(\omega_p)E^{(\text{gate})}(+\omega_g)E^{(\text{gate})}(-\omega_g)\hat{x}_j\left(\hat{x}_k+\hat{y}_k\right)\left(\hat{x}_l+\hat{y}_l\right) \\ &+E^{(\text{probe})}(\omega_p)E^{(\text{gate})}(-\omega_g)E^{(\text{gate})}(+\omega_g)\hat{x}_j\left(\hat{x}_k+\hat{y}_k\right)\left(\hat{x}_l+\hat{y}_l\right) \\ &+E^{(\text{gate})}(+\omega_g)E^{(\text{probe})}(\omega_p)E^{(\text{gate})}(-\omega_g)\left(\hat{x}_j+\hat{y}_j\right)\hat{x}_k\left(\hat{x}_l+\hat{y}_l\right) \\ &+E^{(\text{gate})}(-\omega_g)E^{(\text{probe})}(\omega_p)E^{(\text{gate})}(+\omega_g)\left(\hat{x}_j+\hat{y}_j\right)\hat{x}_k\left(\hat{x}_l+\hat{y}_l\right) \\ &+E^{(\text{gate})}(+\omega_g)E^{(\text{gate})}(-\omega_g)E^{(\text{probe})}(\omega_p)\left(\hat{x}_j+\hat{y}_j\right)\left(\hat{x}_k+\hat{y}_k\right)\hat{x}_l \\ &+E^{(\text{gate})}(-\omega_g)E^{(\text{gate})}(+\omega_g)E^{(\text{probe})}(\omega_p)\left(\hat{x}_j+\hat{y}_j\right)\left(\hat{x}_k+\hat{y}_k\right)\hat{x}_l\Big) \end{aligned} \tag{2.46}$$

evaluating the tensor contractions in equation 2.46 yields the following expression

$$
\begin{aligned}
P_y^{(3)} = \frac{1}{2}\varepsilon_0 \Bigg( & \Big[ \chi^{(3)}_{yxxx}(+\omega_g,-\omega_g,\omega_p) + \chi^{(3)}_{yyxx}(+\omega_g,-\omega_g,\omega_p) + \chi^{(3)}_{yxyx}(+\omega_g,-\omega_g,\omega_p) + \\
& \chi^{(3)}_{yyyx}(+\omega_g,-\omega_g,\omega_p) + \chi^{(3)}_{yxxx}(-\omega_g,+\omega_g,\omega_p) + \chi^{(3)}_{yyxx}(-\omega_g,+\omega_g,\omega_p) + \\
& \chi^{(3)}_{yxyx}(-\omega_g,+\omega_g,\omega_p) + \chi^{(3)}_{yyyx}(-\omega_g,+\omega_g,\omega_p) \Big] + \\
& \Big[ \chi^{(3)}_{yxxx}(+\omega_g,\omega_p,-\omega_g) + \chi^{(3)}_{yyxx}(+\omega_g,\omega_p,-\omega_g) + \chi^{(3)}_{yxxy}(+\omega_g,\omega_p,-\omega_g) + \\
& \chi^{(3)}_{yyxy}(+\omega_g,\omega_p,-\omega_g) + \chi^{(3)}_{yxxx}(-\omega_g,\omega_p,+\omega_g) + \chi^{(3)}_{yyxx}(-\omega_g,\omega_p,+\omega_g) + \\
& \chi^{(3)}_{yxxy}(-\omega_g,\omega_p,+\omega_g) + \chi^{(3)}_{yyxy}(-\omega_g,\omega_p,+\omega_g) \Big] + \\
& \Big[ \chi^{(3)}_{yxxx}(\omega_p,+\omega_g,-\omega_g) + \chi^{(3)}_{yxyx}(\omega_p,+\omega_g,-\omega_g) + \chi^{(3)}_{yxxy}(\omega_p,+\omega_g,-\omega_g) + \\
& \chi^{(3)}_{yxyy}(\omega_p,+\omega_g,-\omega_g) + \chi^{(3)}_{yxxx}(\omega_p,-\omega_g,+\omega_g) + \chi^{(3)}_{yxyx}(\omega_p,-\omega_g,+\omega_g) + \\
& \chi^{(3)}_{yxxy}(\omega_p,-\omega_g,+\omega_g) + \chi^{(3)}_{yxyy}(\omega_p,-\omega_g,+\omega_g) \Big] \Bigg) E^{(\text{gate})} E^{(\text{gate})} E^{(\text{probe})}
\end{aligned}
\tag{2.47}
$$

At this point invoking the intrinsic permutation symmetry of $\chi^{(3)}$ allows us to greatly simplify equation 2.48. By preferencing the arbitrary ordering of $(+\omega_g,-\omega_g,\omega_p)$ we can reexpress equation 2.48 into the following form [39, 36]

$$
\begin{aligned}
P_y^{(3)} = 3\varepsilon_0 \Big( & \chi^{(3)}_{yxxx}(+\omega_g,-\omega_g,\omega_p) + \chi^{(3)}_{yyxx}(+\omega_g,-\omega_g,\omega_p) + \\
& \chi^{(3)}_{yxyx}(+\omega_g,-\omega_g,\omega_p) + \chi^{(3)}_{yyyx}(+\omega_g,-\omega_g,\omega_p) \Big) E^{(\text{gate})} E^{(\text{gate})} E^{(\text{probe})}
\end{aligned}
\tag{2.48}
$$

in the case of an isotropic material, this simplifies even further to the following [36, 39, 47, 70]

$$
P_y^{(3)} = 3\varepsilon_0 \left( \chi^{(3)}_{yxyx}(+\omega_g,-\omega_g,\omega_p) + \chi^{(3)}_{yyxx}(+\omega_g,-\omega_g,\omega_p) \right) E^{(\text{gate})} E^{(\text{gate})} E^{(\text{probe})} \tag{2.49}
$$

Thus for a homodyne OKE experiment of an isotropic system, we identify the following as $\chi^{(3)}_{\text{eff}}$

$$
\chi^{(3)}_{\text{eff/homo}} = 3 \left( \chi^{(3)}_{yxyx}(+\omega_g,-\omega_g,\omega_p) + \chi^{(3)}_{yyxx}(+\omega_g,-\omega_g,\omega_p) \right) \tag{2.50}
$$

We now have written an explicit relation (as seen in expression 2.50) from the tensor elements of $\chi^{(3)}_{\text{iso}}$ to the $\chi^{(3)}_{\text{eff}}$. Also, as seen in expression 2.41, we derived an expression for the intensity

dependent refractive index in terms of this same $\chi^{(3)}_{\text{eff}}$. Lastly, when reviewing the correlation analysis of optical Kerr effect measurements, we related the intrinsic response function ($\mathscr{R}$) of an optical Kerr effect measurement, to the intensity dependent refractive index, using expression 2.27. Combining these relationships allows us to rewrite the expression for the intrinsic response function as follows

$$\begin{aligned}\mathscr{R} &\propto -\frac{i}{4c\varepsilon_0}\frac{d}{dt}\mathscr{F}^{-1}\left[\frac{\chi^{(3)}_{\text{eff}}}{n_0^2}\right](t) \\ &\propto -i\frac{d}{dt}\left(\hat{\chi}^{(3)}_{\text{eff}} * \hat{n}_0^{-2}\right)\end{aligned} \tag{2.51}$$

If the linear refractive index has a constant frequency response over the bandwidth of the pulse envelope, the $\frac{1}{n_0^2}$ term becomes a constant that can be factored out of equation 2.51. This lets us further simplify expression 2.51 and relate the real and imaginary terms of the intrinsic response ($\mathscr{R}$) function to their corresponding real and imaginary terms of the effective third order response function ($\chi^{(3)}_{\text{eff}}$) as follows

$$\mathscr{R}_{n_0} \propto -i\frac{d}{dt}\left(\hat{\chi}^{(3)}_{\text{eff}}(t)\right) \tag{2.52a}$$

$$Re\left(\mathscr{R}_{n_0}\right) \propto -\frac{d}{dt}Im\left(\hat{\chi}^{(3)}_{\text{eff}}(t)\right) \tag{2.52b}$$

$$Im\left(\mathscr{R}_{n_0}\right) \propto \frac{d}{dt}Re\left(\hat{\chi}^{(3)}_{\text{eff}}(t)\right) \tag{2.52c}$$

Physically, equation 2.52 suggests the following interpretation. As implied by equations 2.6, 2.7, 2.11 and 2.12, real Kerr effect phase shifts result in changes in the resultant polarization and imaginary Kerr phase shifts result in shifts in the absorption of the signal. By equations 2.23 and 2.24, the Kerr phase shift is directly proportional to the intrinsic response function in the time domain. In the context of equation 2.52, this suggests that absorption effects in a Kerr effect experiment are due to the first derivative of the real component of $\hat{\chi}^{(3)}_{\text{eff}}(t)$ whereas phase shifts in the polarization are due to first derivative of the imaginary component of $\hat{\chi}^{(3)}_{\text{eff}}(t)$.

When considering the heterodyne experiments, since those measurements involve subtraction of a pair of signals, the approach of only looking at the resulting polarization through 4WM is not as straight forward as compared to the homodyne configuration. However, by using the results of the correlation analysis given the assumption that the sample can be described using equation 2.5, we can generalize the current results to the heterodyne case. Importantly, because the response function as written in equation 2.23 describes both the homodyne and the heterodyne experiments, a derivation of the response function in the homodyne case must also relate back to the heterodyne configuration. Thus by using the result in equation 2.52 we find that we can identify the out-of-phase heterodyne OKE signal as being a function of equation 2.52b and the in-phase heterodyne signal is a function of equation 2.52c.

## 2.3 Analysis of UTPS Signals

One simplifying assumption that's often made when analyzing UTPS signals is that the excitation process is sufficiently decoupled from the signal generation process [61]. This allows us to represent total response function as a weighted sum of the ground state response function ($\mathscr{R}_{\text{OKE}}$) and an excited state response function ($\mathscr{R}_{\text{excited}}$) due to the excited state response [34] with a scalar ($\alpha$) representing the excited state fraction of the sample being observed. Note that the ground state UTPS response function is the response function typically measured in OKE spectroscopy [61]. As $\alpha$ depends on the evolution of the excited state which is initiated by the pump and in principle can be modified by interaction with the gate, $\alpha$ must be a function of both pump-probe delay ($T$) and gate-probe delay ($\tau$). This is in contrast to the ground state response function, which can only depend on the time delay between the gate and probe pulses. In principle, dynamics on the excited state can change the electronic structure as well as transition moments of a molecule, this suggests that the excited state response function in general should be a function of both pump-probe and gate-probe delays. With these considerations we can express the total response function $\mathscr{R}_{\text{tot}}$ as

If the only dynamics on the excited state only impact how the system decays from an excited state , we can consider

$$\begin{aligned}\mathscr{R}_{\text{tot}}(\tau,T) &= (1-\alpha(\tau,T))\,\mathscr{R}_{\text{OKE}}(\tau)+\alpha(\tau,T)\mathscr{R}_{\text{excited}}(\tau,T)\\ &= \mathscr{R}_{\text{OKE}}+\alpha(\tau,T)\,(\mathscr{R}_{\text{excited}}(\tau,T)-\mathscr{R}_{\text{OKE}}(\tau))\end{aligned} \tag{2.53}$$

Experimentally, it can often be more convenient to represent the total response function as a change relative to the ground state due to the excitation pulse ($\Delta\mathscr{R}_{\text{excited}}$) which is both a function of pump-probe delay and gate-probe delay. This allows us to separate the components of the signal that depend only on gate-probe delay from the components that also depend on pump-probe delay. This gives the following alternative expression for the total response function

$$\mathscr{R}_{\text{tot}}(\tau,T) = \mathscr{R}_{\text{OKE}}(\tau)+\Delta\mathscr{R}_{\text{excited}}(\tau,T) \tag{2.54}$$

Briefly, we note that comparing equations 2.53 and 2.54 allows us to identify $\Delta\mathscr{R}_{\text{excited}}$ in terms of the underlying ground state and excited state response functions as seen in equation 2.55.

$$\Delta\mathscr{R}_{\text{excited}} = \alpha\,(\mathscr{R}_{\text{excited}}-\mathscr{R}_{\text{OKE}}) \tag{2.55}$$

We note that the transformations relating $\mathscr{R}$ to $\chi^{(3)}_{\text{eff}}$ as shown in equations 2.51 and 2.52a, are linear. Since equation 2.54 represents the total OKE response function as a sum of the excited and ground state response functions, the linear relationship between $\chi^{(3)}_{\text{eff}}$ and $\mathscr{R}$ suggests that we can also represent $\chi^{(3)}_{\text{eff}}$ as a sum of the ground state susceptibility ($\chi^{(3)}_{\text{eff/OKE}}$) and a change in the susceptibility due the excited state ($\Delta\chi^{(3)}_{\text{eff/Excite}}$). Whatsmore, by inserting expression 2.54 into the previously derived homodyne signal expression of equation 2.28 allows us to express the measured UTPS signal as a function of convolutions of the total response function, the incident gate, and probe pulse, as shown below

$$V_{\text{3-pulse}}^{\text{UTPS-homo}}(\tau,T) \propto I_{\text{probe}} * \left|I_{\text{gate}} * (\mathscr{R}_{\text{OKE}} + \Delta\mathscr{R}_{\text{excited}})\right|^2 + I_{\text{probe}} * \left|I_{\text{excite}} * \mathscr{R}_{\text{OKE}}\right|^2 \tag{2.56}$$

Note that in equation 2.56 we have included the effect of the excitation pulse in two separate ways. First, as expressed in equation 2.54, we have represented the effect of the excitation pulse bringing some population into an excited state and thus modifying the measured OKE signal through the addition of the $\Delta\mathscr{R}_{\text{excited}}$ term. Second we have included the ground state OKE response which can result in a separate ground state Kerr effect signal through interaction between the excitation pulse and the probing pulse. To further simplify equation 2.56, first we break-up the ground state and excited state response functions in terms of their real ($\mathscr{R}'$) and imaginary ($\mathscr{R}''$) components, yielding

$$\begin{aligned} V_{\text{3-pulse}}^{\text{UTPS-homo}}(\tau,T) \propto & I_{\text{probe}} * \left|I_{\text{gate}} * \mathscr{R}_{\text{OKE}}\right|^2 + \\ & I_{\text{probe}} * \left|I_{\text{gate}} * \Delta\mathscr{R}_{\text{excited}}\right|^2 + \\ & 2I_{\text{probe}} * (I_{\text{gate}} * \mathscr{R}'_{\text{OKE}})(I_{\text{gate}} * \Delta\mathscr{R}'_{\text{excited}}) + \\ & 2I_{\text{probe}} * (I_{\text{gate}} * \mathscr{R}''_{\text{OKE}})(I_{\text{gate}} * \Delta\mathscr{R}''_{\text{excited}}) + \\ & I_{\text{probe}} * \left|I_{\text{excite}} * \mathscr{R}_{\text{OKE}}\right|^2 \end{aligned} \tag{2.57}$$

Subtracting the ground state 2-pulse terms between the probe and gate or the probe and excitation pulses leaves us with the resulting expression for the UTPS homodyne signal

$$\begin{aligned} V_{\text{homo}}^{\text{UTPS}}(\tau,T) \propto & I_{\text{probe}} * \left|I_{\text{gate}} * \Delta\mathscr{R}_{\text{excited}}\right|^2 + \\ & 2I_{\text{probe}} * (I_{\text{gate}} * \mathscr{R}'_{\text{OKE}})(I_{\text{gate}} * \Delta\mathscr{R}'_{\text{excited}}) + \\ & 2I_{\text{probe}} * (I_{\text{gate}} * \mathscr{R}''_{\text{OKE}})(I_{\text{gate}} * \Delta\mathscr{R}''_{\text{excited}}) \end{aligned} \tag{2.58}$$

Unlike the OKE case (as seen in expression 2.28), there is no guarantee that the signals from a homodyne UTPS measurement are purely positive. This has to do with the nonlinear interaction between the ground state and excited state response functions in this measurement scheme in combination with the subtraction of the ground state interactions that are encoded in the 2 pulse datasets. Additionally, equation 2.58 further suggests that extracting information from the excited state response function in a UTPS homodyne experiment could be difficult without knowledge of the real ($\mathscr{R}'_{\text{OKE}}$)) and imaginary ($\mathscr{R}''_{\text{OKE}}$)) components of the ground state OKE response function which are most directly accessed through a pair of OKE heterodyne measurements [39, 40, 58].

For a heterodyne UTPS in-phase case, we can again perform a similar procedure as in the homodyne case by substituting equation 2.54 into expression 2.29 for the in-phase OKE signal giving us the following expression for the 3-pulse in-phase UTPS signal

$$V_{\text{in-phase}}^{\text{UTPS-3pulse}}(\tau,T) = I_{\text{probe}} * I_{\text{gate}} * \mathscr{R}''_{\text{OKE}} + I_{\text{probe}} * I_{\text{gate}} * \Delta\mathscr{R}''_{\text{excited}} + I_{\text{probe}} * I_{\text{excitation}} * \mathscr{R}''_{\text{OKE}} \tag{2.59}$$

After subtracting the two-pulse components, the resulting UTPS in-phase signal can be cleanly expressed as

$$V_{\text{in-phase}}^{\text{UTPS}}(\tau,T) = I_{\text{probe}} * I_{\text{gate}} * \Delta\mathscr{R}''_{\text{excited}} \tag{2.60}$$

Allowing for the extraction of the imaginary component of the sample's excited state response function by deconvolving the signal with respect to the probe and gate pulses. Furthermore, as in the case of the in-phase OKE measurement, equation 2.60 suggests that the UTPS in-phase signal is linear with respect to excited state contribution to the Kerr effect absorption.

For the UTPS out-of-phase case, following the same procedure as in the homodyne and heterodyne in-phase examples but starting from the OKE out-of-phase signal expression of equation 2.30 yields

$$\begin{aligned} V_{\text{out-of-phase}}^{\text{UTPS-3pulse}} =& I_{\text{probe}} * \left( e^{I_{\text{gate}} * \mathscr{R}''_{\text{OKE}} + I_{\text{gate}} * \Delta\mathscr{R}''_{\text{excited}}} \left[ I_{\text{gate}} * \mathscr{R}'_{\text{OKE}} + I_{\text{gate}} * \Delta\mathscr{R}'_{\text{excited}} \right] \right) + \\ & I_{\text{probe}} * e^{I_{\text{excitation}} * \mathscr{R}''_{\text{OKE}}} \left( I_{\text{excitation}} * \mathscr{R}'_{\text{OKE}} \right) \end{aligned} \tag{2.61}$$

and subtracting the two-pulse ground state OKE signal from the excitation and probing pulses gives

$$\begin{aligned} V_{\text{out-of-phase}}^{\text{UTPS-subtracted}} &= V_{\text{out-of-phase}}^{\text{UTPS-3pulse}} - V_{\text{out-of-phase}}^{\text{OKE-excite-probe}} \\ &= I_{\text{probe}} * \left( e^{I_{\text{gate}} * \mathscr{R}''_{\text{OKE}} + I_{\text{gate}} * \Delta\mathscr{R}''_{\text{excited}}} \left[ I_{\text{gate}} * \mathscr{R}'_{\text{OKE}} + I_{\text{gate}} * \Delta\mathscr{R}'_{\text{excited}} \right] \right) \end{aligned} \tag{2.62}$$

Equation 2.62 gives us an opportunity to interpret the out-of-phase UTPS signal in reference to the real and imaginary phase shifts of the OKE out-of-phase signal. In the case where the Kerr effect absorption is negligible, the imaginary component of the response function can be ignored. In this case, we can simplify equation 2.62 by both ignoring the contribution of the imaginary component of the response function as well as subtracting the ground state OKE signal, which yields the following simplified expression for the out-of-phase UTPS signal.

$$\begin{aligned} V_{\text{out-of-phase}}^{\text{UTPS-no-absorption}} &= V_{\text{out-of-phase}}^{\text{UTPS-3pulse}} - V_{\text{out-of-phase}}^{\text{OKE-excite-probe}} - V_{\text{out-of-phase}}^{\text{OKE-gate-probe}} \\ &= I_{\text{probe}} * I_{\text{gate}} * \Delta\mathscr{R}'_{\text{excited}} \end{aligned} \tag{2.63}$$

Equations 2.62 and 2.63 suggest that, like the OKE heterodyne signal, the out-of-phase UTPS signal is roughly linear with respect to the real component of the excited state response function. Also like the OKE heterodyne signal, equation 2.62 suggests that the UTPS out-of-phase signal is impacted by both the effects of absorption and refraction. However, equation 2.62 further suggests that in general, information about the Kerr effect absorption from both the ground state and excited state response function is needed in order to extract the real component of the excited state Kerr effect response function. Performing Fourier analysis on equation 2.62 allows us to solve for the real

component of the excited state OKE response function in terms of the following experimentally measurable quantities

$$\mathscr{F}\left[\frac{\mathscr{F}\left[V_{\text{out-of-phase}}^{\text{UTPS-subtracted}}\right]}{\mathscr{F}\left[I_{\text{probe}}\right]}\right] \Big/ e^{V_{\text{in-phase}}^{\text{UTPS-3pulse}} - V_{\text{in-phase}}^{\text{OKE-excite-gate}}} = I_{\text{gate}} * \Delta\mathscr{R}'_{\text{excited}} \tag{2.64}$$

These expressions provide a framework for modeling the responses from a UTPS experiment. Additionally these expressions give us a means to extract information from the 2D excited state response function through a set of 3 pulse and 2 pulse measurements.

## 2.4 Sample UTPS Measurements of Neat Nitrobenzene

In the previous sections, we have discussed how we can collect homodyne and heterodyne UTPS data and how we can analyze the UTPS experimental data in the context of the theory of time resolved OKE spectroscopy. In this section we will present the typical steps taken to collect and process UTPS data in both heterodyne and homodyne configurations. In the following examples of UTPS measurements, we will be considering the case of a sample of neat nitrobenzene being excited by a pump pulse with center frequency at 780 nm, a pulse duration of 40 fs, and an incident intensity of $5 \cdot 10^{11}\text{W}/\text{cm}^2$. This sample was then probed using a pair of gate and probe pulses again with a center frequency at 780 nm and a pulse duration of 40 fs but, with intensities of $2 \cdot 10^{11}\text{W}/\text{cm}^2$ for both the gate and probe pulses. In these cases, the exciting pump, gate, and probe pulses had unperturbed polarizations of 45°, 45°, and 0° respectively.

As suggested by equation 2.57, a typical UTPS measurement in the homodyne configuration where the pulse trains aren't modulated, could consist of three separate measurements. A raw 3 pulse measurement, a pump-probe only measurement (no gate), and a gate-probe only measurement (no-pump). Examples of these measurements can be seen in figure 2.7. Because of the modulated pump pulse train and the use of lock-in amplification to select for pump modulated signal along the probe axis, this had the effect of effectively subtracting the gate-probe only signal from the UTPS homodyne during the three pulse measurement. It's for this reason that we don't see a vertical stripe in the three pulse signal as seen in the no-pump case that would be representative of the ground state signal coming from gate-probe interaction. However, ground state signal from pump-probe only interaction is still present in the three pulse measurement which can be seen as a diagonal stripe along constant pump-probe delay.

Subtracting the no-gate UTPS measurement from three pulse UTPS measurements results in the following homodyne UTPS measurement as seen in figure 2.8. Here we note a few features of these measurements. First, as suggested by equation 2.62 we note that the homodyne UTPS experimental measurements results in both positive and negative signals which we attribute to direct contributions to the signal from the real and imaginary components of the ground and excited state response function of the sample. We also note here that since the diagonal stripe that intersects the peak signal at the temporal overlap occurs with the condition of pump-probe delay being near 0 fs. This means at positive gate-probe delays, signal along the diagonal occurs with the gate arriving

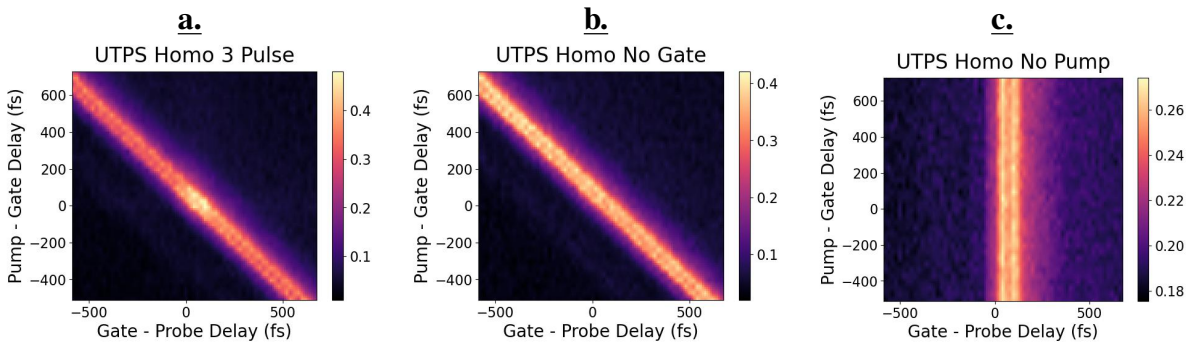


Figure 2.7: Here we show raw three pulse and two pulse polarization sensitive homodyne measurements of neat nitrobenzene that can be further processed into a homodyne UTPS measurement. The three pulse (a.) and the pump-probe only (b.) measurements were made with the pump pulse train being modulated by a mechanical chopper (operating at 137 Hz) and with lock-in amplification being used to amplify the polarization signal along the probe axis that contains the pump modulation. The gate-probe only measurement (c.) was made by feeding the repetition rate of the laser as the lock-in reference frequency so that gate-probe interactions would be detected. In practice only measurements from the pump-probe interaction (b.) and three pulse interaction (c.) are required in order to form a figure representing the UTPS homodyne measurement.

before the pump and probe pulses whereas at negative gate-probe delays, the gate arrives after the pump and probe pulses. Given the ground state OKE heterodyne measurements of nitrobenzene as shown in figure 2.4, this suggests that under the conditions of the gate pulse arriving early, that some component of the excited state response function is strongly negative suggesting that the time derivative of $\hat{\chi}^{(3)}_{\text{eff}}(t)$ undergoes a sign change as a result of excitation. The result of this is a suppression of the 3 pulse signal relative to pump-probe only signal.

We now consider the in-phase heterodyne UTPS measurement. To perform such a measurement with the UTPS set-up, as depicted in figure 2.1, consists of four separate measurements. As suggested by equation 2.59, when combined with lock-in amplification, the heterodyne three pulse UTPS in-phase measurement is sensitive to two terms. The term representing the pump-probe interaction with the ground state response function and the term representing the gate-probe interaction with the excited state response function. To subtract out the pump-probe interaction with the ground state response function term, we must make a separate pump-probe only OKE in-phase measurement that allows us to subtract out this term. As one in-phase measurement involves two separate polarization measurements with a positive and negative perturbation of the analyzing polarizer, to remove the ground state interaction in the three pulse UTPS measurement will require four distinct measurements.

An example of a realization of a complete set of heterodyne in-phase UTPS measurements is shown in figure 2.9. In this case the analyzing polarizer was perturbed by $\pm 2^{\circ}$. After performing the appropriate subtractions we obtain the resulting heterodyne in-phase UTPS measurement.

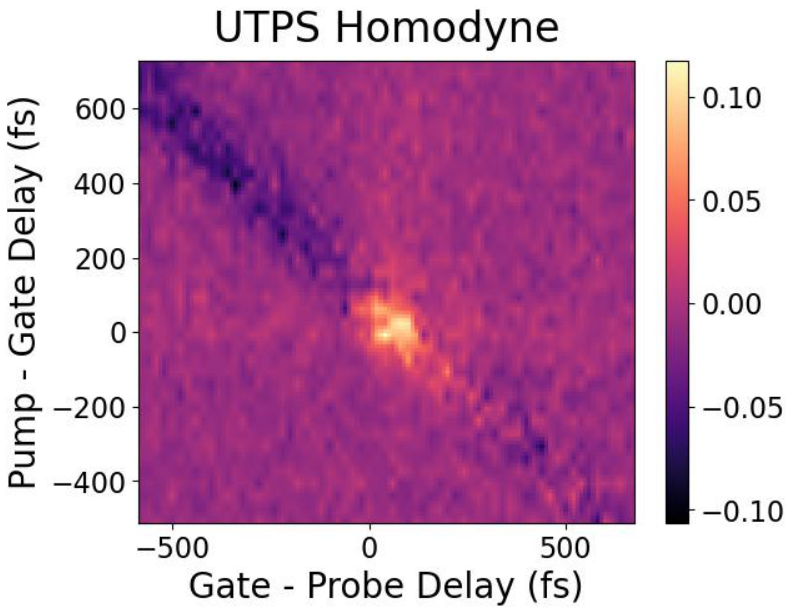


Figure 2.8: A homodyne UTPS measurement of neat nitrobenzene with the pump pulse polarization parallel to the gate pulse. This measurement was formed from the subtraction of the two pulse pump-probe only measurement from the three pulse UTPS measurement. In contrast to homodyne OKE measurements that are purely positive, homodyne UTPS signals can have both positive and negative components to the measurement due to the nonlinear interaction between the excited Kerr effect state response function and the ground state Kerr effect response function.

Importantly, as shown in equation 2.60, since this signal is linear with respect to the imaginary component of the response function, the resultant in-phase heterodyne UTPS measurement gives us a direct probe of this response function.

The out-of-phase heterodyne UTPS measurement has a lot of similarities to the in-phase measurement. One substantial difference is that, according to equation 2.61, due to the effect of Kerr absorption, the real component of the excited state response function is not linear with respect to the measured out-of-phase UTPS signal. In particular, this means that regardless of whether lock-in amplification is performed by modulating the excitation pump pulse train or not, the three pulse signal will still be sensitive to all the terms as shown in equation 2.61. However, under the conditions where the imaginary component of the excited state response function is zero, the out-of-phase UTPS signal reduces to a linear response with respect to the real component of the response function. Under those conditions and while using a lock-in on a pump modulated out-of-phase UTPS signal, the ground state OKE response between the gate and probe pulses will be rejected by the lock-in. This offers an explanation for why, in figure 2.11, the expected vertical stripe representing the UTPS signal that's constant with respect to pump-gate delay doesn't show up in the three pulse out-of-phase UTPS measurements.

After performing the appropriate subtractions given the raw out-of-phase UTPS measurements

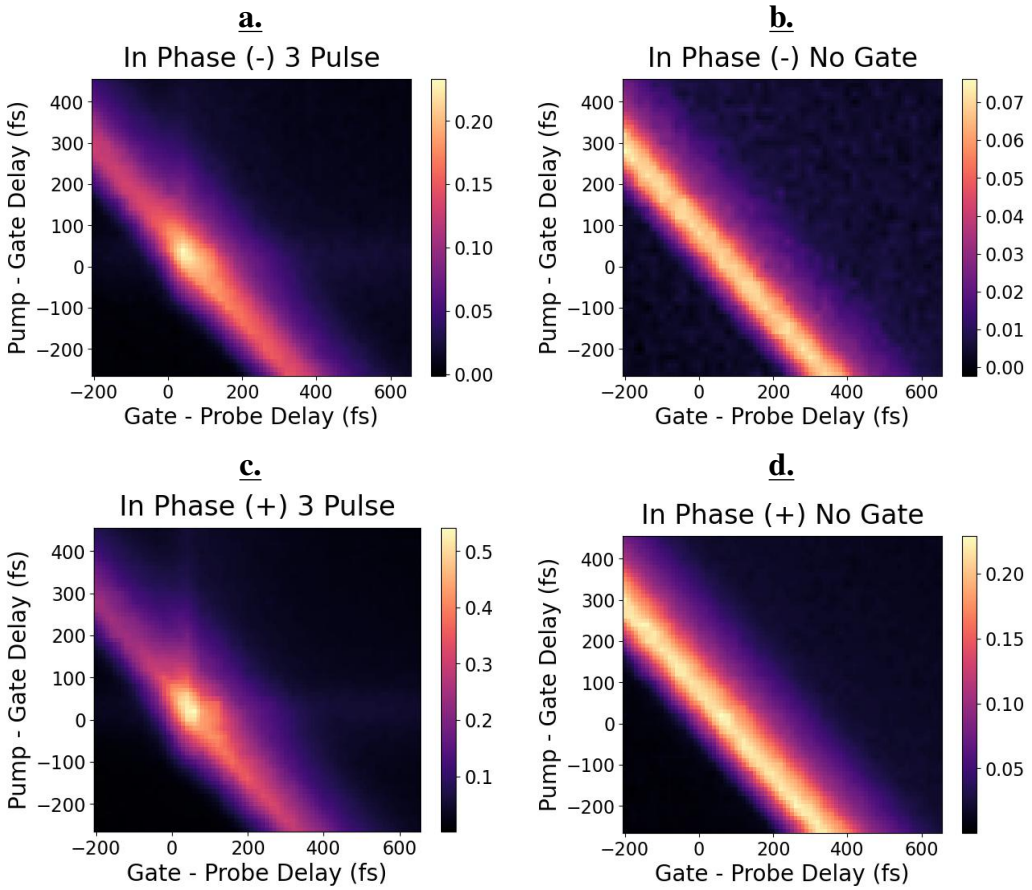


Figure 2.9: Here we show the raw heterodyne in-phase polarization sensitive measurements representing the data needed to form a heterodyne in-phase UTPS measurement of neat liquid nitrobenzene. In these examples, the positive (+) in-phase measurement corresponds to a perturbation of the analyzing-polarizer off from the homodyne condition by $+2^\circ$ and the negative (-) in-phase measurement corresponds to a $-2^\circ$ rotation. Due to the use of lock-in amplification the gate-probe interaction term is suppressed meaning only 4 measurements are needed instead of 6. The difference between panels a and b represent the three pulse in-phase heterodyne measurement as expressed in equation 2.59, whereas the difference between panels b and d represent an in-phase OKE measurement using the pump and probe pulses. The difference between the in-phase three pulse measurement and the pump-probe OKE measurement results in a final UTPS measurement that can be used to extract information about the imaginary component of the excited state Kerr effect response function.

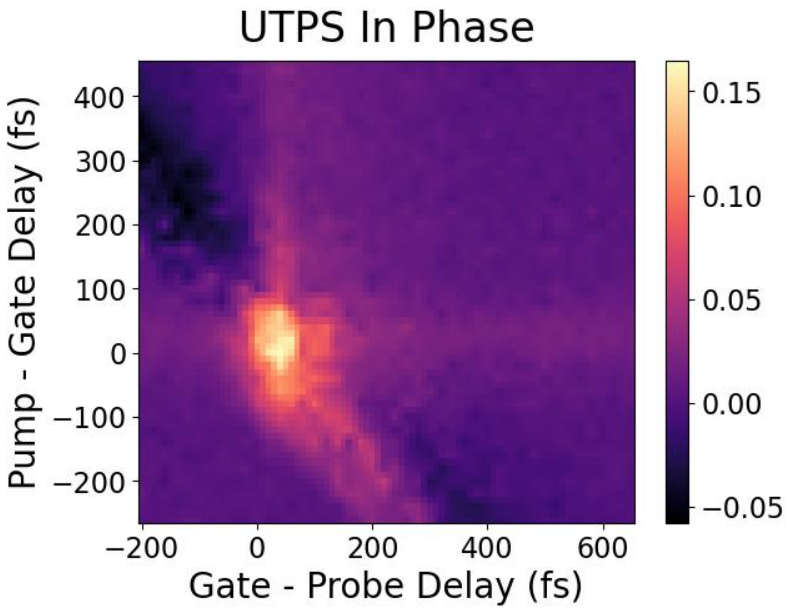


Figure 2.10: This figure gives an example of an in-phase UTPS measurement that is formed after the subtraction of the two pulse pump-gate only in-phase OKE measurement from the three pulse UTPS in-phase measurement. This final in-phase UTPS measurement is linearly related to the imaginary component of the excited state Kerr response function as seen in equation 2.60 and thus gives information about Kerr absorption effects.

we obtain the resultant out-of-phase UTPS signal as shown in figure 2.12. As mentioned previously, in the case of a non-zero imaginary component of the excited state Kerr effect response function, the out-of-phase UTPS signal must be analyzed in the context of the in-phase UTPS measurement.

At this point we've outlined the experimental and analytical tools needed to both take and analyze UTPS measurements. We have also demonstrated the ability for us to prepare a fraction of a sample in a nonequilibrium state and then to sample the dynamics of those systems using methods based on Kerr effect spectroscopy. In chapter 3 we will consider these methods as applied to the analysis of UTPS measurements of neat nitrobenzene. These measurement combined with information about the quantum chemistry of nitrobenzene will allow us to interpret the observed UTPS signal as evidence for wavepacket motion on the $S_1$ excited state.

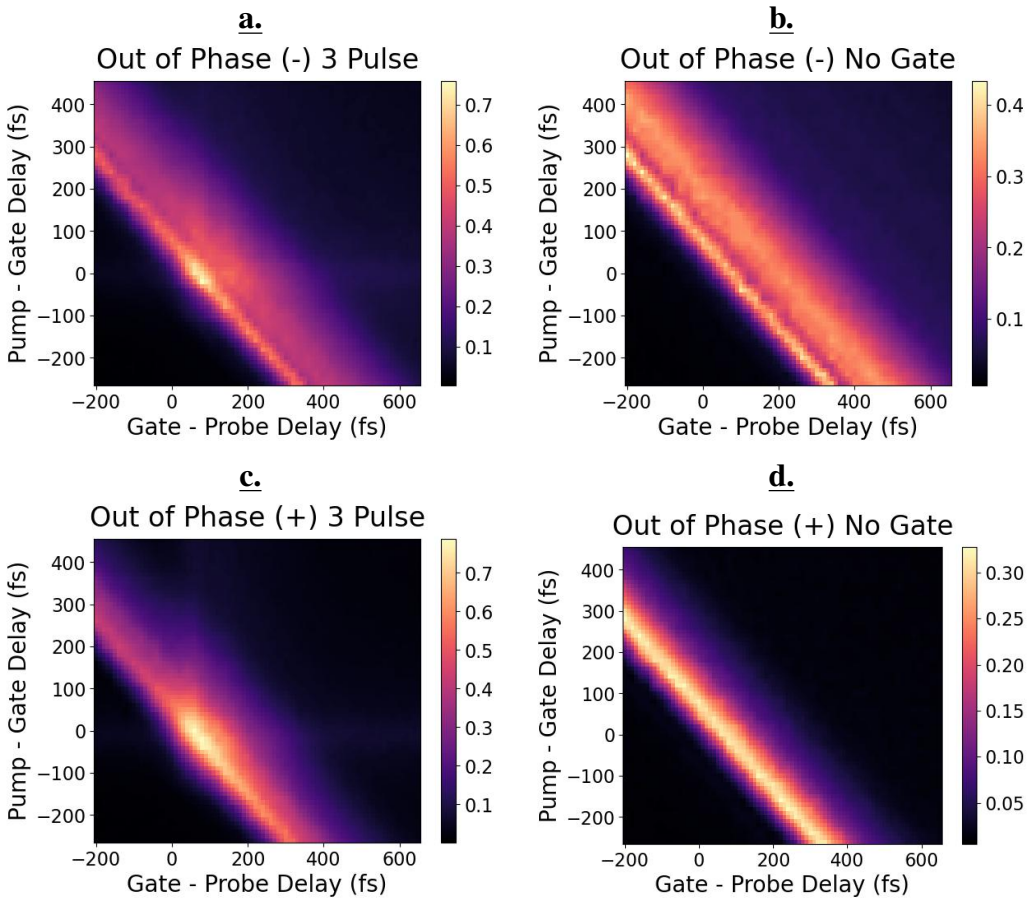


Figure 2.11: Here we show the raw heterodyne out-of-phase polarization sensitive measurements representing the data needed to form a heterodyne out-of-phase UTPS measurement of neat liquid nitrobenzene. In these examples, the positive(+)/negative (-) in-phase measurement corresponds to a perturbation of the ellipticity of the probing pulse prior to interaction with the sample by $\pm 3.4^{\circ}$ as measured through stokes vector measurements of these pulses. The difference between panels a and b represent the three pulse out-of-phase heterodyne measurement as expressed in equation 2.61, whereas the difference between panels b and d represent an out-of-phase OKE measurement using the pump and probe pulses. The difference between the out-of-phase three pulse measurement and the pump-probe out-of-phase OKE measurement results in a final out-of-phase UTPS measurement which can be used to extract information about the real component of the excited state Kerr effect response function in the context of the associated in-phase measurement.

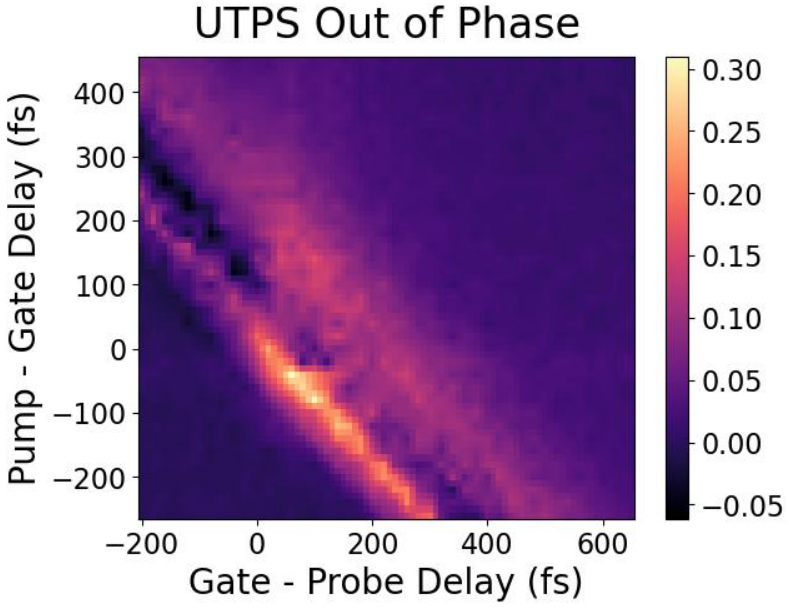


Figure 2.12: This figure gives an example of an out-of-phase UTPS measurement that is formed after the subtraction of the two pulse pump-gate only out-of-phase OKE measurement from the three pulse UTPS in-phase measurement. This final out-of-phase UTPS measurement in general has a nonlinear relationship to the excited state Kerr response function as shown in equation 2.62. This expression suggests that one can extract information about the real component of the excited state Kerr effect response function but only after accounting for the effects of Kerr effect absorption as measured though a set of in-phase UTPS and in-phase OKE measurements.

# Chapter 3

# A Study of Nitrobenzene in the Context of Nonlinear Spectroscopy and Quantum Chemistry

In the previous chapter we provided the framework for taking and analyzing UTPS signals. In this chapter we will apply this technique toward the analysis of the ultrafast dynamics of nitrobenzene.

From a basic science perspective there are several reasons why nitrobenzene is a good target for a polarization sensitive excited state spectroscopic method. First, nitrobenzene has a large and well studied ground state third order response the yields a strong optical Kerr effect signal [36, 65, 88, 89, 90]. This allows us to benchmark our measured ground state response against literature values to ensure we are measuring the third order response of the system.

More specifically, for optical pulses ranging from 1.5 eV to 4 eV, there are effectively two regimes that give rise to distinct dynamics in nitrobenzene as measured with Kerr effect spectroscopy. The first regime occurs with pulses between 1.5 eV and 2.5 eV. At these energies, one photon interaction with nitrobenzene is unable to resonantly interact with the lowest lying singlet excited states which have an energy gap of 3 eV - 4 eV from the ground state as calculated with MCSCF [71] and density functional theory methods [72]. In this energy regime four characteristic decay constants have been measured which have been attributed to the following mechanisms in liquid nitrobenzene. First, a fast electronic component that decays on the 80 fs time scale [65], librational dynamics which occur between 310 fs and 510 fs [65, 66], and reorientational dynamics with the slower rate constant occurring at a time scale between 20 ps - 32 ps [65, 66, 64], with the exact time scale of the dynamics depending on temperature, excitation frequency, solvent viscosity, molecular volume, and molecular shape [64]. A shorter time scale between 0.9 ps and 4 ps has also been observed and attributed to a separate reorientational process [66] or internal structural dynamics in the molecule [64].

Above 3 eV, single photon interactions are able to access the lowest lying electronic states of nitrobenzene [71, 72]. Under these conditions nitrobenzene can break down to form NO and NO2 photo-products [91, 92] or it can relax back down to the ground state [93, 94]. When nitrobenzne relaxes down to the ground state after excitation to the first accessible singlet, three distinct decay

constants have been measured, a fast component < 100 fs, a 6 ps component, and a slow 420 ps componet [93]. With the aid of MCSCF calculations, these components have been interpreted as a fast relaxation from the excited singlet state to the ground state, a triplet to triplet internal conversion, and a slow relaxation of the $T_1$ state back down to the ground state [71]. These, purely electronic mechanisms for the observed dynamics are mediated by conical intersections between the relevant states [71].

Additionally, there several reasons for us to expect that the excited state third order signal of nitrobenzene will be larger than the ground state third order signal. As discussed previously, there are general arguments based on the reduction in the energy gap and the increasing transition dipole moments when a system is in an excited state, that tend to occur across a variety of systems [41, 42]. Later we will show ab initio wavefunction calculations of the third order susceptibility of nitrobenzene using response theory using the dalton quantum chemistry package. In line with the previous points, these calculations will predict excited state enhancement of these third order signals for a range of probe pulse frequencies given a fixed gate frequency. Additionally, a similar set of calculations at the same level of theory as the third order susceptibility calculation will show increased transition dipole moments between excited states as compared to the ground state transition moments for a number of excited states.

In the following experimental study, we aim to further explore the electronic dynamics of nitrobenzene to a low lying excited state using UTPS. To do this we aim to excite nitrobenzene to the first accessible excited state using a multiphoton excitation. We will then probe the time evolution of this excitation using the optical Kerr effect.

## 3.1 Ultrafast Transient Polarization Spectroscopy of Nitrobenzene

Here we present a treatment of UTPS measurements of nitrobenzene. In particular we will focus on homodyne UTPS measurements of neat nitrobenzene using three separate IR pulses. These measurements were performed with liquid samples of nitrobenzene purchased from Sigma-Aldrich (>99% purity). These samples were loaded into a 1 mm path length Spectrosil quartz cuvette with a wall thicknesses of 1 mm. While in principle we can vary the polarization of the incident pumping pulse, for the following set of measurements we will consider the case of the excitation pulse parallel to the Kerr gating pulse.

### Homodyne UTPS Measurement of Nitrobenzene with IR Excitation having Parallel Polarization to the Gate

A schematic of the detection scheme used to collect the homodyne UTPS measurements is shown in figure 3.1. In this detection scheme, the pump pulse train was modulated by a mechanical chopper, allowing us to reduce the number of datasets required in order to process the raw polarization measurements into a 2D map representing the UTPS signal. In the following experiments we set

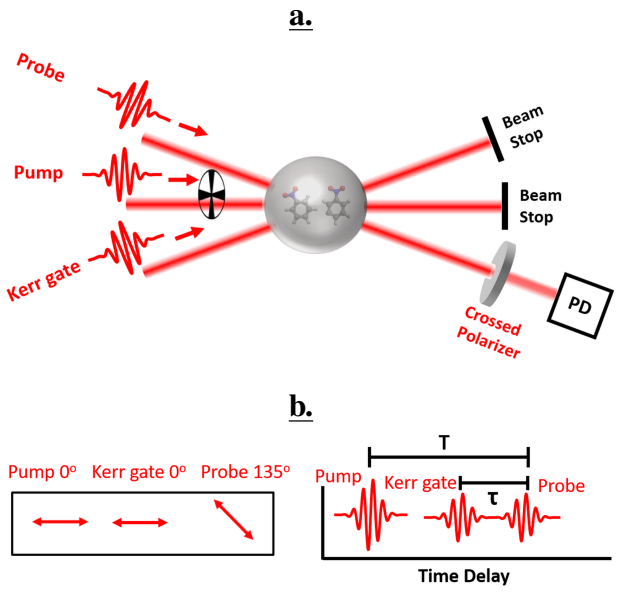


Figure 3.1: Schematic of the homodyne UTPS measurement set-up (a.) used to make the homodyne UTPS measurements of nitrobenzene. Here we also show the polarizations of the incident pulses and time-delay convention (b.) used for the datasets shown in section 3.1. In particular we also note that the polarizations of the pump and gate pulses are aligned, where as the probing pulse is rotated $-45^\circ$ relative to the pump axis.

the pump polarization to be parallel with the gating pulse with the probing pulse set to be $-45^\circ$ offset relative to the probe polarization axis.

To initiate the excited state evolution of nitrobenzene we used a 780 nm pump pulse with an intensity of $5 \times 10^{11}$ W/cm$^2$. This excitation was then sampled by a pair of 780 nm gate and probe pulse each with an intensity of $2 \times 10^{11}$ W/cm$^2$. As seen in figure 2.6, nitrobenzene is transparent to 780 nm optical pulses unless they are intense enough to excite a multiphoton transition. The pump pulse energy was chosen to be within the quadratic absorption regime which is consistent with the 2-photon absorption regime [74]. The gate and probe pulses where chosen to be bellow this threshold. From these measurements we estimate that between 1 - 10% of the sample within the interaction region was brought into the S1 excited electronic state through a multiphoton excitation [34].

As shown in figure 3.2, the intensity cross-correlations of the gate-probe and pump-probe pulses are measured to have a standard deviation of 78 fs and 59 fs respectively. These measurements were made by measuring the second harmonic signal when the pulsed of interest were incident on a BBO crystal [61]. By selecting for the appropriate k-vector we measured the 3-wave mixing signal due to the pair of incident pulses. The cross-correlation measurements give us a means to roughly estimate the time scale of the instrument response function especially in the typical framework of heterodyne time resolved OKE spectroscopy were (as seen in equation 2.3)

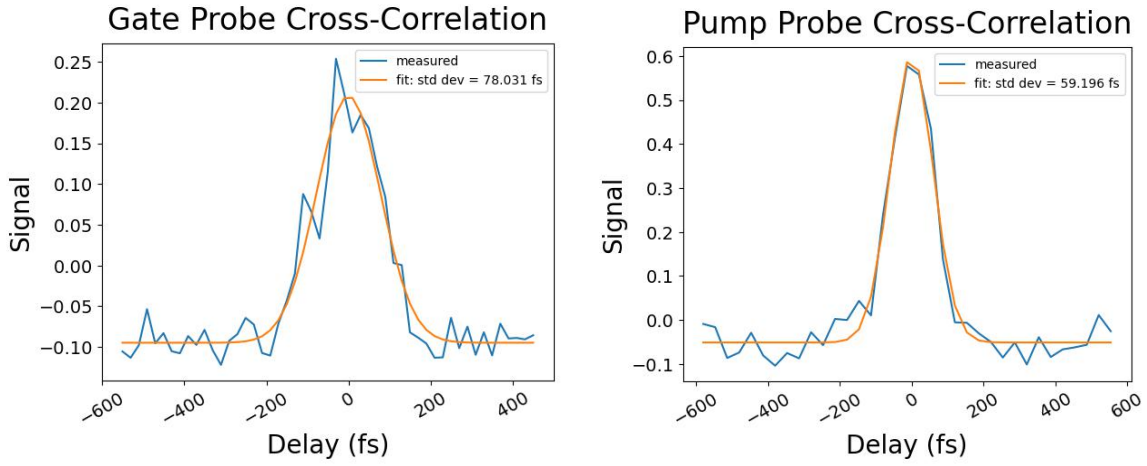


Figure 3.2: Here we show measurements of the cross-correlations of the gate and probe pulses as well as the pump and probe pulses as measured through second harmonic generation using a BBO crystal. These intensity cross correlation fits show a standard deviation of 78 fs and 59 fs for the gate-probe and pump-probe measurements respectively. These measurements give us a means to estimate the instrument response function that convolves the intrinsic response of the sample [61].

the linearity of the final signal allows us to represent the role of the pulses enters the final signal expression as a cross-correlation of the gate and probe pulses [40, 52, 39]. We note here again that this assumption can breakdown under certain conditions when analyzing out-of-phase signals given a non-constant in-phase heterodyne signal as shown in the general expressions 2.30 and 2.34.

The raw polarization sensitive measurements are shown in figure 3.3. For each dataset, one data point represents the lock-in signal acquired over 1500 laser shots at a particular pair of time-delays. Each pair of time-delays were scanned in a randomized sequence until each pair of time delays was sampled once. This process was repeated 24 times with each complete scan being averaged together for this dataset.

We note here a couple of features in the 3-pulse and no-probe datasets that are somewhat atypical for an ideal UTPS measurment. Namely, the diagonal stripe in the 3-pulse and no-probe datasets. In principle, the no-probe dataset, should be exactly zero since there is no probing pulse to sample the transient birefringence of the sample. In practice a small amount of leakage from the gating pulse can make it onto the detector on the probe beamline due to the relatively small incident angles between the pulses and the relatively large divergences from the fairly tight focus of the lenses used [61]. Additionally due to the $45^\circ$ offset polarization of the drive relative to the probe, small amounts of leakage can result in large signals because the analyzing-polarizer is unable to reject all the stray light. The additional 2-pulse contribution from the pump-probe interaction can also be subtracted out in addition to the usual subtraction of the pump-probe two pulse interaction to give the net UTPS homodyne signal.

The resultant homodyne UTPS measurement is shown in figure 3.4. In this figure the amount

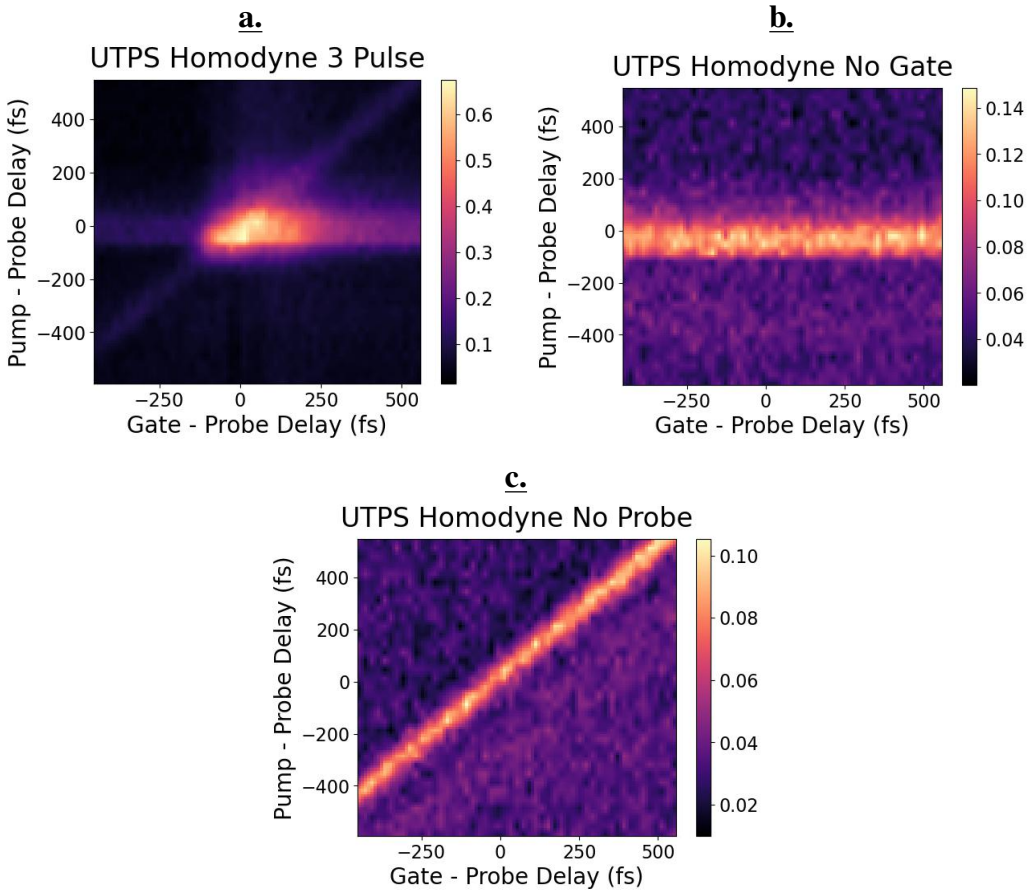


Figure 3.3: Here we show raw three pulse (a.), two pulse no gate (b.), and two pulse no probe (c.) polarization sensitive homodyne measurements of neat nitrobenzene. In principle, the no probe measurement should be exactly zero however due to a small amount of leakage of the gate onto the probe beamline detector, some signal from the gate is detected. As such the additional two-pulse contribution can be subtracted from the 3 pulse in addition to the no-gate two pulse contribution. This pair of subtractions from the three pulse signal gives us the net Homodyne UTPS signal.

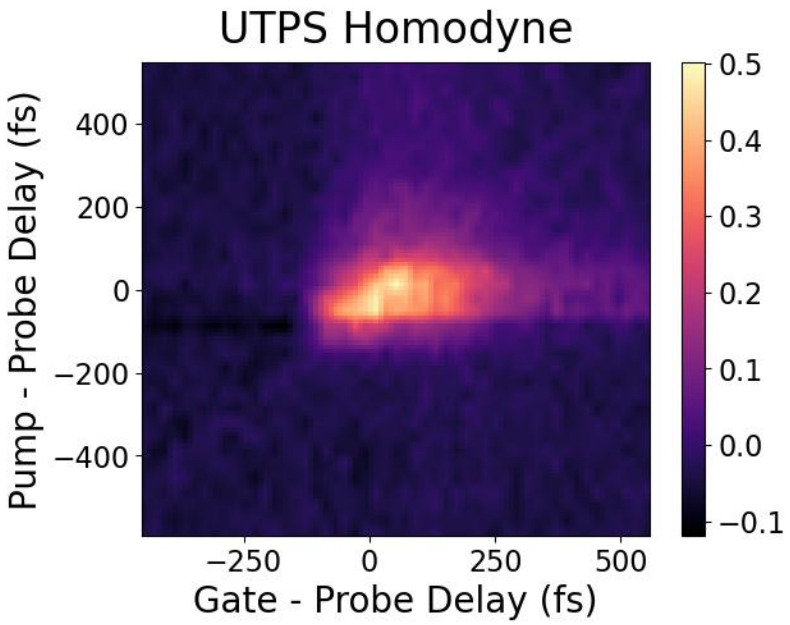


Figure 3.4: A homodyne UTPS measurement of neat nitrobenzene given the gate and pump pulses having parallel polarization relative to each other. This measurement was formed from the subtraction of the two pulse pump-probe only measurement from the three pulse UTPS measurement as well as an additional subtraction from the no-probe measurment as referenced in figure 3.3. Here we note the enhancement of the polarization response near the overlap region.

of positive (negative) signal represents the amount of enhancement (suppression) of the polarization signal as compared to a ground state OKE measurement. In this figure we can clearly see enhancement of the polarization signal near three-pulse overlap. This is consistent with prior studies suggesting that multiple aligned gating pulses can result in the enhancement of a polarization signal due to the additional molecular alignment [53, 54].

To further interpret the UTPS signal we used equation 3.1 as an ansatz to represent the UTPS time delay signal. To justify this ansatz we make the following assumptions. First, we assume that the time delay dependent Signal trace can be thought of as being parameterized by the pump-probe time delay ($T$) and only directly depends on the gate-probe ($\tau$) time delay axis. Next we assume that this parameterized signal can be represented by a convolution between an intrinsic response function and an instrument response function. Here we represent the instrument response function by a Gaussian function ($g(\tau;\sigma)$) which approximates the cross-correlation of a pair of optical pulses [34]. Furthermore, given our short time delay window we make the additional approximation that the intrinsic response function along the gate-probe axis consists of a pair of decay dynamics, a short time scale decay that can be approximated by an exponential ($\exp(-\frac{\tau-t_0}{\gamma})$) and a long time scale decay whose decay rate would not be measurable given the short time window we have to observe the dynamics and can thus be approximated by a constant function. With the

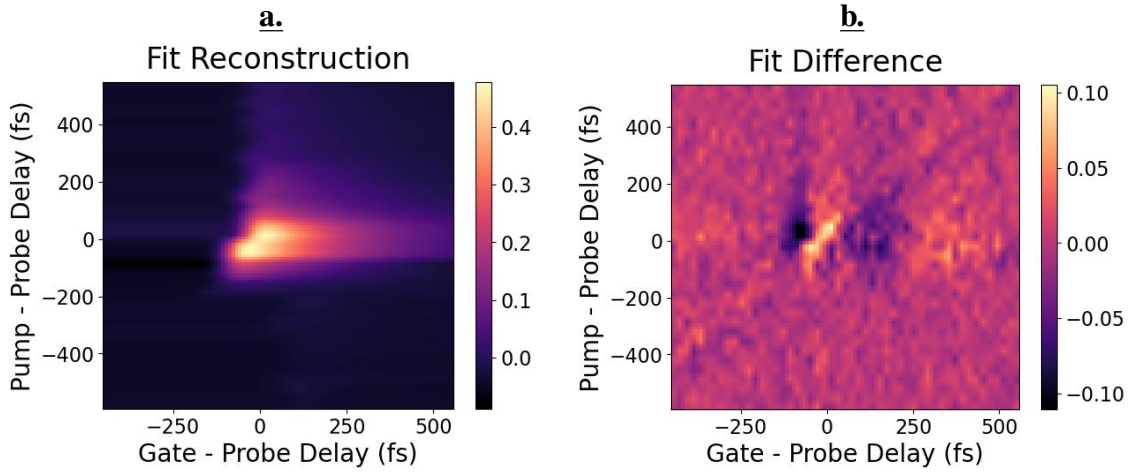


Figure 3.5: This figure shows the reconstruction of the measured homodyne UTPS signal (a.) along with the difference between the reconstructed plot and the measured homodyne signal (b.). We note that the hard edge toward the negative gate-probe side of the signal which we attribute to the sudden approximation as applied to the fitting of this homodyne dataset.

additional use of the sudden approximation we approximate the effective change in the baseline with the Heaviside step function ($\Theta(\tau - t_0)$) with all the scaling factors folded into the amplitude ($A$). As the onset time ($t_0(T)$), scaling amplitude ($A(T)$), and the signal decay rate ($\gamma(T)$), which we interpret as the system's dephasing rate [34], can very depending on the pump-probe time delay scans, we allow these fit parameters to vary between each pump-probe delay step. We note here that in these fits the standard deviation of the Gaussian function that approximated the instrument response was fixed at 30 fs.

$$V^{\text{UTPS Homo}}_{\text{Ansatz Fit}}(\tau;T) = A(T)\left[\Theta(\tau - t_0(T))\exp\left(-\frac{\tau - t_0(T)}{\gamma(T)}\right)\right] * g(\tau:\sigma) \tag{3.1}$$

Fitting the homodyne data in figure 3.4 using equation 3.1 for each pump-probe time delay step allows us to map the fit parameters as a function of pump-probe delay. Whats more, we can use these fit parameters to reconstruct the homodyne data and compute the net difference of this reconstruction as compared to the measured data as one assessment of the quality of the fit in addition to the computed standard deviations of the fit parameters. The results of this reconstruction procedure are seen in figure 3.5. As seen in this figure, there some artifacts in the fit reconstruction that are the result of the choice of fitting function. In particular we note the hard edge along the -47 fs gate-probe delay axis which we attribute to the use of the sudden approximation when approximating the rise of the signal. Further discussion on the limitations of this approach will be discussed in a future section.

The resulting recovered amplitude and signal dephasing rates as parameterized by the pump-probe delay are shown in figure 3.6a. In this case, we interpret $\gamma$ as a measure of the dephasing

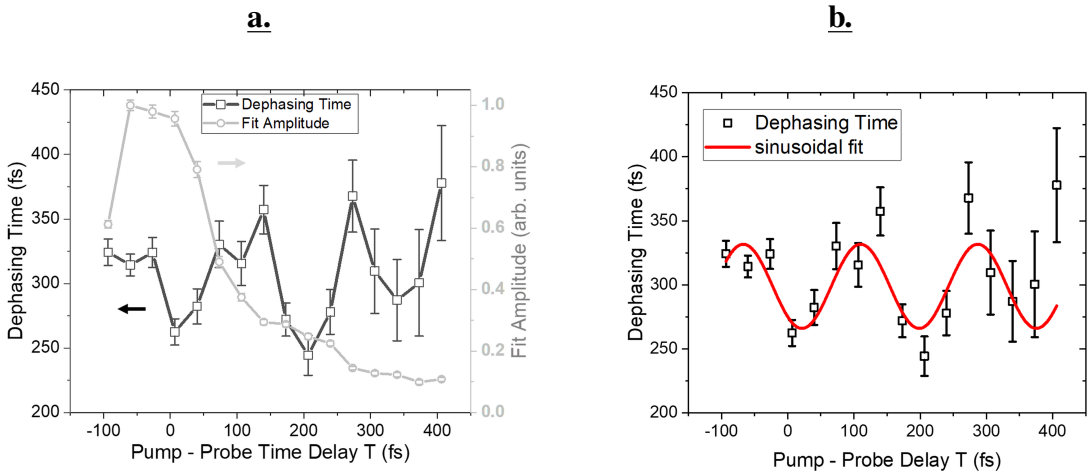


Figure 3.6: Here we show both the fit amplitudes ($A(T)$) and the fit dephasing times ($\gamma(T)$) parameterized by pump-probe delay (panel a.) and a sinusoidal fit of the dephasing time (panel b.). The fit parameters (as shown in a.) were recovered by using equation 3.1 to fit the UTPS signal, as shown in figure 3.4, along the gate-probe time delay axis for each pump-probe delay. Fit parameters from pump-probe time delays bellow -100 fs have particularly large error bars due to the very small signal amplitudes in that region and are not shown. Error bars here represent one standard deviation. A sinusoidal fit of the dephasing time (as shown in panel b.) suggests that $\gamma$ oscilates with a period of $177 \pm 9.6$ fs. We interpret this plot of $\gamma$ as showing oscillations in the dephasing time of vibrational coherences on the $S_1$ excited state [34].

time of the excited state vibrational coherences [34]. This interpretation combined with the fits of $\gamma$ suggest that we see the dephasing time of the excited state vibrational coherences oscillating with a period of $177 \pm 9.6$ fs, as seen in figure 3.6b. Here we note that the amplitude of the oscillation is significantly larger than the observed error bars of the dephasing time, with the error bars here representing one standard deviation of error for the fit parameter.

As established in equations 2.53 and 2.58, a homodyne UTPS signal can be interpreted as being sensitive to a change in the response function relative to the ground state response due to excitation in addition to having components directly related to the ground state response. This means that the net UTPS signal must contain contributions from dynamics on both the excited state and ground state. This hinders our ability to cleanly interpret the decay dynamics in the fit amplitudes ($A(T)$) as dynamics on multiple states contribute to its lifetime [34] and thus the decay rate of the amplitude doesn't necessarily correspond to the excited state lifetime. However the fit amplitudes do suggest the presence of a weak oscillatory component on top of the amplitude that is approximately $\frac{\pi}{2}$ phase shifted relative to the dephasing time oscillation and likely corresponds to excited state dynamics [34].

## Interpretation of the Homodyne UTPS signal with excitation pulse parallel to the gating pulse

As discussed previously, in nitrobenzene, for pulses bellow 3 eV there are three main mechanisms attributed to the time resolved signals associated with Kerr effect measurements. A fast electronic component [65], librational dynamics [65, 66], and relatively slow reorientational dynamics [65, 66, 64]. A fourth process that occurs at a faster time scale then the know reorientational dynamics but slower then the librational dynamics has also been observed which has been attributed to either internal structural dynamics [64] or separate reorientational processes [66]. For excitations above 3 eV, when nitrobenzene relaxes to the ground state, it has separate signals associated with a fast relaxation of the $S_1$ exited state to the ground state mediated by a conical intersection [71], a triplet-triplet internal conversion [71], and a slow relaxation of the $T_1$ state back down to the $S_0$ state [71]. We propose that the oscillatory behavior as observed in figure 3.6, can't be completely explained by the dynamics associated with nuclear motion and that these dynamics are best explained by electronically driven wavepacket dynamics on the $S_1$ excited state [34].

Most of the nuclear dynamics that could contribute to nitrobenzene signals observed in prior studies can be ruled out based on arguments regarding the time scale and the energy scale associated with those mechanisms as discussed in literature. Processes associated with the reorientational dynamics of nitrobenzene have been observed in Kerr effect measurements occurring on the time scale of 20 ps - 32 ps [65, 66, 64], where as mechanisms that can be associated with other nuclear motion in nitrobenzene occur between 0.9 ps - 4 ps [66, 64] which are well beyond the observed time scale of the oscillation of 177 fs. Similarly, librational dynamics in nitrobenzene typically occur on the time scale >300 fs [65, 66], because of this discrepancy we propose that librational dynamics do not play a significant role in this measurement [34].

In principle, raman active modes could compete with the two-photon absorption process however these given our pulse bandwidth of 80 meV, many raman active modes would not be accessible or are particularly weak to the point where they would not be expected to contribute [34, 95]. The modes that could contribute have frequencies of 76 meV, 49 meV, and 22 meV with each mode being expected to contribute to the signal with comparable intensity [34, 95]. We expect that any observed oscillations due to these modes would be due to beating between them, however none of these beating frequencies correspond to the observed oscillation period [34]. For these reasons we suspect that dynamics driven by nuclear motion do not play a significant role in our observed signal.

Prior electronic structure calculations of nitrobenzene [71, 72], in conjunction with experimental measurements of the ground state relaxation mechanisms after a higher energy excitation [91, 72] allow us to suggest the following mechanism for the observed dynamics in the UTPS measurement as schematically shown in figure 3.7. After excitation to the $S_1$ excited state, a nuclear wavepacket evolves by undergoing significant N-C bond distance shorting and O-N-O bond angle shorting [34, 71]. As this wavepacket evolves, it encounters an intersystem crossing [71] that allows a portion of the wavepacket to bifurcate onto the $T_2$ state [34] while the rest of the wavepacket evolves towards the conical intersection between the $S_1$ and $S_0$ states [34]. As the coupling between the $S_1$ and $S_0$ states at the conical intersection is relatively weak [71] and since this intersection is

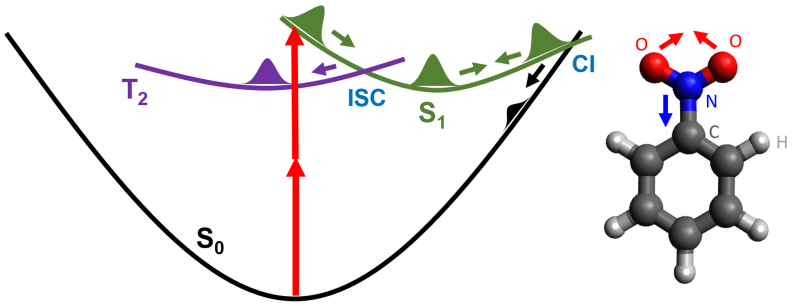


Figure 3.7: A schematic representation of the proposed relaxation mechanism of nitrobenzene after excitation to the S1 excited state. We suggest that after two-photon excitation to the $S_1$ singlet state, an excited state wavepacket evolves on the excited state potential energy surface and oscillates between the ground state (gs) geometry, the $S_1/T_2$ intersystem crossing (ISC) geometry, and the $S_1/S_0$ conical intersection (CI) [34]. This motion primarily involves N-C bond length shortening which moves from 1.476 Å in the gs geometry, to 1.378 Å at the ISC geometry, to 1.241 Å at the CI geometry, [71, 34] and involves O-N-O bond angle closing which start at an angle of 124.94° in the gs geometry, to 113.72° at the ISC geometry, to 94.77° at the CI geometry [71, 34].

| Geometry | $S_0$ | $S_1$ | $T_2$ |
|---|---|---|---|
| $S_0$ minimum | 5.7 | 123.9 | 14.3 |
| $S_1(n\pi^*)$ minimum | 4.5 | 8.4 | 7.5 |
| $T_2(\pi\pi^*)$ minimum | 3.7 | 9.9 | 8.3 |
| $S_1/S_0$ CI | 7.5 | 9.0 | 7.9 |
| $S_1/T_2$ ISC | 4.5 | 8.3 | 7.2 |

Table 3.1: Geometry dependence of $\chi^{(3)}_{\text{eff}}$ in arbitrary units, for the $S_0$, $S_1$, and $T_2$ electronic states. Values for $\chi^{(3)}_{\text{eff}}$ were calculated using the Sum-Over-States method combined with density functional theory that used the B3LYP exchange correlation functional, norm-conserving psudeopotentials, using the Quantum Espresso code [34]. All geometries are from Giussani and Worth [71].

elevated energetically by between 0.3 eV [71] to 0.6 eV [96] relative to the intersystem crossing region, the portion of the remaining wavepacket on the $S_1$ potential energy surface, evolves back toward the intersystem crossing region where the wavepacket can again bifurcate into the triplet manifold [34]. As suggested by the sinusoidal fit and the increasing error bars of the UTPS dephasing time, we propose that this process repeats for three cycles or approximately 530 fs, at which point the remaining wavepacket has either decayed to the ground state or is undergoing an evolution on the triplet state which is not detected in our measurement [34].

We propose that this mechanism is supported by additional electronic structure calculations that compute $\chi^{(3)}_{\text{eff}}$ for nitrobenzene at several different geometries when in either the $S_0$, $S_1$, or $T_2$ states. Details on the specifics of this calculation are presented in the cited reference [34] but to summarize, these $\chi^{(3)}_{\text{eff}}$ calculations were performed using the sum-over-states method with molecular orbital energies and dipole matrix elements calculated using density functional theory using the B3LYP exchange correlation functional, norm-conserving pseudopotentials, and the Quantum Espresso code [34]. All geometries were taken from prior electronic structure calculations performed by Giussani and Worth [71]. Here we assume the sample is under isotropic conditions and we can take $\chi^{(3)}_{\text{eff}}$ to be equal to $\chi^{(3)}_{xyyx} + \chi^{(3)}_{xyxy}$ [39, 34].

We summarize the results of the electronic structure calculation in table 3.1. Here we see that $\chi^{(3)}_{\text{eff}}$ is dominated by the $S_1$ excited state in the ground state geometry as compared to the sampled geometries in either the $S_0$ or $T_2$ states which are all at least an order of magnitude smaller [34]. This suggests that the expected UTPS signal should be dominated by signal from the $S_1$ excited state near the Frank-Condon region and not by wavepacket evolution on the $T_2$ or on $S_0$ states [34]. This is consistent with the proposed relaxation mechanism in that the oscillations on the $S_1$ potential energy surface between configurations near the ground state geometry and configurations near the $S_1/S_0$ conical intersection, can result in large oscillations in $\chi^{(3)}_{\text{eff}}$ and thus the UTPS signal.

## Limitations of Current Analysis in the Context of UTPS Correlation Analysis

There are several limitations with the current analysis as presented. First, the main fitting equation used (as shown in equation 3.1) is inconsistent with the UTPS homodyne signal as derived through a correlation analysis 2.58. In particular we have assumed that the homodyne signal is a linear convolution between the instrument response function and the intrinsic response of the excited state fraction of the sample. Unfortunately none of the three terms are that simple to deconvolve and either involve significant mixing from the real or imaginary component of the ground state response function or transformation by a nonlinear function that isn't one to one. This means that such homodyne UTPS signals shouldn't be interpreted without also taking into account the real and imaginary components of the ground state Kerr effect response which can be obtained from heterodyne OKE measurements.

Additionally, as the first term in the correlation analysis derived UTPS signal expression involves taking the modulus squared of the convolution of the gating pulse with the change in the response function due to excitation, it would also be helpful to involve measurements of the temporal intensity profile of each incident pulse in the analysis. Such single pulse measurements can be obtained with a range of techniques including frequency resolved optical gating in which a single pulse is split and incident on a reference nonlinear medium to obtain a spectrogram which can be used to reconstruct the incident field [82], Spectral Phase Interferometry for Direct Electric-field Reconstruction where the phase of the field is directly measured through by interfering the test pulse with two separate quasi-monochromatic fields in a reference nonlinear crystal and using the

differing spectra to make a phase measurement and thus allowing one to reconstruct the test pulse [83], among other methods [85, 97, 98].

Another limitation stems from the assumption that, in a UTPS measurement, the excitation pulse doesn't significantly contribute to the Kerr effect signal except by bringing the sample into an excited state. This is the assumption that is used to justify splitting the intrinsic response function of an OKE measurement into a ground state response and an excited state response function as shown in equation 2.54 and substituting the resulting expression into the results of the ground state Kerr effect correlation analysis as seen in equations 2.56, 2.59, and 2.61. While there are many conditions in which this assumption is valid (such as for a long lived excited state) [60], near three-pulse overlap the fields have an opportunity to interfere and mix with each other to produce signals that cannot be as easily decoupled.

This is especially evident when considering the plot of the difference between the reconstruction of the UTPS signal and measured response in figure 3.5. In this plot, the largest differences are seen in a window centered around three pulse overlap with a width of approximately $\pm$ 100 fs. This is consistent with the cross-correlation measurements in figure 3.2 of the gate-probe and pump-probe pulses which show a two-standard-deviation-width of 156 fs and 118 fs respectively.

All of this suggests that in order to properly interpret these nonlinear UTPS signals near time overlap, a more sophisticated approach is needed. In particular an approach is needed that can allow for a larger degree of mixing between all the pulses that occur between the three-pulses. In the following chapter we will discuss one such approach.

# Chapter 4

# A Semi-Empirical Approach to the Interpretation of Polarization Sensitive Signals with Ab Initio Parameterization

Thus far, the technique of Ultrafast Transient Polarization Spectroscopy has been presented with methods of analysis that build off of the techniques used to interpret optical Kerr effect measurements. These methods are best applied when the process of excitation is sufficiently decoupled from the measurement of the third order optical response of the sample. The aim of this chapter is to provide the necessary tools to simulate polarization sensitive signals in the time domain, like those detected in UTPS, starting from a foundation in computational quantum chemistry.

There are several reasons why we are particularly interested in simulating these signals in the time domain as apposed to using frequency domain simulations. Recent computational and analytical treatments of 2D electronic spectra [99, 100, 101] have shown that depending on the phase matching conditions, the finite pulse duration and pulse shape can significantly impact the measured response. In particular, these finite pulse duration effects have been shown to alter double quantum signals to the point where the phase and amplitude of vibrational motions could be incorrectly described from these spectra [99], be dependent on the specific double sided Feynman diagram describing the signal [100], and some of these effects may not be completely captured through a perturbative treatment [101]. All of this suggests that incorporating a description of the incident pulses can be important in describing a measured optical signal.

Several simulation methods are commonly employed when simulating nonlinear spectroscopic signals. One method commonly employed is the equation-of-motion (EOM) approach [35], where one directly solves the equations of motion governing the time evolution of a quantum system while also including the effects of a radiation field. Another formalism, dubbed the nonlinear-response-function (NRF) approach [35], involves solving for the effects of an incident field on a system of interest by means of a perturbative treatment taken to lowest order using wavefunctions or the density matrix to represent the quantum system. This approach has been particularly successful especially when considering the applicability of the four-wave mixing and n-wave mixing formalism to a wide variety of optical phenomena [35, 37, 36] with new methods being developed

that can be applied toward predicting nonlinear signals due to nonadiabatic dynamics in molecular systems in the XUV and X-Ray regimes [4].

Recently, Rose and Krich [102] have implemented an efficient means of simulating time domain nonlinear spectra utilizing their $UF^2$ Fourier-based method and a Runge–Kutta–Euler direct propagation method to estimate the spectroscopic signals from the Liouville equation. With these methods as implemented in their open source Ultrafast Spectroscopy Suite, the authors demonstrate the ability to automatically compute signals from all Feynman diagrams up to $5^{th}$ order [103] and treat the case of an open quantum system [104]. As general as these methods are, no specific cases of polarization sensitive measurements are directly considered by these methods.

This chapter is structured as follows. First, computational quantum chemistry methods of modeling the electronic wave function of a molecule are reviewed as a prelude into a discussion of how one can compute dipole moments for electronic transitions between the ground state and excited states, as well as transitions between pairs of excited states, in the molecular frame. After discussing methods of computing an appropriate set of dipole transitions, we will discuss a method of using those dipole transition moments to compute the expected linear and nonlinear corrections to electronic polarization in the context of perturbation theory, in which we treat the interaction of an external electric field with the molecular dipole operator as a perturbation on top of an exactly solvable expression for the time evolution of the system. By applying the results of perturbation theory to a parameterized N-level model of the system of interest, we will be able to compute the time evolution of the $n^{th}$ order polarization responses and the corresponding corrections to the density matrix at the appropriate level of perturbation theory. This gives us a framework for computing molecular frame polarization responses in the time domain that's rooted in ab initio computational quantum chemistry.

Given these nonlinear corrections to the molecular frame time dependent polarizations we will also present techniques to translate these molecular frame responses into the lab frame for the case of an isotropic sample. We will also consider the implications of these transformation methods as applied to the time dependent corrections to the density matrix that correspond to specific components in the total polarization response. We then discuss how to convert these lab frame polarizations to measurable electric fields, thus giving us a way to directly compute measurable transient polarization spectroscopy signals as a function of the time delay between pulses, while allowing for a variety of nonlinear interactions between the sample of interest and the set of incident ultrashort optical pulses.

With this framework, we will apply the model to the 2-level case and validate our time-dependent solutions against exact solutions of the time independent response of a 2-level model. We will also consider the time-dependent response of a 2-level model given an incident time dependent pulse. By appropriately parameterizing the N-level model to represent the polarization response of nitrobenzene, we will compare the simulated electronic responses of nitrobenzene to polarization sensitive measurements of nitrobenzene.

# 4.1 Application of Electronic Structure Methods to the Calculation of Selected Optical Properties of Nitrobenzene

## The Electronic Eigenvalue Problem in the Born-Oppenheimer Approximation

In general, the goal of a wave-function method is to find approximate eigenfunction solutions, $|\Phi\rangle$, of energy eigenvalue equation of a molecule. Such a wavefunction must then depend explicitly on both nuclear and electronic coordinates which are denoted here as $\mathbf{r}_i$ for the coordinates of the $i$th electron and $\mathbf{R}_A$ for the coordinates of the $A$th nucleus. This energy eigenvalue equation for an isolated molecule can then be written as:

$$\mathscr{H}_{\text{mol}}|\Phi(\mathbf{r}_0,...,\mathbf{R}_0,...)\rangle = \varepsilon_{\text{mol}}|\Phi(\mathbf{r}_0,...,\mathbf{R}_0,...)\rangle \tag{4.1}$$

Where the hamiltonian of an isolated molecule, in atomic units, has the following explicit form:

$$\begin{aligned}\mathscr{H}_{\text{mol}} = &\sum_{\text{electrons}} \frac{1}{2}P_i^2 + \sum_{\text{nuclei}} \frac{1}{2M_A}P_A^2 + \sum_{\text{electron pairs}} \frac{1}{|\mathbf{r}_i - \mathbf{r}_j|} + \\ &\sum_{\text{nuclei pairs}} \frac{Z_A Z_B}{|\mathbf{R}_A - \mathbf{R}_B|} + \sum_{\text{electron nuclei pairs}} \frac{-Z_A}{|\mathbf{r}_i - \mathbf{R}_A|}\end{aligned} \tag{4.2}$$

Where the first two terms represent the kinetic energy of the electrons and nuclei respectively, the third and fourth terms represent the coulomb repulsion of the electrons, and the fifth term expresses the coulomb attraction between the nuclei and the electrons [105].

In the Born-Oppenheimer approximation, it's assumed that the part of the molecular wave-function describing the electrons is independent of nuclear motion [105]. Under this assumption, electronic motion is parameterized by but does not explicitly depend on nuclear coordinates. This allows us to decompose the molecular wavefunction into a nuclear component and an electronic component:

$$|\Phi(\mathbf{r}_0,...,\mathbf{R}_0,...)\rangle = |\Phi_{elec}(\mathbf{r}_0,...|\mathbf{R}_0,...)\rangle|\Phi_{nuc}(\mathbf{R}_0,...)\rangle \tag{4.3}$$

Where the electronic component is parameterized by but does not explicitly depend on the nuclear degrees of freedom. Furthermore, under the Born-Oppenheimer approximation the electronic wavefunction can be thought of as a solution to equation 4.1 that depends explicitly on electronic degrees of freedom and therefore only depends on the 1st, 3rd, and 5th terms in equation 4.2. Collecting these terms allows us to write the electronic hamiltonian as:

$$\mathscr{H}_{\text{elec}} = \sum_{\text{electrons}} \frac{1}{2}P_i^2 + \sum_{\text{electron pairs}} \frac{1}{|\mathbf{r}_i - \mathbf{r}_j|} + \sum_{\text{electron nuclei pairs}} \frac{-Z_A}{|\mathbf{r}_i - \mathbf{R}_A|} \tag{4.4}$$

Where the electronic wavefunction $|\Phi_{elec}(\mathbf{r}_0,...|\mathbf{R}_0,...)\rangle$ solves the electronic eigenvalue equation:

$$\mathscr{H}_{\text{elec}}|\Phi_{elec}(\mathbf{r}_0,...|\mathbf{R}_0,...)\rangle = \varepsilon_{\text{elec}}|\Phi_{elec}(\mathbf{r}_0,...|\mathbf{R}_0,...)\rangle \tag{4.5}$$

After approximating wavefunction solutions to the electronic eigenequation, we will then use them to compute various properties of interest including the energy and dipole transitions between the estimated electronic states.

At this point it's useful to discuss some of the limitations of using the Born-Oppenheimer approximation when describing the dynamics of molecular systems as initiated by optical pulses. The Born-Oppenheimer approximation is typically justified by considering the relative mass of the electrons ($m_e$) as compared to the mass of the atoms ($M_l$) and considering solutions of the molecular wave equation that are parameterized by $\kappa$ where $\kappa = \sqrt[4]{m_e/M}$ and where $M$ is a kind of average over the mass of the nuclei [12, 106]. In this formulation, the kinetic energy operator of the nuclei is treated as a perturbation of the electronic hamiltonian with the perturbing factor being $\kappa^4$ [12, 106]. The results of this treatment show that the first, third, and fifth order corrections are exactly 0, with the 2nd order term corresponding to the vibrational energy correction, and the 4th order term corresponding to the rotational energy correction [12]. Together with evidence from numerical simulation, this suggests that the error in the Born-Oppenheimer approximation scales as $(m_e/M)^{3/2}$ [12].

The previous result suggests two regimes were we might expect breakdown of the Born-Oppenheimer approximation. First is when the mass of the negative charge carrier is sufficiently large compared to that of the positive charge carrier which can be achieved when studying exotic molecules where the electron is replaced by the muon or anti-proton [12]. Second, is when the kinetic energy of the nuclei is large relative to the electronic contribution to the energy [12, 11, 3]. This second case where we can expect a breakdown of the Born-Oppenheimer approximation is well known to occur around conical intersections in molecular systems due to the strong coupling of nuclear and electronic dynamics in those regions [107, 11, 12, 3]. With that said, as seen in the electronic structure calculations of nitrobenzene in table 3.1, there are cases where, while the decay dynamics do not abide by the Born-Oppenheimer approximation, the measured signal is generated in configurations where the Born-Oppenheimer approximation does apply [34, 71]. In the following sections we will use results of wave-function calculations in the Born-Oppenheimer approximation to parameterize an N-level model of our system of interest using the Liouville equation [37]. By expressing the time evolution of the system of interest in Liouville space, the decay dynamics can then be added with the addition of a decay matrix [37] which allows us to capture some of these dynamics with an appropriate choice of these decay parameters.

## Applying Multiconfiguration Self Consistent Field Method to Model the Electronic Structure of Nitrobenzene

While a full description of molecular wave function theory in the context of Multiconfiguration Self Consistent Field (MCSCF) methods is beyond the scope of this work, here we present a rough outline of these methods as they haven been applied to the modeling of molecular wave functions of nitrobenzene. In particular we discuss how these methods can be used to construct molecular

wavefunctions that describe ground state and excited singlet states of nitrobenzene as well as triplet state molecular wave functions. With access to these wave functions, we will be able to compute various optical properties given the specified wave function.

Generally speaking, molecular wavefunctions are constructed from single electron molecular spin orbitals that describe the spatial and spin state of a single occupying electron [105, 108]. The spatial component of these molecular orbitals are in turn, constructed from a linear combination of atomic orbitals that are combined in such a way to form an orthonormal basis of spatial orbitals [105, 108, 109]. In order for these multi-electron molecular states to be physical, they must obey the Pauli-exclusion principle, which states that a multi-electron wave function must be anti-symmetric with respect to the interchange of the orbital and spin state of any two electrons [105, 110]. While there are several means of constructing multi-electron wavefunctions that obey the Pauli-exclusion principle from a set of occupied spin orbitals, one common method is to use Slater determinants in which the determinant of a matrix of selected spin orbitals is calculated which results in anti-symmetric determinants that can be used as a basis to construct molecular wavefunctions [105, 110]. A linear combination of determinants used to represent a molecular wavefunction is known as the configuration interaction (CI) [105, 108].

In an MCSCF approach to building these molecular wavefunctions, the determinants and their mixing coefficients are parameterized in such a way that allows for variational optimization of a factor representing the energy of the molecule [105, 108, 111]. In the Dalton quantum chemistry software package, MCSCF wavefunctions are constructed using quadratic optimization techniques which optimize the parameterized wavefunction against the Hessian of the Hamiltonian [112, 109, 113]. While a traditional variational approach that minimizes energy is excellent at producing ground state wavefunctions [105, 108], this procedure allows one to also compute optimized excited state molecular wavefunctions [108] by optimizing the parameter space given the desired number of negative eigenvalues values of the Hessian [112, 109].

In the following sections we will use MCSCF wavefunctions, as implemented in the Dalton quantum chemistry code [114], to model a selected number of states of nitrobenzene. In the following calculations we used an augmented Dunning correlation-consistent basis at the double zeta level of theory. For our active space, we chose to have 14 active electrons distributed among 11 active orbitals. This active space was chosen based on recent electronic structure calculations that studied nondissociative relaxation mechanisms in nitrobenzene after excitation [71]. It was found that this active space is able to to account for the $\pi$ nature of nitrobenzene as well as the lone pairs on the oxygen atoms [71]. This work includes calculations from a number of geometries of nitrobenzene including some ground state optimized geometries as well as geometries from the referenced text [71] with specific geometries being discussed with their associated result.

## Using Response Theory to Compute Nonlinear Molecular Properties of Nitrobenzene

In the following sections we will be using various orders of response theory as applied to a reference multi-electron wavefunction as implemented in the Dalton quantum chemistry package [114,

115, 116]. A full derivation of this technique is beyond the scope of this work however we provide an outline of this computational method to aid in understanding how response theory can give access to information about various molecular properties of interest using the language of perturbation theory.

Start by considering the time evolution of a reference state $|\psi_0(t)\rangle$ under the influence of a perturbing operator $V(t)$. In this framework, we consider the solution of $|\psi_0(t)\rangle$ to be represented by the Fourier transform of the perturbative series expansion of $|\psi_0(\omega)\rangle$ which solves time independent Schödinger equation [115, 116]. This lets us express $|\psi_0(t)\rangle$ in terms of $V(\omega)$ as shown

$$\begin{aligned} |\psi_0(t)\rangle = |\phi_0\rangle &+ \int_{-\infty}^{\infty} d\omega_1 \, e^{(-i\omega_1+\varepsilon)t} \, |\phi_0^{(1)}(\omega_1)\rangle \\ &+ \int_{-\infty}^{\infty}\int_{-\infty}^{\infty} d\omega_1 d\omega_2 \, e^{(-i\omega_1-i\omega_2+2\varepsilon)t} |\phi_0^{(2)}(\omega_1,\omega_2)\,\rangle + ... \end{aligned} \tag{4.6}$$

When considering the time evolution of an observable $\langle A(t)\rangle$ in the Schödenger picture, in which we consider the operator static and the time evolution to be completely contained in the wavefunction, a perturbative solution of this observable can be found in terms of the frequency domain solution for $|\psi_0(t)\rangle$ as seen in equation 4.7. This gives us a series expression for an observable $\langle A(t)\rangle$ in terms of $n^{\text{th}}$ order response functions of the form $\langle\langle A;V^{\omega_1},...\rangle\rangle_{\omega_1,...}$ [115, 116] which can be written as follows

$$\begin{aligned} \langle\psi_0(t)|A|\psi_0(t)\rangle = \langle\phi_0|A|\phi_0\rangle &+ \int_{-\infty}^{\infty} d\omega_1 \, e^{(-i\omega_1+\varepsilon)t} \, \langle\langle A;V^{\omega_1}\rangle\rangle_{\omega_1} \\ &+ \frac{1}{2}\int_{-\infty}^{\infty}\int_{-\infty}^{\infty} d\omega_1 d\omega_2 \, e^{(-i\omega_1-i\omega_2+2\varepsilon)t} \, \langle\langle A;V^{\omega_1},V^{\omega_2}\rangle\rangle_{\omega_1,\omega_2} \\ &+ ... \end{aligned} \tag{4.7}$$

As the explicit time evolution of the observable must obey Ehrenfest's theorem [117], this theorem can be used as an additional constraint that allows us to explicitly solve for the $n^{\text{th}}$ order response functions [115, 116]. By using Ehrenfest's theorem to derive a set of differential equations describing these response functions, solving these differential equations gives explicit solutions in the frequency domain [115, 116] for the desired response function. Moreover, these response functions are in general complex functions with poles that correspond to resonant transitions at particular frequencies [115, 116]. By solving for the residues of these response functions, information about the resonant transitions corresponding to each order of perturbation theory, can be obtained [115, 116]. This allows for the computation of transition dipole moments between the reference and excited sates as well as between excited states depending on the order of the response function computed [115, 116]. Additionally, the response functions themselves can be use to directly represent the $n^{\text{th}}$ order polarizabilities of the molecule of interest [118, 116].

## Calculating Lab Frame Third Order Susceptibilities from Second Order Hyperpolarizabilities

Using response theory as implemented in the Dalton quantum chemistry package, we are able to compute molecular frame polarizabilities of a single molecule up to the second order hyperpolarizability ($\gamma$) of a target molecule [114, 115]. As shown in equation 4.8, to compare these results to experimental measurements of the bulk electronic component of the third order susceptibility, we need to account for three separate factors, the number density of the target molecules in the sample media ($N$) [36, 119, 47], a local field correction ($L$) that provides a transformation of an incident field $\vec{E}$ to the field felt by the target molecule $\vec{F}$ after interaction with the bulk media [36, 119, 47], and the orientation of the target chromophore [47, 119, 120, 121, 122].

$$\chi^{(3)}_{IJKL}\vec{E}\vec{E}\vec{E} = N\langle\gamma_{ijkl}\rangle L(\vec{E})L(\vec{E})L(\vec{E}) \tag{4.8}$$

The local field correction accounts for shifts in the incident fields due to interaction with a surrounding dielectric environment [36, 119, 47]. Two common methods for accounting for this effect are to use either a Lorentz-Lorenz correction and the and the Onsager reaction field model. For a Lorentz-Lorenz correction [36, 119], the effect of the media on the incident field is treated under the assumption that a linearly induced dipole of the media is all that will impact the field. This approximation, while valid for isotropic media, is expected to break down for anisotropic media, and other corrections will need to be considered [119]. The Onsager model is one such correction [119] that also includes the effect of a reaction field which is induced when the induced target molecular dipole interacts with the polarization and polarizability of the embedding media producing the Onsager field correction. For the following calculations, as we are primarily interested in isotropic liquid samples, we accounted for these effects using a Lorentz-Lorenz correction.

The orientation of the target molecules must be treated on a case by case basis depending on the sample of interest. For instance, crystalline samples have a well defined orientation and thus experimental measurements can be compared to molecular frame calculations upon applying a well defined rotation [122]. In experiments considering anisotropic media as in the case of a photo active target attached to a surface [123] or inhomogeneous samples such as a chromophore attached to the surface of suspended particles [124], multiple transformations may be needed to translate the molecule frame $n^{\text{th}}$ order polarizability into a measured lab frame response [123, 124, 121]. In the case of an isotropic sample, as the molecule initially has no preferred orientation, we can account for the orientational response of the molecule through orientational averaging [47, 119, 120]. Additional orientation effects including reorientation due to alignment of the induced molecular dipole to the field can also be accounted for by considering a thermodynamic model given the interaction energy from each term in the series expansion of the polarization in terms of the electric field [47]. In the following calculations we consider only the electronic response of an isotropic sample of target molecules.

## Effective Third Order Susceptibilities of Nitrobenzene as a Function of Electronic State

Here we present the results of a calculation of the effective third order susceptibility ($\chi^{(3)}_{\text{eff}}$)of nitrobenzene as a function of frequency given a $C_{2v}$ symmetric ground state optimized geometry. We note here that $\chi^{(3)}_{\text{eff}}$ is related to third order susceptibility tensor by selecting the specific tensor elements from the full tensor that contribute to the signal being observed [119, 47, 39]. For the case of an optical Kerr effect measurement of a isotropic sample, this simplifies to $\chi^{(3)}_{\text{eff}} = \chi^{(3)}_{yxxy} + \chi^{(3)}_{yxyx}$ given a pulse ordering of probe, gate, gate being used when applying a tensor product of the third order susceptibility with the incident fields [39, 58, 52]. We note that because of the intrinsic permutation symmetry of the third order susceptibility, accounting for other variants of the pulse order is as simple as multiplying by an appropriate factor that counts the different valid simultaneous permutations of the fields and indices [36].

In figure 4.1 we directly compare the results of the computed effective third order susceptibility of nitrobenzene in the ground electronic state with that of literature OKE measurements of the magnitude of nitrobenzene's effective third order susceptibility. Both the experiments from Ho et al. [90] and from Vigil and Kuzyk [88] take measurements of the effective third order susceptibility of nitrobenzene using a probe pulse centered at 532 nm (2.33 eV) and a pump pulse centered at 1064 nm (1.165 eV) with pulse durations around 6 ps in the experiments of Ho et al. and roughly 30 ps pulse duration for Vigil's and Kuzyk's experiments. These experiments resulted in measurements of the effective third order susceptibility of liquid nitrobenzene of $8.6 \times 10^{-22}$ SI [88] and $3.9 \times 10^{-20}$ SI [90]. This compares to our computed effective third order susceptibility at the relevant gate and probe center frequencies of $7.7 \times 10^{-21}$ SI.

Our computed effective third order susceptibility of nitrobenzene lies between the reported measurements and as such, we take this as evidence that our purely electronic model of nitrobenzene is accurate enough to recover some general nonlinear spectroscopic trends of nitrobenzene within the limits of the model. Furthermore, since the first resonant transition occurs beyond 3 eV, the predicted response given the incident frequencies is expected to be in the non-resonant regime. This is evidenced in the purely electronic model of ground state nitrobenzene where the computed frequency dependent $|\chi^{(3)}_{\text{eff}}|$ is fairly consistent within the chosen probe frequency window of 1.51 eV to 2.71 eV with $|\chi^{(3)}_{\text{eff}}|$ smoothly increasing from $6.7 \times 10^{-21}$ SI to $8.5 \times 10^{-21}$ SI over that range. This suggests that the bandwidth differences between the two experiments in this region of the predicted purely electronic response of nitrobenzene is not sufficient to explain the discrepancy between the two experiments. Given that prior studies have suggested that nonlinear optical responses can be quite sensitive to nuclear motion [125, 126], and that prior Kerr effect measurements of nitrobenzene observed separate nuclear dynamics on the time scale of 1-2 ps and 16-35 ps [64], coupled with the difference in pulse duration between these experiments, we suspect that the deviation of the experimental measurements with respect to the computed electronic contribution may be attributable to nuclear motion. One additional consideration is that our model does not account for the electronic continuum above the ionization threshold of nitrobenzene around 9.7 eV [127].

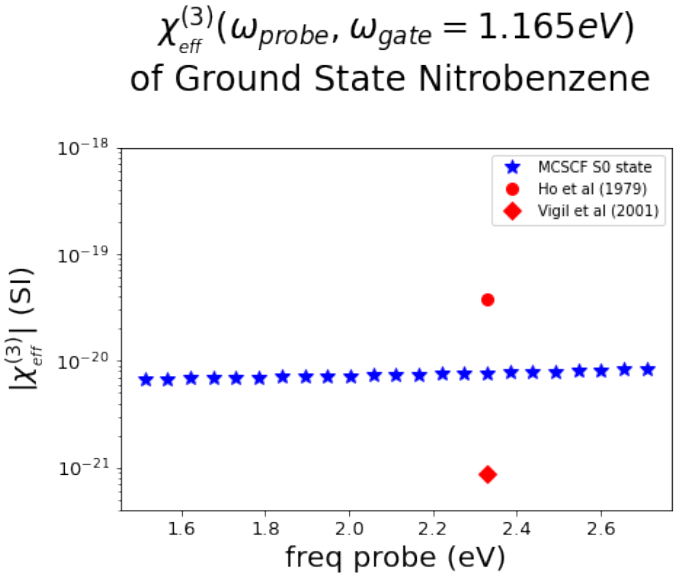


Figure 4.1: This figure shows the predicted effective third order susceptibility on a log scale for nitrobenzene in the planar ground state minimum geometry as calculated using second order response theory using a MCSCF optimized ground state wavefunction with 14 active electrons and 11 active orbitals. The raw hyperpolarizabilities were used to compute effective third order susceptibilities ($\chi^{(3)}_{\text{eff}}$) assuming an OKE measurement, an isotropic sample with a number density equal to that of neat liquid nitrobenzene at standard temperature and pressure, and using the Lorentz-Lorenz local field correct to account for bulk effects on the third order response. Here the calculated response increases from a value of $6.7 \times 10^{-21}$ SI to $8.5 \times 10^{-21}$ SI with a value of $7.7 \times 10^{-21}$ SI when the probe frequency is at 2.33 eV. This compares to prior measurements of nitrobenzene's third order susceptibility of $8.6 \times 10^{-22}$ SI [88] and $3.9 \times 10^{-20}$ SI [90] given a pump frequency of 1.165 eV and probe frequency of 2.33 eV.

In a related calculation, figure 4.2 shows a calculation of the expected effective OKE response as a function of probe frequency given a fixed gate pulse frequency at 780 nm (1.589 eV) for the first four singlet states of nitrobenzene. The computed energy differences relative to the ground state are shown in table A.1 with the first three nonzero energy differences being 4.078 eV, 4.403 eV, and 4.550 eV. The frequencies of the gate and probe pulses were chosen to be representative our non-resonant Kerr effect measurement scheme as used in our previously discussed UTPS measurements [34]. Figure 4.2 shows the following trends and features. First, over a majority of the probe frequencies sampled, nitrobenzene exhibits excited state enhancement of the effective third order susceptibility with the largest enhancements being nearly 3 orders of magnitude larger than the ground state response. This is consistent with previous studies showing excited state enhancements of third order spectroscopic signals in molecular systems [48, 49, 41, 42]. Of particular interest is the predicted excited state depression of the effective third order susceptibility when

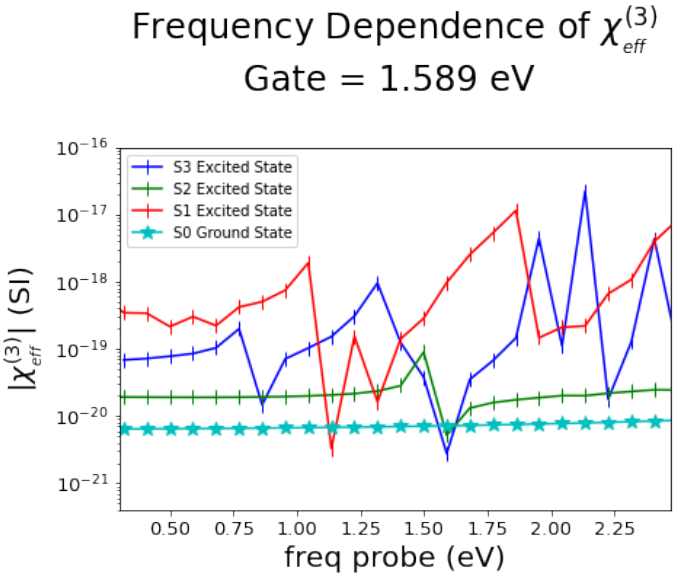


Figure 4.2: This figure shows the predicted effective third order susceptibility on a log scale for nitrobenzene in the planar ground state minimum geometry using MCSCF wavefunctions to represent each molecular state and second order response theory to compute the molecular frame second order hyperpolarizabilities ($\gamma$). These raw hyperpolarizabilities were used to compute effective third order susceptibilities ($\chi^{(3)}_{\text{eff}}$) assuming an OKE measurement and assuming an isotropic sample with a number density equal to that of neat liquid nitrobenzene in standard conditions. Given a fixed gate frequency of 1.589 eV (780 nm), we see excited state enhancement for all the computed excited states over a wide range of probing frequencies. We note that the S2 and S3 excited states do show suppression of the excited state signal for a probing frequency of 1.589 eV. However, these calculations suggest that we could expect up to 2 orders of magnitude increase in OKE signal for nitrobenzene in the S1 excited state at the probing frequency of 1.589 eV (780 nm).

compared against the ground state signal with the center frequencies of the gate and probe pulses having same frequency of 1.589 eV. In particular, the $S_2$ and $S_3$ excited states show a slight excited state depression with a $\chi^{(3)}_{\text{eff}}$'s of $2.77 \times 10^{21}$ S.I. and $5.18 \times 10^{-21}$ S.I. respectively, compared to the ground state which shows a computed $\chi^{(3)}_{\text{eff}}$ of $7.17 \times 10^{-21}$ S.I. given the gate and probe pulses have the same sampling frequency of 1.589 eV. This is in contrast to the relatively large $\chi^{(3)}_{\text{eff}}$ of the $S_1$ state of $9.72 \times 10^{-19}$ S.I. which shows a factor of 135 enhancement compared to the ground state. This suggests that in our experimental conditions, any excited state enhancement of the Kerr effect signal will come from population moving through the $S_1$ excited state.

Unfortunately, using these calculations to directly represent the electronic response of our experimentally measured signals is made more difficult by a few factors. First, these calculations are purely in the frequency domain and our measurements are made with respect to a time delay relative to a set of optical pulses that are most naturally defined in the time domain. This shift in

time delay introduces phase factors in a frequency domain calculation that could be difficult to incorporate into the calculation as performed. Second, the calculations restrict us to only considering the response from excited population states, a not more general nonequilibrium states which may include contributions from coherences. Lastly, these calculations are inherently static and do not include a description of decay processes which play a role in the relaxation mechanism governing the decay of the Kerr effect signal as a function of time-delay.

For these reasons we use a related set of response theory calculations to compute dipole matrix elements between a number of excited states. This will allow us to parameterize the dipole matrix elements in an N-level model that we can explicitly evolve in time. Solving for polarization signal to the appropriate order in perturbation theory, allow us to calculate responses that can be directly compared to our measured signals.

## Response Theory Calculation of the Dipole Transition Matrix Elements of Nitrobenzene

The dipole transition matrix elements were computed using the following procedure. To calculate the dipole matrix elements from the reference ground state wavefunction to a set of excited states, a 1st order response function calculation was performed in which the residues of a set of poles are computed [115]. We can interpret these poles as being directly associated with the resonant transitions, under this interpretation the residues of those poles can be viewed as being related to the transition dipole matrix element with the following expression [115, 116]

$$\lim_{\omega\to\omega_f}(\omega-\omega_f)\langle\langle A;V^{\omega}\rangle\rangle_{\omega}=\langle 0|A|k\rangle\langle k|V^{\omega}|0\rangle \tag{4.9}$$

Similarly, we can follow up the 1st order calculation with a 2nd order response function calculation compute transition dipole moments between exited states [115, 116]. The expression relating the residues of the second order response function to explicit dipole transitions can be written as follows

$$\lim_{\omega_b\to\omega_{f''}}\left[\lim_{\omega_c\to\omega_{f'}}(\omega_c-\omega_{f'})\langle\langle A;V^{\omega_b},V^{\omega_c}\rangle\rangle_{\omega_b,\omega_c}\right](\omega_b+\omega_{f''})= \\ -\langle 0|V^{\omega_b}|f''\rangle\langle f''|\left(A-\langle 0|A|0\rangle\right)|f'\rangle\langle f'|V^{\omega_c}|0\rangle \tag{4.10}$$

After letting the $A$ operator be the dipole operator in the equation 4.10, and after accounting for a shift relative to the ground state dipole moment, we can compute excited state to excited state dipole transition moments without explicitly computing excited state wavefunctions [115, 116].

The results of these calculations for two different geometries are shown in Appendix A. The two geometries for which dipole matrix elements were computed are the ground state $C_{2v}$ symmetric geometry and a geometry with the $NO_2$ group rotated around the CN bond forming a 13° dihedral angle between the plane defined by the benzene ring and the plane defined by the nitro group. These geometries were chosen for the following reasons. First, if we consider the relaxation

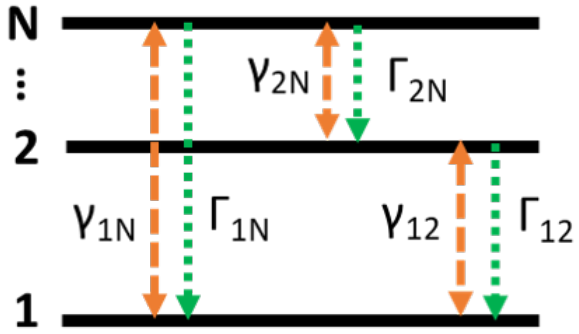


Figure 4.3: A schematic representation of the system under study. Here state populations may non-radiatively decay from higher lying states to lower lying states at their own specified decay rate ($\Gamma$). Coherences between states may also decay at their own decoherence rate ($\gamma$) which is partially determined from the population decay rates [36, 37].

mechanisms of nitrobenzene after excitation to the $S_2$ state, prior calculations sampling multiple potentially relevant geometries [34] seem to suggest that the largest optical signals will primarily be generated when nitrobenzene is in it's ground state minimum $C_{2v}$ symmetric geometry. Additionally, other calculations have shown that the transition between $S_0$ and $S_2$ states, which is thought to be the primary target excited state involved given a resonant excitation above 3 eV [93, 94], is only accessible when the nitro group is twisted out of the plane of the ring [71]. Additionally, gas phase measurements suggest that the nitro group in nitrobenzene naturally has an average 13° dihedral angle [128].

Using the results of these calculations, we can use the computed dipole matrix elements to parameterize an N-level model to represent nitrobenzene. After parameterization, We can then use this model to directly compute the polarization response, and thus an experimentally measurable signal of nitrobenzene in the time-domain. In the following section we will discuss this model and how we can use a Liouville space representation of the density matrix in the context of perturbation theory, to compute signals associated with the third order susceptibility of nitrobenzene.

## 4.2 An N-Level Description of Non-linear Optical Signals

In it's eigenbasis, the time evolution of the density matrix of an N-Level system can be described in terms of the transition energies between each state ($\omega_{nm}$), decoherence rates ($\gamma$), population relaxation rates ($\Gamma$), and a perturbation ($V$) [36, 37].

$$\dot{\rho}_{nn} = -\frac{i}{\hbar}[V,\rho]_{nn} + \sum_{E_m>E_n} \Gamma_{nm}\rho_{mm} - \sum_{E_m<E_n} \Gamma_{mn}\rho_{nn} \tag{4.11a}$$

$$\dot{\rho}_{nm} = -i\omega_{nm}\rho_{nm} - \frac{i}{\hbar}[V,\rho]_{nm} - \gamma_{nm}\rho_{nm}\,,\; n \neq m \tag{4.11b}$$

At this point we can transform equation 4.11 into Liouville space [37], in which we vectorize the density matrix and operators that act on the density matrix are turned into super operators that can be represented as matrix operations on the vectorized density matrix. Completing this transformation, we obtain the following expression for the time evolution of the system where $\mathscr{L}_{mol}$ is the energy operator, $\mathscr{D}$ is a decay operator describing the dephasing rates and decay rates, and $\mathscr{V}$ is the perturbation, all in Liouville space [37].

$$|\dot{\rho}\rangle\rangle = -\frac{i}{\hbar}\mathscr{L}_{\text{mol}}|\rho\rangle\rangle + \mathscr{D}|\rho\rangle\rangle - \frac{i}{\hbar}\mathscr{V}|\rho\rangle\rangle \tag{4.12}$$

A first step in solving equation 4.12, would be to find an appropriate closed form time evolution operator from which a Dyson series solution can be found. Here we consider a simplified expression without the perturbation.

$$|\dot{\rho}\rangle\rangle = -\frac{i}{\hbar}\mathscr{L}_{\text{mol}}|\rho\rangle\rangle + \mathscr{D}|\rho\rangle\rangle \tag{4.13}$$

Note that the addition of the population decay rates has the added effect of breaking the hermiticity of this system which depending on how the hermiticity was broken, may prohibit closed form solutions to this differential equation. However, since population can only decay from higher lying states to lower lying states, the matrix $\mathscr{L}_{\text{mol}} + i\hbar\mathscr{D}$ is diagonalizable and thus, a closed form solution $\mathscr{U}_0(t,t_0)$ is guarantied to exist [129]. This solution can then be used as the basis for an integral solution to equation 4.12.

$$\mathscr{U}(t,t_0) = \mathscr{U}_0(t,t_0) - \frac{i}{\hbar}\int_{t_0}^{t} d\tau\, \mathscr{U}_0(t,t_0)\,\mathscr{U}_0^{-1}(\tau,t_0)\,\mathscr{V}\mathscr{U}(\tau,t_0) \tag{4.14}$$

Iterating equation 4.14 allows for the generation of a Dyson series. Substituting in a stark perturbation and combing the generated series with an initial density matrix $|\rho_0\rangle\rangle$ and the dipole operator $\langle\langle\vec{\mu}|$ allows one to solve for the perturbation expansion of the polarization in the time domain. Explicit solutions for the first few terms in the perturbed polarization expansion are as follows.

$$\begin{aligned}\vec{P}^{(1)}(\mathbf{r},t,t_0) = &-\frac{i}{\hbar}\int_{t_0}^{t} d\tau_1 \\ &\langle\langle\vec{\mu}|\mathscr{U}_0(t-\tau_1)\,\vec{\mu}\,\mathscr{U}_0(\tau_1-t_0)\,|\rho_0\rangle\rangle \\ &\vec{E}(\mathbf{r},\tau_1-t_0)\end{aligned} \tag{4.15a}$$

$$\begin{aligned}\vec{P}^{(2)}(\mathbf{r},t,t_0) = &-\frac{1}{\hbar^2}\int_{t_0}^{t}\int_{t_0}^{\tau_1} d\tau_1 d\tau_2 \\ &\langle\langle\vec{\mu}|\mathscr{U}_0(t-\tau_1)\,\vec{\mu}\,\mathscr{U}_0(\tau_1-\tau_2)\,\vec{\mu}\,\mathscr{U}_0(\tau_2-t_0)\,|\rho_0\rangle\rangle \\ &\vec{E}(\mathbf{r},\tau_1-t_0)\,\vec{E}(\mathbf{r},\tau_2-t_0)\end{aligned} \tag{4.15b}$$

$$\begin{aligned}\vec{P}^{(3)}(\mathbf{r},t,t_0) =& \frac{i}{\hbar^3}\int_{t_0}^{t}\int_{t_0}^{\tau_1}\int_{t_0}^{\tau_2} d\tau_1 d\tau_2 d\tau_3 \\ & \langle\langle\vec{\mu}|\mathscr{U}_0(t-\tau_1)\,\vec{\mu}\,\mathscr{U}_0(\tau_1-\tau_2)\,\vec{\mu}\,\mathscr{U}_0(\tau_2-\tau_3)\,\vec{\mu}\,\mathscr{U}_0(\tau_3-t_0)\,|\rho_0\rangle\rangle \\ & \vec{E}(\mathbf{r},\tau_1-t_0)\,\vec{E}(\mathbf{r},\tau_2-t_0)\,\vec{E}(\mathbf{r},\tau_3-t_0)\end{aligned} \tag{4.15c}$$

With the general expression for the n$^{\text{th}}$ order term being

$$\vec{P}^{(n)} = \left(\frac{-i}{\hbar}\right)^n \langle\langle\vec{\mu}|\int_{t_0}^{t} d\tau_1 \ldots \int_{t_0}^{\tau_{n-1}} d\tau_n \left(\mathscr{U}_0(t-\tau_1)\prod_{m=1}^{n}\vec{\mu}\,\mathscr{U}_0(\Delta\tau_m)\right)|\rho_0\rangle\rangle \prod_{m=1}^{n}\vec{E}_{i_m} \tag{4.16}$$

Where the term $\Delta\tau_m$ is equivalent to $\tau_m - \tau_{m+1}$ for $m < n$ and with $\Delta\tau_n$ being equal to $\tau_n - t_0$. Note that the bra-ket terms in the integrals in equation 4.15 are the time domain form of the polarizability, hyperpolarizability, and second order hyperpolarizability, respectively. Additionally, from equation 4.16 we can identify the n$^{\text{th}}$ order correction term for the density matrix as

$$|\rho^{(n)}\rangle\rangle = \left(\frac{-i}{\hbar}\right)^n \int_{t_0}^{t} d\tau_1 \ldots \int_{t_0}^{\tau_{n-1}} d\tau_n \left(\mathscr{U}_0(t-\tau_1)\prod_{m=1}^{n}\vec{\mu}\,\mathscr{U}_0(\Delta\tau_m)\right)|\rho_0\rangle\rangle \prod_{m=1}^{n}\vec{E}_{i_m} \tag{4.17}$$

These integrals can then be evaluated numerically to estimate the time dependent signal at each order in the perturbation. While not explicitly required to compute a time-domain signal, evaluating equation 4.17 allows us to track the evolution of the density matrix elements giving us a means of interpreting the simulated signals in terms of the relevant dynamics of the populations and coherences.

## 4.3 A Classical Wave Equation Description of Non-linear Optical Signals

In the previous section we discussed methods to compute time domain non-linear polarizations in response to a perturbing electric field for a single molecule. However, this polarization is not directly observable. Instead, experimentally measurable signals are generated from the output lab frame electric field that is generated from the ensemble average of the time dependent polarization that results after the sample has interacted with the incident pulses. There are thus two details that we need to consider when computing experimental measurements from first principles. We first need to consider how to translate a molecular frame calculation of a resultant polarization into the lab frame version of that signal. Second is the question of how to translate a time dependent transient polarization into the propagating signal electric field and then into a measurable signal. These are the two questions we aim to provide a treatment of in this section.

## Computing Lab Frame Polarizations from Molecular frame Calculations

Here we will discuss how one might in general compute a lab frame time dependent polarization from an ostensibly molecular frame calculation given an arbitrary distribution of the orientation of the ensemble molecular target. We will then focus on the case of an isotropic sample and derive explicit formulae that can be used to compute lab frame time dependent polarizations.

First lets consider the case of formally transforming the relation between a molecule's polarization response to an electric field from a lab frame representation to the molecular frame representation. Let $\vec{\mu}_{lab}$, $\vec{E}^{lab}$, and $\chi^{(n)}$ be the lab frame representations of polarization, electric field, and the $n^{\text{th}}$ order susceptibility of a single molecule. Conversely, let the quantities, $\vec{\mu}_{mol}$, $\vec{E}^{mol}$, and $\alpha^{(n)}$, be the molecular frame representations of polarization, electric field, and the $n^{\text{th}}$ order polarizability/hyperpolarizability of a single molecule. These quantities are related by the following expressions:

$$\vec{\mu}_{lab} = \chi^{(n)}_{I_0 \ldots I_n} \prod_{m=1}^{n} \vec{E}^{lab}_{I_m} \tag{4.18a}$$

$$\vec{\mu}_{mol} = \alpha^{(n)}_{i_0 \ldots i_n} \prod_{m=1}^{n} \vec{E}^{mol}_{i_m} \tag{4.18b}$$

Next, there must be some rotation operator $R$ that maps the lab frame axes onto the molecular frame axes such that the following expressions hold.

$$\vec{\mu}_{mol} = R\vec{\mu}_{lab} \tag{4.19a}$$

$$\vec{E}_{mol} = R\vec{E}_{lab} \tag{4.19b}$$

These expressions imply that the molecular polarization response of a single molecule in the molecular frame can be rewritten in terms of rotations of their lab frame counter parts which can be expressed as follows:

$$R\vec{\mu}_{lab} = \alpha^{(n)}_{i_0 \ldots i_n} \left( \prod_{m=1}^{n} R_{i_m I_m} \vec{E}^{lab}_{I_m} \right) \tag{4.20}$$

Or rewritten yields

$$\vec{\mu}_{lab} = \left( R^{-1}_{I_0 i_0} \alpha^{(n)}_{i_0 \ldots i_n} \prod_{m=1}^{n} R_{i_m I_m} \right) \prod_{m=1}^{n} \vec{E}^{lab}_{I_m} \tag{4.21}$$

Comparing equations 4.18a and 4.21 allows us to see that the lab frame $n^{\text{th}}$ order susceptibility of a single molecule is related to the molecular frame polarizability through the following relation.

$$\chi^{(n)}_{I_0 \ldots I_n} = R^{-1}_{I_0 i_0} \alpha^{(n)}_{i_0 \ldots i_n} \prod_{m=1}^{n} R_{i_m I_m} \tag{4.22}$$

In the context of the previous sections expressions 4.22 and 4.21 can be very useful since in an experiment, the electric field is defined in the lab frame and the signal generated from a sample is measured in the lab frame. However, the current expressions are only valid for a single molecule, to connect the polarization response of a single molecule to the ensemble average of orientations that are sampled in experiment. While we consider here the case of an isotropic sample, in principle the results here can be generalized to any anisotropic distribution. To accomplish this, we can modify equation 4.22 by including an appropriate probability density function ($\rho(\Omega)$) to represent the chance that an ensemble of molecules is in a specific lab frame orientation. Integrating the resulting expression over all molecular orientations would then allow us to represent the resultant n$^{\text{th}}$ order susceptibility for a sample with some degree of anisotropy.

For the case of an isotropic sample, $\rho(\Omega)$ is independent of orientation. As such we can simply average $\vec{\mu}_{lab}$ over all possible rotations to yield a polarization response that is proportional to the resultant lab frame polarization, yielding the following expressions.

$$\chi^{(n)} \propto \langle R^{-1}_{I_0 i_0} \alpha^{(n)}_{i_0 \ldots i_n} \prod_{m=1}^{n} R_{i_m I_m} \rangle \tag{4.23a}$$

$$\vec{P}_{lab} \propto \left( \int R^{-1}_{I_0 i_0} \alpha^{(n)}_{i_0 \ldots i_n} \prod_{m=1}^{n} R_{i_m I_m} \, d\Omega \right) \prod_{m=1}^{n} \vec{E}^{lab}_{I_m} \tag{4.23b}$$

Importantly $\alpha^{(n)}$ in equation 4.23 is a calculable quantity in the context of frequency dependent perturbation theory. More specifically, using a wide variety of theoretical methods, electronic structure software packages are able to compute the polarizability, the hyperpolarizability, the second order hyperpolarizability in the molecular frame [130, 118, 131, 132]. Expression 4.23, then gives us a way to map, these molecular frame responses to lab frame measurements in the context of a measurement of an isotropic ensemble.

A very similar approach can be used when considering the case of time dependent perturbation theory. Here, instead of considering the transformation of the frequency dependent polarizabilities or hyperpolarizablities $\alpha^{(n)}$, we consider the time dependent molecular response functions, here denoted as $\vec{\mu}^{(n)}_{mol}$.

One fairly straight forward approach to adapt equation 4.23 to the time domain is to first recognize that, much like the frequency domain quantity $\alpha^{(n)}$, a molecule's $n^{\text{th}}$ order polarization response function $\vec{\mu}^{(n)}_{mol}(t_0, t, \tau_1, ..., \tau_n)$ is a calculable quantity using the methods discussed in section 4.2. When the $\tau_i$ integration variables are integrated over at the appropriate level of perturbation theory, the polarization response function yields a final polarization as a function of time allowing for a more direct comparison with time domain measurements[37, 36]. In Liouville space, these expressions take the following form:

$$\vec{\mu}^{(n)}_{mol} = \langle\langle \vec{\mu}_{i_0} | \mathscr{U}_0 (\Delta T_f) \left[ \prod_{m=1}^{n} \vec{\mu}_{i_m} \mathscr{U}_0 (\Delta \tau_m) \right] | \rho_0 \rangle\rangle \left( \prod_{m=1}^{n} \vec{E}^{mol}_{i_m} \right) \tag{4.24}$$

Where the amount of time evolution between each interaction in perturbation theory, denoted as $\Delta\tau_m$ and $\Delta T_f$, have the following definitions

$$\Delta T_f = t - \tau_1$$

$$\Delta\tau_m = \begin{cases} \tau_m - \tau_{m+1}, & \text{if } m < n \\ \tau_n - t_0, & m = n \end{cases}$$

To simplify equation 4.24, we denote the bra-ket contraction as follows

$$\langle\langle \vec{\mu} | \rho^{(n)} \left(\Delta T_f, \Delta\tau_1, ..., \Delta\tau_n\right) \rangle\rangle_{i_0 \ldots i_n} = \langle\langle \vec{\mu}_{i_0} | \mathscr{U}_0 \left(\Delta T_f\right) \left[ \prod_{m=1}^{n} \vec{\mu}_{i_m} \mathscr{U}_0 \left(\Delta\tau_m\right) \right] | \rho_0 \rangle\rangle \tag{4.26}$$

Thus by substituting equation 4.26 into equation 4.24 and by using the same logic that allowed us to transform equation 4.18b into equation 4.21, we write a lab frame expression for the perturbed time domain response function as follows

$$\vec{\mu}^{(n)}_{lab} = \left( R^{-1}_{I_0 i_0} \langle\langle \vec{\mu} | \rho^{(n)} \rangle\rangle_{i_0 \ldots i_n} \prod_{m=1}^{n} R_{i_m I_m} \right) \prod_{m=1}^{n} \vec{E}^{Lab}_{I_m} \tag{4.27}$$

And again, by applying orientational averaging we can obtain a lab frame expression for the ensemble average of a given single molecule response, giving

$$\langle \vec{\mu}^{(n)}_{lab}(t_0, t, \tau_1, ...\tau_n) \rangle = \int \left( R^{-1}_{I_0 i_0} \langle\langle \vec{\mu} | \rho^{(n)} \rangle\rangle_{i_0 \ldots i_n} \prod_{m=1}^{n} R_{i_m I_m} \right) d\Omega \prod_{m=1}^{n} \vec{E}^{Lab}_{I_m} \tag{4.28}$$

Given the proportionality of $\vec{\mu}_{lab}$ to $\vec{P}_{lab}$, a final expression for the resultant lab frame polarization of a sample that's derived from time domain perturbation theory, can be written whose form is similar to those in equations 4.23.

$$\begin{aligned} \vec{P}^{(n)}_{lab}(t_0, t) \propto & \int_{t_0}^{t} d\tau_1 ... \int_{t_0}^{\tau_{n-1}} d\tau_n \\ & \int \left( R^{-1}_{I_0 i_0}(\Omega) \langle\langle \vec{\mu} | \rho^{(n)} \left(\Delta T_f, \Delta\tau_1, ..., \Delta\tau_n\right) \rangle\rangle_{i_0 \ldots i_n} \prod_{m=1}^{n} R_{i_m I_m}(\Omega) \right) d\Omega \\ & \prod_{m=1}^{n} \vec{E}^{Lab}_{I_m}(\tau_m - t_0) \end{aligned} \tag{4.29}$$

Importantly, as the term $\langle\langle \vec{\mu} | \rho^{(n)} \rangle\rangle_{i_0 \ldots i_n}$ is a molecular frame quantity, it must be independent of the coordinates used to describe the rotation mapping the lab frame to the molecular frame. As such it can be treated as a constant with respect to the Euler angles that describe this rotation for the purpose of evaluating the orientational averaging integrals. This allows us to explicitly evaluate

these integrals by applying cosine matrix integration formulae as tabulated by Kwak and other authors [47, 120].

In summary, we have shown that by using the framework of time dependent perturbation theory, we can computationally evaluate lab frame polarization responses under the assumption of sampling an isotropic system by leveraging isotropic averaging and molecular frame electronic structure calculations for the dipole transition moments. These isotropic averages can be evaluated using cosine matrix integration formulae and, after performing time ordered integration of the averaged quantity, we can compute the time dependent response of the $n^{\text{th}}$ order polarization response. In the next section we will discuss how to translate the resultant time dependent polarization into a measurable signal that can be directly compared with a time delay dependent experiment.

## Computing Experimental Observables from a Driving Non-linear Polarization

Here we will discuss how to compute experimental observables given a driving lab frame polarization. In particular our aim will be to show how to derive relevant expressions for the driven signal electric field starting from Maxwell's equations. Furthermore, we aim to show how one could use this computed signal electric field to further calculate a typical homodyne intensity measurement of the resultant signal.

Maxwell's driven wave equation can be written as

$$\nabla \times \nabla \times \mathbf{E} + \frac{1}{c^2}\frac{\partial^2}{\partial t^2}\mathbf{E} = -\frac{1}{\varepsilon_0 c^2}\frac{\partial^2}{\partial t^2}\mathbf{P} \tag{4.30}$$

or by separating the Linear and non-linear components of the driving polarization [36] we can obtain:

$$\nabla \times \nabla \times \mathbf{E} + \frac{\varepsilon^{(1)}}{c^2}\frac{\partial^2}{\partial t^2}\mathbf{E} = -\frac{1}{\varepsilon_0 c^2}\frac{\partial^2}{\partial t^2}\mathbf{P}^{NL} \tag{4.31}$$

where $\mathbf{E}$ is the resultant electric field from the driving polarization $\mathbf{P}$.

At this point a typical analysis will invoke the unidirectional approximation and the slowly varying envelope approximation and further transform this expression into the frequency domain allowing for the consideration of only plane wave electric fields with the justification that any pulse can be described by a sum of plain-wave fields [36, 39]. Using this analysis we can obtain the following expression for the signal electric field in the frequency domain.

$$\mathbf{E}_{sig} = \frac{i2\pi\omega}{nc} e^{ikL} \int_0^L dz\, e^{-ikz} \mathbf{P}^{NL}(z,\omega) \tag{4.32}$$

While this expression does give us a means of computing the resultant signal field in given a nonlinear driving polarization, This expression requires knowledge of the nonlinear driving polarization in the frequency domain. This presents a drawback when performing time domain simulations of the resultant polarization, namely that the driving polarization is computed in the time

domain. For this reason, we would like an expression that relates the signal field to the driving polarization purely in the time domain. What's more, this expression relies on the previously discussed unidirectional and slowly varying envelope approximations that aren't strictly required to solve this expression given free space conditions [37, 133, 134].

To derive more general expressions for the signal field given a driving polarization, we start by considering Maxwell's equations in the Lorentz gauge in vacuum conditions. Maxwell's equations can then be written in terms of a vector potential ($\vec{A}$) and a scalar potential ($\Phi$) which are determined by solving the following set of inhomogeneous wave equations [134, 133]

$$\nabla^2\vec{A} - \frac{1}{c^2}\frac{\partial^2}{\partial t^2}\vec{A} = -\mu_0\vec{J} \tag{4.33a}$$

$$\nabla^2\Phi - \frac{1}{c^2}\frac{\partial^2}{\partial t^2}\Phi = -\rho/\varepsilon_0 \tag{4.33b}$$

Where $\rho$ is the charge density, $\vec{J}$ is the current density. The fields can be recovered from the potentials using the following expressions

$$\vec{E} = -\nabla\Phi - \frac{\partial^2}{\partial t^2}\vec{A} \tag{4.34a}$$

$$\vec{B} = \nabla \times A \tag{4.34b}$$

For free space conditions, these equations can solved using the retarded Green's function which allows us to encode a causal relationship between a source and the output field [134, 133]. Using this procedure we arrive at the following classic solution for the electric field at an observation point ($\vec{x}$) in terms of the source charge density and the source current density [134].

$$\vec{E}(\vec{x},t) = \frac{1}{4\pi\varepsilon_0}\int d^3x_{\mathrm{sr}}\left(\frac{\hat{R}}{R^2}\left[\rho(\vec{x}_{\mathrm{sr}},t')\right]_{\mathrm{ret}} + \frac{\hat{R}}{cR}\left[\frac{\partial}{\partial t'}\rho(\vec{x}_{\mathrm{sr}},t')\right]_{\mathrm{ret}} - \frac{1}{c^2R}\left[\frac{\partial}{\partial t'}\vec{J}(\vec{x}_{\mathrm{sr}},t')\right]_{\mathrm{ret}}\right) \tag{4.35}$$

where we denote the distance vector between a source point ($\vec{x}_{\mathrm{sr}}$) and the observation point ($\vec{x}$) as $\vec{R}$, the magnitude of the distance as $R$, and the unit vector representing the direction as $\hat{R}$. We also note that a function of the retarded time $t'$ is related to normal time $t$ through the following transformation, $[f(\vec{x}_{\mathrm{sr}},t')]_{\mathrm{ret}} = f(\vec{x}_{\mathrm{sr}},t-R/c)$, which is used to explicitly enforce causality [134].

To explicitly solve for the electric field given a driving polarization we use the following expressions to relate that quantity to the charge and current densities [37].

$$\rho = \rho_0 - \nabla\cdot\vec{P} \tag{4.36a}$$

$$\vec{J} = \frac{\partial}{\partial t}\vec{P} + \nabla\times\mathscr{M} \tag{4.36b}$$

Here we make the following simplifying assumptions. First we assume that, all fluctuations of the charge density are contained in the polarization and we can consider the initial charge distribution ($\rho_0$) as a static quantity and can be ignored. Next, we assume that the contribution of the magnetization density ($\mathscr{M}$) can be ignored. This allows us to rewrite equation 4.36 in the following simplified form.

$$\rho = -\nabla \cdot \vec{P} \tag{4.37a}$$

$$\vec{J} = \frac{\partial}{\partial t}\vec{P} \tag{4.37b}$$

Lastly, we use the common point dipole approximation [37] where we express the polarization in terms of a point dipole source ($\vec{\mu}(t')$) centered at the origin. Note that $\vec{\mu}(t')$ only contains information about the time dependence of the dipole source, whereas the spatial dependence can be expressed in terms of a delta function ($\delta(\vec{x}_{\text{sr}})$). Under these assumptions, we can re-express the source terms in equation 4.37 as

$$\rho = -\sum_{i=0}^{2} \mu_i \delta'(x_{i\%3})\delta(x_{i+1\%3})\delta(x_{i+2\%3}) \tag{4.38a}$$

$$\vec{J} = \frac{\partial \vec{\mu}}{\partial t}\delta(\vec{x}_{\text{sr}}) \tag{4.38b}$$

where $\delta'(x_i)$ is the spatial derivative of the delta function along the $x_i$ th Cartesian coordinate [135, 136]. Substituting equation 4.38 into equation 4.35 and evaluating the integrals yields the following expression for the time dependence of the detected field

$$\begin{aligned}\vec{E}(\vec{x},t) = \frac{1}{4\pi\varepsilon_0}\Bigg(&\frac{3\left([\vec{\mu}]_{\text{ret}}\cdot\hat{R}\right)\hat{R} - [\vec{\mu}]_{\text{ret}}}{R^3} \\ &+ \frac{3\left(\left[\frac{\partial}{\partial t'}\vec{\mu}\right]_{\text{ret}}\cdot\hat{R}\right)\hat{R} - \left[\frac{\partial}{\partial t'}\vec{\mu}\right]_{\text{ret}}}{cR^2} \\ &+ \frac{\left(\left[\frac{\partial^2}{\partial t'^2}\vec{\mu}\right]_{\text{ret}}\cdot\hat{R}\right)\hat{R} - \left[\frac{\partial^2}{\partial t'^2}\vec{\mu}\right]_{\text{ret}}}{c^2R}\Bigg)\end{aligned} \tag{4.39}$$

To simplify equation 4.39, we make the following set of assumptions. First we assume that the detector is placed along some particular axis (here the $\hat{z}$ axis), and that this detector is placed far from the source. As the spatial dependence of the first two terms in equation 4.39 decay more rapidly then the last term, this assumption allows us to consider the net field to only depend on the last term in expression as shown.

$$\vec{E}(z,t) = \frac{1}{4\pi\varepsilon_0}\left(\frac{\left[\frac{\partial^2}{\partial t'^2}\mu_z\right]_{\text{ret}}\hat{z} - \left[\frac{\partial^2}{\partial t'^2}\vec{\mu}\right]_{\text{ret}}}{c^2R}\right) \tag{4.40}$$

Next we assume that we are detecting signals from a sample whose polarization is primarily orthogonal to the propagation direction. Essentially this allows us to ignore factors dependent on $\vec{\mu}_z$. This assumption is justified for a wide class of signals, but as we are particularly interested in third order signals of isotropic samples we focus on this case. If we assume that the incident fields have some polarization in the $\hat{x}$ and $\hat{y}$ axes due to the intrinsic symmetries of isotropic systems, the only resulting polarizations can be in the $\hat{x}$ and $\hat{y}$ directions [36, 137]. Together with the addition of a polarizer in front of the detector that is orientated along the $\hat{y}$ axis allows us to express the field at a detector as

$$E_y(z,t) = \frac{1}{4\pi\varepsilon_0}\left(\frac{-\left[\frac{\partial^2}{\partial t'^2}\mu_y\right]_{\text{ret}}}{c^2 R}\right) \tag{4.41}$$

Since what's measured is the time-averaged square magnitude of the signal electric field in equation 4.41, by performing this operation we can compute a signal proportional to an experimentally measured polarization sensitive signal.

$$\mathrm{V}_{signal} \propto \int_{-\infty}^{\infty} dt \left| \left[\frac{\partial^2}{\partial t'^2}\mu_y\right]_{\text{ret}}(t)\right|^2 \tag{4.42}$$

Equation 4.42 shows final expression that we use to compute the simulated UTPS signal given a computation of the time dependent driving third order polarization.

## 4.4 Orientational Averaging and the Perturbed Density Matrix - An Introduction to the Projected Density Matrix

To compute a orientationally averaged density matrix in the context of perturbation theory, we start by following a similar procedure as used in section 4.3. Namely, we apply the rotation operator that transforms a lab frame vector into a molecular frame vector as implicitly defined in equation 4.19 to the expression for the n$^{\text{th}}$ order correction term of the density matrix as expressed in equation 4.17. Doing this gives the following general expression for a density matrix of a molecule with a given orientation under rotation

$$|\rho^{(n)}\rangle\rangle \propto \int_{t_0}^{t} d\tau_1 \ldots \int_{t_0}^{\tau_{n-1}} d\tau_n \left[\left(\mathscr{U}_0\left(\Delta T_f\right)\prod_{m=1}^{n}\vec{\mu}\,\mathscr{U}_0\left(\Delta\tau_m\right)|\rho_0\rangle\rangle\right)\prod_{m=1}^{n}R_{i_m I_m}\right]\prod_{m=1}^{n}\vec{E}_{I_m}^{lab} \tag{4.43}$$

where we use the following convention for $\Delta T_f$ and $\Delta\tau_m$

$$\Delta T_f = t - \tau_1$$

$$\Delta\tau_m = \begin{cases} \tau_m - \tau_{m+1}, & \text{if } m < n \\ \tau_n - t_0, & n = 0 \end{cases}$$

We point out here that in equation 4.43 the term in the parentheses is nearly identical to the term $\langle\langle\vec{\mu}|\rho^{(n)}\rangle\rangle_{i_0\ldots i_n}$ as defined in equation 4.26 save for the removal of the final contracting dipole operator $\langle\langle\vec{\mu}|$. Given this identification we make the following definition

$$|\rho^{(n)}\rangle\rangle_{i_1\ldots i_n} = \mathscr{U}_0\left(\Delta T_f\right)\prod_{m=1}^{n}\vec{\mu}_{i_m}\mathscr{U}_0\left(\Delta\tau_m\right)|\rho_0\rangle\rangle \tag{4.45}$$

Which allows us to rewrite equation 4.43 as

$$|\rho^{(n)}\rangle\rangle = \left(\frac{-i}{\hbar}\right)^n\int_{t_0}^{t}d\tau_1\ldots\int_{t_0}^{\tau_{n-1}}d\tau_n\left[|\rho^{(n)}\rangle\rangle_{i_1\ldots i_n}\prod_{m=1}^{n}R_{i_mI_m}\right]\prod_{m=1}^{n}\vec{E}^{lab}_{I_m} \tag{4.46}$$

Orientationally averaging the result in equation 4.46 under the assumption of an isotropic system gives us

$$|\rho^{(n)}\rangle\rangle_{ave} = \left(\frac{-i}{\hbar}\right)^n\int_{t_0}^{t}d\tau_1\ldots\int_{t_0}^{\tau_{n-1}}d\tau_n\int\left[|\rho^{(n)}\rangle\rangle_{i_1\ldots i_n}\prod_{m=1}^{n}R_{i_mI_m}\right]d\Omega\prod_{m=1}^{n}\vec{E}^{lab}_{I_m} \tag{4.47}$$

Comparing this equation to equation 4.28 we note a number of similarities but one particularly notable difference. Much like $\langle\langle\vec{\mu}|\rho^{(n)}\rangle\rangle_{i_0\ldots i_n}$, the term $|\rho^{(n)}\rangle\rangle_{i_1\ldots i_n}$ is independent of the orientation of the system in the lab frame. This means that we can use the same cosine matrix formulae to solve the orientational averaging component of the integral as was used when rotationally averaging the signals as shown in equation 4.29 [47, 120]. However, in terms of the effect under orientational averaging, equation 4.47 differs from equation 4.28 by a factor of $R^{-1}$. This difference implies that the perturbed correction to the density matrix has different transformation properties then that of the signal that is generated at that the same level of perturbation theory [47, 120]. Under several circumstances, this implies that the orientationally averaged $n^{th}$ order correction to the density matrix can be exactly zero even when the signal is nonzero.

As a worked example we consider the case of first order perturbation theory. As per equations 4.29 and 4.47, the expression representing a orientationally averaged $1^{st}$ order polarization response is

$$\vec{P}^{(1)}_{lab}(t_0,t)\propto\int_{t_0}^{t}d\tau_1\left[\int R^{-1}_{I_0i_0}\langle\langle\vec{\mu}|\rho^{(n)}\rangle\rangle_{i_0i_1}R_{i_1I_1}\,d\Omega\right]\vec{E}^{lab}_{I_1} \tag{4.48}$$

whereas the orientationally averaged $1^{st}$ order correction of the density matrix can be written as

$$|\rho^{(1)}\rangle\rangle_{ave} = \left(\frac{-i}{\hbar}\right)^n\int_{t_0}^{t}d\tau_1\left[\int|\rho^{(n)}\rangle\rangle_{i_1}R_{i_1I_1}d\Omega\right]\vec{E}^{lab}_{I_1} \tag{4.49}$$

In general, the bracketed term in equation 4.48 is nonzero [36, 47, 120] and the integral of these terms over the integration constant $\tau_1$ allows this term to represent the linear polarization in the time domain. However, the bracketed term in equation 4.49 is exactly zero, since the rotational average

of a vector that samples all orientations must be zero. This forces $|\rho^{(1)}\rangle\rangle_{ave} = 0$ and illustrates some of the challenges when trying to perform an orientational average of the density matrix while still preserving information about the evolution of the relevant density matrix elements.

One approach to address this concern in the context of polarization sensitive measurements, is to invoke the fact that in polarization spectroscopy, there is a preferred lab frame axis of measurement defined by the analyzing polarizer. By associating this preferred lab frame defined axis with the density matrix we reintroduce this missing rotation operator and create an object related to the density matrix that transforms like the signal it represents. We denote this object the polarization projected density matrix.

## Derivation of the Projected Density Matrix

In general, the Liouville space representation of the relation between the molecular frame dipole and the lab frame dipole, as seen in equation 4.19a, can be written as

$$\langle\langle \vec{\mu}_{lab}|\rho\rangle\rangle = R^{-1}\langle\langle \vec{\mu}_{mol}|\rho\rangle\rangle \tag{4.50}$$

The addition of a polarizer with it's major axis along $\hat{\mathbf{e}}^{pol}$ means that we are only sensitive to the component of the dipole projected along this lab frame defined axis. In essence, the lab frame defined analyzing polarizer axis defines a **preferred measurement axis** in the molecular frame, where only the component of the dipole signal along this preferred measurement axis contributes to the measured response. Here we can explicitly add the effect of this preferred measurement axis to equation 4.50 in the following manner

$$\hat{\mathbf{e}}^{pol}\cdot\langle\langle \vec{\mu}_{lab}|\rho\rangle\rangle = \hat{\mathbf{e}}^{pol}\cdot R^{-1}\langle\langle \vec{\mu}_{mol}|\rho\rangle\rangle \tag{4.51}$$

Expanding the right hand side of equation 4.51 in terms of it's components and collecting terms under the trace allows us to write

$$\begin{aligned}
\hat{\mathbf{e}}^{pol}\cdot\langle\langle \vec{\mu}_{lab}|\rho\rangle\rangle &= \langle\langle \mu_x^{mol}|\rho\rangle\rangle\hat{\mathbf{e}}^{pol}\cdot R^{-1}\hat{\mathbf{e}}_x^{mol} + \langle\langle \mu_y^{mol}|\rho\rangle\rangle\hat{\mathbf{e}}^{pol}\cdot R^{-1}\hat{\mathbf{e}}_y^{mol} + \langle\langle \mu_z^{mol}|\rho\rangle\rangle\hat{\mathbf{e}}^{pol}\cdot R^{-1}\hat{\mathbf{e}}_z^{mol} \\
&= Tr\left(\mu_x^{mol}\rho\right)s_x + Tr\left(\mu_y^{mol}\rho\right)s_y + Tr\left(\mu_z^{mol}\rho\right)s_z \\
&= Tr\left(\mu_x^{mol}s_x\rho + \mu_y^{mol}s_y\rho + \mu_z^{mol}s_z\rho\right) \\
&= Tr\left(\left(\mu_x^{mol},\mu_y^{mol},\mu_z^{mol}\right)\cdot\left(s_x\rho, s_y\rho, s_z\rho\right)\right)
\end{aligned} \tag{4.52}$$

where we have defined the components $s_x$, $s_y$, $s_z$, to be the components of the preferred polarization axis after rotation into the molecular frame. Equation 4.52 then suggests the following definition for the polarization projected density matrix

$$|\vec{\rho}_{proj}\rangle\rangle = \begin{pmatrix}\hat{\mathbf{e}}^{pol}\cdot R^{-1}\hat{\mathbf{e}}_x^{mol}|\rho\rangle\rangle \\ \hat{\mathbf{e}}^{pol}\cdot R^{-1}\hat{\mathbf{e}}_y^{mol}|\rho\rangle\rangle \\ \hat{\mathbf{e}}^{pol}\cdot R^{-1}\hat{\mathbf{e}}_z^{mol}|\rho\rangle\rangle\end{pmatrix} = \begin{pmatrix}s_x|\rho\rangle\rangle \\ s_y|\rho\rangle\rangle \\ s_z|\rho\rangle\rangle\end{pmatrix} = \mathbf{s}\otimes|\rho\rangle\rangle \tag{4.53}$$

With this definition we can rewrite equation 4.51 as

$$\hat{\mathbf{e}}^{pol} \cdot \langle\langle \vec{\mu}_{lab} | \rho \rangle\rangle = \langle\langle \vec{\mu}_{mol} | \vec{\rho}_{proj} \rangle\rangle \tag{4.54}$$

Under orientational averaging, the projected density matrix can be written as

$$|\vec{\rho}_{proj}\rangle\rangle_{ave} = \int \mathbf{s}(\Omega) \otimes |\rho(\Omega)\rangle\rangle d\Omega = \begin{pmatrix} \int \hat{\mathbf{e}}^{pol} \cdot R^{-1}(\Omega) \hat{\mathbf{e}}_x^{mol} |\rho(\Omega)\rangle\rangle d\Omega \\ \int \hat{\mathbf{e}}^{pol} \cdot R^{-1}(\Omega) \hat{\mathbf{e}}_y^{mol} |\rho(\Omega)\rangle\rangle d\Omega \\ \int \hat{\mathbf{e}}^{pol} \cdot R^{-1}(\Omega) \hat{\mathbf{e}}_z^{mol} |\rho(\Omega)\rangle\rangle d\Omega \end{pmatrix} \tag{4.55}$$

Applying the results of perturbation theory to equation 4.55 lets us write the n$^{\text{th}}$ order correction to the density matrix as

$$\begin{aligned} |\vec{\rho}^{(n)}_{proj}\rangle\rangle_{ave} =& \int \mathbf{s}(\Omega) \otimes |\rho^{(n)}(\Omega)\rangle\rangle d\Omega \\ =& \hat{\mathbf{e}}^{pol} \cdot \begin{pmatrix} \int R^{-1}(\Omega) \hat{\mathbf{e}}_x^{mol} |\rho^{(n)}(\Omega)\rangle\rangle d\Omega \\ \int R^{-1}(\Omega) \hat{\mathbf{e}}_y^{mol} |\rho^{(n)}(\Omega)\rangle\rangle d\Omega \\ \int R^{-1}(\Omega) \hat{\mathbf{e}}_z^{mol} |\rho^{(n)}(\Omega)\rangle\rangle d\Omega \end{pmatrix} \end{aligned} \tag{4.56}$$

Where the term $|\rho^{(n)}\rangle\rangle$ is the n$^{\text{th}}$ order correction to the density matrix given lab frame perturbing fields being rotated into the molecular frame as expressed in equation 4.46.

Given the definition of the projected density matrix, there are several useful implications that we wish to discuss. One effect of the projected density matrix is to provide an implicit transformation of a the molecular frame density matrix into the lab frame. As a consequence, and as explicitly shown in equation 4.53, the components of the projected density matrix include the rotation that translates molecular frame quantities into their lab frame counter parts that was missing when we considered the orientationally averaged density matrix in equation 4.47. This means means that the components of the projected density matrix transform like the signal they represent. In conjunction with equation 4.54, this suggests that we can interpret the $|\vec{\rho}\rangle\rangle_x$, $|\vec{\rho}\rangle\rangle_y$, or $|\vec{\rho}\rangle\rangle_z$ elements of the projected density matrix as the relative proportion of the density matrix that contributes to the selected polarization signal through a molecular frame defined $\mu_x^{mol}$, $\mu_y^{mol}$, or $\mu_z^{mol}$ respectively.

In essence, the implicit transformation from the molecular frame to lab frame provided by the projected density matrix gives us access to relevant molecular frame quantities through lab frame defined signals. In future sections we will exploit this property of the projected density matrix to aid in the interpretation of orientationally averaged signals.

## Using the Orientationally Averaged Projected Density Matrix to Estimate a Preferred Sampling Orientation of a Molecular System

In the previous section we derived the projected density matrix and showed that it transforms like the signal measured through a preferred measurement axis. Therefore, it can retain information about the relevant quantum state of a system of interest. In this section we will discuss a set of approximations that can be used to recover preferred lab frame orientations of a molecule.

Importantly, the following approximations allow us to recover an explicit transformation into the most relevant molecular frame orientation that provide dominant contributions to the measured lab frame signal.

The core assumption that we will make in this section is that the we can approximate the orientationally averaged projected density matrix as the the projected density matrix for a single molecular orientation. Effectively, we assume that there is a single dominant orientation of the molecule that contributes to a measured polarization selective signal. This can be justified as follows. For a signal that can be described through a finite sequence of transition dipole matrix elements, each transition will be maximized in isolation if the perturbing field is aligned along the transition dipole axis. This suggests that, for any given sequence of transitions, there should be some molecular orientation that maximizes the projection of the perturbing fields with the mediating transition dipoles and thus the resulting signal. While many such sequences of transitions can and do exist, the pathways that have major contributions to the net signal may go through a similar sequence of dipole transitions. If this is the case, the orientation that maximizes all of these contributions could be representative of the net orientationally averaged signal. This approximation can be seen in the following equation

$$|\vec{\rho}_{proj}\rangle\rangle_{\text{ave}} = \int \mathbf{s}(\Omega) \otimes |\rho(\Omega)\rangle\rangle d\Omega \approx \tilde{\mathbf{s}} \otimes |\rho_{\text{approx}}\rangle\rangle \tag{4.57}$$

We note here that by definition, the vector $\tilde{\mathbf{s}}$ is the unit vector representing the rotation of the preferred measurement axis into the molecular frame. This means that $\tilde{\mathbf{s}}$ is a 3-vector with real components of unit magnitude as shown in equation 4.58. By solving for $\tilde{\mathbf{s}}$ and given knowledge of the preferred measurement axis in the lab frame, we aim to determine the rotation matrix describing this transformation of the preferred measurement axis into the molecular frame.

$$||\tilde{\mathbf{s}}||_{\text{real}} = \sqrt{(\tilde{s}_x)^2 + (\tilde{s}_y)^2 + (\tilde{s}_z)^2} = 1 \tag{4.58}$$

Consider the following relationship between the density matrix elements of the orientationally averaged projected density matrix and the single orientation approximation.

$$\langle\langle ij|\vec{\rho}_{proj}\rangle\rangle_{\text{ave}} \approx \tilde{\mathbf{s}}_{ij}\langle\langle ij|\rho_{\text{approx}}\rangle\rangle \tag{4.59}$$

Since we are only selecting for one density matrix element in equation 4.59, this equation represents a complex three component vector. Additionally we note that because $\tilde{\mathbf{s}}_{ij}$ is a real 3 vector of unit length, the term $\tilde{\mathbf{s}}_{ij}\langle\langle ij|\rho_{\text{approx}}\rangle\rangle$ contains only one complex scalar quantity in the density matrix element $\langle\langle ij|\rho_{\text{approx}}\rangle\rangle$. This suggests that we can use equation 4.59 to solve for $\tilde{\mathbf{s}}_{ij}$ using the complex vector quantity $\langle\langle ij|\vec{\rho}_{proj}\rangle\rangle_{\text{ave}}$ with the following procedure.

First we separate equation 4.59 into it's real and imaginary components, giving us two separate expressions for $\tilde{\mathbf{s}}_{ij}$. Since $\tilde{\mathbf{s}}_{ij}$ is of unit length, by taking the magnitude of the vectors derived from the real component and the imaginary component of equation 4.59, we can solve for $\tilde{\mathbf{s}}_{ij}$ up to a sign. Here we show the resulting expression where we denote the raw unit vectors derived from the real and imaginary components of equation 4.59 as $\tilde{\mathbf{s}}_{ij}^{\text{real}}$ and $\tilde{\mathbf{s}}_{ij}^{\text{imag}}$ respectively. The result from this procedure is shown as follows

$$\frac{\mathscr{R}\left[\langle\langle ij|\vec{\rho}_{proj}\rangle\rangle_{\text{ave}}\right]}{\left|\left|\mathscr{R}\left[\langle\langle ij|\vec{\rho}_{proj}\rangle\rangle_{\text{ave}}\right]\right|\right|_{\text{real}}} \equiv \pm\tilde{\mathbf{s}}_{ij}^{\text{real}} \approx \pm\tilde{\mathbf{s}}_{ij} \tag{4.60a}$$

$$\frac{\mathscr{I}\left[\langle\langle ij|\vec{\rho}_{proj}\rangle\rangle_{\text{ave}}\right]}{\left|\left|\mathscr{I}\left[\langle\langle ij|\vec{\rho}_{proj}\rangle\rangle_{\text{ave}}\right]\right|\right|_{\text{real}}} \equiv \pm\tilde{\mathbf{s}}_{ij}^{\text{imag}} \approx \pm\tilde{\mathbf{s}}_{ij} \tag{4.60b}$$

In principle, based on the approximation in equation 4.59, the terms $\tilde{\mathbf{s}}_{ij}^{\text{real}}$ and $\tilde{\mathbf{s}}_{ij}^{\text{imag}}$ should be equal. However, in the exact equation, the real and imaginary component of each matrix element can be associated with their own unique preferred orientation. We can interpret this orientation as being reflective of the set of dipole transitions that maximizes the contribution of the given density matrix element. To arrive at a single $\tilde{\mathbf{s}}$ from the set of $\tilde{\mathbf{s}}_{ij}^{\text{real}}$'s and $\tilde{\mathbf{s}}_{ij}^{\text{imag}}$'s, after assuming the positive sign convention for the vectors, we simply take the average of all $\tilde{\mathbf{s}}_{ij}^{\text{real}}$'s and $\tilde{\mathbf{s}}_{ij}^{\text{imag}}$'s that are associated with nonzero components of their associated density matrix elements as shown in equation 4.61.

$$\frac{\langle\tilde{\mathbf{s}}^{\text{imag}}\rangle + \langle\tilde{\mathbf{s}}^{\text{real}}\rangle}{2} = \tilde{\mathbf{s}} \tag{4.61}$$

This procedure allows us to compute the direction of the preferred measurement axis ($\hat{\mathbf{e}}_1$) in the molecular frame ($\tilde{\mathbf{s}}_1$) from an orientationally averaged projected density matrix calculation. Unfortunately, one unit vector is insufficient to completely define the molecular frame basis in the lab frame. However, two unique unit vectors can be used to determine this molecular frame basis. If $\tilde{\mathbf{s}}_1$ and $\tilde{\mathbf{s}}_2$ are orthogonal, taking the cross product will give the unit vector $\tilde{\mathbf{s}}_3$ which would be orthogonal to both, giving us a complete basis.

To find this $\tilde{\mathbf{s}}_2$, we repeat the same procedure to compute $\tilde{\mathbf{s}}$ using an analyzer-polarizer axis ($\hat{\mathbf{e}}_2$) that's orthogonal to the original axis ($\hat{\mathbf{e}}_1$). Under the assumption that the preferred orientation of the molecule is the same for a signal measured along $\hat{\mathbf{e}}_2$ as compared to a signal measured along $\hat{\mathbf{e}}_1$, the second resulting molecular frame preferred axis vector ($\tilde{\mathbf{s}}_2$) should be orthogonal to the first one ($\tilde{\mathbf{s}}_1$). By taking the cross-product, this allows us to determine the basis representing the molecular frame coordinates in the lab frame and thus the rotation matrix. However, a polarization signal along $\hat{\mathbf{e}}_1$ is not guaranteed to occur through the same transitions as a separate orthogonal axis $\hat{\mathbf{e}}_2$. When we consider the case of third order signals from an isotropic system, these two analyzing polarizers can be sensitive to independent tensor elements whose signals can be preferred through a separate set of transitions.

To estimate the orientation of the molecule whose lab frame signal is measured along $\hat{\mathbf{e}}_1$ we perform the following procedure. First, we assume that the plane defining $\tilde{\mathbf{s}}_1$ and $\tilde{\mathbf{s}}_2$ is the same as the plane defined by $\hat{\mathbf{e}}_1$ and $\hat{\mathbf{e}}_2$. By taking the cross-product of $\tilde{\mathbf{s}}_1$ and $\tilde{\mathbf{s}}_2$ we can solve for $\tilde{\mathbf{s}}_3'$ which is orthonormal to the prior two s-vectors. By taking a second cross-product between $\tilde{\mathbf{s}}_1$ and $\tilde{\mathbf{s}}_3'$ we can define a vector $\tilde{\mathbf{s}}_2'$ which is orthonormal to $\tilde{\mathbf{s}}_1$ and $\tilde{\mathbf{s}}_3'$. Thus the vectors $\tilde{\mathbf{s}}_1$, $\tilde{\mathbf{s}}_2'$, and $\tilde{\mathbf{s}}_3'$ form an orthonormal basis which we interpret as defining the preferred molecular orientation describing the measured signal.

At this point it's useful to contrast this result with other techniques of determining molecular orientations, particularity that of alignment. Thus far, as described in expression 4.57, we have shown how we can use orientationally averaged projected density matrix calculations to find preferred molecular frame orientations that describe the electronic response of an isotropic ensemble of molecules. We can interpret this result as the orientation of the molecule that dominates the signal generation given an isotropic distribution of orientations. This is in contrast to alignment techniques where, after interaction with an aligning field, rotational dynamics shift the orientational distribution of the sampled molecules changing the signal being generated in some manner [138]. Additionally, in the case of isotropic samples, all orientations are present and in principle there can be situations where more than one molecular orientation has dominant contributions to the measured signal. In these situations, the approximation in expression 4.57 would breakdown and to more appropriately approximate the signal one would need to consider a larger number of orientations.

In this work we will only consider the case of a single molecular orientation approximating the result of an orientationally averaged calculation. In future sections we use this procedure to compute these preferred orientations of signal generation and compare the signal generated from them as compared to that from the signal computed from explicit orientational averaging. While these orientationally averaged calculations can be expensive, by performing these calculations over a relatively short time window to obtain an approximate lab frame molecular orientation, we can use this preferred orientation in a much less expensive molecular frame calculation in which the incident fields are rotated into the molecular frame and the output polarization is rotated out of the molecular frame using the explicit rotation matrix as derived in this section.

## 4.5 Perturbative Simulations Of Polarization Sensitive Signals

In the previous sections we outlined the theoretical basis with which we can use ab initio calculations to parameterize an N-level system, compute polarization sensitive signals associated with their response to incident fields, and interpret the resulting the electronic response with the aid of the projected density matrix. Here we aim to detail our software implementation of these techniques and to apply this method to study the responses from an arbitrary two level system and to an n-level model we parameterize in such a way to represent the isotropic response of nitrobenzene.

In the following calculations we performed either a molecular frame calculation where we directly estimate the integrals of section 4.2 for a specific orientation of the input system or a lab frame calculation where we employ orientational averaging of the projected density matrix to compute the resultant signal as shown in section 4.4. In our implementation, we estimate the integrals as discussed in the previous sections using left handed Riemann sums over a truncated time window. This allows us to compute the electronic polarization as a function of simulation time. Given this response as a function of simulation time, we then use equation **??** to compute the signal reported by a time averaging detector when considering the response from a sequence of

Gaussian pulses, or we use the fast Fourier transform to compute the amplitude of the frequency response when considering the case of an incident continuous wave field.

For the case of a sequence of Gaussian pulses, we compute the time averaged signal as parameterized by the time delay between these pulses. To reduce the effects of clipping when the desired time delay window can risk temporal clipping of either the one of the incident pulses or of the raw polarization response, we set the simulation time window to include at least an extra standard deviation of pulse width on both the positive and negative ends of the simulation time window. Additionally in these simulations, we assume the incident fields are all co-propagating along the z-axis and we only simulate the response from a molecule centered at the origin. The effect of these approximations is that we neglect any spatial effects and do not have k-vector selectivity.

In the following sections, we will first validate our methods against an analytical description of the nonlinear steady state response of an arbitrary 2-level system. We will then consider the case of a 2-level system under the influence of a Gaussian pulse and compare these results against the signals obtained from direct iteration of the Liouville equation. Lastly, we will then compute nonlinear polarization sensitive signals from an n-level model parameterized to represent the electronic response from nitrobenzene.

## The Steady State Response of a 2-Level System

To validate the time domain model we consider the case of a 2 level system, described in equation 4.11, with a level spacing $\omega_{ab}$, a population decay time of $T_1$, a characteristic dephasing time of $T_2$, a transition dipole moment of $\mu_{ba}$, and an unsaturated line-center absorption coefficient of $\alpha_0(0)$. This two level system is influenced by a continuous wave (CW) beam with a frequency of $\omega$ which is modeled as a Stark perturbation ($V = \vec{\mu} \cdot \vec{E}$). Analytical solutions for the steady state signal have been derived for this case as shown in equation 4.62, note that only the first and third order susceptibilities are are shown since, in the case of a 2 level atom, all other orders are zero [36]. By estimating the steady state solutions using the time domain method described in section 4.2 and comparing against the analytical solution, we can validate our time domain model.

$$\chi^{(1)} = \frac{-\alpha_0(0)}{\omega_{ab}/c} \frac{(\omega - \omega_{ab})T_2 - i}{1 + (\omega - \omega_{ab})^2 T_2^2} \tag{4.62a}$$

$$\chi^{(3)} = \frac{-\alpha_0(0)}{3\omega_{ab}/c} \frac{(\omega - \omega_{ab})T_2 - i}{\left(1 + (\omega - \omega_{ab})^2 T_2^2\right)^2} \frac{4|\mu_{ba}|^2 T_1 T_2}{\hbar^2} \tag{4.62b}$$

To convert our time domain signals into the frequency dependent steady state signals we perform the following procedure, first we numerically evaluate the time ordered integrals of equation 4.29 over a length of time. Next we take the time domain polarization signal and convert it into the frequency domain. In the steady state case, the frequency of the incident field will be the same as the output polarization signal and this will be the main source of signal [36]. Thus to compute an estimated steady state signal we perform a FFT on the computed time domain data and pick out the maximal frequency domain signal. The amplitude of this signal is what's used to compare

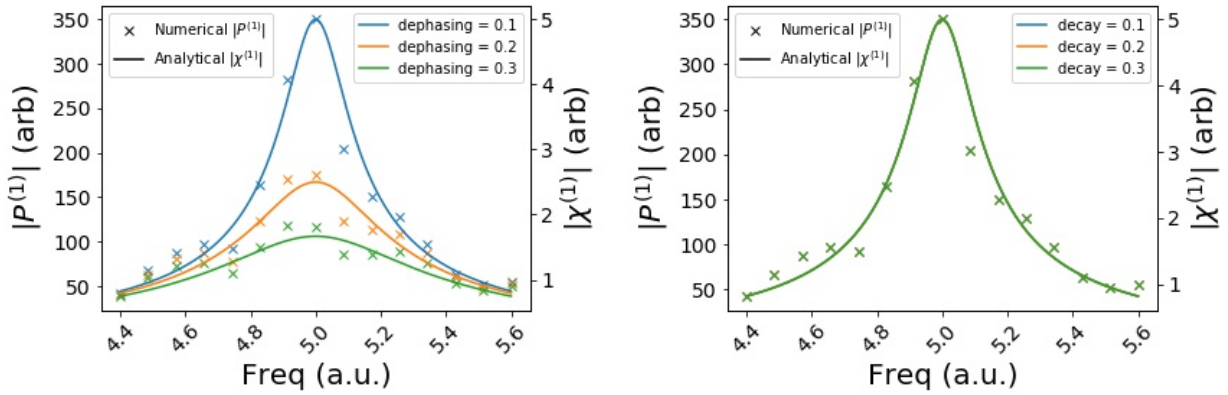


Figure 4.4: This figure compares the analytical solution of $\chi^{(1)}$ to a time dependent numerical estimate of $P^{(1)}$ for a 2-level system with a level spacing of 5 a.u. given a CW incident beam of variable frequency and variable decay and dephasing rates. In both the case of variable dephasing rates and variable decay rates, the numerical estimates peak heights show very good quantitative agreement as compared to the analytical solution. Additionally the line shapes also show good quatitative agreement with the steady state solution. There is some deviation from these plots but we attribute these errors to a combination of finite spacing and boundary cut off effects associated with the FFT. Note that the analytical solution for $\chi^{(1)}$ for this system is independent of decay rate and this behaviour is observed in the numerical estimate.

against the expected amplitudes from the analytical steady state values. As a further verification we compared the frequencies of the input and output fields to ensure that they match. Note that since the estimate computes a value proportional to $P^{(n)}$ and the analytical solution computes $\chi^{(n)}$, the numerical estimates and analytical values can only be qualitatively compared.

In the first order case, we evaluated the signal from 150a.u. of time to 2000 a.u. of time (see Figure 4.4). This range was chosen in order to remove contributions from the initial transient response as well as provide sufficient resolution to recover the oscilating signals. In the third order case, signals were evaluated from 0 a.u. of time to 100 a.u. of time (see Figure 4.5). While this range does include some of the initial response of the system before equilibrium is reached, this range was chosen to limit the cost of the simulations. In each run of these simulations, the energy separation was 5 a.u., the transition dipole moment was 0.1 a.u., and the frequency of the input electric field was varied from 4.4 a.u. to 5.6 a.u.. To qualitatively compare the trends between different runs, the decay rates were varied from 0.1 a.u. to 0.6 a.u. and the dephasing rates were varied from 0.1 a.u. to 0.5 a.u.

As shown in figure 4.4 and figure 4.5, these calculations show fairly good qualitative agreement between the calculated estimate and the analytical solutions with particularly good agreement of the peak signal at the transition frequency. There is some error in tracking the line widths of the various decays but those can be attributed to a combination of boundary cut off effects, finite time spacing, and finite duration of the calculation.

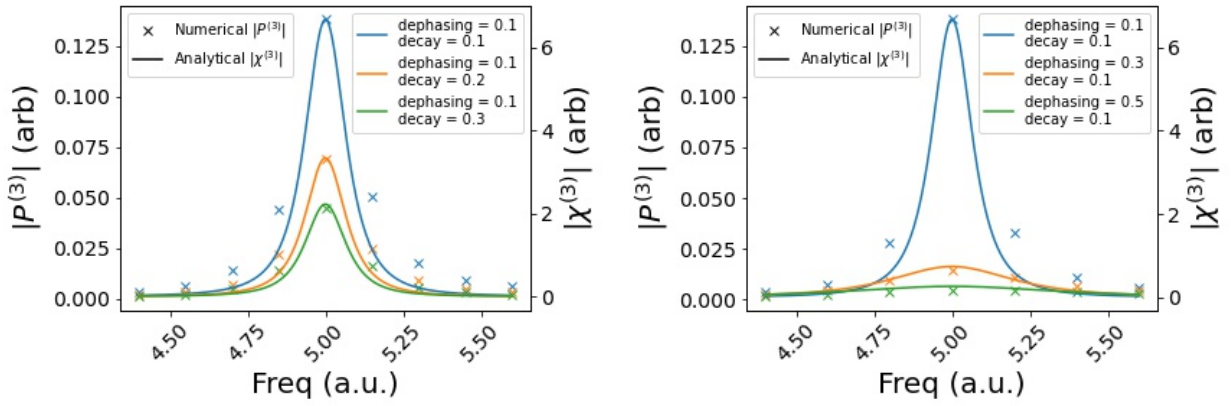


Figure 4.5: This figure compares the analytical solution of $\chi^{(3)}$ to a time dependent numerical estimate of $P^{(3)}$ for a 2-level system with a level spacing of 5 a.u. given a CW incident beam of variable frequency and variable dephasing rates. In contrast with the solution of $\chi^{(1)}$ which is expected to be independent of the decay rate, $\chi^{(3)}$ for this system is expected to be dependent on both the dephasing rate and decay rate. This behaviour is recovered in the numerical estimate. We additionally see good qualitative agreement between the numerical and analytical estimates particularly when comparing peak heights of the two sets of curves. Similar to the $\chi^{(1)}$ calculation we attribute the errors in the qualitative width of the curves to boundary cut off effects, the finite time spacing, and the finite duration of the calculation, used to compute the estimated $P^{(3)}$. The finite duration of the calculation plays a bigger role in third order calculations as they are substantially more expensive then first order calculations.

## The Transient Response of a 2-Level Isotropic System with Incident Gaussian Pulses

In the previous section, we described the steady state response of a two level system using perturbative time domain representation of the polarization response. While useful when comparing against analytical solutions, this computational technique is most capable at representing transient time domain information. Here we explore some of the results of such a calculation in the context of Gaussian pulses.

### Comparison of the Polarization Response from Perturbative Lab frame Calculations and Direct Iteration of the Liouville Equation

Here we present results comparing calculations of the transient polarization response of a two level system performed using two different methods. The first method relying on a lab frame perturbation theory framework as discussed in sections 4.2 and 4.3 and the second method [139] being a molecular frame calculation using direct iterations of the quantum Liouville equation (as expressed in equation 4.11) performed in collaboration with Dr. Liang Z. Tan. In this pair of

calculations, the model parameterization used in these calculations is identical to that in table 4.1.

| Parameter | Value (atomic units) |
|---|---|
| $\mu_{ab}$ | 0.001 |
| $\mu_{aa}$ | 0 |
| $\mu_{bb}$ | 0 |
| $\omega_{ba}$ | 0.1 |
| $\Gamma$ | 0.0002 |
| $\gamma$ | 0.0001 |

Table 4.1: Model parameters of the two level model used in the following calculations. Here, $\mu$ represents the dipole matrix elements along a specific axis with other matrices representing the transitions along orthogonal axes being 0, $\omega_{ba}$ is the transition energy between the ground state ($a$) and the excited state ($b$), $\gamma$ is the dephasing rate of the coherence's between the model states, and $\Gamma$ is the minimal spontaneous decay rate of the excited state population ignoring collisional effects [36, 37].

The results from the lab frame perturbation calculation are shown in figure 4.6. Here the incident driving lab frame field is chosen to have an arbitrary amplitude of 0.1 (a.u.) with the output polarization axis being the same as the chosen polarization of the driving field. We note that because this simulation includes the response of the system that samples all orientations, the relative magnitude of the responses differs compared to a molecular frame calculation which was performed in the alternative simulation method. However, because the shape of the signals computed at the same order of perturbation theory doesn't change when scaling all incident fields by the same factor (as implied by equation 4.15c), these results can be normalized and directly compared to the results from the alternative calculation method shown in figure 4.7.

Figure 4.7 shows the results of the total polarization response of this two level system and an estimate for the 3$^{\text{rd}}$ order polarization along with the driving electric field. As illustrated in equation 4.63, this estimate was calculated by subtracting from the total polarization signal, a factor of 10 scaled up polarization signal that was computed using a factor of 10 scaled down electric field.

$$P^{(3)}_{\text{est}} = P(E) - 10P(0.1E) \tag{4.63}$$

As the third order signal will scale up faster then the linear scaling, the result of this estimate should remove the linear contribution of the polarization while leaving the nonlinear contributions of which we expect the third order response should dominate.

We note here that while the center frequency and the width of the driving field is the same as that used in the perturbative calculation, the amplitude of the field differs from that used in the calculation of the perturbative response as shown in figure 4.6. While this along with the difference in the lab vs molecular frame calculations makes comparison of the total polarization signal somewhat more difficult, since the result of the perturbation calculation scales with respect to the amplitude of the one incident pulse, comparison between the perturbative third order response

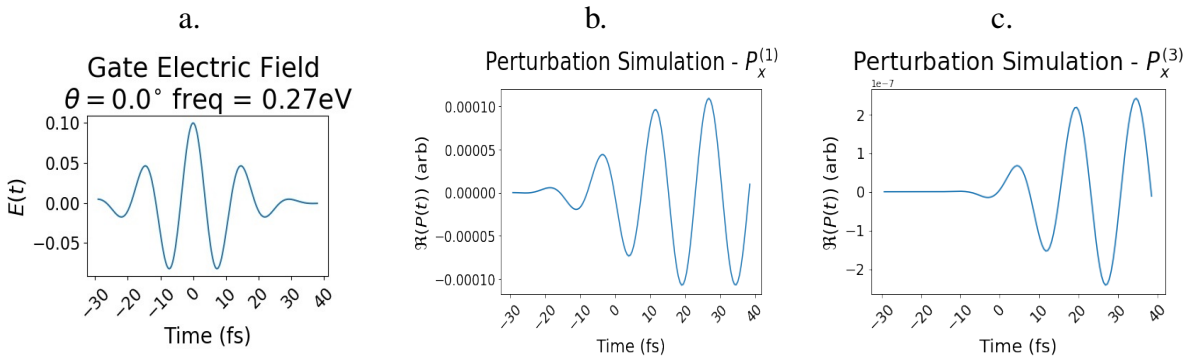


Figure 4.6: Results from a lab frame 2-level model when using a computing method relying on a perturbative treatment of the Liouville equation as discussed in sections 4.2 and 4.3 where the driving E-field and the selected polarization response have the same polarization. Here we show the incident electric field whose center frequency was chosen to be resonant with the transition energy of the system (Panel a.), the computed first order polarization response (Panel b.), and the computed third order polarization response (Panel c.).

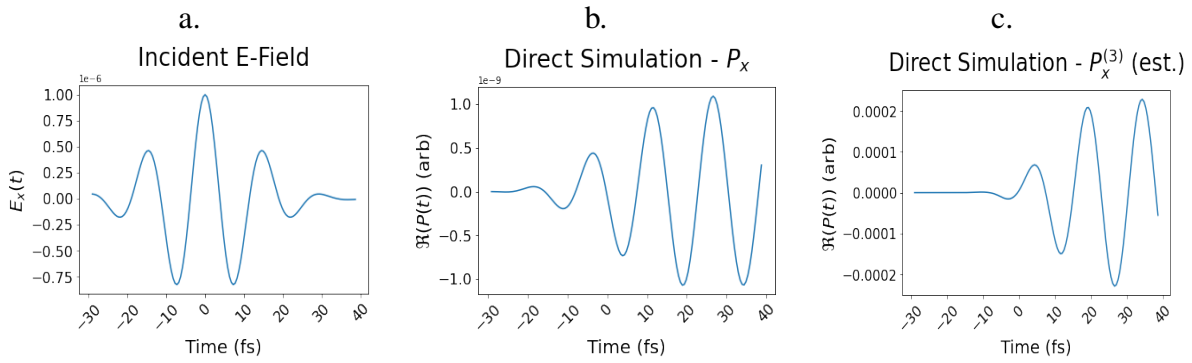


Figure 4.7: Results from a 2-level model when using a simulation method [139] relying on direct iteration of the Liouville equation with the resonant driving E-field and the selected polarization response have the same polarization. Here we show the incident electric field whose center frequency was chosen to be resonant with the transition energy of the system (Panel a.), the total computed polarization response from the simulation (Panel b.), and an estimate for third order polarization response (Panel c.) using equation 4.63. These calculations were performed in collaboration with Dr. Liang Tan.

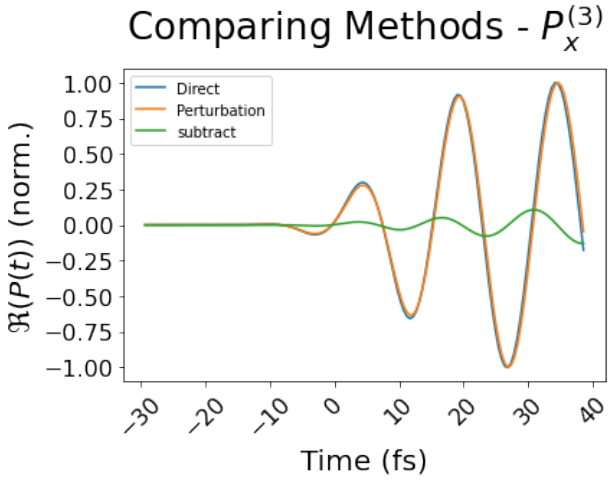


Figure 4.8: A comparison of the computed normalized third order polarization response from a two level system. This figure shows the result from a perturbative calculation in which the third order correction is directly calculated, and the results from a simulation method that estimates the third order polarization by directly propagating the Liouville equation. We note some small differences within the window of the simulation between these calculation methods as seen in the subtraction between the direct and perturbation calculations with a peak magnitude of the difference being 0.107. We attribute these differences to the potential contribution of higher order correction terms in the direct simulation that aren't present in the perturbative calculation.

with the estimated third order signal can be done using their normalized responses. The result of this comparison can be seen in figure 4.8.

Figure 4.8, shows excellent agreement between the two methods of simulation. We do note some small differences between the calculations, especially at the later simulation times, but we attribute this to the method used to estimate the third order polarization. In principle, we may expect some differences between the direct iteration approach and the response function approach due to the different time stepping methods implemented in either method. In the direct iteration method, a forward Euler method was used to compute the next result whereas in the response function approach, integrals were directly numerically estimated using left-handed Riemann sums. As these two methods take fundamentally different approaches to estimating the same result, we expect that differences due to the method of time-stepping should result in noisy differences between the two methods. However, we also note that the estimate (equation 4.63) is designed to remove the linear contribution and is not guarantied to only include the third order response. As such higher order correction terms in the polarization response may contribute to the $P^{(3)}_{\text{direct}}$ estimate which show up as deviations from the polarization computed through perturbative methods. Such a deviation from higher order contributions would have similar oscillatory behaviour and growth behaviour of the peak amplitude as compared to a lower order contribution, however the higher order contribution would be expected to be weaker and/or shifted. As this is similar to the behaviour

| Parameter | Value (atomic units) |
|---|---|
| $\mu_{ab}$ | 0.001 - 0.01 |
| $\mu_{aa}$ | 0.0 - 1.0 |
| $\mu_{bb}$ | 0.0 - 2.0 |
| $\omega_{ba}$ | 0.1 |
| $\Gamma$ | 0.0002 |
| $\gamma$ | 0.0001 |

Table 4.2: Here we show a summary of the model parameters of the two level model used in of the following calculations of the orientationally averaged density matrix, the orientationally averaged projected density matrix, and their associated transient polarizations. The single incident pulse frequency was chosen with center frequency resonant with the transition energy, a peak amplitude of 1 a.u., and a pulse duration of 20 fs. In the following calculations the polarization of the incident pulse and the selected signal polarization were set to the same axis.

of the difference between the two simulation results, we attribute the primary difference between these methods as a result of additional higher order terms contributing to the direct simulation estimate of $P^{(3)}_{\text{direct}}$. These results, serve as an additional validation of the perturbative approach in simulating the polarization response of the system.

**The Polarization Response As a Function of Simulation Parameters**

The following calculations show the result of simulations in which the we varied the dipole matrix elements of a two level system while keeping the incident pulse parameters the same. A summary of the model parameters sampled can be seen in table 4.2, with the incident pulse duration being 20 fs, with an amplitude of 1 a.u. and the peak of the pulse occurring at $t = 0$.

A summary of the resulting sampled signals can be seen in figure 4.9. We note here the following trends that can be seen when comparing the results of these simulations. First, when the ground state dipole increases (as seen when comparing figures 4.9c and 4.9d), the magnitude of the 3$^{\text{rd}}$ order polarization response decreases. This can be explained by the ground and excited state dipole moments having the same orientation and thus, when population moves out of the ground state population to the excited state, the contribution of the ground state dipole to the net instantaneous response goes down in proportion to the population that has left the ground state. This is further evidenced by comparing figures 4.9b and 4.9d which result in the same realization of the net polarization response despite the lack of a strong ground state dipole moment in 4.9b. Additionally, we note a big difference in the shape of the signal when the only contribution to the polarization response is from the transition dipole moment (figure 4.9a) as compared to when there is a nonzero population state dipole moment (4.9b). In figure 4.9a, we see a relatively slowly growing but longer lived polarization, whereas in figure 4.9b we see the inclusion of a strong but short lived but quickly decaying polarization response.

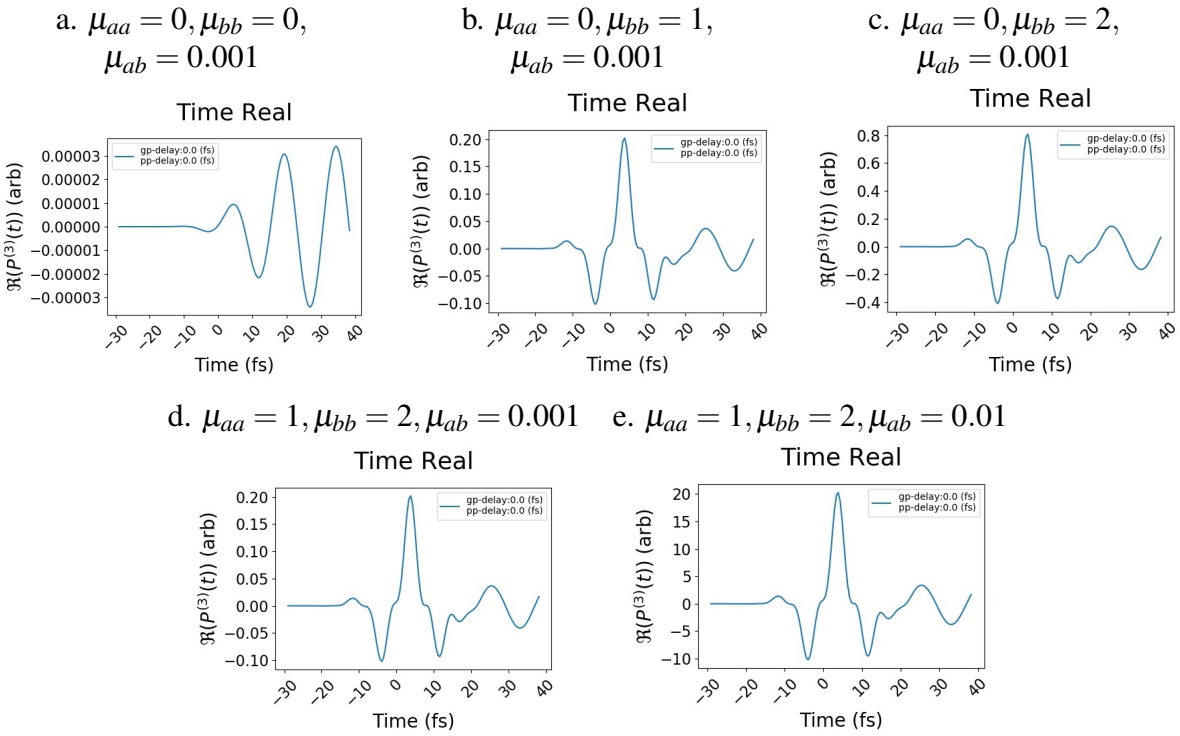


Figure 4.9: Transient polarization responses of a two level model with the model parameters as in table 4.2. Here we show the orientationally averaged transient polarization responses and the associated dipole matrix elements of the two level system corresponding to the simulation.

These results suggest, that the transition dipole matrix element and the corresponding coherences are primarily responsible for a relatively small amplitude and slowly rising but longer lived signal that could be associated with the decay of the off diagonal coherences, where as the strong peak polarization that occurs within 10 fs of the peak amplitude of the driving field is due to the effects of population state dipole moments and the associated population dynamics. Also as the period of the oscillations after the 20 fs simulation time don't change and they scale with increasing excited state $\mu_{bb}$, it's possible that while the transition state dipole moment mediates the transitions, it doesn't directly contribute to the overall signal and that population dynamics are the primary driver of these signals. Comparing panels d and e of figure 4.9, does not allow us to conclude that coherences are playing a significant role in the net polarization response outside of mediating the population dynamics since, increasing the transition dipole by a factor of 10 increases the magnitude of the polarization by a factor of 10.

To further explore the orientationally averaged transient polarization responses of figure 4.9, we explicitly compare calculations of the third order correction to density matrix under orientational averaging (equation 4.47) as compared with the orientationally averaged third order correction of the projected density matrix (equation 4.55). The $\mu$ parameters in table 4.2 are associated with the

dipole transitions along the molecular frame z-axis, with the x and y dipole matrix elements being set to zero. Thus only transitions that occur through the z dipole matrix are able to contribute to a transient polarization signal. In the following examples, we have fixed the z dipole matrix elements to be $\mu_{aa} = 1$, $\mu_{ba} = 2$, and $\mu_{ab} = 0.001$. The resulting signal associated with these parameters is shown in figure 4.9d, with the peak of the polarization occurring within the first 10 fs after the peak of the incident pulse.

Due to the number of rotation matrices involved in the molecular frame to lab frame transformation, we can expect that the orientationally averaged $|\rho^{(3)}\rangle\rangle$ will have the analogous transformation properties as $\chi^{(2)}$ under orientationally averaging. We note that $\chi^{(2)}$ under these conditions has six nonzero elements $\chi^{(2)}_{zyx}$, $\chi^{(2)}_{yxz}$, $\chi^{(2)}_{xzy}$, $\chi^{(2)}_{zxy}$, $\chi^{(2)}_{yzx}$, and $\chi^{(2)}_{xyz}$ with these tensor elements being equal to each other up to a sign [140]. When considering how these transformation properties of $\chi^{(2)}$ would apply to $|\rho^{(3)}\rangle\rangle$, this means that in order for the orientationally averaged $|\rho^{(3)}\rangle\rangle$ to be nonzero, the perturbing fields must have polarization components along the x, y, and z axes. Since the perturbing fields all have polarizations in the x-y plane, these relations suggest we should expect the orientationally averaged density matrix to be identically zero even though the orientationally averaged signal that is represented at this order of perturbation theory is nonzero. This is in contrast to the projected density matrix which, as discussed previously, has Cartesian elements that transform like the signal they represent under orientational averaging.

Additionally, previously we discussed an interpretation of the Cartesian elements of the projected density matrix as representing a proportion of the density matrix that contributes to the lab frame signal through the specific molecular molecular frame dipole transitions that occur through that same Cartesian axis. Given that only $\mu_z$ has nonzero transitions, and the transformation properties previously discussed, this suggests that the z component of the projected density matrix will be the only one to have nonzero components. Given this, we should expect $\langle\rho^{(3)}\rangle$, $\langle\vec{\rho}^{(3)}_x\rangle$, and $\langle\vec{\rho}^{(3)}_y\rangle$ to be identically zero with only the term $\langle\vec{\rho}^{(3)}_z\rangle$ being nonzero.

Figure 4.10 shows the magnitude of the Cartesian elements of the third order correction to the projected density matrix and the third order correction to the density matrix under orientational averaging. As expected, the z component of the projected density matrix has a nonzero contribution, with the other components are identically zero since only $\mu_z$ contains nonzero elements. These results demonstrate the ability of the projected density matrix to provide access to a quantity related to the density matrix after orientational averaging. Given that the averaged projected density matrix samples all orientations of a molecule, this provides us a means of sampling all orientations of a molecule while still maintaining the ability to interpret which elements are contributing to a specific signal.

In this example, because the model is so simple the interpretation is also relatively simple. Given a resonant pulse with a given lab frame polarization and a polarizer oriented along the same polarization axis, for a system parameterized as in table 4.2, only the z transitions are demonstrated to contribute to the signal. Additionally, looking at the magnitude of the coherences relative to the populations, despite the strong population dipole moments, the coherences seam to have a very strong contribution to the output polarization. This is particularly evident when looking at the magnitude of the $|\vec{\rho}_z\rangle\rangle$ in figure 4.10 at simulation times greater than 20 fs. When compared

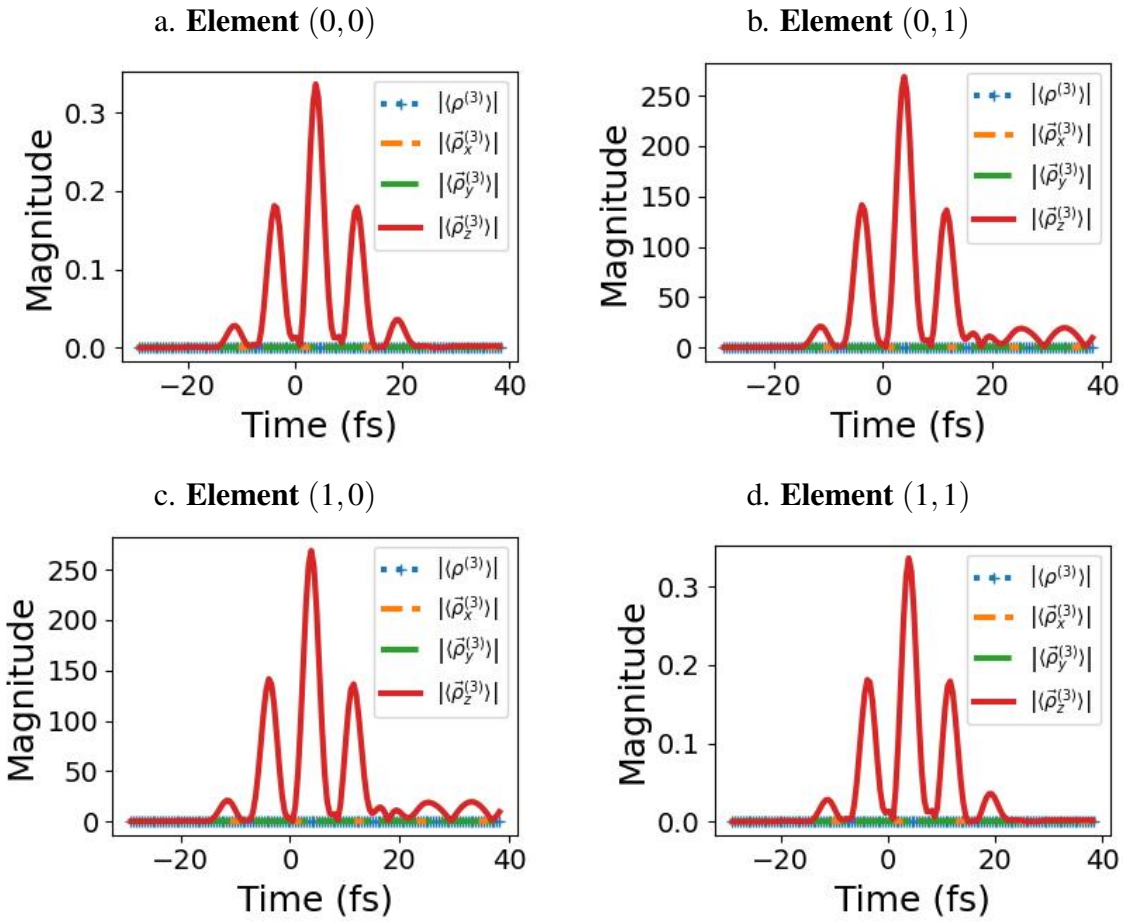


Figure 4.10: This figure shows the magnitude of the elements of the 3rd order density matrix and the 3rd order correction to the projected density matrix, both as a function of simulation time after orientaional averaging. Here, 0 refers to the ground state and 1 refers to the first excited state. Thus $(0,0)$ and $(1,1)$ refer to the ground state and excited state populations respectively, whereas $(0,1)$, and $(1,0)$ refer to the complex conjugates of the orientationally averaged coherence between these states at the third order of perturbation theory. Here we see that $\vec{\rho}_z^{(3)}$ is the only nonzero Cartesian component of the orientationally averaged projected density matrix and $\rho^{(3)}$ is exactly zero under orientationally averaging.

against the computed third order polarization in figure 4.9d, this suggests that, while the peak polarization, as seen within the first 10 fs of when the sample experiences the peak field, has significant contributions from the dynamics of the population states, the coherences appear to be driving the longer tail of the signal while also having a significant contribution to the peak amplitude polarization. This is in contrast to the previously discussed interpretation of these signals which suggested that these signals were primarily driven solely by population dynamics mediated by coherences as apposed to the coherences having a major contribution to the signal.

This particular case is a little simple to fully demonstrate the full utility of the projected density matrix. Since the only major transition is along the molecular frame z-axis, it's simple to assume the sample is aligned along the lab frame z-axis when performing a calculation, this has all the benefits of interpretability as orientational averaging is not required giving access to the $n^{th}$ order corrections to the density matrix, while also avoiding the additional expense of explicit orientational averaging.

In future calculations we will demonstrate how this explicit orientational averaging allows for the determination of preferential molecular orientations that have dominant contributions to the computed polarization when there are many potential transitions and decay pathways that can modify and/or contribute to the net signal.

## Simulating the Nonlinear Electronic Response of Nitrobenzene through Perturbative Calculations of an N-Level Model

### Parameterization of the N-Level Model to simulate the electronic response of Nitrobenzene

In this section we will discuss the procedure by which we parameterized the N-level model as depicted in section 4.2 to best represent the electronic response from nitrobenzene. As shown in equation 4.11 there are four matrices that need to be parameterized in order to represent the signal from a specific molecule, the transition energies between each state ($\omega_{nm}$), decoherence rates ($\gamma$), population relaxation rates ($\Gamma$), and a perturbation ($V$), where we take the perturbation to be due to the energy of external electric fields ($\vec{E}$) interacting with the dipole operator ($\vec{\mu}$).

To determine the values to be used for the matrix elements of the dipole operator used in the following calculations, we performed a set of response theory calculations as described in section 4.1. With these calculations we are able to determine the ground-to-excited state transition dipoles as well as the excited-to-excited state dipole matrix elements. Together with a calculation of the ground state dipole moment, we are able to determine the transition dipole moments between a number of chosen excited states. In these response theory calculations, the transition energies are also computed which further allows for the parameterization of the transition energies between each state.

In the following sections we used the dipole moments from nitrobenzene with a 13° dihedral angle between the plane of the benzene ring and by the plane defined by the $NO_2$ functional group. This geometry was chosen since prior calculations [71] suggest that this geometry helps facilitate the dipole transitions between the ground state and the lower lying excited states. Additionally, When comparing the transition dipoles given the current level of theory (as shown in appendix

A) between the $C_{2v}$ planar geometry and the $C_1$ 13° twisted geometry, many of the ground to excited state transitions in the $C_{2v}$ geometry are particularly weak with only excited state transition moment bellow 4.7 eV with a magnitude of the transition dipole larger than $10^{-10}$ (a.u.) being the $S_0$ to $S_3$ transition moment with a magnitude of 0.0564 a.u. and an energy difference of 4.55 eV. In contrast, the 13° twisted geometry shows strong ground to $S_1$ and $S_2$ transitions with ground to excited state transition moment magnitudes and energy differences of 0.0743 a.u. / 4.17 eV and 0.0346 a.u. / 4.56 eV respectively.

To determine the pulse parameters we started by approximating the incident pulses with a set of Gaussian functions using the FROG measurements to determine the pulse width and pulse energy measurements to set the field amplitude. Depending on the time scale of the simulation the width of these fields were modified to reduce edge effects from clipping the edges of the fields in time.

The most difficult terms to parameterize through ab initio methods are the dephasing ($\gamma$) and population decay terms ($\Gamma$) which are contained in the Liouville space decay matrix ($\mathscr{D}$). The most complete way to express the ability of molecules to dissipate energy into other degrees of freedom is by explicitly solving for nonadiabatic dynamics especially those around conical intersections [3, 4]. Here, by including the decay matrix ($\mathscr{D}$), we can approximate the effects of these nonradiative decay processes. In general the dephasing and decay terms are related through the following expression [37, 36]

$$\gamma_{ij} = \Gamma_i + \Gamma_j + \gamma_c \tag{4.64}$$

where $\Gamma_i$ and $\Gamma_j$ are the population decay rates for the i$^{\text{th}}$ and j$^{\text{th}}$ states, $\gamma_c$ is the collisional contribution to the dephasing rate, and $\gamma_{ij}$ is the dephasing rate of the coherence between the i$^{\text{th}}$ and j$^{\text{th}}$ states. To approximate the decay terms $\Gamma_i$ and $\Gamma_j$, we started by including the decay rate due to spontaneous emission [117] which lets us set a lower bound of the decay rates. These decay rates were then scaled to be roughly the same order of magnitude as the measured electronic decay rates of nitrobenzene [65, 93] around 10-100 fs or longer. Once these estimates for the population decay rates were chosen, we then used expression 4.64 to estimate the associated dephasing rates assuming negligible $\gamma_c$.

### Comparison of N-Level Model simulation to OKE measurements of Nitrobenzene

Here we describe a series of calculations aimed at describing the electronic response of an optical Kerr effect signal of nitrobenzene. To perform this calculation we used the parameterized N-level model to simulate the third order response from nitrobenzene as described in section 4.2 using the parameterization method as described in section 4.5. The aim of these calculations is to first find an appropriate representative orientation of nitrobenzene by performing orientationally averaged calculations over a short time delay window. After validating this preferred orientation, we will then exploit the cost saving difference between the lab frame and molecular frame calculations to compute longer lab frame calculations using this representative orientation. We then aim to use this representative orientation to compute polarization signals that appropriately represent the electronic response from an isotropic sample of nitrobenzene. With this response we then aim to

compare this molecular frame calculation against recent measured optical Kerr effect signals of nitrobenzene.

To start, we performed a series of orientationally averaged third order calculations of nitrobenzene given a set number of included states and pulse durations included in the model. In these calculations, both the probing pulse and the Kerr gating pulse were represented by Gaussian pulses with equal amplitudes and equal pulse duration with the gate having a 45° relative polarization as compared to the probe where we defined the probe polarization axis to be along the lab frame x-axis and the lab frame z-axis was defined to be the propagation axis. The signal polarization was taken along the lab frame y-axis. To aid in comparing these simulations to experimental measurements, the amplitudes of the Gaussian pulses were determined from the pulse intensities used in our recent observations of the optical Kerr effect signal in nitrobenzene [61] as shown in section 2.1.

$$\mathbf{R}_{\text{mol}\rightarrow\text{lab}} = Y(\theta_1)\,Z(\theta_2)\,Y(\theta_3) \tag{4.65}$$

| Included States | Pulse Width (fs) | $\theta_1$ (rad.) | $\theta_2$ (rad.) | $\theta_3$ (rad.) |
|---|---|---|---|---|
| $S_0$, $S_1$, $S_2$ | 7.5 | $0.9669 \pm 0.0044$ | $1.272 \pm 0.012$ | $-0.22 \pm 0.23$ |
| $S_0$, $S_1$, $S_2$ | 15 | $0.9573 \pm 0.0030$ | $1.2706 \pm 0.0070$ | $-0.21 \pm 0.25$ |
| $S_0$, $S_1$, $S_2$ | 30 | $1.0042 \pm 0.0074$ | $1.2778 \pm 0.0037$ | $-0.25 \pm 0.20$ |
| $S_0$, $S_1$, $S_2$, $S_8$, $S_{12}$ | 7.5 | $0.9764 \pm 0.0035$ | $1.288 \pm 0.010$ | $-0.176 \pm 0.099$ |
| $S_0$, $S_1$, $S_2$, $S_8$, $S_{12}$ | 15 | $0.9887 \pm 0.0036$ | $1.2666 \pm 0.0049$ | $0.01 \pm 0.15$ |
| $S_0$, $S_1$, $S_2$, $S_8$, $S_{12}$ | 30 | $0.9832 \pm 0.0040$ | $1.2909 \pm 0.0040$ | $-0.08 \pm 0.19$ |

Table 4.3: Recovered Euler angles and standard errors from third order orientationally averaged projected density matrix calculations using a pair of incident Gaussian pulses with a center frequency at 780 nm. In these calculations the full width at half max pulse duration of the both the Kerr gate and the probe were set to be equal to the pulse width in the table.

After performing these orientationally averaged calculation for a fixed set of model parameters, we were able to extract representative orientations of nitrobenzene as a function of time-delay between the Kerr gate and probe pulses. Here we represent the recovered orientation using a set of extrinsic Euler angles using the Y-Z-Y convention as seen in equation 4.65. To settle on a final value for the Euler angles, we averaged the recovered Euler angles over the sampled set of time delays and computed the standard error for that mean value.

In table 4.3, we show the average Euler angles and associated standard errors for a variable set of model parameters. We note that, as discussed in section 4.4, projecting one preferred axis into the molecular frame is not enough to completely determine the preferred molecular orientation. In essence this is because rotations about this axis can't be distinguished from one another which leave one additional degree of freedom. This means that using the orientationally averaged projected density matrix calculation using the lab frame y-axis as the preferred axis we can determine the two Euler angles $\theta_1$ and $\theta_2$. The third Euler angle $\theta_3$ on the other hand, must be determined by

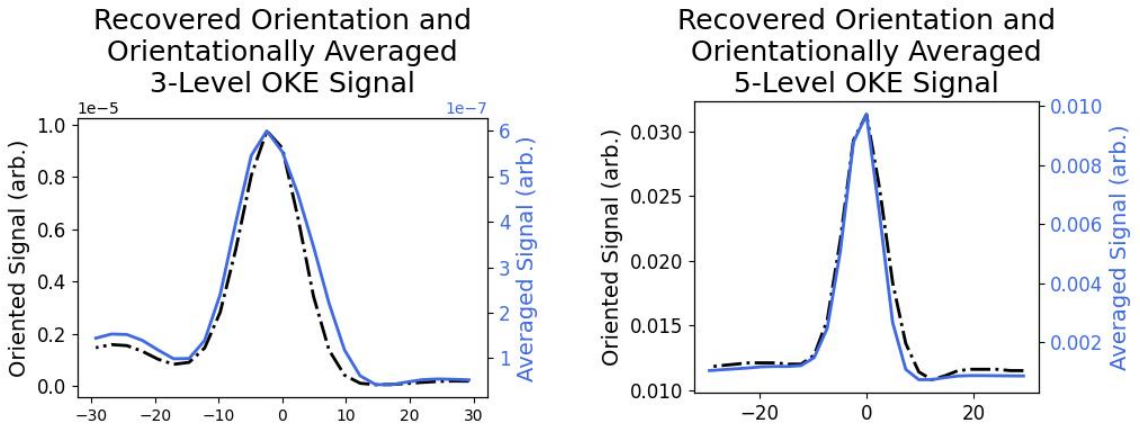


Figure 4.11: A sample comparison of the third order orientationally averaged polarization signal against the third order polarization signal from an oriented molecular frame calculation. For the molecular frame calculation, the orientation supplied was recovered from the orientationally averaged projected density matrix calculation that was used to compute the orientationally averaged signal. In the 3-level case, the included states were $S_0$, $S_1$, and $S_2$. Whereas in the 5-level case, we included $S_0$, $S_1$, $S_2$, $S_8$, and $S_{12}$ in the model. In these calculations, the 780 nm IR fields had full width half max pulse durations of 15 fs and equal amplitudes.

computing a second orientationally averaged projected density matrix with the x-axis being the preferred axis. However, since this second preferred measurement axis can accept polarization signals from different tensor elements of $\chi^{(3)}$, we aren't guarantied to sample the same preferred orientation of nitrobenzene, as compared to the case where the y-axis is the preferred measurement direction. These differences help to explain why our reported uncertainties in $\theta_1$ and $\theta_2$ is roughly 1-2 orders of magnitude smaller then the uncertainty in $\theta_3$.

Interestingly, as seen in table 4.3, regardless of the changes in the included states or the pulse duration, the recovered orientations are all fairly close to one another. This suggests that for a wide number of states, this orientation of nitrobenzene is particularly sensitive to this configuration of incident IR fields regardless of pulse duration or the number of included states.

To validate these recovered orientations, within a set of fixed model parameters, we compared the polarization signal calculated from a molecular frame calculation using the recovered orientation against the signal from the orientationally averaged calculation. An example of these comparisons for the 3-level ($S_0$, $S_1$, $S_2$) and 5-level ($S_0$, $S_1$, $S_2$, $S_8$, $S_{12}$) cases with 15 fs incident Gaussian pulses are shown in figure 4.11. Here we note fairly good qualitative agreement even though the magnitude of the signal between these two cases differs by a factor of 2 in the 5-level case, and roughly a factor of 20 in the 3-level case. Since other weaker signals aren't being averaged together to result in the final signal in the oriented molecular frame case, it's not unexpected that the orientationally averaged signal will be weaker then the signal calculated from the oriented molecular

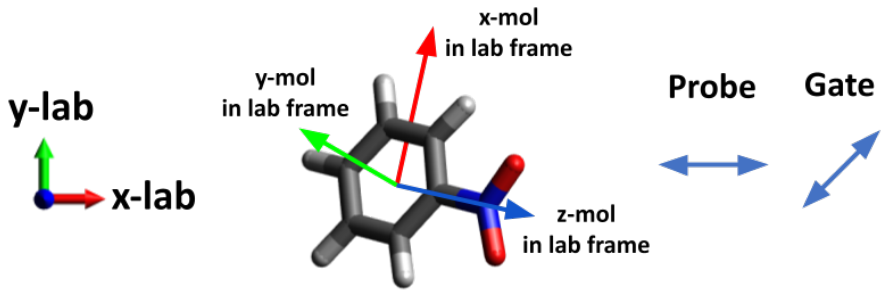


Figure 4.12: Recovered lab frame orientation of nitrobenzene from a 3-level orientationally averaged third order projected density matrix calculation of nitrobenzene. In this calculation the included states were $S_0$, $S_1$, and $S_2$ and the pulse duration was 15 fs. We note that here that to define the lab frame axes, $\hat{z}_{\text{lab}}$ is the pulse propagation axis, $\hat{x}_{\text{lab}}$ is aligned along the probe polarization axis, and $\hat{y}_{\text{lab}}$ is the analysing polarizer axis. To define the molecular frame axes, $\hat{z}_{mol}$ is along the CN bond axis, $\hat{y}_{mol}$ is normal to the plane of the ring, and $\hat{x}_{mol}$ is in the plane of the ring. The specific lab frame representation of the individual molecular axes are shown in table 4.4.

| lab frame $\hat{x}_{\text{mol}}$ | lab frame $\hat{y}_{\text{mol}}$ | lab frame $\hat{z}_{\text{mol}}$ |
|---|---|---|
| 0.34 | -0.55 | 0.76 |
| 0.93 | 0.30 | -0.20 |
| -0.12 | 0.78 | 0.61 |

Table 4.4: Here we show explicit representations of the molecular frame axes in the lab frame given the recovered orientation from a 3-level ($S_0$, $S_1$, and $S_2$) third order projected density matrix calculation with the incident IR pulses having full width half max pulse durations of 15 fs. We note that the definitions for the lab frame and molecular frame axes are the same as in figure 4.12.

frame calculation.

We note here that we observed a significant decrease in computational cost between the orientationally averaged calculation and the molecular frame calculation in both the 3-level (factor of 1000 decrease) and 5-level (factor of 500 decrease) cases. It's possible that these efficiency differences point to additional optimizations that can be made to the current iteration of the code, however in general, we would always expect the orientationally averaged calculation to take significantly longer then a molecular frame calculation using the recovered orientation of the molecule.

Additionally, in figure 4.12, we present the representative orientation of nitrobenzene in lab frame coordinates from the recovered orientation taken from of the 3-level model representation of nitrobenzene with 15 fs incident IR Gaussian pulses. The specific lab frame representations of the molecular frame axes of nitrobenzene are shown in table 4.4 where we define $\hat{z}_{mol}$ to be along the CN bond axis, $\hat{y}_{mol}$ to be normal to the plane of the ring, and $\hat{x}_{mol}$ to be in the plane of the ring. One might expect that since the population states have polarizations primarily along $\hat{z}_{mol}$ and

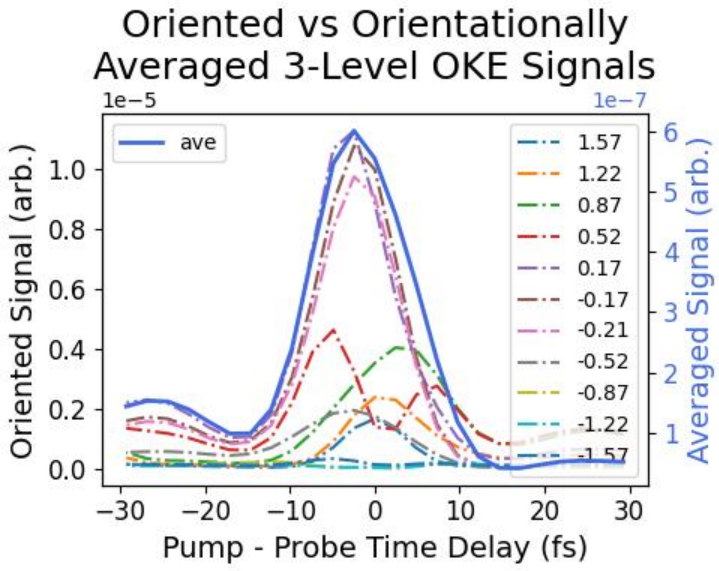


Figure 4.13: Here we compare the simulated molecular frame signal after scanning the third Euler angle $\theta_3$ to that of the orientationally averaged signal. We note here that the recovered $\theta_3$ from the orientationally averaged calculation is $-0.21 \pm 0.25$ radians. Additionally from these scans, the sampled angles from $-0.17$ to $0.21$ radians appear to have the greatest contribution to the signal and most closely match the shape of the orientationally averaged signal. The other Euler angles were fixed at 0.9573 radians and 1.2706 radians for $\theta_1$ and $\theta_2$ respectively.

since the preferred measurement axis is primarily along the lab frame y-axis, that the molecule would prefer to have the $\hat{z}_{mol}$ axis oriented along the y polarization axis. However, as can be seen in table A.4 the transition dipole moments of the coherences can have strong transitions mediated through the $\hat{x}_{mol}$ and $\hat{y}_{mol}$ axes. The contribution of these coherences to the measured polarizations is what shifts the representative orientation away from the expected lab frame y-axis orientation to the orientation depicted in figure 4.12.

To further validate the recovered orientation, we performed a scan of the third Euler angle $\theta_3$ from $-\pi$ to $\pi$ radians using the 3-level ($S_0$, $S_1$, and $S_2$) model of nitrobenzene with 15 fs FWHM incident IR pulses. The result of this scan can be seen in figure 4.13. As seen in this figure, the sampled $\theta_3$ angles near 0.17 to $-0.21$ radians tend to both have larger net contributions to the signal and they tend to qualitatively match the orientationally averaged signal better. Directly comparing the peak signal magnitudes around $\theta_3$ being equal to 0.17 to $-0.21$ radians to signals outside of the region, angles outside of that region have a factor of 2 to factor of 10 smaller peak magnitude compared to peaks around 0.17 to $-0.21$ radians. Here we note that the recovered $\theta_3$ in this case, has a value of $-0.21 \pm 0.25$ radians which appears to roughly align with the identified range.

To directly compare simulated 3$^{\text{rd}}$ order polarization sensitive measurements with experiment

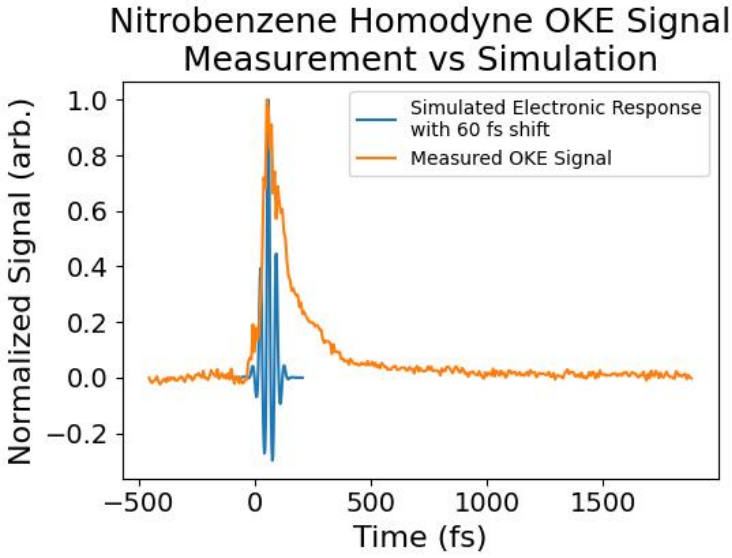


Figure 4.14: Comparison of a normalized homodyne OKE measurement of liquid nitrobenzene to that of the predicted 3rd order polarization response given due to the electronic dynamics in nitrobenzene. In this case, the simulated signal from the the recovered representative orientation of nitrobenzene, has also been normalized and shifted by 60 fs to match the peak amplitudes. We attribute this shift to potential errors in overlap measurement, but future work will needed to confirm this as the source of the shift.

we performed the following calculations. First using the 5-level recovered orientation of nitrobenzene in table 4.3, we computed the 3rd order polarization signal cross to the probe pulse orientation. Using this selected orientation, we extended the simulation time window to 400 fs and the FWHM pulse duration of the pair of IR pulses was extended from 30 fs to 40 fs to better match experimental conditions. To avoid clipping effects, we computed the signal from a set of time delays between $\pm$150 fs. This was then compared to the experimentally measured OKE signal of neat liquid nitrobenzene as measured in figure 2.3. The comparison between the simulation and measurement is shown in figure 4.14.

We additionally note the following regarding the third order simulation of the electronic component of the OKE signal of nitrobenzene. The raw simulation has a signal that peaks when the time delay is 0 and has a nonzero baseline, we additionally see periodic behaviour in the signal amplitude as a function of time delay. Some of these effects are due to limitations of the simulation method compared to experiment. In the experiment, the incident fields are not co-propagating perfectly along the same axis as each other and due to phase matching, we can select for the signal propagating along the probe axis. This is not implemented in the current code base and as such, we are sensitive to signals generated solely from third order interaction with the gate or would result from phase matching conditions that we would not be sensitive to experimentally. We would not

expect to be sensitive to third order interactions solely from the probe since the resulting polarization would be aligned along the lab frame x-axis and the crossed polarizer axis would reject this signal. However, since the gate polarization is 45° relative to the probe, the gate can result in a nonlinear signal that is independent of time delay. To account for this we subtracted the baseline from the simulated response when normalizing the computed signal. This is also a likely reason for the observed oscillations in signal magnitude which could be caused by relatively slow beating between the signals generated from different phase matching in the experiment all contributing to the signal in the simulation.

We additionally note that the peak of the simulated response differs from the measured OKE response by 60 fs. Potentially, this points to an experimental error in the determination of overlap where type II phase matching conditions were used to find overlap as apposed to type I conditions, given this difference, a 60 fs shift in time delay overlap could explained if the pulses meet 150 microns into the BBO sample. Additionally, this shift in time delay overlap is not reported in other literature OKE measurements of liquid nitrobenzene [66, 65].

We additionally note that, while the width of the simulated electronic response is roughly 80 fs which is consistent with other OKE measurements of the electronic response, the peak itself is highly symmetric about the peak. Given the conservative approach to setting the decay parameters and no inclusion of collisional dephasing, the observed symmetry in the rise and fall of the simulated peak could be due to these dephasing parameters being incorrect. Additionally, recent results from Walz et al. suggest that asymmetric line shapes as a function of time delay can be attributed to effects from phase matching [86].

# Chapter 5

# Future Directions

Over the previous chapters, we have demonstrated an experimental realization of ultrafast transient polarization spectroscopy and applied this technique to the study of excited state spectroscopic signals of nitrobenzene. We then presented a systematic method to simulate lab frame signals from the electronic component of the polarization using a parameterized n-level model of nitrobenzene. In the context of the projected density matrix, we were able to recover representative orientations of nitrobenzene that produce signals most closely representing the orientation-averaged signals in the laboratory frame. Here we discuss some of the possible future directions that are enabled by this work. First we discuss some of the future theoretical work such as potential avenues for extending the current simulation methods and in potential development of the projected density matrix formalism. Then we discuss some potential experimental directions including a proposed measurement scheme of the projected density matrix, and potential avenues to extend UTPS into XUV/x-ray energy regimes.

## 5.1 Future Theoretical Directions

### Extending the Perturbative Simulations

In principle, when considering the phase matching conditions of UTPS, the lowest order interaction that includes interactions with the resulting signal traveling along the probe direction is $k_{\text{sig}} = k_{\text{probe}} + k_{\text{gate}} - k_{\text{gate}} + k_{\text{pump}} - k_{\text{pump}}$. This suggests that the lowest order UTPS signal will be in general represented by $\chi^{(5)}$. However the current code base is only able to simulate up to third order responses. There are several options that can be taken to extend the capability of the current simulation methods to address this issue. One potential avenue to address this limitation avenue could be the inclusion of non-equilibrium states through linear and nonlinear pumping schemes. By including non-equilibrium states into the calculation, such a scheme may allow us to more appropriately simulate UTPS signals by simulating the general higher order interaction with a sequence of lower order interactions. This could allow for the efficient computation of orientationally averaged signals given a specific electronic excitation scheme.

One method to include these non-equilibrium states would be to follow the work of Agarwalla et al. [60] where the authors use a lower order of perturbation theory to compute an initial state of the density matrix after interaction with a number of fields. In effect, this allows the authors to compute effects from a higher order in perturbation theory as a sequence of lower order calculations. The method utilized by Agarwalla et al. mainly relied on computing the appropriate order correction to the density matrix in the molecular frame [60]. This suggests that by appropriately adapting the projected density matrix formalism we may be able to compute orientationally averaged signals from nonequilibrium states to more closely simulate the electronic response of UTPS measurements.

Another approach to more closely simulate higher order UTPS signals could be to simply extend the code base to compute higher orders of perturbation theory. While such a calculation is straight forward to implement for the molecular frame calculation, the lab frame case poses some difficulty. One barrier in implementation would be the need for exact solutions of static molecular frame $5^{\text{th}}$ order tensors under orientational averaging. Currently, solutions have been tabulated for orientational averaging up to $3^{\text{rd}}$ order [47, 137], so to treat the case of $5^{\text{th}}$ order signals from isotropic samples, one would need to derive these expressions for the orientationally averaged $5^{\text{th}}$ order tensor to avoid unnecessary orientational sampling. There is also a limitation in computational cost. As currently implemented, the perturbative calculation of $n^{\text{th}}$ order nonlinear signals is of order $(t/\delta)^n$ where $t$ is the length of the simulation and $\delta$ is the simulation step size. For a single set of time delays representing the nonparallelized portion of a calculation, on current hardware, the orientationally averaged third order signal can take over 24 hours to complete given a time window on the order of 100 fs wide, depending on the resolution. This suggests that the equivalent $5^{\text{th}}$ order calculation given the same time window and resolution could take take nearly a factor of 10 longer which on current hardware would take over 200 hours to complete. Even with this extra cost it still might be useful to implement this method, due to the relative simplicity in implementation and it's ability to be used as a reference method to cross check more approximate methods.

An additional factor that isn't currently taken into account is the lack of k-vector selectivity. In the simulations presented in section 4.5, because the spatial effects aren't explicitly taken into account, these simulated signals are not k-vector selective. In both OKE and UTPS measurements, the signal propagates along the probe propagation direction. However, since the field order is arbitrary, there can be signals that propagate along other directions, such as the gate or pump propagation directions. Such signals aren't detected in the experiment, but are detected in the simulation, because all of the propagation directions are degenerate in the simulation. To account for this we have a couple options. Firstly, in equation 4.32 we can follow the procedure as suggested by Dickson [39], where we can explicitly compute the time dependent polarization for a set of points in a sample volume. However, this fails to exploit the spatial periodicity of the resulting signal. Another option would be to incorporate phase matching conditions, by selecting for specific field interaction terms in the selected order in perturbation theory [36]. A third option could be to select for signals propagating along a specific axis in phase space, by sampling the incident output polarizations given spatial dependent phase shifts of the fields along the axis of interest. By sampling these incident fields and selecting for the spatially coherent component of

the sampled polarizations, we may be able to account for the phase matching conditions directly from simulation while also taking advantage of the spatial periodicity of the signal[35].

Since this code calculates nonlinear optical signals through perturbation theory, a natural extension of this code could be to include Feynman diagram selectivity. It has been shown that some 2D spectroscopic signals show a Feynman diagram dependence [100]. Additionally, methods for automatically calculating the nonlinear spectroscopic signals associated with the set of Feynman diagrams that can contribute to a signal have been implemented [103]. Adapting this method into the existing code base would allow for the calculation of polarization sensitive and Feynman diagram dependent nonlinear spectroscopic signals.

## Extending the Projected Density Matrix Formalism

In principle, the formalism of the projected density matrix can be extended in a couple of different ways. One limitation of the current projected density matrix formalism is that, in order to completely recover a representative molecular orientation, two separate projected density matrices with orthogonal preferred measurement axes need to be obtained. With these two projected density matrices we then make the assumption that the preferred orientation of a molecule is approximately the same for both preferred axes. However, given that the different output polarizations can result in the signal resulting from a different set of tensor elements of the $n^{th}$ order susceptibility, the two different preferred measurement axes could produce different representative molecular orientations. Mathematically, the reason a unique orientation is not completely determined from one projected density matrix is that the 3D unit vector describing the preferred orientation can be described with two degrees of freedom (essentially two different angles) whereas a rotation matrix is described using 3 degrees of freedom (3 Euler angles). This suggests that a version of the projected density matrix that represents a quadrupole sensitive measurement may include enough information to fully describe a representative orientation of a molecule.

Such quadrupole selective measurements, can be difficult and for measurements of the electric quadrupole moment typically involve the measurement of the sample's response due to an applied electric field gradient [141, 142]. Theoretically, the quadrupole field interaction contributes to a variety of spectroscopic signals [37]. However, a theoretical treatment [143] of the quadrupole contribution to 2D circularly polarized photon echo spectroscopy found that, for a set of peptides, the quadrupole contribution can be an order of magnitude weaker then the magnetic dipole contribution to the signal. A recent proposal [144] has suggested a scheme by which the magnetic quadrupole moment of a simple heavy molecular system could be measured by considering the response of a superposition of molecules to parallel incident electric and magnetic fields.

If such a quadrupole selective measurement scheme can be justified, this could potentially provide a means of determining a preferred molecular orientation directly from a determination of one projected density matrix where the preferred measurement axis is from a specific quadrupole moment.

Another direction that could be useful in extending these projected density matrix calculations would be to consider the case of anisotropic systems and how the addition of anisotropy could change the measured response. In considering the case of anisotropic systems we can potentially

connect this object to a wider set of measurements beyond solely the electronic response of a system. In particular, we can consider the result from considering anisotropic samples which could occur at surfaces [145] where the restricted degrees of freedom limit the possible orientations of relevant moieties. Additionally, by considering the effects of time evolution of an orientationally distribution through the lens of the projected density matrix, we can connect this object to the effects of induced anisotropy from molecular alignment in an electric field [47, 138] or librational motion [146, 147]. Additionally, comparison of the projected density matrix from an orientationally averaged isotropic sample, to an oriented sample, may provide a means of recovering a measure of anisotropy in such samples.

## Future Calculations

As implemented, the current simulation software allows for computation of polarization sensitive, time-delay dependent electronic signals with 3 separate pulses described by 2 sets of time-delays. Thus far we have applied this software to simple two level systems and nitrobenzene with the $NO_2$ group twisted 13° out of plane with the aim of computing polarization sensitive signals to OKE and UTPS measurements. In principle, this software package can be applied to the simulation of any polarization sensitive experiment that can be described with up to 3$^{\text{rd}}$ order in perturbation theory. Additionally, while the current simulation software is unable to exactly account for phase matching conditions, one potential way around this issue would be to consider the signals generated from sets of signals with different colors for each of the incident pulses. This suggests some directions for future calculations.

Initially, given the computed dipole transitions from planer $C_{2v}$ symmetric nitrobenzene, a good next set of calculations would be to compute polarization sensitive signals from this geometry of nitrobenzene. This could be particularly interesting given the symmetry of nitrobenzene in this geometry which may imprint some symmetry on the polarization sensitive signals. There have also been some calculations [71, 34] that suggest that the planer $C_{2v}$ symmetric geometry may be primarily responsible for the electronic signal after resonant excitation to the $S_2$ state. With a related set of calculations one could consider the addition of a resonant UV excitation pulse. Such pulses are readily accessible through the use of a tripler [148] and in our laboratory some polarization sensitive data with a UV pulse and two IR pulses has been taken.

Currently, we have only considered the case of homodyne OKE/UTPS measurements however changing the simulation configuration to consider the response from elliptically polarized pulses, or to change the orientation of the lab frame polarizer relative to the probe polarization axis. By performing a pair of simulations and subtracting the resulting signals, we could directly simulate the of out-of-phase and in-phase heterodyne OKE/UTPS signals. We can also consider modifying the chirp parameters of these input pulses which could allow for the computation of polarization sensitive spectroscopic measurements like chirped heterodyne OKE spectroscopy [149].

Lastly, we can also consider simply applying this software package to a different system. So long as the transitions from ground to excited state, and from excited state to excited state are appropriately parameterized, this software package is able to compute responses given appropriate parameterization. Currently, we parameterized this model by referencing electronic structure

calculations of nitrobenzene, however by preforming a similar set of calculations, we can use this model to represent the optical response from a number of molecules including systems like water or other benzene derivatives. For instance, one system that could prove interesting to explore could be a simpler system like $N_2$ or $H_2$. As these systems have simpler nuclear dynamics such a system could be convenient for testing extensions of this simulation method that incorporate nuclear dynamics. In principle larger systems or few-molecule systems systems, like hydration shells around a charged ion, could also be treated with this n-level model approach but appropriately parameterizing the dipole transitions between excited states could be expensive using the methods discussed in chapter 4.

## 5.2 Future Experimental Directions

### Measurement of the Projected Density Matrix

For all intents and purposes, the projected density matrix contains a representation of a density matrix and thus like a density matrix, such an object should be measurable. One approach to measure the density matrix of a molecule, as implemented using time resolved fluorescence [150] and ultrafast electron diffraction experiments [151] is to use time resolved experimental measurements of a probability distribution and it's derivative to determine a Wigner distribution which has a one-to-one mapping to the density matrix. Another approach to density matrix measurement is to consider it as a phase retrieval problem, in which an iterative algorithmic approach is use to recover the phase of the wavefunction given the constraints of a valid density matrix and time resolved electron diffraction measurements [152]. Additionally, if one is interested in the density matrix of light, these measurements have been made by making quadrature-amplitude measurements [153, 154] that allow for the determination of a Wigner distribution and thus the density matrix. More recently, measurements of a rotationally resolved lab frame density matrix of $NH_3$ has been made by recovering coefficients of molecular angular distribution moments given resonant enhanced multiphoton ionization measurements [155]. Given these prior density matrix measurements, it should be possible to find an analogous projected density matrix measurement method.

One approach that can be considered would be by using a determined set of dipole matrix elements with the assumption that there is only one preferred orientation that dominates a measured signal. From equation 4.57 the measured polarization signal will be proportional to the following expression.

$$\langle\langle \vec{\mu}_{mol} | \vec{\rho}_{proj} \rangle\rangle_{\text{ave}} = \langle\langle \vec{\mu}_{mol} | \cdot \int \mathbf{s}(\Omega) \otimes |\rho(\Omega)\rangle\rangle d\Omega \approx \langle\langle \vec{\mu}_{mol} | \cdot \tilde{\mathbf{s}} \otimes |\rho_{\text{approx}}\rangle\rangle \tag{5.1}$$

Note that for any lab frame defined preferred measurement axis $\hat{\mathbf{e}}^{pol}$ the projected density matrix can be written as

$$|\vec{\rho}_{proj}\rangle\rangle \approx \tilde{\mathbf{s}} \otimes |\rho_{\text{approx}}\rangle\rangle = \hat{\mathbf{e}}^{pol} \cdot \begin{pmatrix} R^{-1}\hat{\mathbf{e}}_x^{mol}|\rho\rangle\rangle \\ R^{-1}\hat{\mathbf{e}}_y^{mol}|\rho\rangle\rangle \\ R^{-1}\hat{\mathbf{e}}_z^{mol}|\rho\rangle\rangle \end{pmatrix} = \hat{\mathbf{e}}^{pol} \cdot |\vec{\rho}_{preproj}\rangle\rangle \tag{5.2}$$

with the term $|\vec{\rho}_{preproj}\rangle\rangle$ being independent of any given lab frame preferred measurement axis. Since, this term represents the projected density matrix, prior to the polarization signal being projected onto the preferred measurement axis, we call this factor the pre-projected density matrix.

In principle, if we consider every term in the pre-projected density matrix density matrix to be independent of every other term, this implies that there would be up to $9n(n+1)/2$ pre-projected density matrix elements that would need to be determined given that $n$ states play a role in the generation of the signal. Thus given $9n(n+1)/2$ separate polarization sensitive measurements, and accurate determinations of the appropriate $\mu_x$, $\mu_y$, and $\mu_z$ mediated transitions, one could potentially reconstruct an approximate rotationally averaged projected density matrix by performing a least squares fit of the pre-projected density matrix. Note that since this pre-projected density matrix also contains the density matrix, the transitions that resulted in that density matrix are also encoded in the pre-projected density matrix. Thus, any sufficiently angle resolved polarization measurement method should be able to recover the projected density matrix.

There are some limitations with this approach however, depending on the recovered orientation, and the symmetry of the transitions, there may be multiple mathematically valid reconstructions of the pre-projected density matrix. Additionally, over a 90° arc, a 4 state system could require a resolution of 1° or better in order to be determined. Thus, depending on the number of states involved in the dynamics of interest, the required angular resolution of the polarization could make a measurement infeasible. Additionally, since this approach assumes that there is only one dominant orientation of a molecular system, this approach would not be expected to be effective for systems with high degrees of molecular symmetry or for systems that rotate or align during the dynamical process that produces the signal of interest. However, more work is needed to determine the specific constraints of such a measurement.

## Extension of UTPS to XUV Energy Regimes

The development of ultrafast table top coherent XUV and x-ray sources [156] as well as intense coherent x-ray pulses at free electron lasers [157] has enabled the development of attosecond science [158] which has given researchers access to core shell dynamics as well a direct probe of charge transfer and charge migration processes in molecular systems. In the future, these sources are even expected to be provide enough sensitivity to see nonlinear spectroscopic effects in a variety of targets [159, 160, 161, 162]. The continued development of x-ray polarization optics [163, 164], as well as increased control of polarization state of these x-ray sources [165, 166], suggests several avenues of future research to extend UTPS into the XUV and x-ray regime. Here we discuss some of these future possibilities and some of the experimental challenges in realizing such an experiment.

One such natural extension of the UTPS experimental scheme is to consider the case of an XUV or x-ray pump pulse, and probing with a pair of optical pulses. This scheme presents itself with several natural advantages. First, depending on the excited state of interest, many of the near ionization threshold states and excited ionic states that can be generated from these pumping wavelengths, can be quite long lived. For instance, in $N_2$, time resolved studies of the near ionization states [167] measured lifetimes on the order of hundreds of picoseconds to nanoseconds. Related

studies of excited ionic states of $N_2$ [168] have measured excited state lifetimes on the order of tens of nanoseconds. These relatively long excited states relative to the pulse duration of available femtosecond/attosecond light sources suggest that the excitation process can be considered separately from the probing process and that the assumptions required to apply the UTPS formalism would be applicable for such states. Second, using a pair of optical probing pulses allows one to tap into existing high quality off-the-shelf polarization optics including the ultra-high contrast polarizers used in our first demonstration of the UTPS technique [61]. Such an experimental scheme would be particularly applicable in a tabletop XUV/soft x-ray source where leakage from the IR pulse that generated the XUV light through high harmonic generation [169], can be split and delayed separately from the generated XUV pulse to act as a coherent pair of probing pulses. With that said, there are proposals to integrate separate optical probes into free electron laser facilities [170, 171] which once implemented, could enable the application of UTPS as applied to states only accessible through these light sources.

Another approach that can be considered is the case of optical pump and XUV/x-ray probe. Because of the increased time resolution as well as the frequencies of the probing pulses, such an experimental scheme could be sensitive to a number of optically driven dynamics that would not be accessible through an optical probe scheme. One such example would be a direct probe of charge transfer dynamics in the proteins involved in photosynthesis such as Photosystems I and II. Previous studies of such dynamics in Photosystem II [172] used 2D electronic spectra to measure decay rates of <200 fs and $\tilde{1}$.5 ps which the authors associated with two separate electronic decay pathways. Additionally, recent results of Photosystem II from experiments at free electron lasers [173] have shown that there are two distinct protein confirmations in photosystem II. In principle, monitoring nonlinear x-ray spectra as a function of time delay of the optical excitation pulse could allow for the direct monitoring of these charge transfer dynamics.

However such a measurement scheme also presents itself with a number of technical challenges. One major limitation is the lack of many established nonlinear spectroscopic signals with x-ray free electron laser light sources. That being said, nonlinear x-ray interactions have been observed at x-ray free electron lasers with recent results [174] even demonstrating electronic state population transfer through an impulsive stimulated x-ray Raman scattering process. With that said, nonlinear x-ray spectroscopy methods like 2D coherent x-ray spectroscopy [162] and transient redistribution of ultrafast electronic coherences in attosecond Raman signals [159] have been proposed as methods that can elucidate some of these signals, but are still under development at this time.

# Appendix A

# Computed Dipole and Energy Level Transitions of Nitrobenzene

## A.1 Nitrobenzene In $C_{2v}$ Symmetric Ground State Geometry

Table A.1: Calculated singlet energy levels of nitrobenzene in planer ground state $C_{2v}$ symmetric geometry as calculated though 1$^{st}$ and 2$^{nd}$ order response theory calculations as implemented in the Dalton quantum chemistry software package.

| State | Symmetry | Energy (eV) |
|---|---|---|
| $S_0$ | $A_1$ | 0.0 |
| $S_1$ | $A_1$ | 4.078125376 |
| $S_2$ | $A_2$ | 4.402586832 |
| $S_3$ | $B_1$ | 4.54990312 |
| $S_4$ | $B_1$ | 4.694980032 |
| $S_5$ | $B_2$ | 4.766720847999999 |
| $S_6$ | $B_1$ | 5.028521392 |
| $S_7$ | $B_1$ | 5.29077808 |
| $S_8$ | $A_1$ | 5.308655279999999 |
| $S_9$ | $A_1$ | 6.5275656159999995 |
| $S_{10}$ | $A_1$ | 7.454652319999999 |
| $S_{11}$ | $B_1$ | 7.475949920000001 |
| $S_{12}$ | $B_1$ | 7.535815759999999 |
| $S_{13}$ | $A_1$ | 7.615821567999999 |
| $S_{14}$ | $A_1$ | 7.79218936 |
| $S_{15}$ | $A_2$ | 7.7949273119999996 |
| $S_{16}$ | $B_2$ | 7.914057872 |
| $S_{17}$ | $B_1$ | 8.037114208 |

| State | Symmetry | Energy (eV) |
|---|---|---|
| $S_{18}$ | $B_1$ | 8.043606303999999 |
| $S_{19}$ | $B_1$ | 8.122820864 |
| $S_{20}$ | $B_2$ | 8.367476432 |
| $S_{21}$ | $B_1$ | 8.546321872 |
| $S_{22}$ | $A_1$ | 8.580052319999998 |
| $S_{23}$ | $A_2$ | 8.62920544 |
| $S_{24}$ | $B_2$ | 8.708331328 |
| $S_{25}$ | $A_2$ | 8.88608768 |
| $S_{26}$ | $A_1$ | 8.894325744 |
| $S_{27}$ | $A_2$ | 8.970613584 |
| $S_{28}$ | $A_1$ | 9.152767359999999 |
| $S_{29}$ | $B_1$ | 9.157682672 |
| $S_{30}$ | $B_2$ | 9.230290624 |
| $S_{31}$ | $A_1$ | 9.291999808 |
| $S_{32}$ | $A_2$ | 9.306558063999999 |
| $S_{33}$ | $B_2$ | 9.448690304 |
| $S_{34}$ | $B_2$ | 9.5963096 |
| $S_{35}$ | $A_2$ | 9.597904336 |
| $S_{36}$ | $B_2$ | 9.716337216 |
| $S_{37}$ | $A_2$ | 9.834712976 |
| $S_{38}$ | $B_2$ | 9.866701264 |
| $S_{39}$ | $A_1$ | 9.978627904 |
| $S_{40}$ | $A_2$ | 10.037657344 |
| $S_{41}$ | $A_2$ | 10.166617984 |
| $S_{42}$ | $A_2$ | 10.412013936000001 |
| $S_{43}$ | $B_2$ | 10.615077984 |
| $S_{44}$ | $B_2$ | 10.681055936 |

Table A.2: Singlet to Singlet dipole transitions of nitrobenzene from in planer ground state $C_{2v}$ symmetric geometry as calculated though 1st and 2nd order response theory calculations as implemented in the Dalton quantum chemistry software package. Here $S_{\text{init}}$ and $S_{\text{final}}$ are used to represent the initial and final states of a dipole mediated transition, and $\mu_x$, $\mu_y$, $\mu_z$ represent the strength of the dipole transition in atomic units.

| $S_{\text{init}}$ | $S_{\text{final}}$ | $\mu_x$ | $\mu_y$ | $\mu_z$ |
|---|---|---|---|---|
| $S_0$ | $S_0$ | 0.0 | 0.0 | -1.65568481 |
| $S_0$ | $S_1$ | 0.0 | 0.0 | 8.79e-14 |
| $S_0$ | $S_2$ | 0.0 | 0.0 | 0.0 |
| $S_0$ | $S_3$ | -0.056396416 | 0.0 | 0.0 |

| $S_{\text{init}}$ | $S_{\text{final}}$ | $\mu_x$ | $\mu_y$ | $\mu_z$ |
|---|---|---|---|---|
| $S_0$ | $S_4$ | -2.31e-14 | 0.0 | 0.0 |
| $S_0$ | $S_5$ | 0.0 | -0.05474994 | 0.0 |
| $S_0$ | $S_6$ | 1.0340975 | 0.0 | 0.0 |
| $S_0$ | $S_7$ | 2.24e-13 | 0.0 | 0.0 |
| $S_0$ | $S_8$ | 0.0 | 0.0 | 1.59e-13 |
| $S_0$ | $S_9$ | 0.0 | 0.0 | -1.1507304 |
| $S_0$ | $S_{10}$ | 0.0 | 0.0 | -1.08e-13 |
| $S_0$ | $S_{11}$ | -3.31e-13 | 0.0 | 0.0 |
| $S_0$ | $S_{12}$ | -1.4312231 | 0.0 | 0.0 |
| $S_0$ | $S_{13}$ | 0.0 | 0.0 | -1.6951899 |
| $S_0$ | $S_{14}$ | 0.0 | 0.0 | 0.3543636 |
| $S_0$ | $S_{15}$ | 0.0 | 0.0 | 0.0 |
| $S_0$ | $S_{16}$ | 0.0 | 0.33398909 | 0.0 |
| $S_0$ | $S_{17}$ | -5.56e-13 | 0.0 | 0.0 |
| $S_0$ | $S_{18}$ | 0.26802037 | 0.0 | 0.0 |
| $S_0$ | $S_{19}$ | 1.0014635 | 0.0 | 0.0 |
| $S_0$ | $S_{20}$ | 0.0 | -0.40811402 | 0.0 |
| $S_0$ | $S_{21}$ | -1.36e-14 | 0.0 | 0.0 |
| $S_0$ | $S_{22}$ | 0.0 | 0.0 | 0.42989645 |
| $S_0$ | $S_{23}$ | 0.0 | 0.0 | 0.0 |
| $S_0$ | $S_{24}$ | 0.0 | 0.11297427 | 0.0 |
| $S_0$ | $S_{25}$ | 0.0 | 0.0 | 0.0 |
| $S_0$ | $S_{26}$ | 0.0 | 0.0 | 0.35816647 |
| $S_0$ | $S_{27}$ | 0.0 | 0.0 | 0.0 |
| $S_0$ | $S_{28}$ | 0.0 | 0.0 | 9.11e-06 |
| $S_0$ | $S_{29}$ | 0.12135457 | 0.0 | 0.0 |
| $S_0$ | $S_{30}$ | 0.0 | -0.12430957 | 0.0 |
| $S_0$ | $S_{31}$ | 0.0 | 0.0 | 0.1551809 |
| $S_0$ | $S_{32}$ | 0.0 | 0.0 | 0.0 |
| $S_0$ | $S_{33}$ | 0.0 | 0.089432572 | 0.0 |
| $S_0$ | $S_{34}$ | 0.0 | 0.14071966 | 0.0 |
| $S_0$ | $S_{35}$ | 0.0 | 0.0 | 0.0 |
| $S_0$ | $S_{36}$ | 0.0 | -0.15787347 | 0.0 |
| $S_0$ | $S_{37}$ | 0.0 | 0.0 | 0.0 |
| $S_0$ | $S_{38}$ | 0.0 | -0.099872701 | 0.0 |
| $S_0$ | $S_{39}$ | 0.0 | 0.0 | -0.014518617 |
| $S_0$ | $S_{40}$ | 0.0 | 0.0 | 0.0 |
| $S_0$ | $S_{41}$ | 0.0 | 0.0 | 0.0 |
| $S_0$ | $S_{42}$ | 0.0 | 0.0 | 0.0 |
| $S_0$ | $S_{43}$ | 0.0 | 0.48888005 | 0.0 |

| $S_{\text{init}}$ | $S_{\text{final}}$ | $\mu_x$ | $\mu_y$ | $\mu_z$ |
|---|---|---|---|---|
| $S_0$ | $S_{44}$ | 0.0 | 0.6128152 | 0.0 |
| $S_1$ | $S_0$ | 0.0 | 0.0 | 8.79e-14 |
| $S_1$ | $S_1$ | 0.0 | 0.0 | -1.66438708 |
| $S_1$ | $S_2$ | 0.0 | 0.0 | 0.0 |
| $S_1$ | $S_3$ | 6.06e-05 | 0.0 | 0.0 |
| $S_1$ | $S_4$ | -0.20545412 | 0.0 | 0.0 |
| $S_1$ | $S_5$ | 0.0 | -1e-08 | 0.0 |
| $S_1$ | $S_6$ | -0.00044792 | 0.0 | 0.0 |
| $S_1$ | $S_7$ | 0.16000613 | 0.0 | 0.0 |
| $S_1$ | $S_8$ | 0.0 | 0.0 | 0.10028309 |
| $S_1$ | $S_9$ | 0.0 | 0.0 | -7e-08 |
| $S_1$ | $S_{10}$ | 0.0 | 0.0 | 0.09722287 |
| $S_1$ | $S_{11}$ | -0.06732052 | 0.0 | 0.0 |
| $S_1$ | $S_{12}$ | -9.54e-05 | 0.0 | 0.0 |
| $S_1$ | $S_{13}$ | 0.0 | 0.0 | 4e-08 |
| $S_1$ | $S_{14}$ | 0.0 | 0.0 | -1e-07 |
| $S_1$ | $S_{15}$ | 0.0 | 0.0 | 0.0 |
| $S_1$ | $S_{16}$ | 0.0 | 0.0 | 0.0 |
| $S_1$ | $S_{17}$ | 0.02173414 | 0.0 | 0.0 |
| $S_1$ | $S_{18}$ | 0.00021788 | 0.0 | 0.0 |
| $S_1$ | $S_{19}$ | -1.05e-06 | 0.0 | 0.0 |
| $S_1$ | $S_{20}$ | 0.0 | 1e-08 | 0.0 |
| $S_1$ | $S_{21}$ | -1.07684047 | 0.0 | 0.0 |
| $S_1$ | $S_{22}$ | 0.0 | 0.0 | -1.2e-07 |
| $S_1$ | $S_{23}$ | 0.0 | 0.0 | 0.0 |
| $S_1$ | $S_{24}$ | 0.0 | -4e-08 | 0.0 |
| $S_1$ | $S_{25}$ | 0.0 | 0.0 | 0.0 |
| $S_1$ | $S_{26}$ | 0.0 | 0.0 | 1.13e-06 |
| $S_1$ | $S_{27}$ | 0.0 | 0.0 | 0.0 |
| $S_1$ | $S_{28}$ | 0.0 | 0.0 | 0.0 |
| $S_1$ | $S_{29}$ | 0.00045583 | 0.0 | 0.0 |
| $S_1$ | $S_{30}$ | 0.0 | 0.0 | 0.0 |
| $S_1$ | $S_{31}$ | 0.0 | 0.0 | -9.7e-07 |
| $S_1$ | $S_{32}$ | 0.0 | 0.0 | 0.0 |
| $S_1$ | $S_{33}$ | 0.0 | 2e-08 | 0.0 |
| $S_1$ | $S_{34}$ | 0.0 | 0.0 | 0.0 |
| $S_1$ | $S_{35}$ | 0.0 | 0.0 | 0.0 |
| $S_1$ | $S_{36}$ | 0.0 | -4e-08 | 0.0 |
| $S_1$ | $S_{37}$ | 0.0 | 0.0 | 0.0 |
| $S_1$ | $S_{38}$ | 0.0 | 5e-08 | 0.0 |

| $S_{\text{init}}$ | $S_{\text{final}}$ | $\mu_x$ | $\mu_y$ | $\mu_z$ |
|---|---|---|---|---|
| $S_1$ | $S_{39}$ | 0.0 | 0.0 | 1.8e-07 |
| $S_1$ | $S_{40}$ | 0.0 | 0.0 | 0.0 |
| $S_1$ | $S_{41}$ | 0.0 | 0.0 | 0.0 |
| $S_1$ | $S_{42}$ | 0.0 | 0.0 | 0.0 |
| $S_1$ | $S_{43}$ | 0.0 | -2e-08 | 0.0 |
| $S_1$ | $S_{44}$ | 0.0 | -1.1e-07 | 0.0 |
| $S_2$ | $S_0$ | 0.0 | 0.0 | 0.0 |
| $S_2$ | $S_1$ | 0.0 | 0.0 | 0.0 |
| $S_2$ | $S_2$ | 0.0 | 0.0 | -2.2806388 |
| $S_2$ | $S_3$ | 0.0 | 0.00075088 | 0.0 |
| $S_2$ | $S_4$ | 0.0 | 8e-08 | 0.0 |
| $S_2$ | $S_5$ | 1.15884729 | 0.0 | 0.0 |
| $S_2$ | $S_6$ | 0.0 | -0.02334204 | 0.0 |
| $S_2$ | $S_7$ | 0.0 | -1e-08 | 0.0 |
| $S_2$ | $S_8$ | 0.0 | 0.0 | 0.0 |
| $S_2$ | $S_9$ | 0.0 | 0.0 | 0.0 |
| $S_2$ | $S_{10}$ | 0.0 | 0.0 | 0.0 |
| $S_2$ | $S_{11}$ | 0.0 | 3e-08 | 0.0 |
| $S_2$ | $S_{12}$ | 0.0 | -0.01048305 | 0.0 |
| $S_2$ | $S_{13}$ | 0.0 | 0.0 | 0.0 |
| $S_2$ | $S_{14}$ | 0.0 | 0.0 | 0.0 |
| $S_2$ | $S_{15}$ | 0.0 | 0.0 | 0.00341002 |
| $S_2$ | $S_{16}$ | 0.0032621 | 0.0 | 0.0 |
| $S_2$ | $S_{17}$ | 0.0 | 0.0 | 0.0 |
| $S_2$ | $S_{18}$ | 0.0 | 0.00111904 | 0.0 |
| $S_2$ | $S_{19}$ | 0.0 | 0.00435573 | 0.0 |
| $S_2$ | $S_{20}$ | -0.0041803 | 0.0 | 0.0 |
| $S_2$ | $S_{21}$ | 0.0 | -1.8e-07 | 0.0 |
| $S_2$ | $S_{22}$ | 0.0 | 0.0 | 0.0 |
| $S_2$ | $S_{23}$ | 0.0 | 0.0 | -0.00641344 |
| $S_2$ | $S_{24}$ | -0.00112696 | 0.0 | 0.0 |
| $S_2$ | $S_{25}$ | 0.0 | 0.0 | 0.00326279 |
| $S_2$ | $S_{26}$ | 0.0 | 0.0 | 0.0 |
| $S_2$ | $S_{27}$ | 0.0 | 0.0 | -0.00563205 |
| $S_2$ | $S_{28}$ | 0.0 | 0.0 | 0.0 |
| $S_2$ | $S_{29}$ | 0.0 | 0.00788064 | 0.0 |
| $S_2$ | $S_{30}$ | 0.2102812 | 0.0 | 0.0 |
| $S_2$ | $S_{31}$ | 0.0 | 0.0 | 0.0 |
| $S_2$ | $S_{32}$ | 0.0 | 0.0 | -0.10914128 |
| $S_2$ | $S_{33}$ | -3.63905489 | 0.0 | 0.0 |

| $S_{\text{init}}$ | $S_{\text{final}}$ | $\mu_x$ | $\mu_y$ | $\mu_z$ |
|---|---|---|---|---|
| $S_2$ | $S_{34}$ | -0.75972659 | 0.0 | 0.0 |
| $S_2$ | $S_{35}$ | 0.0 | 0.0 | -0.00223599 |
| $S_2$ | $S_{36}$ | -0.34139901 | 0.0 | 0.0 |
| $S_2$ | $S_{37}$ | 0.0 | 0.0 | 0.0163813 |
| $S_2$ | $S_{38}$ | 0.18134976 | 0.0 | 0.0 |
| $S_2$ | $S_{39}$ | 0.0 | 0.0 | 0.0 |
| $S_2$ | $S_{40}$ | 0.0 | 0.0 | 0.12977326 |
| $S_2$ | $S_{41}$ | 0.0 | 0.0 | -0.45434527 |
| $S_2$ | $S_{42}$ | 0.0 | 0.0 | -0.27125127 |
| $S_2$ | $S_{43}$ | 0.00453275 | 0.0 | 0.0 |
| $S_2$ | $S_{44}$ | -0.03161371 | 0.0 | 0.0 |
| $S_3$ | $S_0$ | -0.056396416 | 0.0 | 0.0 |
| $S_3$ | $S_1$ | 6.06e-05 | 0.0 | 0.0 |
| $S_3$ | $S_2$ | 0.0 | 0.00075088 | 0.0 |
| $S_3$ | $S_3$ | 0.0 | 0.0 | -1.505958 |
| $S_3$ | $S_4$ | 0.0 | 0.0 | 1.2e-07 |
| $S_3$ | $S_5$ | 0.0 | 0.0 | 0.0 |
| $S_3$ | $S_6$ | 0.0 | 0.0 | -0.14913614 |
| $S_3$ | $S_7$ | 0.0 | 0.0 | 5.4e-07 |
| $S_3$ | $S_8$ | -2.45e-05 | 0.0 | 0.0 |
| $S_3$ | $S_9$ | -0.07859916 | 0.0 | 0.0 |
| $S_3$ | $S_{10}$ | 1.07e-05 | 0.0 | 0.0 |
| $S_3$ | $S_{11}$ | 0.0 | 0.0 | 8.5e-07 |
| $S_3$ | $S_{12}$ | 0.0 | 0.0 | 0.52041003 |
| $S_3$ | $S_{13}$ | -0.00728764 | 0.0 | 0.0 |
| $S_3$ | $S_{14}$ | -0.11844719 | 0.0 | 0.0 |
| $S_3$ | $S_{15}$ | 0.0 | -0.109404 | 0.0 |
| $S_3$ | $S_{16}$ | 0.0 | 0.0 | 0.0 |
| $S_3$ | $S_{17}$ | 0.0 | 0.0 | 1.42e-06 |
| $S_3$ | $S_{18}$ | 0.0 | 0.0 | 0.17104704 |
| $S_3$ | $S_{19}$ | 0.0 | 0.0 | -0.200965 |
| $S_3$ | $S_{20}$ | 0.0 | 0.0 | 0.0 |
| $S_3$ | $S_{21}$ | 0.0 | 0.0 | -9.9e-07 |
| $S_3$ | $S_{22}$ | 0.82506097 | 0.0 | 0.0 |
| $S_3$ | $S_{23}$ | 0.0 | 0.22850685 | 0.0 |
| $S_3$ | $S_{24}$ | 0.0 | 0.0 | 0.0 |
| $S_3$ | $S_{25}$ | 0.0 | -0.08125627 | 0.0 |
| $S_3$ | $S_{26}$ | 0.40269755 | 0.0 | 0.0 |
| $S_3$ | $S_{27}$ | 0.0 | 0.13465421 | 0.0 |
| $S_3$ | $S_{28}$ | -0.00101797 | 0.0 | 0.0 |

| $S_{\text{init}}$ | $S_{\text{final}}$ | $\mu_x$ | $\mu_y$ | $\mu_z$ |
|---|---|---|---|---|
| $S_3$ | $S_{29}$ | 0.0 | 0.0 | -0.09795714 |
| $S_3$ | $S_{30}$ | 0.0 | 0.0 | 0.0 |
| $S_3$ | $S_{31}$ | 0.069526 | 0.0 | 0.0 |
| $S_3$ | $S_{32}$ | 0.0 | -0.27046693 | 0.0 |
| $S_3$ | $S_{33}$ | 0.0 | 0.0 | 0.0 |
| $S_3$ | $S_{34}$ | 0.0 | 0.0 | 0.0 |
| $S_3$ | $S_{35}$ | 0.0 | 0.21976406 | 0.0 |
| $S_3$ | $S_{36}$ | 0.0 | 0.0 | 0.0 |
| $S_3$ | $S_{37}$ | 0.0 | 0.01408031 | 0.0 |
| $S_3$ | $S_{38}$ | 0.0 | 0.0 | 0.0 |
| $S_3$ | $S_{39}$ | 0.36096969 | 0.0 | 0.0 |
| $S_3$ | $S_{40}$ | 0.0 | 0.00687869 | 0.0 |
| $S_3$ | $S_{41}$ | 0.0 | -0.00328068 | 0.0 |
| $S_3$ | $S_{42}$ | 0.0 | -0.06112969 | 0.0 |
| $S_3$ | $S_{43}$ | 0.0 | 0.0 | 0.0 |
| $S_3$ | $S_{44}$ | 0.0 | 0.0 | 0.0 |
| $S_4$ | $S_0$ | -2.31e-14 | 0.0 | 0.0 |
| $S_4$ | $S_1$ | -0.20545412 | 0.0 | 0.0 |
| $S_4$ | $S_2$ | 0.0 | 8e-08 | 0.0 |
| $S_4$ | $S_3$ | 0.0 | 0.0 | 1.2e-07 |
| $S_4$ | $S_4$ | 0.0 | 0.0 | -2.86744137 |
| $S_4$ | $S_5$ | 0.0 | 0.0 | 0.0 |
| $S_4$ | $S_6$ | 0.0 | 0.0 | -2.2e-07 |
| $S_4$ | $S_7$ | 0.0 | 0.0 | 0.14835982 |
| $S_4$ | $S_8$ | -0.19282368 | 0.0 | 0.0 |
| $S_4$ | $S_9$ | 0.00018906 | 0.0 | 0.0 |
| $S_4$ | $S_{10}$ | 0.46023443 | 0.0 | 0.0 |
| $S_4$ | $S_{11}$ | 0.0 | 0.0 | 0.08766735 |
| $S_4$ | $S_{12}$ | 0.0 | 0.0 | 1.9e-07 |
| $S_4$ | $S_{13}$ | -0.00011341 | 0.0 | 0.0 |
| $S_4$ | $S_{14}$ | -2.88e-05 | 0.0 | 0.0 |
| $S_4$ | $S_{15}$ | 0.0 | -1e-08 | 0.0 |
| $S_4$ | $S_{16}$ | 0.0 | 0.0 | 0.0 |
| $S_4$ | $S_{17}$ | 0.0 | 0.0 | -0.08532609 |
| $S_4$ | $S_{18}$ | 0.0 | 0.0 | -8e-07 |
| $S_4$ | $S_{19}$ | 0.0 | 0.0 | -3.4e-07 |
| $S_4$ | $S_{20}$ | 0.0 | 0.0 | 0.0 |
| $S_4$ | $S_{21}$ | 0.0 | 0.0 | -0.03341141 |
| $S_4$ | $S_{22}$ | -7.15e-05 | 0.0 | 0.0 |
| $S_4$ | $S_{23}$ | 0.0 | 1e-08 | 0.0 |

| $S_{\text{init}}$ | $S_{\text{final}}$ | $\mu_x$ | $\mu_y$ | $\mu_z$ |
|---|---|---|---|---|
| $S_4$ | $S_{24}$ | 0.0 | 0.0 | 0.0 |
| $S_4$ | $S_{25}$ | 0.0 | 0.0 | 0.0 |
| $S_4$ | $S_{26}$ | 0.00026817 | 0.0 | 0.0 |
| $S_4$ | $S_{27}$ | 0.0 | 0.0 | 0.0 |
| $S_4$ | $S_{28}$ | 2e-08 | 0.0 | 0.0 |
| $S_4$ | $S_{29}$ | 0.0 | 0.0 | 0.0 |
| $S_4$ | $S_{30}$ | 0.0 | 0.0 | 0.0 |
| $S_4$ | $S_{31}$ | -0.00037081 | 0.0 | 0.0 |
| $S_4$ | $S_{32}$ | 0.0 | -1.3e-07 | 0.0 |
| $S_4$ | $S_{33}$ | 0.0 | 0.0 | 0.0 |
| $S_4$ | $S_{34}$ | 0.0 | 0.0 | 0.0 |
| $S_4$ | $S_{35}$ | 0.0 | 1e-08 | 0.0 |
| $S_4$ | $S_{36}$ | 0.0 | 0.0 | 0.0 |
| $S_4$ | $S_{37}$ | 0.0 | 2e-08 | 0.0 |
| $S_4$ | $S_{38}$ | 0.0 | 0.0 | 0.0 |
| $S_4$ | $S_{39}$ | -0.00030318 | 0.0 | 0.0 |
| $S_4$ | $S_{40}$ | 0.0 | -3e-08 | 0.0 |
| $S_4$ | $S_{41}$ | 0.0 | 1.1e-07 | 0.0 |
| $S_4$ | $S_{42}$ | 0.0 | -8e-08 | 0.0 |
| $S_4$ | $S_{43}$ | 0.0 | 0.0 | 0.0 |
| $S_4$ | $S_{44}$ | 0.0 | 0.0 | 0.0 |
| $S_5$ | $S_0$ | 0.0 | -0.05474994 | 0.0 |
| $S_5$ | $S_1$ | 0.0 | -1e-08 | 0.0 |
| $S_5$ | $S_2$ | 1.15884729 | 0.0 | 0.0 |
| $S_5$ | $S_3$ | 0.0 | 0.0 | 0.0 |
| $S_5$ | $S_4$ | 0.0 | 0.0 | 0.0 |
| $S_5$ | $S_5$ | 0.0 | 0.0 | -2.22515025 |
| $S_5$ | $S_6$ | 0.0 | 0.0 | 0.0 |
| $S_5$ | $S_7$ | 0.0 | 0.0 | 0.0 |
| $S_5$ | $S_8$ | 0.0 | 1e-08 | 0.0 |
| $S_5$ | $S_9$ | 0.0 | -0.00230065 | 0.0 |
| $S_5$ | $S_{10}$ | 0.0 | -8e-08 | 0.0 |
| $S_5$ | $S_{11}$ | 0.0 | 0.0 | 0.0 |
| $S_5$ | $S_{12}$ | 0.0 | 0.0 | 0.0 |
| $S_5$ | $S_{13}$ | 0.0 | -0.00138134 | 0.0 |
| $S_5$ | $S_{14}$ | 0.0 | 0.00522468 | 0.0 |
| $S_5$ | $S_{15}$ | -0.00673943 | 0.0 | 0.0 |
| $S_5$ | $S_{16}$ | 0.0 | 0.0 | 0.00498287 |
| $S_5$ | $S_{17}$ | 0.0 | 0.0 | 0.0 |
| $S_5$ | $S_{18}$ | 0.0 | 0.0 | 0.0 |

| $S_{\text{init}}$ | $S_{\text{final}}$ | $\mu_x$ | $\mu_y$ | $\mu_z$ |
|---|---|---|---|---|
| $S_5$ | $S_{19}$ | 0.0 | 0.0 | 0.0 |
| $S_5$ | $S_{20}$ | 0.0 | 0.0 | 0.00313974 |
| $S_5$ | $S_{21}$ | 0.0 | 0.0 | 0.0 |
| $S_5$ | $S_{22}$ | 0.0 | 0.00446851 | 0.0 |
| $S_5$ | $S_{23}$ | -0.00310139 | 0.0 | 0.0 |
| $S_5$ | $S_{24}$ | 0.0 | 0.0 | -0.00732068 |
| $S_5$ | $S_{25}$ | 0.00101141 | 0.0 | 0.0 |
| $S_5$ | $S_{26}$ | 0.0 | -0.00259816 | 0.0 |
| $S_5$ | $S_{27}$ | 0.02133952 | 0.0 | 0.0 |
| $S_5$ | $S_{28}$ | 0.0 | -1.53e-05 | 0.0 |
| $S_5$ | $S_{29}$ | 0.0 | 0.0 | 0.0 |
| $S_5$ | $S_{30}$ | 0.0 | 0.0 | -0.02782557 |
| $S_5$ | $S_{31}$ | 0.0 | -0.01245941 | 0.0 |
| $S_5$ | $S_{32}$ | 0.02560625 | 0.0 | 0.0 |
| $S_5$ | $S_{33}$ | 0.0 | 0.0 | 0.00728102 |
| $S_5$ | $S_{34}$ | 0.0 | 0.0 | -0.08067379 |
| $S_5$ | $S_{35}$ | -0.00640241 | 0.0 | 0.0 |
| $S_5$ | $S_{36}$ | 0.0 | 0.0 | -0.06249239 |
| $S_5$ | $S_{37}$ | -0.29662635 | 0.0 | 0.0 |
| $S_5$ | $S_{38}$ | 0.0 | 0.0 | 0.06806973 |
| $S_5$ | $S_{39}$ | 0.0 | -0.00073808 | 0.0 |
| $S_5$ | $S_{40}$ | -0.5216897 | 0.0 | 0.0 |
| $S_5$ | $S_{41}$ | 0.11998352 | 0.0 | 0.0 |
| $S_5$ | $S_{42}$ | 0.01663566 | 0.0 | 0.0 |
| $S_5$ | $S_{43}$ | 0.0 | 0.0 | 0.01683917 |
| $S_5$ | $S_{44}$ | 0.0 | 0.0 | -0.36756218 |
| $S_6$ | $S_0$ | 1.0340975 | 0.0 | 0.0 |
| $S_6$ | $S_1$ | -0.00044792 | 0.0 | 0.0 |
| $S_6$ | $S_2$ | 0.0 | -0.02334204 | 0.0 |
| $S_6$ | $S_3$ | 0.0 | 0.0 | -0.14913614 |
| $S_6$ | $S_4$ | 0.0 | 0.0 | -2.2e-07 |
| $S_6$ | $S_5$ | 0.0 | 0.0 | 0.0 |
| $S_6$ | $S_6$ | 0.0 | 0.0 | -0.98594977 |
| $S_6$ | $S_7$ | 0.0 | 0.0 | -1.1e-07 |
| $S_6$ | $S_8$ | -0.00013785 | 0.0 | 0.0 |
| $S_6$ | $S_9$ | 0.98060848 | 0.0 | 0.0 |
| $S_6$ | $S_{10}$ | -9.72e-05 | 0.0 | 0.0 |
| $S_6$ | $S_{11}$ | 0.0 | 0.0 | -1.45e-06 |
| $S_6$ | $S_{12}$ | 0.0 | 0.0 | 0.04214257 |
| $S_6$ | $S_{13}$ | -0.73603536 | 0.0 | 0.0 |

| $S_{\text{init}}$ | $S_{\text{final}}$ | $\mu_x$ | $\mu_y$ | $\mu_z$ |
|---|---|---|---|---|
| $S_6$ | $S_{14}$ | -0.3327061 | 0.0 | 0.0 |
| $S_6$ | $S_{15}$ | 0.0 | 0.04459811 | 0.0 |
| $S_6$ | $S_{16}$ | 0.0 | 0.0 | 0.0 |
| $S_6$ | $S_{17}$ | 0.0 | 0.0 | -5.71e-06 |
| $S_6$ | $S_{18}$ | 0.0 | 0.0 | -0.78432778 |
| $S_6$ | $S_{19}$ | 0.0 | 0.0 | -0.09765134 |
| $S_6$ | $S_{20}$ | 0.0 | 0.0 | 0.0 |
| $S_6$ | $S_{21}$ | 0.0 | 0.0 | -7.92e-06 |
| $S_6$ | $S_{22}$ | -0.95001385 | 0.0 | 0.0 |
| $S_6$ | $S_{23}$ | 0.0 | -0.03502104 | 0.0 |
| $S_6$ | $S_{24}$ | 0.0 | 0.0 | 0.0 |
| $S_6$ | $S_{25}$ | 0.0 | 0.03215045 | 0.0 |
| $S_6$ | $S_{26}$ | 2.67227019 | 0.0 | 0.0 |
| $S_6$ | $S_{27}$ | 0.0 | 0.00838117 | 0.0 |
| $S_6$ | $S_{28}$ | 0.00417707 | 0.0 | 0.0 |
| $S_6$ | $S_{29}$ | 0.0 | 0.0 | 0.03100295 |
| $S_6$ | $S_{30}$ | 0.0 | 0.0 | 0.0 |
| $S_6$ | $S_{31}$ | -1.3971058 | 0.0 | 0.0 |
| $S_6$ | $S_{32}$ | 0.0 | 0.04787316 | 0.0 |
| $S_6$ | $S_{33}$ | 0.0 | 0.0 | 0.0 |
| $S_6$ | $S_{34}$ | 0.0 | 0.0 | 0.0 |
| $S_6$ | $S_{35}$ | 0.0 | 0.11869513 | 0.0 |
| $S_6$ | $S_{36}$ | 0.0 | 0.0 | 0.0 |
| $S_6$ | $S_{37}$ | 0.0 | -0.05298093 | 0.0 |
| $S_6$ | $S_{38}$ | 0.0 | 0.0 | 0.0 |
| $S_6$ | $S_{39}$ | 5.71798923 | 0.0 | 0.0 |
| $S_6$ | $S_{40}$ | 0.0 | -0.0406418 | 0.0 |
| $S_6$ | $S_{41}$ | 0.0 | 0.08012559 | 0.0 |
| $S_6$ | $S_{42}$ | 0.0 | 0.46330796 | 0.0 |
| $S_6$ | $S_{43}$ | 0.0 | 0.0 | 0.0 |
| $S_6$ | $S_{44}$ | 0.0 | 0.0 | 0.0 |
| $S_7$ | $S_0$ | 2.24e-13 | 0.0 | 0.0 |
| $S_7$ | $S_1$ | 0.16000613 | 0.0 | 0.0 |
| $S_7$ | $S_2$ | 0.0 | -1e-08 | 0.0 |
| $S_7$ | $S_3$ | 0.0 | 0.0 | 5.4e-07 |
| $S_7$ | $S_4$ | 0.0 | 0.0 | 0.14835982 |
| $S_7$ | $S_5$ | 0.0 | 0.0 | 0.0 |
| $S_7$ | $S_6$ | 0.0 | 0.0 | -1.1e-07 |
| $S_7$ | $S_7$ | 0.0 | 0.0 | -1.55004782 |
| $S_7$ | $S_8$ | 0.01338481 | 0.0 | 0.0 |

| $S_{\text{init}}$ | $S_{\text{final}}$ | $\mu_x$ | $\mu_y$ | $\mu_z$ |
|---|---|---|---|---|
| $S_7$ | $S_9$ | -4.7e-05 | 0.0 | 0.0 |
| $S_7$ | $S_{10}$ | 0.21866795 | 0.0 | 0.0 |
| $S_7$ | $S_{11}$ | 0.0 | 0.0 | 0.11116286 |
| $S_7$ | $S_{12}$ | 0.0 | 0.0 | 1.9e-07 |
| $S_7$ | $S_{13}$ | 1.26e-05 | 0.0 | 0.0 |
| $S_7$ | $S_{14}$ | 4.73e-06 | 0.0 | 0.0 |
| $S_7$ | $S_{15}$ | 0.0 | 1e-08 | 0.0 |
| $S_7$ | $S_{16}$ | 0.0 | 0.0 | 0.0 |
| $S_7$ | $S_{17}$ | 0.0 | 0.0 | -0.44296353 |
| $S_7$ | $S_{18}$ | 0.0 | 0.0 | 2e-08 |
| $S_7$ | $S_{19}$ | 0.0 | 0.0 | -1e-08 |
| $S_7$ | $S_{20}$ | 0.0 | 0.0 | 0.0 |
| $S_7$ | $S_{21}$ | 0.0 | 0.0 | -0.0428357 |
| $S_7$ | $S_{22}$ | 6.31e-05 | 0.0 | 0.0 |
| $S_7$ | $S_{23}$ | 0.0 | -1e-08 | 0.0 |
| $S_7$ | $S_{24}$ | 0.0 | 0.0 | 0.0 |
| $S_7$ | $S_{25}$ | 0.0 | 0.0 | 0.0 |
| $S_7$ | $S_{26}$ | -9.18e-05 | 0.0 | 0.0 |
| $S_7$ | $S_{27}$ | 0.0 | -1e-08 | 0.0 |
| $S_7$ | $S_{28}$ | -4e-08 | 0.0 | 0.0 |
| $S_7$ | $S_{29}$ | 0.0 | 0.0 | 4.2e-07 |
| $S_7$ | $S_{30}$ | 0.0 | 0.0 | 0.0 |
| $S_7$ | $S_{31}$ | 2.01e-05 | 0.0 | 0.0 |
| $S_7$ | $S_{32}$ | 0.0 | 1e-08 | 0.0 |
| $S_7$ | $S_{33}$ | 0.0 | 0.0 | 0.0 |
| $S_7$ | $S_{34}$ | 0.0 | 0.0 | 0.0 |
| $S_7$ | $S_{35}$ | 0.0 | 0.0 | 0.0 |
| $S_7$ | $S_{36}$ | 0.0 | 0.0 | 0.0 |
| $S_7$ | $S_{37}$ | 0.0 | -1e-08 | 0.0 |
| $S_7$ | $S_{38}$ | 0.0 | 0.0 | 0.0 |
| $S_7$ | $S_{39}$ | 2.74e-05 | 0.0 | 0.0 |
| $S_7$ | $S_{40}$ | 0.0 | -2.8e-07 | 0.0 |
| $S_7$ | $S_{41}$ | 0.0 | -1e-08 | 0.0 |
| $S_7$ | $S_{42}$ | 0.0 | 3e-08 | 0.0 |
| $S_7$ | $S_{43}$ | 0.0 | 0.0 | 0.0 |
| $S_7$ | $S_{44}$ | 0.0 | 0.0 | 0.0 |
| $S_8$ | $S_0$ | 0.0 | 0.0 | 1.59e-13 |
| $S_8$ | $S_1$ | 0.0 | 0.0 | 0.10028309 |
| $S_8$ | $S_2$ | 0.0 | 0.0 | 0.0 |
| $S_8$ | $S_3$ | -2.45e-05 | 0.0 | 0.0 |

| $S_{\text{init}}$ | $S_{\text{final}}$ | $\mu_x$ | $\mu_y$ | $\mu_z$ |
|---|---|---|---|---|
| $S_8$ | $S_4$ | -0.19282368 | 0.0 | 0.0 |
| $S_8$ | $S_5$ | 0.0 | 1e-08 | 0.0 |
| $S_8$ | $S_6$ | -0.00013785 | 0.0 | 0.0 |
| $S_8$ | $S_7$ | 0.01338481 | 0.0 | 0.0 |
| $S_8$ | $S_8$ | 0.0 | 0.0 | -1.55867957 |
| $S_8$ | $S_9$ | 0.0 | 0.0 | -1e-07 |
| $S_8$ | $S_{10}$ | 0.0 | 0.0 | 0.17095642 |
| $S_8$ | $S_{11}$ | 0.08339075 | 0.0 | 0.0 |
| $S_8$ | $S_{12}$ | -5.15e-06 | 0.0 | 0.0 |
| $S_8$ | $S_{13}$ | 0.0 | 0.0 | 1.5e-07 |
| $S_8$ | $S_{14}$ | 0.0 | 0.0 | -1.9e-07 |
| $S_8$ | $S_{15}$ | 0.0 | 0.0 | 0.0 |
| $S_8$ | $S_{16}$ | 0.0 | -1e-08 | 0.0 |
| $S_8$ | $S_{17}$ | 0.04947754 | 0.0 | 0.0 |
| $S_8$ | $S_{18}$ | 1.04e-05 | 0.0 | 0.0 |
| $S_8$ | $S_{19}$ | 1.26e-05 | 0.0 | 0.0 |
| $S_8$ | $S_{20}$ | 0.0 | -1e-08 | 0.0 |
| $S_8$ | $S_{21}$ | -0.40688586 | 0.0 | 0.0 |
| $S_8$ | $S_{22}$ | 0.0 | 0.0 | 6.1e-07 |
| $S_8$ | $S_{23}$ | 0.0 | 0.0 | 0.0 |
| $S_8$ | $S_{24}$ | 0.0 | 0.0 | 0.0 |
| $S_8$ | $S_{25}$ | 0.0 | 0.0 | 0.0 |
| $S_8$ | $S_{26}$ | 0.0 | 0.0 | -1.18e-06 |
| $S_8$ | $S_{27}$ | 0.0 | 0.0 | 0.0 |
| $S_8$ | $S_{28}$ | 0.0 | 0.0 | 0.0 |
| $S_8$ | $S_{29}$ | 1.47e-05 | 0.0 | 0.0 |
| $S_8$ | $S_{30}$ | 0.0 | -2e-08 | 0.0 |
| $S_8$ | $S_{31}$ | 0.0 | 0.0 | 3.7e-07 |
| $S_8$ | $S_{32}$ | 0.0 | 0.0 | 0.0 |
| $S_8$ | $S_{33}$ | 0.0 | 0.0 | 0.0 |
| $S_8$ | $S_{34}$ | 0.0 | -2e-08 | 0.0 |
| $S_8$ | $S_{35}$ | 0.0 | 0.0 | 0.0 |
| $S_8$ | $S_{36}$ | 0.0 | 0.0 | 0.0 |
| $S_8$ | $S_{37}$ | 0.0 | 0.0 | 0.0 |
| $S_8$ | $S_{38}$ | 0.0 | -5e-08 | 0.0 |
| $S_8$ | $S_{39}$ | 0.0 | 0.0 | -4.6e-07 |
| $S_8$ | $S_{40}$ | 0.0 | 0.0 | 0.0 |
| $S_8$ | $S_{41}$ | 0.0 | 0.0 | 0.0 |
| $S_8$ | $S_{42}$ | 0.0 | 0.0 | 0.0 |
| $S_8$ | $S_{43}$ | 0.0 | 1e-08 | 0.0 |

| $S_{\text{init}}$ | $S_{\text{final}}$ | $\mu_x$ | $\mu_y$ | $\mu_z$ |
|---|---|---|---|---|
| $S_8$ | $S_{44}$ | 0.0 | -4e-08 | 0.0 |
| $S_9$ | $S_0$ | 0.0 | 0.0 | -1.1507304 |
| $S_9$ | $S_1$ | 0.0 | 0.0 | -7e-08 |
| $S_9$ | $S_2$ | 0.0 | 0.0 | 0.0 |
| $S_9$ | $S_3$ | -0.07859916 | 0.0 | 0.0 |
| $S_9$ | $S_4$ | 0.00018906 | 0.0 | 0.0 |
| $S_9$ | $S_5$ | 0.0 | -0.00230065 | 0.0 |
| $S_9$ | $S_6$ | 0.98060848 | 0.0 | 0.0 |
| $S_9$ | $S_7$ | -4.7e-05 | 0.0 | 0.0 |
| $S_9$ | $S_8$ | 0.0 | 0.0 | -1e-07 |
| $S_9$ | $S_9$ | 0.0 | 0.0 | -0.47978844 |
| $S_9$ | $S_{10}$ | 0.0 | 0.0 | -9.5e-07 |
| $S_9$ | $S_{11}$ | 1.25e-06 | 0.0 | 0.0 |
| $S_9$ | $S_{12}$ | -0.04598203 | 0.0 | 0.0 |
| $S_9$ | $S_{13}$ | 0.0 | 0.0 | -0.55569674 |
| $S_9$ | $S_{14}$ | 0.0 | 0.0 | 0.4968288 |
| $S_9$ | $S_{15}$ | 0.0 | 0.0 | 0.0 |
| $S_9$ | $S_{16}$ | 0.0 | -0.07359199 | 0.0 |
| $S_9$ | $S_{17}$ | -6.49e-05 | 0.0 | 0.0 |
| $S_9$ | $S_{18}$ | -0.12210857 | 0.0 | 0.0 |
| $S_9$ | $S_{19}$ | -0.09315332 | 0.0 | 0.0 |
| $S_9$ | $S_{20}$ | 0.0 | -0.09963052 | 0.0 |
| $S_9$ | $S_{21}$ | -4.23e-05 | 0.0 | 0.0 |
| $S_9$ | $S_{22}$ | 0.0 | 0.0 | -0.04440032 |
| $S_9$ | $S_{23}$ | 0.0 | 0.0 | 0.0 |
| $S_9$ | $S_{24}$ | 0.0 | 0.37540006 | 0.0 |
| $S_9$ | $S_{25}$ | 0.0 | 0.0 | 0.0 |
| $S_9$ | $S_{26}$ | 0.0 | 0.0 | 0.741929 |
| $S_9$ | $S_{27}$ | 0.0 | 0.0 | 0.0 |
| $S_9$ | $S_{28}$ | 0.0 | 0.0 | -0.00035467 |
| $S_9$ | $S_{29}$ | 0.03515388 | 0.0 | 0.0 |
| $S_9$ | $S_{30}$ | 0.0 | -0.22430954 | 0.0 |
| $S_9$ | $S_{31}$ | 0.0 | 0.0 | 0.1766759 |
| $S_9$ | $S_{32}$ | 0.0 | 0.0 | 0.0 |
| $S_9$ | $S_{33}$ | 0.0 | -0.02699422 | 0.0 |
| $S_9$ | $S_{34}$ | 0.0 | 0.05094284 | 0.0 |
| $S_9$ | $S_{35}$ | 0.0 | 0.0 | 0.0 |
| $S_9$ | $S_{36}$ | 0.0 | 0.09332107 | 0.0 |
| $S_9$ | $S_{37}$ | 0.0 | 0.0 | 0.0 |
| $S_9$ | $S_{38}$ | 0.0 | 0.10241905 | 0.0 |

| $S_{\text{init}}$ | $S_{\text{final}}$ | $\mu_x$ | $\mu_y$ | $\mu_z$ |
|---|---|---|---|---|
| $S_9$ | $S_{39}$ | 0.0 | 0.0 | -0.0233868 |
| $S_9$ | $S_{40}$ | 0.0 | 0.0 | 0.0 |
| $S_9$ | $S_{41}$ | 0.0 | 0.0 | 0.0 |
| $S_9$ | $S_{42}$ | 0.0 | 0.0 | 0.0 |
| $S_9$ | $S_{43}$ | 0.0 | 0.11717236 | 0.0 |
| $S_9$ | $S_{44}$ | 0.0 | 0.07798317 | 0.0 |
| $S_{10}$ | $S_0$ | 0.0 | 0.0 | -1.08e-13 |
| $S_{10}$ | $S_1$ | 0.0 | 0.0 | 0.09722287 |
| $S_{10}$ | $S_2$ | 0.0 | 0.0 | 0.0 |
| $S_{10}$ | $S_3$ | 1.07e-05 | 0.0 | 0.0 |
| $S_{10}$ | $S_4$ | 0.46023443 | 0.0 | 0.0 |
| $S_{10}$ | $S_5$ | 0.0 | -8e-08 | 0.0 |
| $S_{10}$ | $S_6$ | -9.72e-05 | 0.0 | 0.0 |
| $S_{10}$ | $S_7$ | 0.21866795 | 0.0 | 0.0 |
| $S_{10}$ | $S_8$ | 0.0 | 0.0 | 0.17095642 |
| $S_{10}$ | $S_9$ | 0.0 | 0.0 | -9.5e-07 |
| $S_{10}$ | $S_{10}$ | 0.0 | 0.0 | -1.55053621 |
| $S_{10}$ | $S_{11}$ | 0.13936823 | 0.0 | 0.0 |
| $S_{10}$ | $S_{12}$ | 2.78e-05 | 0.0 | 0.0 |
| $S_{10}$ | $S_{13}$ | 0.0 | 0.0 | -6e-08 |
| $S_{10}$ | $S_{14}$ | 0.0 | 0.0 | 7.6e-07 |
| $S_{10}$ | $S_{15}$ | 0.0 | 0.0 | 0.0 |
| $S_{10}$ | $S_{16}$ | 0.0 | 0.0 | 0.0 |
| $S_{10}$ | $S_{17}$ | -0.4903393 | 0.0 | 0.0 |
| $S_{10}$ | $S_{18}$ | 2.41e-05 | 0.0 | 0.0 |
| $S_{10}$ | $S_{19}$ | -9.72e-06 | 0.0 | 0.0 |
| $S_{10}$ | $S_{20}$ | 0.0 | 0.0 | 0.0 |
| $S_{10}$ | $S_{21}$ | 0.20367732 | 0.0 | 0.0 |
| $S_{10}$ | $S_{22}$ | 0.0 | 0.0 | -2.3e-07 |
| $S_{10}$ | $S_{23}$ | 0.0 | 0.0 | 0.0 |
| $S_{10}$ | $S_{24}$ | 0.0 | 1e-08 | 0.0 |
| $S_{10}$ | $S_{25}$ | 0.0 | 0.0 | 0.0 |
| $S_{10}$ | $S_{26}$ | 0.0 | 0.0 | 1.8e-07 |
| $S_{10}$ | $S_{27}$ | 0.0 | 0.0 | 0.0 |
| $S_{10}$ | $S_{28}$ | 0.0 | 0.0 | 0.0 |
| $S_{10}$ | $S_{29}$ | -5.72e-06 | 0.0 | 0.0 |
| $S_{10}$ | $S_{30}$ | 0.0 | 0.0 | 0.0 |
| $S_{10}$ | $S_{31}$ | 0.0 | 0.0 | -2.8e-07 |
| $S_{10}$ | $S_{32}$ | 0.0 | 0.0 | 0.0 |
| $S_{10}$ | $S_{33}$ | 0.0 | 1e-08 | 0.0 |

| $S_{\text{init}}$ | $S_{\text{final}}$ | $\mu_x$ | $\mu_y$ | $\mu_z$ |
|---|---|---|---|---|
| $S_{10}$ | $S_{34}$ | 0.0 | 1e-08 | 0.0 |
| $S_{10}$ | $S_{35}$ | 0.0 | 0.0 | 0.0 |
| $S_{10}$ | $S_{36}$ | 0.0 | 3e-08 | 0.0 |
| $S_{10}$ | $S_{37}$ | 0.0 | 0.0 | 0.0 |
| $S_{10}$ | $S_{38}$ | 0.0 | 1e-08 | 0.0 |
| $S_{10}$ | $S_{39}$ | 0.0 | 0.0 | -4e-07 |
| $S_{10}$ | $S_{40}$ | 0.0 | 0.0 | 0.0 |
| $S_{10}$ | $S_{41}$ | 0.0 | 0.0 | 0.0 |
| $S_{10}$ | $S_{42}$ | 0.0 | 0.0 | 0.0 |
| $S_{10}$ | $S_{43}$ | 0.0 | 0.0 | 0.0 |
| $S_{10}$ | $S_{44}$ | 0.0 | 2e-08 | 0.0 |
| $S_{11}$ | $S_0$ | -3.31e-13 | 0.0 | 0.0 |
| $S_{11}$ | $S_1$ | -0.06732052 | 0.0 | 0.0 |
| $S_{11}$ | $S_2$ | 0.0 | 3e-08 | 0.0 |
| $S_{11}$ | $S_3$ | 0.0 | 0.0 | 8.5e-07 |
| $S_{11}$ | $S_4$ | 0.0 | 0.0 | 0.08766735 |
| $S_{11}$ | $S_5$ | 0.0 | 0.0 | 0.0 |
| $S_{11}$ | $S_6$ | 0.0 | 0.0 | -1.45e-06 |
| $S_{11}$ | $S_7$ | 0.0 | 0.0 | 0.11116286 |
| $S_{11}$ | $S_8$ | 0.08339075 | 0.0 | 0.0 |
| $S_{11}$ | $S_9$ | 1.25e-06 | 0.0 | 0.0 |
| $S_{11}$ | $S_{10}$ | 0.13936823 | 0.0 | 0.0 |
| $S_{11}$ | $S_{11}$ | 0.0 | 0.0 | -1.04445506 |
| $S_{11}$ | $S_{12}$ | 0.0 | 0.0 | -1.9e-07 |
| $S_{11}$ | $S_{13}$ | -1.81e-05 | 0.0 | 0.0 |
| $S_{11}$ | $S_{14}$ | -3.5e-07 | 0.0 | 0.0 |
| $S_{11}$ | $S_{15}$ | 0.0 | 2e-08 | 0.0 |
| $S_{11}$ | $S_{16}$ | 0.0 | 0.0 | 0.0 |
| $S_{11}$ | $S_{17}$ | 0.0 | 0.0 | -0.66163373 |
| $S_{11}$ | $S_{18}$ | 0.0 | 0.0 | 1.1e-07 |
| $S_{11}$ | $S_{19}$ | 0.0 | 0.0 | -1.6e-07 |
| $S_{11}$ | $S_{20}$ | 0.0 | 0.0 | 0.0 |
| $S_{11}$ | $S_{21}$ | 0.0 | 0.0 | 0.05005918 |
| $S_{11}$ | $S_{22}$ | -2.31e-05 | 0.0 | 0.0 |
| $S_{11}$ | $S_{23}$ | 0.0 | -1e-08 | 0.0 |
| $S_{11}$ | $S_{24}$ | 0.0 | 0.0 | 0.0 |
| $S_{11}$ | $S_{25}$ | 0.0 | 1e-08 | 0.0 |
| $S_{11}$ | $S_{26}$ | 4.58e-05 | 0.0 | 0.0 |
| $S_{11}$ | $S_{27}$ | 0.0 | -1e-08 | 0.0 |
| $S_{11}$ | $S_{28}$ | 0.0 | 0.0 | 0.0 |

| $S_{\text{init}}$ | $S_{\text{final}}$ | $\mu_x$ | $\mu_y$ | $\mu_z$ |
|---|---|---|---|---|
| $S_{11}$ | $S_{29}$ | 0.0 | 0.0 | -4e-08 |
| $S_{11}$ | $S_{30}$ | 0.0 | 0.0 | 0.0 |
| $S_{11}$ | $S_{31}$ | -4.05e-05 | 0.0 | 0.0 |
| $S_{11}$ | $S_{32}$ | 0.0 | -1e-08 | 0.0 |
| $S_{11}$ | $S_{33}$ | 0.0 | 0.0 | 0.0 |
| $S_{11}$ | $S_{34}$ | 0.0 | 0.0 | 0.0 |
| $S_{11}$ | $S_{35}$ | 0.0 | 0.0 | 0.0 |
| $S_{11}$ | $S_{36}$ | 0.0 | 0.0 | 0.0 |
| $S_{11}$ | $S_{37}$ | 0.0 | -3e-08 | 0.0 |
| $S_{11}$ | $S_{38}$ | 0.0 | 0.0 | 0.0 |
| $S_{11}$ | $S_{39}$ | -8.05e-06 | 0.0 | 0.0 |
| $S_{11}$ | $S_{40}$ | 0.0 | 1e-08 | 0.0 |
| $S_{11}$ | $S_{41}$ | 0.0 | -4e-08 | 0.0 |
| $S_{11}$ | $S_{42}$ | 0.0 | 0.0 | 0.0 |
| $S_{11}$ | $S_{43}$ | 0.0 | 0.0 | 0.0 |
| $S_{11}$ | $S_{44}$ | 0.0 | 0.0 | 0.0 |
| $S_{12}$ | $S_0$ | -1.4312231 | 0.0 | 0.0 |
| $S_{12}$ | $S_1$ | -9.54e-05 | 0.0 | 0.0 |
| $S_{12}$ | $S_2$ | 0.0 | -0.01048305 | 0.0 |
| $S_{12}$ | $S_3$ | 0.0 | 0.0 | 0.52041003 |
| $S_{12}$ | $S_4$ | 0.0 | 0.0 | 1.9e-07 |
| $S_{12}$ | $S_5$ | 0.0 | 0.0 | 0.0 |
| $S_{12}$ | $S_6$ | 0.0 | 0.0 | 0.04214257 |
| $S_{12}$ | $S_7$ | 0.0 | 0.0 | 1.9e-07 |
| $S_{12}$ | $S_8$ | -5.15e-06 | 0.0 | 0.0 |
| $S_{12}$ | $S_9$ | -0.04598203 | 0.0 | 0.0 |
| $S_{12}$ | $S_{10}$ | 2.78e-05 | 0.0 | 0.0 |
| $S_{12}$ | $S_{11}$ | 0.0 | 0.0 | -1.9e-07 |
| $S_{12}$ | $S_{12}$ | 0.0 | 0.0 | -0.62575167 |
| $S_{12}$ | $S_{13}$ | -0.32874555 | 0.0 | 0.0 |
| $S_{12}$ | $S_{14}$ | -0.40957006 | 0.0 | 0.0 |
| $S_{12}$ | $S_{15}$ | 0.0 | -0.51231349 | 0.0 |
| $S_{12}$ | $S_{16}$ | 0.0 | 0.0 | 0.0 |
| $S_{12}$ | $S_{17}$ | 0.0 | 0.0 | -5.9e-07 |
| $S_{12}$ | $S_{18}$ | 0.0 | 0.0 | 0.11250891 |
| $S_{12}$ | $S_{19}$ | 0.0 | 0.0 | 0.10899779 |
| $S_{12}$ | $S_{20}$ | 0.0 | 0.0 | 0.0 |
| $S_{12}$ | $S_{21}$ | 0.0 | 0.0 | -4.8e-07 |
| $S_{12}$ | $S_{22}$ | 0.0701525 | 0.0 | 0.0 |
| $S_{12}$ | $S_{23}$ | 0.0 | 0.23606345 | 0.0 |

| $S_{\text{init}}$ | $S_{\text{final}}$ | $\mu_x$ | $\mu_y$ | $\mu_z$ |
|---|---|---|---|---|
| $S_{12}$ | $S_{24}$ | 0.0 | 0.0 | 0.0 |
| $S_{12}$ | $S_{25}$ | 0.0 | -0.35096681 | 0.0 |
| $S_{12}$ | $S_{26}$ | -0.0025709 | 0.0 | 0.0 |
| $S_{12}$ | $S_{27}$ | 0.0 | -0.0977081 | 0.0 |
| $S_{12}$ | $S_{28}$ | 0.00016949 | 0.0 | 0.0 |
| $S_{12}$ | $S_{29}$ | 0.0 | 0.0 | -0.17949751 |
| $S_{12}$ | $S_{30}$ | 0.0 | 0.0 | 0.0 |
| $S_{12}$ | $S_{31}$ | 0.18070589 | 0.0 | 0.0 |
| $S_{12}$ | $S_{32}$ | 0.0 | 0.02381181 | 0.0 |
| $S_{12}$ | $S_{33}$ | 0.0 | 0.0 | 0.0 |
| $S_{12}$ | $S_{34}$ | 0.0 | 0.0 | 0.0 |
| $S_{12}$ | $S_{35}$ | 0.0 | -0.2782631 | 0.0 |
| $S_{12}$ | $S_{36}$ | 0.0 | 0.0 | 0.0 |
| $S_{12}$ | $S_{37}$ | 0.0 | -0.02977205 | 0.0 |
| $S_{12}$ | $S_{38}$ | 0.0 | 0.0 | 0.0 |
| $S_{12}$ | $S_{39}$ | 0.83403812 | 0.0 | 0.0 |
| $S_{12}$ | $S_{40}$ | 0.0 | -0.02463636 | 0.0 |
| $S_{12}$ | $S_{41}$ | 0.0 | -0.01920126 | 0.0 |
| $S_{12}$ | $S_{42}$ | 0.0 | 0.05821775 | 0.0 |
| $S_{12}$ | $S_{43}$ | 0.0 | 0.0 | 0.0 |
| $S_{12}$ | $S_{44}$ | 0.0 | 0.0 | 0.0 |
| $S_{13}$ | $S_0$ | 0.0 | 0.0 | -1.6951899 |
| $S_{13}$ | $S_1$ | 0.0 | 0.0 | 4e-08 |
| $S_{13}$ | $S_2$ | 0.0 | 0.0 | 0.0 |
| $S_{13}$ | $S_3$ | -0.00728764 | 0.0 | 0.0 |
| $S_{13}$ | $S_4$ | -0.00011341 | 0.0 | 0.0 |
| $S_{13}$ | $S_5$ | 0.0 | -0.00138134 | 0.0 |
| $S_{13}$ | $S_6$ | -0.73603536 | 0.0 | 0.0 |
| $S_{13}$ | $S_7$ | 1.26e-05 | 0.0 | 0.0 |
| $S_{13}$ | $S_8$ | 0.0 | 0.0 | 1.5e-07 |
| $S_{13}$ | $S_9$ | 0.0 | 0.0 | -0.55569674 |
| $S_{13}$ | $S_{10}$ | 0.0 | 0.0 | -6e-08 |
| $S_{13}$ | $S_{11}$ | -1.81e-05 | 0.0 | 0.0 |
| $S_{13}$ | $S_{12}$ | -0.32874555 | 0.0 | 0.0 |
| $S_{13}$ | $S_{13}$ | 0.0 | 0.0 | -1.40398691 |
| $S_{13}$ | $S_{14}$ | 0.0 | 0.0 | -0.05128066 |
| $S_{13}$ | $S_{15}$ | 0.0 | 0.0 | 0.0 |
| $S_{13}$ | $S_{16}$ | 0.0 | -0.19453049 | 0.0 |
| $S_{13}$ | $S_{17}$ | 8.44e-05 | 0.0 | 0.0 |
| $S_{13}$ | $S_{18}$ | -0.02171607 | 0.0 | 0.0 |

| $S_{\text{init}}$ | $S_{\text{final}}$ | $\mu_x$ | $\mu_y$ | $\mu_z$ |
|---|---|---|---|---|
| $S_{13}$ | $S_{19}$ | -0.37607242 | 0.0 | 0.0 |
| $S_{13}$ | $S_{20}$ | 0.0 | 0.16202334 | 0.0 |
| $S_{13}$ | $S_{21}$ | 3.95e-05 | 0.0 | 0.0 |
| $S_{13}$ | $S_{22}$ | 0.0 | 0.0 | 0.19598621 |
| $S_{13}$ | $S_{23}$ | 0.0 | 0.0 | 0.0 |
| $S_{13}$ | $S_{24}$ | 0.0 | -0.04163952 | 0.0 |
| $S_{13}$ | $S_{25}$ | 0.0 | 0.0 | 0.0 |
| $S_{13}$ | $S_{26}$ | 0.0 | 0.0 | -0.21378941 |
| $S_{13}$ | $S_{27}$ | 0.0 | 0.0 | 0.0 |
| $S_{13}$ | $S_{28}$ | 0.0 | 0.0 | -0.00035587 |
| $S_{13}$ | $S_{29}$ | 0.17701141 | 0.0 | 0.0 |
| $S_{13}$ | $S_{30}$ | 0.0 | -0.1759825 | 0.0 |
| $S_{13}$ | $S_{31}$ | 0.0 | 0.0 | -0.16453133 |
| $S_{13}$ | $S_{32}$ | 0.0 | 0.0 | 0.0 |
| $S_{13}$ | $S_{33}$ | 0.0 | -0.4014728 | 0.0 |
| $S_{13}$ | $S_{34}$ | 0.0 | 0.0133298 | 0.0 |
| $S_{13}$ | $S_{35}$ | 0.0 | 0.0 | 0.0 |
| $S_{13}$ | $S_{36}$ | 0.0 | -0.0966466 | 0.0 |
| $S_{13}$ | $S_{37}$ | 0.0 | 0.0 | 0.0 |
| $S_{13}$ | $S_{38}$ | 0.0 | -0.19623435 | 0.0 |
| $S_{13}$ | $S_{39}$ | 0.0 | 0.0 | -0.81683341 |
| $S_{13}$ | $S_{40}$ | 0.0 | 0.0 | 0.0 |
| $S_{13}$ | $S_{41}$ | 0.0 | 0.0 | 0.0 |
| $S_{13}$ | $S_{42}$ | 0.0 | 0.0 | 0.0 |
| $S_{13}$ | $S_{43}$ | 0.0 | -0.12668579 | 0.0 |
| $S_{13}$ | $S_{44}$ | 0.0 | -0.03527538 | 0.0 |
| $S_{14}$ | $S_0$ | 0.0 | 0.0 | 0.3543636 |
| $S_{14}$ | $S_1$ | 0.0 | 0.0 | -1e-07 |
| $S_{14}$ | $S_2$ | 0.0 | 0.0 | 0.0 |
| $S_{14}$ | $S_3$ | -0.11844719 | 0.0 | 0.0 |
| $S_{14}$ | $S_4$ | -2.88e-05 | 0.0 | 0.0 |
| $S_{14}$ | $S_5$ | 0.0 | 0.00522468 | 0.0 |
| $S_{14}$ | $S_6$ | -0.3327061 | 0.0 | 0.0 |
| $S_{14}$ | $S_7$ | 4.73e-06 | 0.0 | 0.0 |
| $S_{14}$ | $S_8$ | 0.0 | 0.0 | -1.9e-07 |
| $S_{14}$ | $S_9$ | 0.0 | 0.0 | 0.4968288 |
| $S_{14}$ | $S_{10}$ | 0.0 | 0.0 | 7.6e-07 |
| $S_{14}$ | $S_{11}$ | -3.5e-07 | 0.0 | 0.0 |
| $S_{14}$ | $S_{12}$ | -0.40957006 | 0.0 | 0.0 |
| $S_{14}$ | $S_{13}$ | 0.0 | 0.0 | -0.05128066 |

| $S_{\text{init}}$ | $S_{\text{final}}$ | $\mu_x$ | $\mu_y$ | $\mu_z$ |
|---|---|---|---|---|
| $S_{14}$ | $S_{14}$ | 0.0 | 0.0 | -1.48055988 |
| $S_{14}$ | $S_{15}$ | 0.0 | 0.0 | 0.0 |
| $S_{14}$ | $S_{16}$ | 0.0 | -0.0283167 | 0.0 |
| $S_{14}$ | $S_{17}$ | 1.97e-05 | 0.0 | 0.0 |
| $S_{14}$ | $S_{18}$ | 0.32878579 | 0.0 | 0.0 |
| $S_{14}$ | $S_{19}$ | 0.04960033 | 0.0 | 0.0 |
| $S_{14}$ | $S_{20}$ | 0.0 | 0.09844367 | 0.0 |
| $S_{14}$ | $S_{21}$ | 8.93e-05 | 0.0 | 0.0 |
| $S_{14}$ | $S_{22}$ | 0.0 | 0.0 | 0.15358366 |
| $S_{14}$ | $S_{23}$ | 0.0 | 0.0 | 0.0 |
| $S_{14}$ | $S_{24}$ | 0.0 | 0.0982201 | 0.0 |
| $S_{14}$ | $S_{25}$ | 0.0 | 0.0 | 0.0 |
| $S_{14}$ | $S_{26}$ | 0.0 | 0.0 | -0.23538562 |
| $S_{14}$ | $S_{27}$ | 0.0 | 0.0 | 0.0 |
| $S_{14}$ | $S_{28}$ | 0.0 | 0.0 | 4.72e-05 |
| $S_{14}$ | $S_{29}$ | 0.1454049 | 0.0 | 0.0 |
| $S_{14}$ | $S_{30}$ | 0.0 | 0.08135873 | 0.0 |
| $S_{14}$ | $S_{31}$ | 0.0 | 0.0 | 0.11547155 |
| $S_{14}$ | $S_{32}$ | 0.0 | 0.0 | 0.0 |
| $S_{14}$ | $S_{33}$ | 0.0 | -0.04625261 | 0.0 |
| $S_{14}$ | $S_{34}$ | 0.0 | -0.01644056 | 0.0 |
| $S_{14}$ | $S_{35}$ | 0.0 | 0.0 | 0.0 |
| $S_{14}$ | $S_{36}$ | 0.0 | 0.05606147 | 0.0 |
| $S_{14}$ | $S_{37}$ | 0.0 | 0.0 | 0.0 |
| $S_{14}$ | $S_{38}$ | 0.0 | 0.13075132 | 0.0 |
| $S_{14}$ | $S_{39}$ | 0.0 | 0.0 | -0.15600373 |
| $S_{14}$ | $S_{40}$ | 0.0 | 0.0 | 0.0 |
| $S_{14}$ | $S_{41}$ | 0.0 | 0.0 | 0.0 |
| $S_{14}$ | $S_{42}$ | 0.0 | 0.0 | 0.0 |
| $S_{14}$ | $S_{43}$ | 0.0 | 0.02188728 | 0.0 |
| $S_{14}$ | $S_{44}$ | 0.0 | -0.00529488 | 0.0 |
| $S_{15}$ | $S_0$ | 0.0 | 0.0 | 0.0 |
| $S_{15}$ | $S_1$ | 0.0 | 0.0 | 0.0 |
| $S_{15}$ | $S_2$ | 0.0 | 0.0 | 0.00341002 |
| $S_{15}$ | $S_3$ | 0.0 | -0.109404 | 0.0 |
| $S_{15}$ | $S_4$ | 0.0 | -1e-08 | 0.0 |
| $S_{15}$ | $S_5$ | -0.00673943 | 0.0 | 0.0 |
| $S_{15}$ | $S_6$ | 0.0 | 0.04459811 | 0.0 |
| $S_{15}$ | $S_7$ | 0.0 | 1e-08 | 0.0 |
| $S_{15}$ | $S_8$ | 0.0 | 0.0 | 0.0 |

| $S_{\text{init}}$ | $S_{\text{final}}$ | $\mu_x$ | $\mu_y$ | $\mu_z$ |
|---|---|---|---|---|
| $S_{15}$ | $S_9$ | 0.0 | 0.0 | 0.0 |
| $S_{15}$ | $S_{10}$ | 0.0 | 0.0 | 0.0 |
| $S_{15}$ | $S_{11}$ | 0.0 | 2e-08 | 0.0 |
| $S_{15}$ | $S_{12}$ | 0.0 | -0.51231349 | 0.0 |
| $S_{15}$ | $S_{13}$ | 0.0 | 0.0 | 0.0 |
| $S_{15}$ | $S_{14}$ | 0.0 | 0.0 | 0.0 |
| $S_{15}$ | $S_{15}$ | 0.0 | 0.0 | -3.29110192 |
| $S_{15}$ | $S_{16}$ | 1.00853941 | 0.0 | 0.0 |
| $S_{15}$ | $S_{17}$ | 0.0 | -1e-08 | 0.0 |
| $S_{15}$ | $S_{18}$ | 0.0 | -0.10097816 | 0.0 |
| $S_{15}$ | $S_{19}$ | 0.0 | 0.32029667 | 0.0 |
| $S_{15}$ | $S_{20}$ | -3.80570339 | 0.0 | 0.0 |
| $S_{15}$ | $S_{21}$ | 0.0 | 0.0 | 0.0 |
| $S_{15}$ | $S_{22}$ | 0.0 | 0.0 | 0.0 |
| $S_{15}$ | $S_{23}$ | 0.0 | 0.0 | -2.32138397 |
| $S_{15}$ | $S_{24}$ | -0.94875204 | 0.0 | 0.0 |
| $S_{15}$ | $S_{25}$ | 0.0 | 0.0 | 2.04532817 |
| $S_{15}$ | $S_{26}$ | 0.0 | 0.0 | 0.0 |
| $S_{15}$ | $S_{27}$ | 0.0 | 0.0 | -0.63366242 |
| $S_{15}$ | $S_{28}$ | 0.0 | 0.0 | 0.0 |
| $S_{15}$ | $S_{29}$ | 0.0 | -2.91732357 | 0.0 |
| $S_{15}$ | $S_{30}$ | 0.04382184 | 0.0 | 0.0 |
| $S_{15}$ | $S_{31}$ | 0.0 | 0.0 | 0.0 |
| $S_{15}$ | $S_{32}$ | 0.0 | 0.0 | 0.09617966 |
| $S_{15}$ | $S_{33}$ | -0.01653095 | 0.0 | 0.0 |
| $S_{15}$ | $S_{34}$ | 0.10610204 | 0.0 | 0.0 |
| $S_{15}$ | $S_{35}$ | 0.0 | 0.0 | -0.008548 |
| $S_{15}$ | $S_{36}$ | -0.16202175 | 0.0 | 0.0 |
| $S_{15}$ | $S_{37}$ | 0.0 | 0.0 | -0.60818192 |
| $S_{15}$ | $S_{38}$ | 0.04094303 | 0.0 | 0.0 |
| $S_{15}$ | $S_{39}$ | 0.0 | 0.0 | 0.0 |
| $S_{15}$ | $S_{40}$ | 0.0 | 0.0 | 0.15983938 |
| $S_{15}$ | $S_{41}$ | 0.0 | 0.0 | 0.06666785 |
| $S_{15}$ | $S_{42}$ | 0.0 | 0.0 | -0.17655561 |
| $S_{15}$ | $S_{43}$ | 0.28186078 | 0.0 | 0.0 |
| $S_{15}$ | $S_{44}$ | -0.79247351 | 0.0 | 0.0 |
| $S_{16}$ | $S_0$ | 0.0 | 0.33398909 | 0.0 |
| $S_{16}$ | $S_1$ | 0.0 | 0.0 | 0.0 |
| $S_{16}$ | $S_2$ | 0.0032621 | 0.0 | 0.0 |
| $S_{16}$ | $S_3$ | 0.0 | 0.0 | 0.0 |

| $S_{\text{init}}$ | $S_{\text{final}}$ | $\mu_x$ | $\mu_y$ | $\mu_z$ |
|---|---|---|---|---|
| $S_{16}$ | $S_4$ | 0.0 | 0.0 | 0.0 |
| $S_{16}$ | $S_5$ | 0.0 | 0.0 | 0.00498287 |
| $S_{16}$ | $S_6$ | 0.0 | 0.0 | 0.0 |
| $S_{16}$ | $S_7$ | 0.0 | 0.0 | 0.0 |
| $S_{16}$ | $S_8$ | 0.0 | -1e-08 | 0.0 |
| $S_{16}$ | $S_9$ | 0.0 | -0.07359199 | 0.0 |
| $S_{16}$ | $S_{10}$ | 0.0 | 0.0 | 0.0 |
| $S_{16}$ | $S_{11}$ | 0.0 | 0.0 | 0.0 |
| $S_{16}$ | $S_{12}$ | 0.0 | 0.0 | 0.0 |
| $S_{16}$ | $S_{13}$ | 0.0 | -0.19453049 | 0.0 |
| $S_{16}$ | $S_{14}$ | 0.0 | -0.0283167 | 0.0 |
| $S_{16}$ | $S_{15}$ | 1.00853941 | 0.0 | 0.0 |
| $S_{16}$ | $S_{16}$ | 0.0 | 0.0 | -4.72355912 |
| $S_{16}$ | $S_{17}$ | 0.0 | 0.0 | 0.0 |
| $S_{16}$ | $S_{18}$ | 0.0 | 0.0 | 0.0 |
| $S_{16}$ | $S_{19}$ | 0.0 | 0.0 | 0.0 |
| $S_{16}$ | $S_{20}$ | 0.0 | 0.0 | 0.42868013 |
| $S_{16}$ | $S_{21}$ | 0.0 | 0.0 | 0.0 |
| $S_{16}$ | $S_{22}$ | 0.0 | 0.1766467 | 0.0 |
| $S_{16}$ | $S_{23}$ | 2.353645 | 0.0 | 0.0 |
| $S_{16}$ | $S_{24}$ | 0.0 | 0.0 | -2.83265618 |
| $S_{16}$ | $S_{25}$ | 2.52239017 | 0.0 | 0.0 |
| $S_{16}$ | $S_{26}$ | 0.0 | -0.62481902 | 0.0 |
| $S_{16}$ | $S_{27}$ | 0.0432952 | 0.0 | 0.0 |
| $S_{16}$ | $S_{28}$ | 0.0 | -1.03e-05 | 0.0 |
| $S_{16}$ | $S_{29}$ | 0.0 | 0.0 | 0.0 |
| $S_{16}$ | $S_{30}$ | 0.0 | 0.0 | 0.39690106 |
| $S_{16}$ | $S_{31}$ | 0.0 | -2.75794913 | 0.0 |
| $S_{16}$ | $S_{32}$ | -0.16940101 | 0.0 | 0.0 |
| $S_{16}$ | $S_{33}$ | 0.0 | 0.0 | -0.58716726 |
| $S_{16}$ | $S_{34}$ | 0.0 | 0.0 | -0.12099537 |
| $S_{16}$ | $S_{35}$ | 0.13511452 | 0.0 | 0.0 |
| $S_{16}$ | $S_{36}$ | 0.0 | 0.0 | -0.3396049 |
| $S_{16}$ | $S_{37}$ | 0.16763394 | 0.0 | 0.0 |
| $S_{16}$ | $S_{38}$ | 0.0 | 0.0 | -0.39857214 |
| $S_{16}$ | $S_{39}$ | 0.0 | -0.34810622 | 0.0 |
| $S_{16}$ | $S_{40}$ | -0.13258434 | 0.0 | 0.0 |
| $S_{16}$ | $S_{41}$ | -0.0310257 | 0.0 | 0.0 |
| $S_{16}$ | $S_{42}$ | 0.25439561 | 0.0 | 0.0 |
| $S_{16}$ | $S_{43}$ | 0.0 | 0.0 | -0.25302563 |

| $S_{\text{init}}$ | $S_{\text{final}}$ | $\mu_x$ | $\mu_y$ | $\mu_z$ |
|---|---|---|---|---|
| $S_{16}$ | $S_{44}$ | 0.0 | 0.0 | 1.28976177 |
| $S_{17}$ | $S_0$ | -5.56e-13 | 0.0 | 0.0 |
| $S_{17}$ | $S_1$ | 0.02173414 | 0.0 | 0.0 |
| $S_{17}$ | $S_2$ | 0.0 | 0.0 | 0.0 |
| $S_{17}$ | $S_3$ | 0.0 | 0.0 | 1.42e-06 |
| $S_{17}$ | $S_4$ | 0.0 | 0.0 | -0.08532609 |
| $S_{17}$ | $S_5$ | 0.0 | 0.0 | 0.0 |
| $S_{17}$ | $S_6$ | 0.0 | 0.0 | -5.71e-06 |
| $S_{17}$ | $S_7$ | 0.0 | 0.0 | -0.44296353 |
| $S_{17}$ | $S_8$ | 0.04947754 | 0.0 | 0.0 |
| $S_{17}$ | $S_9$ | -6.49e-05 | 0.0 | 0.0 |
| $S_{17}$ | $S_{10}$ | -0.4903393 | 0.0 | 0.0 |
| $S_{17}$ | $S_{11}$ | 0.0 | 0.0 | -0.66163373 |
| $S_{17}$ | $S_{12}$ | 0.0 | 0.0 | -5.9e-07 |
| $S_{17}$ | $S_{13}$ | 8.44e-05 | 0.0 | 0.0 |
| $S_{17}$ | $S_{14}$ | 1.97e-05 | 0.0 | 0.0 |
| $S_{17}$ | $S_{15}$ | 0.0 | -1e-08 | 0.0 |
| $S_{17}$ | $S_{16}$ | 0.0 | 0.0 | 0.0 |
| $S_{17}$ | $S_{17}$ | 0.0 | 0.0 | -1.83619928 |
| $S_{17}$ | $S_{18}$ | 0.0 | 0.0 | 1.8e-07 |
| $S_{17}$ | $S_{19}$ | 0.0 | 0.0 | 8e-08 |
| $S_{17}$ | $S_{20}$ | 0.0 | 0.0 | 0.0 |
| $S_{17}$ | $S_{21}$ | 0.0 | 0.0 | -0.00281451 |
| $S_{17}$ | $S_{22}$ | 3.29e-05 | 0.0 | 0.0 |
| $S_{17}$ | $S_{23}$ | 0.0 | 1e-08 | 0.0 |
| $S_{17}$ | $S_{24}$ | 0.0 | 0.0 | 0.0 |
| $S_{17}$ | $S_{25}$ | 0.0 | -1e-08 | 0.0 |
| $S_{17}$ | $S_{26}$ | -1.25e-05 | 0.0 | 0.0 |
| $S_{17}$ | $S_{27}$ | 0.0 | 1e-08 | 0.0 |
| $S_{17}$ | $S_{28}$ | -1e-08 | 0.0 | 0.0 |
| $S_{17}$ | $S_{29}$ | 0.0 | 0.0 | -3.8e-07 |
| $S_{17}$ | $S_{30}$ | 0.0 | 0.0 | 0.0 |
| $S_{17}$ | $S_{31}$ | 7.04e-05 | 0.0 | 0.0 |
| $S_{17}$ | $S_{32}$ | 0.0 | 2e-08 | 0.0 |
| $S_{17}$ | $S_{33}$ | 0.0 | 0.0 | 0.0 |
| $S_{17}$ | $S_{34}$ | 0.0 | 0.0 | 0.0 |
| $S_{17}$ | $S_{35}$ | 0.0 | -1e-08 | 0.0 |
| $S_{17}$ | $S_{36}$ | 0.0 | 0.0 | 0.0 |
| $S_{17}$ | $S_{37}$ | 0.0 | 2e-08 | 0.0 |
| $S_{17}$ | $S_{38}$ | 0.0 | 0.0 | 0.0 |

| $S_{\text{init}}$ | $S_{\text{final}}$ | $\mu_x$ | $\mu_y$ | $\mu_z$ |
|---|---|---|---|---|
| $S_{17}$ | $S_{39}$ | -5.18e-05 | 0.0 | 0.0 |
| $S_{17}$ | $S_{40}$ | 0.0 | -3e-08 | 0.0 |
| $S_{17}$ | $S_{41}$ | 0.0 | 8e-08 | 0.0 |
| $S_{17}$ | $S_{42}$ | 0.0 | 1e-08 | 0.0 |
| $S_{17}$ | $S_{43}$ | 0.0 | 0.0 | 0.0 |
| $S_{17}$ | $S_{44}$ | 0.0 | 0.0 | 0.0 |
| $S_{18}$ | $S_0$ | 0.26802037 | 0.0 | 0.0 |
| $S_{18}$ | $S_1$ | 0.00021788 | 0.0 | 0.0 |
| $S_{18}$ | $S_2$ | 0.0 | 0.00111904 | 0.0 |
| $S_{18}$ | $S_3$ | 0.0 | 0.0 | 0.17104704 |
| $S_{18}$ | $S_4$ | 0.0 | 0.0 | -8e-07 |
| $S_{18}$ | $S_5$ | 0.0 | 0.0 | 0.0 |
| $S_{18}$ | $S_6$ | 0.0 | 0.0 | -0.78432778 |
| $S_{18}$ | $S_7$ | 0.0 | 0.0 | 2e-08 |
| $S_{18}$ | $S_8$ | 1.04e-05 | 0.0 | 0.0 |
| $S_{18}$ | $S_9$ | -0.12210857 | 0.0 | 0.0 |
| $S_{18}$ | $S_{10}$ | 2.41e-05 | 0.0 | 0.0 |
| $S_{18}$ | $S_{11}$ | 0.0 | 0.0 | 1.1e-07 |
| $S_{18}$ | $S_{12}$ | 0.0 | 0.0 | 0.11250891 |
| $S_{18}$ | $S_{13}$ | -0.02171607 | 0.0 | 0.0 |
| $S_{18}$ | $S_{14}$ | 0.32878579 | 0.0 | 0.0 |
| $S_{18}$ | $S_{15}$ | 0.0 | -0.10097816 | 0.0 |
| $S_{18}$ | $S_{16}$ | 0.0 | 0.0 | 0.0 |
| $S_{18}$ | $S_{17}$ | 0.0 | 0.0 | 1.8e-07 |
| $S_{18}$ | $S_{18}$ | 0.0 | 0.0 | -2.95962391 |
| $S_{18}$ | $S_{19}$ | 0.0 | 0.0 | 0.05595836 |
| $S_{18}$ | $S_{20}$ | 0.0 | 0.0 | 0.0 |
| $S_{18}$ | $S_{21}$ | 0.0 | 0.0 | 2e-07 |
| $S_{18}$ | $S_{22}$ | 0.16638965 | 0.0 | 0.0 |
| $S_{18}$ | $S_{23}$ | 0.0 | 0.06933528 | 0.0 |
| $S_{18}$ | $S_{24}$ | 0.0 | 0.0 | 0.0 |
| $S_{18}$ | $S_{25}$ | 0.0 | -0.06745455 | 0.0 |
| $S_{18}$ | $S_{26}$ | -0.00491268 | 0.0 | 0.0 |
| $S_{18}$ | $S_{27}$ | 0.0 | -0.0420427 | 0.0 |
| $S_{18}$ | $S_{28}$ | 0.00071758 | 0.0 | 0.0 |
| $S_{18}$ | $S_{29}$ | 0.0 | 0.0 | 0.07318101 |
| $S_{18}$ | $S_{30}$ | 0.0 | 0.0 | 0.0 |
| $S_{18}$ | $S_{31}$ | 0.09932671 | 0.0 | 0.0 |
| $S_{18}$ | $S_{32}$ | 0.0 | 0.00337075 | 0.0 |
| $S_{18}$ | $S_{33}$ | 0.0 | 0.0 | 0.0 |

| $S_{\text{init}}$ | $S_{\text{final}}$ | $\mu_x$ | $\mu_y$ | $\mu_z$ |
|---|---|---|---|---|
| $S_{18}$ | $S_{34}$ | 0.0 | 0.0 | 0.0 |
| $S_{18}$ | $S_{35}$ | 0.0 | -0.03333661 | 0.0 |
| $S_{18}$ | $S_{36}$ | 0.0 | 0.0 | 0.0 |
| $S_{18}$ | $S_{37}$ | 0.0 | 0.03746665 | 0.0 |
| $S_{18}$ | $S_{38}$ | 0.0 | 0.0 | 0.0 |
| $S_{18}$ | $S_{39}$ | -0.02749808 | 0.0 | 0.0 |
| $S_{18}$ | $S_{40}$ | 0.0 | -0.01026132 | 0.0 |
| $S_{18}$ | $S_{41}$ | 0.0 | 0.02084872 | 0.0 |
| $S_{18}$ | $S_{42}$ | 0.0 | -0.19969176 | 0.0 |
| $S_{18}$ | $S_{43}$ | 0.0 | 0.0 | 0.0 |
| $S_{18}$ | $S_{44}$ | 0.0 | 0.0 | 0.0 |
| $S_{19}$ | $S_0$ | 1.0014635 | 0.0 | 0.0 |
| $S_{19}$ | $S_1$ | -1.05e-06 | 0.0 | 0.0 |
| $S_{19}$ | $S_2$ | 0.0 | 0.00435573 | 0.0 |
| $S_{19}$ | $S_3$ | 0.0 | 0.0 | -0.200965 |
| $S_{19}$ | $S_4$ | 0.0 | 0.0 | -3.4e-07 |
| $S_{19}$ | $S_5$ | 0.0 | 0.0 | 0.0 |
| $S_{19}$ | $S_6$ | 0.0 | 0.0 | -0.09765134 |
| $S_{19}$ | $S_7$ | 0.0 | 0.0 | -1e-08 |
| $S_{19}$ | $S_8$ | 1.26e-05 | 0.0 | 0.0 |
| $S_{19}$ | $S_9$ | -0.09315332 | 0.0 | 0.0 |
| $S_{19}$ | $S_{10}$ | -9.72e-06 | 0.0 | 0.0 |
| $S_{19}$ | $S_{11}$ | 0.0 | 0.0 | -1.6e-07 |
| $S_{19}$ | $S_{12}$ | 0.0 | 0.0 | 0.10899779 |
| $S_{19}$ | $S_{13}$ | -0.37607242 | 0.0 | 0.0 |
| $S_{19}$ | $S_{14}$ | 0.04960033 | 0.0 | 0.0 |
| $S_{19}$ | $S_{15}$ | 0.0 | 0.32029667 | 0.0 |
| $S_{19}$ | $S_{16}$ | 0.0 | 0.0 | 0.0 |
| $S_{19}$ | $S_{17}$ | 0.0 | 0.0 | 8e-08 |
| $S_{19}$ | $S_{18}$ | 0.0 | 0.0 | 0.05595836 |
| $S_{19}$ | $S_{19}$ | 0.0 | 0.0 | -2.1622551 |
| $S_{19}$ | $S_{20}$ | 0.0 | 0.0 | 0.0 |
| $S_{19}$ | $S_{21}$ | 0.0 | 0.0 | 3.5e-07 |
| $S_{19}$ | $S_{22}$ | 0.13582691 | 0.0 | 0.0 |
| $S_{19}$ | $S_{23}$ | 0.0 | -0.2012096 | 0.0 |
| $S_{19}$ | $S_{24}$ | 0.0 | 0.0 | 0.0 |
| $S_{19}$ | $S_{25}$ | 0.0 | 0.20874397 | 0.0 |
| $S_{19}$ | $S_{26}$ | 0.12028194 | 0.0 | 0.0 |
| $S_{19}$ | $S_{27}$ | 0.0 | -0.06646385 | 0.0 |
| $S_{19}$ | $S_{28}$ | -0.00106219 | 0.0 | 0.0 |

| $S_{\text{init}}$ | $S_{\text{final}}$ | $\mu_x$ | $\mu_y$ | $\mu_z$ |
|---|---|---|---|---|
| $S_{19}$ | $S_{29}$ | 0.0 | 0.0 | -0.16706648 |
| $S_{19}$ | $S_{30}$ | 0.0 | 0.0 | 0.0 |
| $S_{19}$ | $S_{31}$ | -0.0359892 | 0.0 | 0.0 |
| $S_{19}$ | $S_{32}$ | 0.0 | 0.02295032 | 0.0 |
| $S_{19}$ | $S_{33}$ | 0.0 | 0.0 | 0.0 |
| $S_{19}$ | $S_{34}$ | 0.0 | 0.0 | 0.0 |
| $S_{19}$ | $S_{35}$ | 0.0 | 0.14194528 | 0.0 |
| $S_{19}$ | $S_{36}$ | 0.0 | 0.0 | 0.0 |
| $S_{19}$ | $S_{37}$ | 0.0 | 0.23134195 | 0.0 |
| $S_{19}$ | $S_{38}$ | 0.0 | 0.0 | 0.0 |
| $S_{19}$ | $S_{39}$ | -0.65328002 | 0.0 | 0.0 |
| $S_{19}$ | $S_{40}$ | 0.0 | 0.02226051 | 0.0 |
| $S_{19}$ | $S_{41}$ | 0.0 | 0.00239209 | 0.0 |
| $S_{19}$ | $S_{42}$ | 0.0 | 0.00999551 | 0.0 |
| $S_{19}$ | $S_{43}$ | 0.0 | 0.0 | 0.0 |
| $S_{19}$ | $S_{44}$ | 0.0 | 0.0 | 0.0 |
| $S_{20}$ | $S_0$ | 0.0 | -0.40811402 | 0.0 |
| $S_{20}$ | $S_1$ | 0.0 | 1e-08 | 0.0 |
| $S_{20}$ | $S_2$ | -0.0041803 | 0.0 | 0.0 |
| $S_{20}$ | $S_3$ | 0.0 | 0.0 | 0.0 |
| $S_{20}$ | $S_4$ | 0.0 | 0.0 | 0.0 |
| $S_{20}$ | $S_5$ | 0.0 | 0.0 | 0.00313974 |
| $S_{20}$ | $S_6$ | 0.0 | 0.0 | 0.0 |
| $S_{20}$ | $S_7$ | 0.0 | 0.0 | 0.0 |
| $S_{20}$ | $S_8$ | 0.0 | -1e-08 | 0.0 |
| $S_{20}$ | $S_9$ | 0.0 | -0.09963052 | 0.0 |
| $S_{20}$ | $S_{10}$ | 0.0 | 0.0 | 0.0 |
| $S_{20}$ | $S_{11}$ | 0.0 | 0.0 | 0.0 |
| $S_{20}$ | $S_{12}$ | 0.0 | 0.0 | 0.0 |
| $S_{20}$ | $S_{13}$ | 0.0 | 0.16202334 | 0.0 |
| $S_{20}$ | $S_{14}$ | 0.0 | 0.09844367 | 0.0 |
| $S_{20}$ | $S_{15}$ | -3.80570339 | 0.0 | 0.0 |
| $S_{20}$ | $S_{16}$ | 0.0 | 0.0 | 0.42868013 |
| $S_{20}$ | $S_{17}$ | 0.0 | 0.0 | 0.0 |
| $S_{20}$ | $S_{18}$ | 0.0 | 0.0 | 0.0 |
| $S_{20}$ | $S_{19}$ | 0.0 | 0.0 | 0.0 |
| $S_{20}$ | $S_{20}$ | 0.0 | 0.0 | -2.79192924 |
| $S_{20}$ | $S_{21}$ | 0.0 | 0.0 | 0.0 |
| $S_{20}$ | $S_{22}$ | 0.0 | 0.10728878 | 0.0 |
| $S_{20}$ | $S_{23}$ | 0.56085722 | 0.0 | 0.0 |

| $S_{\text{init}}$ | $S_{\text{final}}$ | $\mu_x$ | $\mu_y$ | $\mu_z$ |
|---|---|---|---|---|
| $S_{20}$ | $S_{24}$ | 0.0 | 0.0 | -0.74744624 |
| $S_{20}$ | $S_{25}$ | 0.37478615 | 0.0 | 0.0 |
| $S_{20}$ | $S_{26}$ | 0.0 | -0.37791542 | 0.0 |
| $S_{20}$ | $S_{27}$ | 2.99901163 | 0.0 | 0.0 |
| $S_{20}$ | $S_{28}$ | 0.0 | -1.87e-05 | 0.0 |
| $S_{20}$ | $S_{29}$ | 0.0 | 0.0 | 0.0 |
| $S_{20}$ | $S_{30}$ | 0.0 | 0.0 | 1.56674918 |
| $S_{20}$ | $S_{31}$ | 0.0 | -0.82587227 | 0.0 |
| $S_{20}$ | $S_{32}$ | -0.2133184 | 0.0 | 0.0 |
| $S_{20}$ | $S_{33}$ | 0.0 | 0.0 | 2.49171549 |
| $S_{20}$ | $S_{34}$ | 0.0 | 0.0 | -0.22794205 |
| $S_{20}$ | $S_{35}$ | 0.24125662 | 0.0 | 0.0 |
| $S_{20}$ | $S_{36}$ | 0.0 | 0.0 | -0.18416303 |
| $S_{20}$ | $S_{37}$ | -1.19670086 | 0.0 | 0.0 |
| $S_{20}$ | $S_{38}$ | 0.0 | 0.0 | -0.25271534 |
| $S_{20}$ | $S_{39}$ | 0.0 | 2.33334705 | 0.0 |
| $S_{20}$ | $S_{40}$ | 0.25686337 | 0.0 | 0.0 |
| $S_{20}$ | $S_{41}$ | -0.00597277 | 0.0 | 0.0 |
| $S_{20}$ | $S_{42}$ | -0.42895554 | 0.0 | 0.0 |
| $S_{20}$ | $S_{43}$ | 0.0 | 0.0 | -0.04338927 |
| $S_{20}$ | $S_{44}$ | 0.0 | 0.0 | -0.39380595 |
| $S_{21}$ | $S_0$ | -1.36e-14 | 0.0 | 0.0 |
| $S_{21}$ | $S_1$ | -1.07684047 | 0.0 | 0.0 |
| $S_{21}$ | $S_2$ | 0.0 | -1.8e-07 | 0.0 |
| $S_{21}$ | $S_3$ | 0.0 | 0.0 | -9.9e-07 |
| $S_{21}$ | $S_4$ | 0.0 | 0.0 | -0.03341141 |
| $S_{21}$ | $S_5$ | 0.0 | 0.0 | 0.0 |
| $S_{21}$ | $S_6$ | 0.0 | 0.0 | -7.92e-06 |
| $S_{21}$ | $S_7$ | 0.0 | 0.0 | -0.0428357 |
| $S_{21}$ | $S_8$ | -0.40688586 | 0.0 | 0.0 |
| $S_{21}$ | $S_9$ | -4.23e-05 | 0.0 | 0.0 |
| $S_{21}$ | $S_{10}$ | 0.20367732 | 0.0 | 0.0 |
| $S_{21}$ | $S_{11}$ | 0.0 | 0.0 | 0.05005918 |
| $S_{21}$ | $S_{12}$ | 0.0 | 0.0 | -4.8e-07 |
| $S_{21}$ | $S_{13}$ | 3.95e-05 | 0.0 | 0.0 |
| $S_{21}$ | $S_{14}$ | 8.93e-05 | 0.0 | 0.0 |
| $S_{21}$ | $S_{15}$ | 0.0 | 0.0 | 0.0 |
| $S_{21}$ | $S_{16}$ | 0.0 | 0.0 | 0.0 |
| $S_{21}$ | $S_{17}$ | 0.0 | 0.0 | -0.00281451 |
| $S_{21}$ | $S_{18}$ | 0.0 | 0.0 | 2e-07 |

| $S_{\text{init}}$ | $S_{\text{final}}$ | $\mu_x$ | $\mu_y$ | $\mu_z$ |
|---|---|---|---|---|
| $S_{21}$ | $S_{19}$ | 0.0 | 0.0 | 3.5e-07 |
| $S_{21}$ | $S_{20}$ | 0.0 | 0.0 | 0.0 |
| $S_{21}$ | $S_{21}$ | 0.0 | 0.0 | -2.92845918 |
| $S_{21}$ | $S_{22}$ | 5.53e-05 | 0.0 | 0.0 |
| $S_{21}$ | $S_{23}$ | 0.0 | 1e-08 | 0.0 |
| $S_{21}$ | $S_{24}$ | 0.0 | 0.0 | 0.0 |
| $S_{21}$ | $S_{25}$ | 0.0 | 1e-08 | 0.0 |
| $S_{21}$ | $S_{26}$ | -8.75e-05 | 0.0 | 0.0 |
| $S_{21}$ | $S_{27}$ | 0.0 | 1e-08 | 0.0 |
| $S_{21}$ | $S_{28}$ | -1e-08 | 0.0 | 0.0 |
| $S_{21}$ | $S_{29}$ | 0.0 | 0.0 | 0.0 |
| $S_{21}$ | $S_{30}$ | 0.0 | 0.0 | 0.0 |
| $S_{21}$ | $S_{31}$ | 6.54e-06 | 0.0 | 0.0 |
| $S_{21}$ | $S_{32}$ | 0.0 | -2e-08 | 0.0 |
| $S_{21}$ | $S_{33}$ | 0.0 | 0.0 | 0.0 |
| $S_{21}$ | $S_{34}$ | 0.0 | 0.0 | 0.0 |
| $S_{21}$ | $S_{35}$ | 0.0 | -3e-08 | 0.0 |
| $S_{21}$ | $S_{36}$ | 0.0 | 0.0 | 0.0 |
| $S_{21}$ | $S_{37}$ | 0.0 | -1e-08 | 0.0 |
| $S_{21}$ | $S_{38}$ | 0.0 | 0.0 | 0.0 |
| $S_{21}$ | $S_{39}$ | -1.15e-05 | 0.0 | 0.0 |
| $S_{21}$ | $S_{40}$ | 0.0 | 2e-08 | 0.0 |
| $S_{21}$ | $S_{41}$ | 0.0 | -6e-08 | 0.0 |
| $S_{21}$ | $S_{42}$ | 0.0 | -2e-08 | 0.0 |
| $S_{21}$ | $S_{43}$ | 0.0 | 0.0 | 0.0 |
| $S_{21}$ | $S_{44}$ | 0.0 | 0.0 | 0.0 |
| $S_{22}$ | $S_0$ | 0.0 | 0.0 | 0.42989645 |
| $S_{22}$ | $S_1$ | 0.0 | 0.0 | -1.2e-07 |
| $S_{22}$ | $S_2$ | 0.0 | 0.0 | 0.0 |
| $S_{22}$ | $S_3$ | 0.82506097 | 0.0 | 0.0 |
| $S_{22}$ | $S_4$ | -7.15e-05 | 0.0 | 0.0 |
| $S_{22}$ | $S_5$ | 0.0 | 0.00446851 | 0.0 |
| $S_{22}$ | $S_6$ | -0.95001385 | 0.0 | 0.0 |
| $S_{22}$ | $S_7$ | 6.31e-05 | 0.0 | 0.0 |
| $S_{22}$ | $S_8$ | 0.0 | 0.0 | 6.1e-07 |
| $S_{22}$ | $S_9$ | 0.0 | 0.0 | -0.04440032 |
| $S_{22}$ | $S_{10}$ | 0.0 | 0.0 | -2.3e-07 |
| $S_{22}$ | $S_{11}$ | -2.31e-05 | 0.0 | 0.0 |
| $S_{22}$ | $S_{12}$ | 0.0701525 | 0.0 | 0.0 |
| $S_{22}$ | $S_{13}$ | 0.0 | 0.0 | 0.19598621 |

| $S_{\text{init}}$ | $S_{\text{final}}$ | $\mu_x$ | $\mu_y$ | $\mu_z$ |
|---|---|---|---|---|
| $S_{22}$ | $S_{14}$ | 0.0 | 0.0 | 0.15358366 |
| $S_{22}$ | $S_{15}$ | 0.0 | 0.0 | 0.0 |
| $S_{22}$ | $S_{16}$ | 0.0 | 0.1766467 | 0.0 |
| $S_{22}$ | $S_{17}$ | 3.29e-05 | 0.0 | 0.0 |
| $S_{22}$ | $S_{18}$ | 0.16638965 | 0.0 | 0.0 |
| $S_{22}$ | $S_{19}$ | 0.13582691 | 0.0 | 0.0 |
| $S_{22}$ | $S_{20}$ | 0.0 | 0.10728878 | 0.0 |
| $S_{22}$ | $S_{21}$ | 5.53e-05 | 0.0 | 0.0 |
| $S_{22}$ | $S_{22}$ | 0.0 | 0.0 | -3.30205588 |
| $S_{22}$ | $S_{23}$ | 0.0 | 0.0 | 0.0 |
| $S_{22}$ | $S_{24}$ | 0.0 | -0.01363048 | 0.0 |
| $S_{22}$ | $S_{25}$ | 0.0 | 0.0 | 0.0 |
| $S_{22}$ | $S_{26}$ | 0.0 | 0.0 | -1.19058477 |
| $S_{22}$ | $S_{27}$ | 0.0 | 0.0 | 0.0 |
| $S_{22}$ | $S_{28}$ | 0.0 | 0.0 | 0.0008985 |
| $S_{22}$ | $S_{29}$ | 0.03423862 | 0.0 | 0.0 |
| $S_{22}$ | $S_{30}$ | 0.0 | -0.17870505 | 0.0 |
| $S_{22}$ | $S_{31}$ | 0.0 | 0.0 | 0.30419901 |
| $S_{22}$ | $S_{32}$ | 0.0 | 0.0 | 0.0 |
| $S_{22}$ | $S_{33}$ | 0.0 | 0.24876836 | 0.0 |
| $S_{22}$ | $S_{34}$ | 0.0 | -0.00779733 | 0.0 |
| $S_{22}$ | $S_{35}$ | 0.0 | 0.0 | 0.0 |
| $S_{22}$ | $S_{36}$ | 0.0 | -0.02640432 | 0.0 |
| $S_{22}$ | $S_{37}$ | 0.0 | 0.0 | 0.0 |
| $S_{22}$ | $S_{38}$ | 0.0 | -0.14380123 | 0.0 |
| $S_{22}$ | $S_{39}$ | 0.0 | 0.0 | 0.21736769 |
| $S_{22}$ | $S_{40}$ | 0.0 | 0.0 | 0.0 |
| $S_{22}$ | $S_{41}$ | 0.0 | 0.0 | 0.0 |
| $S_{22}$ | $S_{42}$ | 0.0 | 0.0 | 0.0 |
| $S_{22}$ | $S_{43}$ | 0.0 | -0.05445384 | 0.0 |
| $S_{22}$ | $S_{44}$ | 0.0 | -0.05063163 | 0.0 |
| $S_{23}$ | $S_0$ | 0.0 | 0.0 | 0.0 |
| $S_{23}$ | $S_1$ | 0.0 | 0.0 | 0.0 |
| $S_{23}$ | $S_2$ | 0.0 | 0.0 | -0.00641344 |
| $S_{23}$ | $S_3$ | 0.0 | 0.22850685 | 0.0 |
| $S_{23}$ | $S_4$ | 0.0 | 1e-08 | 0.0 |
| $S_{23}$ | $S_5$ | -0.00310139 | 0.0 | 0.0 |
| $S_{23}$ | $S_6$ | 0.0 | -0.03502104 | 0.0 |
| $S_{23}$ | $S_7$ | 0.0 | -1e-08 | 0.0 |
| $S_{23}$ | $S_8$ | 0.0 | 0.0 | 0.0 |

| $S_{\text{init}}$ | $S_{\text{final}}$ | $\mu_x$ | $\mu_y$ | $\mu_z$ |
|---|---|---|---|---|
| $S_{23}$ | $S_9$ | 0.0 | 0.0 | 0.0 |
| $S_{23}$ | $S_{10}$ | 0.0 | 0.0 | 0.0 |
| $S_{23}$ | $S_{11}$ | 0.0 | -1e-08 | 0.0 |
| $S_{23}$ | $S_{12}$ | 0.0 | 0.23606345 | 0.0 |
| $S_{23}$ | $S_{13}$ | 0.0 | 0.0 | 0.0 |
| $S_{23}$ | $S_{14}$ | 0.0 | 0.0 | 0.0 |
| $S_{23}$ | $S_{15}$ | 0.0 | 0.0 | -2.32138397 |
| $S_{23}$ | $S_{16}$ | 2.353645 | 0.0 | 0.0 |
| $S_{23}$ | $S_{17}$ | 0.0 | 1e-08 | 0.0 |
| $S_{23}$ | $S_{18}$ | 0.0 | 0.06933528 | 0.0 |
| $S_{23}$ | $S_{19}$ | 0.0 | -0.2012096 | 0.0 |
| $S_{23}$ | $S_{20}$ | 0.56085722 | 0.0 | 0.0 |
| $S_{23}$ | $S_{21}$ | 0.0 | 1e-08 | 0.0 |
| $S_{23}$ | $S_{22}$ | 0.0 | 0.0 | 0.0 |
| $S_{23}$ | $S_{23}$ | 0.0 | 0.0 | -3.13711844 |
| $S_{23}$ | $S_{24}$ | -0.45012152 | 0.0 | 0.0 |
| $S_{23}$ | $S_{25}$ | 0.0 | 0.0 | 0.04062429 |
| $S_{23}$ | $S_{26}$ | 0.0 | 0.0 | 0.0 |
| $S_{23}$ | $S_{27}$ | 0.0 | 0.0 | -0.7357419 |
| $S_{23}$ | $S_{28}$ | 0.0 | 0.0 | 0.0 |
| $S_{23}$ | $S_{29}$ | 0.0 | 0.92765686 | 0.0 |
| $S_{23}$ | $S_{30}$ | 3.16341007 | 0.0 | 0.0 |
| $S_{23}$ | $S_{31}$ | 0.0 | 0.0 | 0.0 |
| $S_{23}$ | $S_{32}$ | 0.0 | 0.0 | 0.36413527 |
| $S_{23}$ | $S_{33}$ | 0.53579209 | 0.0 | 0.0 |
| $S_{23}$ | $S_{34}$ | -0.23081812 | 0.0 | 0.0 |
| $S_{23}$ | $S_{35}$ | 0.0 | 0.0 | -2.27555895 |
| $S_{23}$ | $S_{36}$ | 0.32625869 | 0.0 | 0.0 |
| $S_{23}$ | $S_{37}$ | 0.0 | 0.0 | 1.50465859 |
| $S_{23}$ | $S_{38}$ | 1.3435305 | 0.0 | 0.0 |
| $S_{23}$ | $S_{39}$ | 0.0 | 0.0 | 0.0 |
| $S_{23}$ | $S_{40}$ | 0.0 | 0.0 | -0.17458642 |
| $S_{23}$ | $S_{41}$ | 0.0 | 0.0 | -0.13969005 |
| $S_{23}$ | $S_{42}$ | 0.0 | 0.0 | -0.28541972 |
| $S_{23}$ | $S_{43}$ | -0.40796856 | 0.0 | 0.0 |
| $S_{23}$ | $S_{44}$ | -1.12878757 | 0.0 | 0.0 |
| $S_{24}$ | $S_0$ | 0.0 | 0.11297427 | 0.0 |
| $S_{24}$ | $S_1$ | 0.0 | -4e-08 | 0.0 |
| $S_{24}$ | $S_2$ | -0.00112696 | 0.0 | 0.0 |
| $S_{24}$ | $S_3$ | 0.0 | 0.0 | 0.0 |

| $S_{\text{init}}$ | $S_{\text{final}}$ | $\mu_x$ | $\mu_y$ | $\mu_z$ |
|---|---|---|---|---|
| $S_{24}$ | $S_4$ | 0.0 | 0.0 | 0.0 |
| $S_{24}$ | $S_5$ | 0.0 | 0.0 | -0.00732068 |
| $S_{24}$ | $S_6$ | 0.0 | 0.0 | 0.0 |
| $S_{24}$ | $S_7$ | 0.0 | 0.0 | 0.0 |
| $S_{24}$ | $S_8$ | 0.0 | 0.0 | 0.0 |
| $S_{24}$ | $S_9$ | 0.0 | 0.37540006 | 0.0 |
| $S_{24}$ | $S_{10}$ | 0.0 | 1e-08 | 0.0 |
| $S_{24}$ | $S_{11}$ | 0.0 | 0.0 | 0.0 |
| $S_{24}$ | $S_{12}$ | 0.0 | 0.0 | 0.0 |
| $S_{24}$ | $S_{13}$ | 0.0 | -0.04163952 | 0.0 |
| $S_{24}$ | $S_{14}$ | 0.0 | 0.0982201 | 0.0 |
| $S_{24}$ | $S_{15}$ | -0.94875204 | 0.0 | 0.0 |
| $S_{24}$ | $S_{16}$ | 0.0 | 0.0 | -2.83265618 |
| $S_{24}$ | $S_{17}$ | 0.0 | 0.0 | 0.0 |
| $S_{24}$ | $S_{18}$ | 0.0 | 0.0 | 0.0 |
| $S_{24}$ | $S_{19}$ | 0.0 | 0.0 | 0.0 |
| $S_{24}$ | $S_{20}$ | 0.0 | 0.0 | -0.74744624 |
| $S_{24}$ | $S_{21}$ | 0.0 | 0.0 | 0.0 |
| $S_{24}$ | $S_{22}$ | 0.0 | -0.01363048 | 0.0 |
| $S_{24}$ | $S_{23}$ | -0.45012152 | 0.0 | 0.0 |
| $S_{24}$ | $S_{24}$ | 0.0 | 0.0 | -3.11970659 |
| $S_{24}$ | $S_{25}$ | -0.65330736 | 0.0 | 0.0 |
| $S_{24}$ | $S_{26}$ | 0.0 | 0.31614445 | 0.0 |
| $S_{24}$ | $S_{27}$ | 0.29333195 | 0.0 | 0.0 |
| $S_{24}$ | $S_{28}$ | 0.0 | 2.61e-05 | 0.0 |
| $S_{24}$ | $S_{29}$ | 0.0 | 0.0 | 0.0 |
| $S_{24}$ | $S_{30}$ | 0.0 | 0.0 | 1.2183888 |
| $S_{24}$ | $S_{31}$ | 0.0 | 1.355854 | 0.0 |
| $S_{24}$ | $S_{32}$ | -0.11035278 | 0.0 | 0.0 |
| $S_{24}$ | $S_{33}$ | 0.0 | 0.0 | 0.11721876 |
| $S_{24}$ | $S_{34}$ | 0.0 | 0.0 | -0.11241332 |
| $S_{24}$ | $S_{35}$ | 3.00759483 | 0.0 | 0.0 |
| $S_{24}$ | $S_{36}$ | 0.0 | 0.0 | 0.78694926 |
| $S_{24}$ | $S_{37}$ | 0.67753381 | 0.0 | 0.0 |
| $S_{24}$ | $S_{38}$ | 0.0 | 0.0 | 2.45300293 |
| $S_{24}$ | $S_{39}$ | 0.0 | 0.02388821 | 0.0 |
| $S_{24}$ | $S_{40}$ | 0.02933747 | 0.0 | 0.0 |
| $S_{24}$ | $S_{41}$ | 0.14040019 | 0.0 | 0.0 |
| $S_{24}$ | $S_{42}$ | -0.36480875 | 0.0 | 0.0 |
| $S_{24}$ | $S_{43}$ | 0.0 | 0.0 | 0.25675728 |

| $S_{\text{init}}$ | $S_{\text{final}}$ | $\mu_x$ | $\mu_y$ | $\mu_z$ |
|---|---|---|---|---|
| $S_{24}$ | $S_{44}$ | 0.0 | 0.0 | 1.53792337 |
| $S_{25}$ | $S_0$ | 0.0 | 0.0 | 0.0 |
| $S_{25}$ | $S_1$ | 0.0 | 0.0 | 0.0 |
| $S_{25}$ | $S_2$ | 0.0 | 0.0 | 0.00326279 |
| $S_{25}$ | $S_3$ | 0.0 | -0.08125627 | 0.0 |
| $S_{25}$ | $S_4$ | 0.0 | 0.0 | 0.0 |
| $S_{25}$ | $S_5$ | 0.00101141 | 0.0 | 0.0 |
| $S_{25}$ | $S_6$ | 0.0 | 0.03215045 | 0.0 |
| $S_{25}$ | $S_7$ | 0.0 | 0.0 | 0.0 |
| $S_{25}$ | $S_8$ | 0.0 | 0.0 | 0.0 |
| $S_{25}$ | $S_9$ | 0.0 | 0.0 | 0.0 |
| $S_{25}$ | $S_{10}$ | 0.0 | 0.0 | 0.0 |
| $S_{25}$ | $S_{11}$ | 0.0 | 1e-08 | 0.0 |
| $S_{25}$ | $S_{12}$ | 0.0 | -0.35096681 | 0.0 |
| $S_{25}$ | $S_{13}$ | 0.0 | 0.0 | 0.0 |
| $S_{25}$ | $S_{14}$ | 0.0 | 0.0 | 0.0 |
| $S_{25}$ | $S_{15}$ | 0.0 | 0.0 | 2.04532817 |
| $S_{25}$ | $S_{16}$ | 2.52239017 | 0.0 | 0.0 |
| $S_{25}$ | $S_{17}$ | 0.0 | -1e-08 | 0.0 |
| $S_{25}$ | $S_{18}$ | 0.0 | -0.06745455 | 0.0 |
| $S_{25}$ | $S_{19}$ | 0.0 | 0.20874397 | 0.0 |
| $S_{25}$ | $S_{20}$ | 0.37478615 | 0.0 | 0.0 |
| $S_{25}$ | $S_{21}$ | 0.0 | 1e-08 | 0.0 |
| $S_{25}$ | $S_{22}$ | 0.0 | 0.0 | 0.0 |
| $S_{25}$ | $S_{23}$ | 0.0 | 0.0 | 0.04062429 |
| $S_{25}$ | $S_{24}$ | -0.65330736 | 0.0 | 0.0 |
| $S_{25}$ | $S_{25}$ | 0.0 | 0.0 | -4.69717255 |
| $S_{25}$ | $S_{26}$ | 0.0 | 0.0 | 0.0 |
| $S_{25}$ | $S_{27}$ | 0.0 | 0.0 | 1.02957859 |
| $S_{25}$ | $S_{28}$ | 0.0 | 0.0 | 0.0 |
| $S_{25}$ | $S_{29}$ | 0.0 | -0.23507329 | 0.0 |
| $S_{25}$ | $S_{30}$ | 0.88742679 | 0.0 | 0.0 |
| $S_{25}$ | $S_{31}$ | 0.0 | 0.0 | 0.0 |
| $S_{25}$ | $S_{32}$ | 0.0 | 0.0 | -0.0731955 |
| $S_{25}$ | $S_{33}$ | -3.86463316 | 0.0 | 0.0 |
| $S_{25}$ | $S_{34}$ | 0.18487407 | 0.0 | 0.0 |
| $S_{25}$ | $S_{35}$ | 0.0 | 0.0 | -1.69387457 |
| $S_{25}$ | $S_{36}$ | 0.02857661 | 0.0 | 0.0 |
| $S_{25}$ | $S_{37}$ | 0.0 | 0.0 | -2.74261219 |
| $S_{25}$ | $S_{38}$ | 0.88058418 | 0.0 | 0.0 |

| $S_{\text{init}}$ | $S_{\text{final}}$ | $\mu_x$ | $\mu_y$ | $\mu_z$ |
|---|---|---|---|---|
| $S_{25}$ | $S_{39}$ | 0.0 | 0.0 | 0.0 |
| $S_{25}$ | $S_{40}$ | 0.0 | 0.0 | 0.33106317 |
| $S_{25}$ | $S_{41}$ | 0.0 | 0.0 | 0.01053986 |
| $S_{25}$ | $S_{42}$ | 0.0 | 0.0 | 0.22486905 |
| $S_{25}$ | $S_{43}$ | -0.33105435 | 0.0 | 0.0 |
| $S_{25}$ | $S_{44}$ | -1.27526208 | 0.0 | 0.0 |
| $S_{26}$ | $S_0$ | 0.0 | 0.0 | 0.35816647 |
| $S_{26}$ | $S_1$ | 0.0 | 0.0 | 1.13e-06 |
| $S_{26}$ | $S_2$ | 0.0 | 0.0 | 0.0 |
| $S_{26}$ | $S_3$ | 0.40269755 | 0.0 | 0.0 |
| $S_{26}$ | $S_4$ | 0.00026817 | 0.0 | 0.0 |
| $S_{26}$ | $S_5$ | 0.0 | -0.00259816 | 0.0 |
| $S_{26}$ | $S_6$ | 2.67227019 | 0.0 | 0.0 |
| $S_{26}$ | $S_7$ | -9.18e-05 | 0.0 | 0.0 |
| $S_{26}$ | $S_8$ | 0.0 | 0.0 | -1.18e-06 |
| $S_{26}$ | $S_9$ | 0.0 | 0.0 | 0.741929 |
| $S_{26}$ | $S_{10}$ | 0.0 | 0.0 | 1.8e-07 |
| $S_{26}$ | $S_{11}$ | 4.58e-05 | 0.0 | 0.0 |
| $S_{26}$ | $S_{12}$ | -0.0025709 | 0.0 | 0.0 |
| $S_{26}$ | $S_{13}$ | 0.0 | 0.0 | -0.21378941 |
| $S_{26}$ | $S_{14}$ | 0.0 | 0.0 | -0.23538562 |
| $S_{26}$ | $S_{15}$ | 0.0 | 0.0 | 0.0 |
| $S_{26}$ | $S_{16}$ | 0.0 | -0.62481902 | 0.0 |
| $S_{26}$ | $S_{17}$ | -1.25e-05 | 0.0 | 0.0 |
| $S_{26}$ | $S_{18}$ | -0.00491268 | 0.0 | 0.0 |
| $S_{26}$ | $S_{19}$ | 0.12028194 | 0.0 | 0.0 |
| $S_{26}$ | $S_{20}$ | 0.0 | -0.37791542 | 0.0 |
| $S_{26}$ | $S_{21}$ | -8.75e-05 | 0.0 | 0.0 |
| $S_{26}$ | $S_{22}$ | 0.0 | 0.0 | -1.19058477 |
| $S_{26}$ | $S_{23}$ | 0.0 | 0.0 | 0.0 |
| $S_{26}$ | $S_{24}$ | 0.0 | 0.31614445 | 0.0 |
| $S_{26}$ | $S_{25}$ | 0.0 | 0.0 | 0.0 |
| $S_{26}$ | $S_{26}$ | 0.0 | 0.0 | -1.76387152 |
| $S_{26}$ | $S_{27}$ | 0.0 | 0.0 | 0.0 |
| $S_{26}$ | $S_{28}$ | 0.0 | 0.0 | 0.00012529 |
| $S_{26}$ | $S_{29}$ | -0.15966516 | 0.0 | 0.0 |
| $S_{26}$ | $S_{30}$ | 0.0 | 0.38257109 | 0.0 |
| $S_{26}$ | $S_{31}$ | 0.0 | 0.0 | -0.29176772 |
| $S_{26}$ | $S_{32}$ | 0.0 | 0.0 | 0.0 |
| $S_{26}$ | $S_{33}$ | 0.0 | -0.47770016 | 0.0 |

| $S_{\text{init}}$ | $S_{\text{final}}$ | $\mu_x$ | $\mu_y$ | $\mu_z$ |
|---|---|---|---|---|
| $S_{26}$ | $S_{34}$ | 0.0 | 0.02976766 | 0.0 |
| $S_{26}$ | $S_{35}$ | 0.0 | 0.0 | 0.0 |
| $S_{26}$ | $S_{36}$ | 0.0 | 0.04690854 | 0.0 |
| $S_{26}$ | $S_{37}$ | 0.0 | 0.0 | 0.0 |
| $S_{26}$ | $S_{38}$ | 0.0 | 0.23127148 | 0.0 |
| $S_{26}$ | $S_{39}$ | 0.0 | 0.0 | -0.40459768 |
| $S_{26}$ | $S_{40}$ | 0.0 | 0.0 | 0.0 |
| $S_{26}$ | $S_{41}$ | 0.0 | 0.0 | 0.0 |
| $S_{26}$ | $S_{42}$ | 0.0 | 0.0 | 0.0 |
| $S_{26}$ | $S_{43}$ | 0.0 | 0.1066169 | 0.0 |
| $S_{26}$ | $S_{44}$ | 0.0 | 0.1428613 | 0.0 |
| $S_{27}$ | $S_0$ | 0.0 | 0.0 | 0.0 |
| $S_{27}$ | $S_1$ | 0.0 | 0.0 | 0.0 |
| $S_{27}$ | $S_2$ | 0.0 | 0.0 | -0.00563205 |
| $S_{27}$ | $S_3$ | 0.0 | 0.13465421 | 0.0 |
| $S_{27}$ | $S_4$ | 0.0 | 0.0 | 0.0 |
| $S_{27}$ | $S_5$ | 0.02133952 | 0.0 | 0.0 |
| $S_{27}$ | $S_6$ | 0.0 | 0.00838117 | 0.0 |
| $S_{27}$ | $S_7$ | 0.0 | -1e-08 | 0.0 |
| $S_{27}$ | $S_8$ | 0.0 | 0.0 | 0.0 |
| $S_{27}$ | $S_9$ | 0.0 | 0.0 | 0.0 |
| $S_{27}$ | $S_{10}$ | 0.0 | 0.0 | 0.0 |
| $S_{27}$ | $S_{11}$ | 0.0 | -1e-08 | 0.0 |
| $S_{27}$ | $S_{12}$ | 0.0 | -0.0977081 | 0.0 |
| $S_{27}$ | $S_{13}$ | 0.0 | 0.0 | 0.0 |
| $S_{27}$ | $S_{14}$ | 0.0 | 0.0 | 0.0 |
| $S_{27}$ | $S_{15}$ | 0.0 | 0.0 | -0.63366242 |
| $S_{27}$ | $S_{16}$ | 0.0432952 | 0.0 | 0.0 |
| $S_{27}$ | $S_{17}$ | 0.0 | 1e-08 | 0.0 |
| $S_{27}$ | $S_{18}$ | 0.0 | -0.0420427 | 0.0 |
| $S_{27}$ | $S_{19}$ | 0.0 | -0.06646385 | 0.0 |
| $S_{27}$ | $S_{20}$ | 2.99901163 | 0.0 | 0.0 |
| $S_{27}$ | $S_{21}$ | 0.0 | 1e-08 | 0.0 |
| $S_{27}$ | $S_{22}$ | 0.0 | 0.0 | 0.0 |
| $S_{27}$ | $S_{23}$ | 0.0 | 0.0 | -0.7357419 |
| $S_{27}$ | $S_{24}$ | 0.29333195 | 0.0 | 0.0 |
| $S_{27}$ | $S_{25}$ | 0.0 | 0.0 | 1.02957859 |
| $S_{27}$ | $S_{26}$ | 0.0 | 0.0 | 0.0 |
| $S_{27}$ | $S_{27}$ | 0.0 | 0.0 | -2.36011534 |
| $S_{27}$ | $S_{28}$ | 0.0 | 0.0 | 0.0 |

| $S_{\text{init}}$ | $S_{\text{final}}$ | $\mu_x$ | $\mu_y$ | $\mu_z$ |
|---|---|---|---|---|
| $S_{27}$ | $S_{29}$ | 0.0 | -1.52688311 | 0.0 |
| $S_{27}$ | $S_{30}$ | 1.36001343 | 0.0 | 0.0 |
| $S_{27}$ | $S_{31}$ | 0.0 | 0.0 | 0.0 |
| $S_{27}$ | $S_{32}$ | 0.0 | 0.0 | 0.32301934 |
| $S_{27}$ | $S_{33}$ | 0.3589172 | 0.0 | 0.0 |
| $S_{27}$ | $S_{34}$ | -0.13846707 | 0.0 | 0.0 |
| $S_{27}$ | $S_{35}$ | 0.0 | 0.0 | -0.86945332 |
| $S_{27}$ | $S_{36}$ | 0.02101643 | 0.0 | 0.0 |
| $S_{27}$ | $S_{37}$ | 0.0 | 0.0 | 1.48041238 |
| $S_{27}$ | $S_{38}$ | 0.26738953 | 0.0 | 0.0 |
| $S_{27}$ | $S_{39}$ | 0.0 | 0.0 | 0.0 |
| $S_{27}$ | $S_{40}$ | 0.0 | 0.0 | 0.13646126 |
| $S_{27}$ | $S_{41}$ | 0.0 | 0.0 | -0.20383087 |
| $S_{27}$ | $S_{42}$ | 0.0 | 0.0 | 0.65779117 |
| $S_{27}$ | $S_{43}$ | 0.40273576 | 0.0 | 0.0 |
| $S_{27}$ | $S_{44}$ | 0.41284317 | 0.0 | 0.0 |
| $S_{28}$ | $S_0$ | 0.0 | 0.0 | 9.11e-06 |
| $S_{28}$ | $S_1$ | 0.0 | 0.0 | 0.0 |
| $S_{28}$ | $S_2$ | 0.0 | 0.0 | 0.0 |
| $S_{28}$ | $S_3$ | -0.00101797 | 0.0 | 0.0 |
| $S_{28}$ | $S_4$ | 2e-08 | 0.0 | 0.0 |
| $S_{28}$ | $S_5$ | 0.0 | -1.53e-05 | 0.0 |
| $S_{28}$ | $S_6$ | 0.00417707 | 0.0 | 0.0 |
| $S_{28}$ | $S_7$ | -4e-08 | 0.0 | 0.0 |
| $S_{28}$ | $S_8$ | 0.0 | 0.0 | 0.0 |
| $S_{28}$ | $S_9$ | 0.0 | 0.0 | -0.00035467 |
| $S_{28}$ | $S_{10}$ | 0.0 | 0.0 | 0.0 |
| $S_{28}$ | $S_{11}$ | 0.0 | 0.0 | 0.0 |
| $S_{28}$ | $S_{12}$ | 0.00016949 | 0.0 | 0.0 |
| $S_{28}$ | $S_{13}$ | 0.0 | 0.0 | -0.00035587 |
| $S_{28}$ | $S_{14}$ | 0.0 | 0.0 | 4.72e-05 |
| $S_{28}$ | $S_{15}$ | 0.0 | 0.0 | 0.0 |
| $S_{28}$ | $S_{16}$ | 0.0 | -1.03e-05 | 0.0 |
| $S_{28}$ | $S_{17}$ | -1e-08 | 0.0 | 0.0 |
| $S_{28}$ | $S_{18}$ | 0.00071758 | 0.0 | 0.0 |
| $S_{28}$ | $S_{19}$ | -0.00106219 | 0.0 | 0.0 |
| $S_{28}$ | $S_{20}$ | 0.0 | -1.87e-05 | 0.0 |
| $S_{28}$ | $S_{21}$ | -1e-08 | 0.0 | 0.0 |
| $S_{28}$ | $S_{22}$ | 0.0 | 0.0 | 0.0008985 |
| $S_{28}$ | $S_{23}$ | 0.0 | 0.0 | 0.0 |

| $S_{\text{init}}$ | $S_{\text{final}}$ | $\mu_x$ | $\mu_y$ | $\mu_z$ |
|---|---|---|---|---|
| $S_{28}$ | $S_{24}$ | 0.0 | 2.61e-05 | 0.0 |
| $S_{28}$ | $S_{25}$ | 0.0 | 0.0 | 0.0 |
| $S_{28}$ | $S_{26}$ | 0.0 | 0.0 | 0.00012529 |
| $S_{28}$ | $S_{27}$ | 0.0 | 0.0 | 0.0 |
| $S_{28}$ | $S_{28}$ | 0.0 | 0.0 | -1.5482213 |
| $S_{28}$ | $S_{29}$ | 0.00109863 | 0.0 | 0.0 |
| $S_{28}$ | $S_{30}$ | 0.0 | -9.65e-06 | 0.0 |
| $S_{28}$ | $S_{31}$ | 0.0 | 0.0 | -5.85e-05 |
| $S_{28}$ | $S_{32}$ | 0.0 | 0.0 | 0.0 |
| $S_{28}$ | $S_{33}$ | 0.0 | -1.93e-05 | 0.0 |
| $S_{28}$ | $S_{34}$ | 0.0 | -1.38e-05 | 0.0 |
| $S_{28}$ | $S_{35}$ | 0.0 | 0.0 | 0.0 |
| $S_{28}$ | $S_{36}$ | 0.0 | 2.15e-05 | 0.0 |
| $S_{28}$ | $S_{37}$ | 0.0 | 0.0 | 0.0 |
| $S_{28}$ | $S_{38}$ | 0.0 | 4.17e-05 | 0.0 |
| $S_{28}$ | $S_{39}$ | 0.0 | 0.0 | 8.45e-05 |
| $S_{28}$ | $S_{40}$ | 0.0 | 0.0 | 0.0 |
| $S_{28}$ | $S_{41}$ | 0.0 | 0.0 | 0.0 |
| $S_{28}$ | $S_{42}$ | 0.0 | 0.0 | 0.0 |
| $S_{28}$ | $S_{43}$ | 0.0 | -8.96e-06 | 0.0 |
| $S_{28}$ | $S_{44}$ | 0.0 | 3.51e-06 | 0.0 |
| $S_{29}$ | $S_0$ | 0.12135457 | 0.0 | 0.0 |
| $S_{29}$ | $S_1$ | 0.00045583 | 0.0 | 0.0 |
| $S_{29}$ | $S_2$ | 0.0 | 0.00788064 | 0.0 |
| $S_{29}$ | $S_3$ | 0.0 | 0.0 | -0.09795714 |
| $S_{29}$ | $S_4$ | 0.0 | 0.0 | 0.0 |
| $S_{29}$ | $S_5$ | 0.0 | 0.0 | 0.0 |
| $S_{29}$ | $S_6$ | 0.0 | 0.0 | 0.03100295 |
| $S_{29}$ | $S_7$ | 0.0 | 0.0 | 4.2e-07 |
| $S_{29}$ | $S_8$ | 1.47e-05 | 0.0 | 0.0 |
| $S_{29}$ | $S_9$ | 0.03515388 | 0.0 | 0.0 |
| $S_{29}$ | $S_{10}$ | -5.72e-06 | 0.0 | 0.0 |
| $S_{29}$ | $S_{11}$ | 0.0 | 0.0 | -4e-08 |
| $S_{29}$ | $S_{12}$ | 0.0 | 0.0 | -0.17949751 |
| $S_{29}$ | $S_{13}$ | 0.17701141 | 0.0 | 0.0 |
| $S_{29}$ | $S_{14}$ | 0.1454049 | 0.0 | 0.0 |
| $S_{29}$ | $S_{15}$ | 0.0 | -2.91732357 | 0.0 |
| $S_{29}$ | $S_{16}$ | 0.0 | 0.0 | 0.0 |
| $S_{29}$ | $S_{17}$ | 0.0 | 0.0 | -3.8e-07 |
| $S_{29}$ | $S_{18}$ | 0.0 | 0.0 | 0.07318101 |

| $S_{\text{init}}$ | $S_{\text{final}}$ | $\mu_x$ | $\mu_y$ | $\mu_z$ |
|---|---|---|---|---|
| $S_{29}$ | $S_{19}$ | 0.0 | 0.0 | -0.16706648 |
| $S_{29}$ | $S_{20}$ | 0.0 | 0.0 | 0.0 |
| $S_{29}$ | $S_{21}$ | 0.0 | 0.0 | 0.0 |
| $S_{29}$ | $S_{22}$ | 0.03423862 | 0.0 | 0.0 |
| $S_{29}$ | $S_{23}$ | 0.0 | 0.92765686 | 0.0 |
| $S_{29}$ | $S_{24}$ | 0.0 | 0.0 | 0.0 |
| $S_{29}$ | $S_{25}$ | 0.0 | -0.23507329 | 0.0 |
| $S_{29}$ | $S_{26}$ | -0.15966516 | 0.0 | 0.0 |
| $S_{29}$ | $S_{27}$ | 0.0 | -1.52688311 | 0.0 |
| $S_{29}$ | $S_{28}$ | 0.00109863 | 0.0 | 0.0 |
| $S_{29}$ | $S_{29}$ | 0.0 | 0.0 | -2.46751914 |
| $S_{29}$ | $S_{30}$ | 0.0 | 0.0 | 0.0 |
| $S_{29}$ | $S_{31}$ | 0.10123366 | 0.0 | 0.0 |
| $S_{29}$ | $S_{32}$ | 0.0 | -0.01101952 | 0.0 |
| $S_{29}$ | $S_{33}$ | 0.0 | 0.0 | 0.0 |
| $S_{29}$ | $S_{34}$ | 0.0 | 0.0 | 0.0 |
| $S_{29}$ | $S_{35}$ | 0.0 | 0.20305962 | 0.0 |
| $S_{29}$ | $S_{36}$ | 0.0 | 0.0 | 0.0 |
| $S_{29}$ | $S_{37}$ | 0.0 | -0.48915476 | 0.0 |
| $S_{29}$ | $S_{38}$ | 0.0 | 0.0 | 0.0 |
| $S_{29}$ | $S_{39}$ | 2.07701422 | 0.0 | 0.0 |
| $S_{29}$ | $S_{40}$ | 0.0 | 0.10858511 | 0.0 |
| $S_{29}$ | $S_{41}$ | 0.0 | -0.0082569 | 0.0 |
| $S_{29}$ | $S_{42}$ | 0.0 | 0.11554395 | 0.0 |
| $S_{29}$ | $S_{43}$ | 0.0 | 0.0 | 0.0 |
| $S_{29}$ | $S_{44}$ | 0.0 | 0.0 | 0.0 |
| $S_{30}$ | $S_0$ | 0.0 | -0.12430957 | 0.0 |
| $S_{30}$ | $S_1$ | 0.0 | 0.0 | 0.0 |
| $S_{30}$ | $S_2$ | 0.2102812 | 0.0 | 0.0 |
| $S_{30}$ | $S_3$ | 0.0 | 0.0 | 0.0 |
| $S_{30}$ | $S_4$ | 0.0 | 0.0 | 0.0 |
| $S_{30}$ | $S_5$ | 0.0 | 0.0 | -0.02782557 |
| $S_{30}$ | $S_6$ | 0.0 | 0.0 | 0.0 |
| $S_{30}$ | $S_7$ | 0.0 | 0.0 | 0.0 |
| $S_{30}$ | $S_8$ | 0.0 | -2e-08 | 0.0 |
| $S_{30}$ | $S_9$ | 0.0 | -0.22430954 | 0.0 |
| $S_{30}$ | $S_{10}$ | 0.0 | 0.0 | 0.0 |
| $S_{30}$ | $S_{11}$ | 0.0 | 0.0 | 0.0 |
| $S_{30}$ | $S_{12}$ | 0.0 | 0.0 | 0.0 |
| $S_{30}$ | $S_{13}$ | 0.0 | -0.1759825 | 0.0 |

| $S_{\text{init}}$ | $S_{\text{final}}$ | $\mu_x$ | $\mu_y$ | $\mu_z$ |
|---|---|---|---|---|
| $S_{30}$ | $S_{14}$ | 0.0 | 0.08135873 | 0.0 |
| $S_{30}$ | $S_{15}$ | 0.04382184 | 0.0 | 0.0 |
| $S_{30}$ | $S_{16}$ | 0.0 | 0.0 | 0.39690106 |
| $S_{30}$ | $S_{17}$ | 0.0 | 0.0 | 0.0 |
| $S_{30}$ | $S_{18}$ | 0.0 | 0.0 | 0.0 |
| $S_{30}$ | $S_{19}$ | 0.0 | 0.0 | 0.0 |
| $S_{30}$ | $S_{20}$ | 0.0 | 0.0 | 1.56674918 |
| $S_{30}$ | $S_{21}$ | 0.0 | 0.0 | 0.0 |
| $S_{30}$ | $S_{22}$ | 0.0 | -0.17870505 | 0.0 |
| $S_{30}$ | $S_{23}$ | 3.16341007 | 0.0 | 0.0 |
| $S_{30}$ | $S_{24}$ | 0.0 | 0.0 | 1.2183888 |
| $S_{30}$ | $S_{25}$ | 0.88742679 | 0.0 | 0.0 |
| $S_{30}$ | $S_{26}$ | 0.0 | 0.38257109 | 0.0 |
| $S_{30}$ | $S_{27}$ | 1.36001343 | 0.0 | 0.0 |
| $S_{30}$ | $S_{28}$ | 0.0 | -9.65e-06 | 0.0 |
| $S_{30}$ | $S_{29}$ | 0.0 | 0.0 | 0.0 |
| $S_{30}$ | $S_{30}$ | 0.0 | 0.0 | -2.35920848 |
| $S_{30}$ | $S_{31}$ | 0.0 | 0.99411998 | 0.0 |
| $S_{30}$ | $S_{32}$ | -0.03781458 | 0.0 | 0.0 |
| $S_{30}$ | $S_{33}$ | 0.0 | 0.0 | 0.2429992 |
| $S_{30}$ | $S_{34}$ | 0.0 | 0.0 | 0.0797226 |
| $S_{30}$ | $S_{35}$ | -1.52543837 | 0.0 | 0.0 |
| $S_{30}$ | $S_{36}$ | 0.0 | 0.0 | -0.19388086 |
| $S_{30}$ | $S_{37}$ | 0.95122715 | 0.0 | 0.0 |
| $S_{30}$ | $S_{38}$ | 0.0 | 0.0 | -1.05444082 |
| $S_{30}$ | $S_{39}$ | 0.0 | 0.3028504 | 0.0 |
| $S_{30}$ | $S_{40}$ | 0.02665194 | 0.0 | 0.0 |
| $S_{30}$ | $S_{41}$ | -0.28551412 | 0.0 | 0.0 |
| $S_{30}$ | $S_{42}$ | 0.77476974 | 0.0 | 0.0 |
| $S_{30}$ | $S_{43}$ | 0.0 | 0.0 | 1.23339905 |
| $S_{30}$ | $S_{44}$ | 0.0 | 0.0 | -0.42025641 |
| $S_{31}$ | $S_0$ | 0.0 | 0.0 | 0.1551809 |
| $S_{31}$ | $S_1$ | 0.0 | 0.0 | -9.7e-07 |
| $S_{31}$ | $S_2$ | 0.0 | 0.0 | 0.0 |
| $S_{31}$ | $S_3$ | 0.069526 | 0.0 | 0.0 |
| $S_{31}$ | $S_4$ | -0.00037081 | 0.0 | 0.0 |
| $S_{31}$ | $S_5$ | 0.0 | -0.01245941 | 0.0 |
| $S_{31}$ | $S_6$ | -1.3971058 | 0.0 | 0.0 |
| $S_{31}$ | $S_7$ | 2.01e-05 | 0.0 | 0.0 |
| $S_{31}$ | $S_8$ | 0.0 | 0.0 | 3.7e-07 |

| $S_{\text{init}}$ | $S_{\text{final}}$ | $\mu_x$ | $\mu_y$ | $\mu_z$ |
|---|---|---|---|---|
| $S_{31}$ | $S_9$ | 0.0 | 0.0 | 0.1766759 |
| $S_{31}$ | $S_{10}$ | 0.0 | 0.0 | -2.8e-07 |
| $S_{31}$ | $S_{11}$ | -4.05e-05 | 0.0 | 0.0 |
| $S_{31}$ | $S_{12}$ | 0.18070589 | 0.0 | 0.0 |
| $S_{31}$ | $S_{13}$ | 0.0 | 0.0 | -0.16453133 |
| $S_{31}$ | $S_{14}$ | 0.0 | 0.0 | 0.11547155 |
| $S_{31}$ | $S_{15}$ | 0.0 | 0.0 | 0.0 |
| $S_{31}$ | $S_{16}$ | 0.0 | -2.75794913 | 0.0 |
| $S_{31}$ | $S_{17}$ | 7.04e-05 | 0.0 | 0.0 |
| $S_{31}$ | $S_{18}$ | 0.09932671 | 0.0 | 0.0 |
| $S_{31}$ | $S_{19}$ | -0.0359892 | 0.0 | 0.0 |
| $S_{31}$ | $S_{20}$ | 0.0 | -0.82587227 | 0.0 |
| $S_{31}$ | $S_{21}$ | 6.54e-06 | 0.0 | 0.0 |
| $S_{31}$ | $S_{22}$ | 0.0 | 0.0 | 0.30419901 |
| $S_{31}$ | $S_{23}$ | 0.0 | 0.0 | 0.0 |
| $S_{31}$ | $S_{24}$ | 0.0 | 1.355854 | 0.0 |
| $S_{31}$ | $S_{25}$ | 0.0 | 0.0 | 0.0 |
| $S_{31}$ | $S_{26}$ | 0.0 | 0.0 | -0.29176772 |
| $S_{31}$ | $S_{27}$ | 0.0 | 0.0 | 0.0 |
| $S_{31}$ | $S_{28}$ | 0.0 | 0.0 | -5.85e-05 |
| $S_{31}$ | $S_{29}$ | 0.10123366 | 0.0 | 0.0 |
| $S_{31}$ | $S_{30}$ | 0.0 | 0.99411998 | 0.0 |
| $S_{31}$ | $S_{31}$ | 0.0 | 0.0 | -2.71813103 |
| $S_{31}$ | $S_{32}$ | 0.0 | 0.0 | 0.0 |
| $S_{31}$ | $S_{33}$ | 0.0 | -0.24503197 | 0.0 |
| $S_{31}$ | $S_{34}$ | 0.0 | -0.02724396 | 0.0 |
| $S_{31}$ | $S_{35}$ | 0.0 | 0.0 | 0.0 |
| $S_{31}$ | $S_{36}$ | 0.0 | -0.34149335 | 0.0 |
| $S_{31}$ | $S_{37}$ | 0.0 | 0.0 | 0.0 |
| $S_{31}$ | $S_{38}$ | 0.0 | -0.68418227 | 0.0 |
| $S_{31}$ | $S_{39}$ | 0.0 | 0.0 | -0.25524489 |
| $S_{31}$ | $S_{40}$ | 0.0 | 0.0 | 0.0 |
| $S_{31}$ | $S_{41}$ | 0.0 | 0.0 | 0.0 |
| $S_{31}$ | $S_{42}$ | 0.0 | 0.0 | 0.0 |
| $S_{31}$ | $S_{43}$ | 0.0 | -0.67348906 | 0.0 |
| $S_{31}$ | $S_{44}$ | 0.0 | 0.0478078 | 0.0 |
| $S_{32}$ | $S_0$ | 0.0 | 0.0 | 0.0 |
| $S_{32}$ | $S_1$ | 0.0 | 0.0 | 0.0 |
| $S_{32}$ | $S_2$ | 0.0 | 0.0 | -0.10914128 |
| $S_{32}$ | $S_3$ | 0.0 | -0.27046693 | 0.0 |

| $S_{\text{init}}$ | $S_{\text{final}}$ | $\mu_x$ | $\mu_y$ | $\mu_z$ |
|---|---|---|---|---|
| $S_{32}$ | $S_4$ | 0.0 | -1.3e-07 | 0.0 |
| $S_{32}$ | $S_5$ | 0.02560625 | 0.0 | 0.0 |
| $S_{32}$ | $S_6$ | 0.0 | 0.04787316 | 0.0 |
| $S_{32}$ | $S_7$ | 0.0 | 1e-08 | 0.0 |
| $S_{32}$ | $S_8$ | 0.0 | 0.0 | 0.0 |
| $S_{32}$ | $S_9$ | 0.0 | 0.0 | 0.0 |
| $S_{32}$ | $S_{10}$ | 0.0 | 0.0 | 0.0 |
| $S_{32}$ | $S_{11}$ | 0.0 | -1e-08 | 0.0 |
| $S_{32}$ | $S_{12}$ | 0.0 | 0.02381181 | 0.0 |
| $S_{32}$ | $S_{13}$ | 0.0 | 0.0 | 0.0 |
| $S_{32}$ | $S_{14}$ | 0.0 | 0.0 | 0.0 |
| $S_{32}$ | $S_{15}$ | 0.0 | 0.0 | 0.09617966 |
| $S_{32}$ | $S_{16}$ | -0.16940101 | 0.0 | 0.0 |
| $S_{32}$ | $S_{17}$ | 0.0 | 2e-08 | 0.0 |
| $S_{32}$ | $S_{18}$ | 0.0 | 0.00337075 | 0.0 |
| $S_{32}$ | $S_{19}$ | 0.0 | 0.02295032 | 0.0 |
| $S_{32}$ | $S_{20}$ | -0.2133184 | 0.0 | 0.0 |
| $S_{32}$ | $S_{21}$ | 0.0 | -2e-08 | 0.0 |
| $S_{32}$ | $S_{22}$ | 0.0 | 0.0 | 0.0 |
| $S_{32}$ | $S_{23}$ | 0.0 | 0.0 | 0.36413527 |
| $S_{32}$ | $S_{24}$ | -0.11035278 | 0.0 | 0.0 |
| $S_{32}$ | $S_{25}$ | 0.0 | 0.0 | -0.0731955 |
| $S_{32}$ | $S_{26}$ | 0.0 | 0.0 | 0.0 |
| $S_{32}$ | $S_{27}$ | 0.0 | 0.0 | 0.32301934 |
| $S_{32}$ | $S_{28}$ | 0.0 | 0.0 | 0.0 |
| $S_{32}$ | $S_{29}$ | 0.0 | -0.01101952 | 0.0 |
| $S_{32}$ | $S_{30}$ | -0.03781458 | 0.0 | 0.0 |
| $S_{32}$ | $S_{31}$ | 0.0 | 0.0 | 0.0 |
| $S_{32}$ | $S_{32}$ | 0.0 | 0.0 | -1.29106939 |
| $S_{32}$ | $S_{33}$ | 0.23875151 | 0.0 | 0.0 |
| $S_{32}$ | $S_{34}$ | -0.0681219 | 0.0 | 0.0 |
| $S_{32}$ | $S_{35}$ | 0.0 | 0.0 | 0.3097347 |
| $S_{32}$ | $S_{36}$ | -0.16379181 | 0.0 | 0.0 |
| $S_{32}$ | $S_{37}$ | 0.0 | 0.0 | -0.28168723 |
| $S_{32}$ | $S_{38}$ | -0.16453956 | 0.0 | 0.0 |
| $S_{32}$ | $S_{39}$ | 0.0 | 0.0 | 0.0 |
| $S_{32}$ | $S_{40}$ | 0.0 | 0.0 | 0.0314753 |
| $S_{32}$ | $S_{41}$ | 0.0 | 0.0 | -0.1672382 |
| $S_{32}$ | $S_{42}$ | 0.0 | 0.0 | -0.17908045 |
| $S_{32}$ | $S_{43}$ | 0.17099422 | 0.0 | 0.0 |

| $S_{\text{init}}$ | $S_{\text{final}}$ | $\mu_x$ | $\mu_y$ | $\mu_z$ |
|---|---|---|---|---|
| $S_{32}$ | $S_{44}$ | -0.00491693 | 0.0 | 0.0 |
| $S_{33}$ | $S_0$ | 0.0 | 0.089432572 | 0.0 |
| $S_{33}$ | $S_1$ | 0.0 | 2e-08 | 0.0 |
| $S_{33}$ | $S_2$ | -3.63905489 | 0.0 | 0.0 |
| $S_{33}$ | $S_3$ | 0.0 | 0.0 | 0.0 |
| $S_{33}$ | $S_4$ | 0.0 | 0.0 | 0.0 |
| $S_{33}$ | $S_5$ | 0.0 | 0.0 | 0.00728102 |
| $S_{33}$ | $S_6$ | 0.0 | 0.0 | 0.0 |
| $S_{33}$ | $S_7$ | 0.0 | 0.0 | 0.0 |
| $S_{33}$ | $S_8$ | 0.0 | 0.0 | 0.0 |
| $S_{33}$ | $S_9$ | 0.0 | -0.02699422 | 0.0 |
| $S_{33}$ | $S_{10}$ | 0.0 | 1e-08 | 0.0 |
| $S_{33}$ | $S_{11}$ | 0.0 | 0.0 | 0.0 |
| $S_{33}$ | $S_{12}$ | 0.0 | 0.0 | 0.0 |
| $S_{33}$ | $S_{13}$ | 0.0 | -0.4014728 | 0.0 |
| $S_{33}$ | $S_{14}$ | 0.0 | -0.04625261 | 0.0 |
| $S_{33}$ | $S_{15}$ | -0.01653095 | 0.0 | 0.0 |
| $S_{33}$ | $S_{16}$ | 0.0 | 0.0 | -0.58716726 |
| $S_{33}$ | $S_{17}$ | 0.0 | 0.0 | 0.0 |
| $S_{33}$ | $S_{18}$ | 0.0 | 0.0 | 0.0 |
| $S_{33}$ | $S_{19}$ | 0.0 | 0.0 | 0.0 |
| $S_{33}$ | $S_{20}$ | 0.0 | 0.0 | 2.49171549 |
| $S_{33}$ | $S_{21}$ | 0.0 | 0.0 | 0.0 |
| $S_{33}$ | $S_{22}$ | 0.0 | 0.24876836 | 0.0 |
| $S_{33}$ | $S_{23}$ | 0.53579209 | 0.0 | 0.0 |
| $S_{33}$ | $S_{24}$ | 0.0 | 0.0 | 0.11721876 |
| $S_{33}$ | $S_{25}$ | -3.86463316 | 0.0 | 0.0 |
| $S_{33}$ | $S_{26}$ | 0.0 | -0.47770016 | 0.0 |
| $S_{33}$ | $S_{27}$ | 0.3589172 | 0.0 | 0.0 |
| $S_{33}$ | $S_{28}$ | 0.0 | -1.93e-05 | 0.0 |
| $S_{33}$ | $S_{29}$ | 0.0 | 0.0 | 0.0 |
| $S_{33}$ | $S_{30}$ | 0.0 | 0.0 | 0.2429992 |
| $S_{33}$ | $S_{31}$ | 0.0 | -0.24503197 | 0.0 |
| $S_{33}$ | $S_{32}$ | 0.23875151 | 0.0 | 0.0 |
| $S_{33}$ | $S_{33}$ | 0.0 | 0.0 | -2.7795261 |
| $S_{33}$ | $S_{34}$ | 0.0 | 0.0 | -0.02135719 |
| $S_{33}$ | $S_{35}$ | -0.2236083 | 0.0 | 0.0 |
| $S_{33}$ | $S_{36}$ | 0.0 | 0.0 | 0.36034684 |
| $S_{33}$ | $S_{37}$ | 2.88642652 | 0.0 | 0.0 |
| $S_{33}$ | $S_{38}$ | 0.0 | 0.0 | 0.81623304 |

| $S_{\text{init}}$ | $S_{\text{final}}$ | $\mu_x$ | $\mu_y$ | $\mu_z$ |
|---|---|---|---|---|
| $S_{33}$ | $S_{39}$ | 0.0 | 0.29206351 | 0.0 |
| $S_{33}$ | $S_{40}$ | -0.04005131 | 0.0 | 0.0 |
| $S_{33}$ | $S_{41}$ | -0.26773563 | 0.0 | 0.0 |
| $S_{33}$ | $S_{42}$ | 0.81616565 | 0.0 | 0.0 |
| $S_{33}$ | $S_{43}$ | 0.0 | 0.0 | -1.89146496 |
| $S_{33}$ | $S_{44}$ | 0.0 | 0.0 | 0.47228967 |
| $S_{34}$ | $S_0$ | 0.0 | 0.14071966 | 0.0 |
| $S_{34}$ | $S_1$ | 0.0 | 0.0 | 0.0 |
| $S_{34}$ | $S_2$ | -0.75972659 | 0.0 | 0.0 |
| $S_{34}$ | $S_3$ | 0.0 | 0.0 | 0.0 |
| $S_{34}$ | $S_4$ | 0.0 | 0.0 | 0.0 |
| $S_{34}$ | $S_5$ | 0.0 | 0.0 | -0.08067379 |
| $S_{34}$ | $S_6$ | 0.0 | 0.0 | 0.0 |
| $S_{34}$ | $S_7$ | 0.0 | 0.0 | 0.0 |
| $S_{34}$ | $S_8$ | 0.0 | -2e-08 | 0.0 |
| $S_{34}$ | $S_9$ | 0.0 | 0.05094284 | 0.0 |
| $S_{34}$ | $S_{10}$ | 0.0 | 1e-08 | 0.0 |
| $S_{34}$ | $S_{11}$ | 0.0 | 0.0 | 0.0 |
| $S_{34}$ | $S_{12}$ | 0.0 | 0.0 | 0.0 |
| $S_{34}$ | $S_{13}$ | 0.0 | 0.0133298 | 0.0 |
| $S_{34}$ | $S_{14}$ | 0.0 | -0.01644056 | 0.0 |
| $S_{34}$ | $S_{15}$ | 0.10610204 | 0.0 | 0.0 |
| $S_{34}$ | $S_{16}$ | 0.0 | 0.0 | -0.12099537 |
| $S_{34}$ | $S_{17}$ | 0.0 | 0.0 | 0.0 |
| $S_{34}$ | $S_{18}$ | 0.0 | 0.0 | 0.0 |
| $S_{34}$ | $S_{19}$ | 0.0 | 0.0 | 0.0 |
| $S_{34}$ | $S_{20}$ | 0.0 | 0.0 | -0.22794205 |
| $S_{34}$ | $S_{21}$ | 0.0 | 0.0 | 0.0 |
| $S_{34}$ | $S_{22}$ | 0.0 | -0.00779733 | 0.0 |
| $S_{34}$ | $S_{23}$ | -0.23081812 | 0.0 | 0.0 |
| $S_{34}$ | $S_{24}$ | 0.0 | 0.0 | -0.11241332 |
| $S_{34}$ | $S_{25}$ | 0.18487407 | 0.0 | 0.0 |
| $S_{34}$ | $S_{26}$ | 0.0 | 0.02976766 | 0.0 |
| $S_{34}$ | $S_{27}$ | -0.13846707 | 0.0 | 0.0 |
| $S_{34}$ | $S_{28}$ | 0.0 | -1.38e-05 | 0.0 |
| $S_{34}$ | $S_{29}$ | 0.0 | 0.0 | 0.0 |
| $S_{34}$ | $S_{30}$ | 0.0 | 0.0 | 0.0797226 |
| $S_{34}$ | $S_{31}$ | 0.0 | -0.02724396 | 0.0 |
| $S_{34}$ | $S_{32}$ | -0.0681219 | 0.0 | 0.0 |
| $S_{34}$ | $S_{33}$ | 0.0 | 0.0 | -0.02135719 |

| $S_{\text{init}}$ | $S_{\text{final}}$ | $\mu_x$ | $\mu_y$ | $\mu_z$ |
|---|---|---|---|---|
| $S_{34}$ | $S_{34}$ | 0.0 | 0.0 | -1.24501866 |
| $S_{34}$ | $S_{35}$ | 0.14154775 | 0.0 | 0.0 |
| $S_{34}$ | $S_{36}$ | 0.0 | 0.0 | 0.2806624 |
| $S_{34}$ | $S_{37}$ | -0.16072222 | 0.0 | 0.0 |
| $S_{34}$ | $S_{38}$ | 0.0 | 0.0 | -0.03338928 |
| $S_{34}$ | $S_{39}$ | 0.0 | -0.20744199 | 0.0 |
| $S_{34}$ | $S_{40}$ | 0.02255223 | 0.0 | 0.0 |
| $S_{34}$ | $S_{41}$ | -0.01666352 | 0.0 | 0.0 |
| $S_{34}$ | $S_{42}$ | -0.10882037 | 0.0 | 0.0 |
| $S_{34}$ | $S_{43}$ | 0.0 | 0.0 | 0.03897392 |
| $S_{34}$ | $S_{44}$ | 0.0 | 0.0 | 0.00529624 |
| $S_{35}$ | $S_0$ | 0.0 | 0.0 | 0.0 |
| $S_{35}$ | $S_1$ | 0.0 | 0.0 | 0.0 |
| $S_{35}$ | $S_2$ | 0.0 | 0.0 | -0.00223599 |
| $S_{35}$ | $S_3$ | 0.0 | 0.21976406 | 0.0 |
| $S_{35}$ | $S_4$ | 0.0 | 1e-08 | 0.0 |
| $S_{35}$ | $S_5$ | -0.00640241 | 0.0 | 0.0 |
| $S_{35}$ | $S_6$ | 0.0 | 0.11869513 | 0.0 |
| $S_{35}$ | $S_7$ | 0.0 | 0.0 | 0.0 |
| $S_{35}$ | $S_8$ | 0.0 | 0.0 | 0.0 |
| $S_{35}$ | $S_9$ | 0.0 | 0.0 | 0.0 |
| $S_{35}$ | $S_{10}$ | 0.0 | 0.0 | 0.0 |
| $S_{35}$ | $S_{11}$ | 0.0 | 0.0 | 0.0 |
| $S_{35}$ | $S_{12}$ | 0.0 | -0.2782631 | 0.0 |
| $S_{35}$ | $S_{13}$ | 0.0 | 0.0 | 0.0 |
| $S_{35}$ | $S_{14}$ | 0.0 | 0.0 | 0.0 |
| $S_{35}$ | $S_{15}$ | 0.0 | 0.0 | -0.008548 |
| $S_{35}$ | $S_{16}$ | 0.13511452 | 0.0 | 0.0 |
| $S_{35}$ | $S_{17}$ | 0.0 | -1e-08 | 0.0 |
| $S_{35}$ | $S_{18}$ | 0.0 | -0.03333661 | 0.0 |
| $S_{35}$ | $S_{19}$ | 0.0 | 0.14194528 | 0.0 |
| $S_{35}$ | $S_{20}$ | 0.24125662 | 0.0 | 0.0 |
| $S_{35}$ | $S_{21}$ | 0.0 | -3e-08 | 0.0 |
| $S_{35}$ | $S_{22}$ | 0.0 | 0.0 | 0.0 |
| $S_{35}$ | $S_{23}$ | 0.0 | 0.0 | -2.27555895 |
| $S_{35}$ | $S_{24}$ | 3.00759483 | 0.0 | 0.0 |
| $S_{35}$ | $S_{25}$ | 0.0 | 0.0 | -1.69387457 |
| $S_{35}$ | $S_{26}$ | 0.0 | 0.0 | 0.0 |
| $S_{35}$ | $S_{27}$ | 0.0 | 0.0 | -0.86945332 |
| $S_{35}$ | $S_{28}$ | 0.0 | 0.0 | 0.0 |

| $S_{\text{init}}$ | $S_{\text{final}}$ | $\mu_x$ | $\mu_y$ | $\mu_z$ |
|---|---|---|---|---|
| $S_{35}$ | $S_{29}$ | 0.0 | 0.20305962 | 0.0 |
| $S_{35}$ | $S_{30}$ | -1.52543837 | 0.0 | 0.0 |
| $S_{35}$ | $S_{31}$ | 0.0 | 0.0 | 0.0 |
| $S_{35}$ | $S_{32}$ | 0.0 | 0.0 | 0.3097347 |
| $S_{35}$ | $S_{33}$ | -0.2236083 | 0.0 | 0.0 |
| $S_{35}$ | $S_{34}$ | 0.14154775 | 0.0 | 0.0 |
| $S_{35}$ | $S_{35}$ | 0.0 | 0.0 | -2.04701446 |
| $S_{35}$ | $S_{36}$ | 1.37834785 | 0.0 | 0.0 |
| $S_{35}$ | $S_{37}$ | 0.0 | 0.0 | 0.69086742 |
| $S_{35}$ | $S_{38}$ | 2.49062097 | 0.0 | 0.0 |
| $S_{35}$ | $S_{39}$ | 0.0 | 0.0 | 0.0 |
| $S_{35}$ | $S_{40}$ | 0.0 | 0.0 | 0.14380874 |
| $S_{35}$ | $S_{41}$ | 0.0 | 0.0 | -0.16779504 |
| $S_{35}$ | $S_{42}$ | 0.0 | 0.0 | 0.57913384 |
| $S_{35}$ | $S_{43}$ | -2.89674572 | 0.0 | 0.0 |
| $S_{35}$ | $S_{44}$ | 0.0458868 | 0.0 | 0.0 |
| $S_{36}$ | $S_0$ | 0.0 | -0.15787347 | 0.0 |
| $S_{36}$ | $S_1$ | 0.0 | -4e-08 | 0.0 |
| $S_{36}$ | $S_2$ | -0.34139901 | 0.0 | 0.0 |
| $S_{36}$ | $S_3$ | 0.0 | 0.0 | 0.0 |
| $S_{36}$ | $S_4$ | 0.0 | 0.0 | 0.0 |
| $S_{36}$ | $S_5$ | 0.0 | 0.0 | -0.06249239 |
| $S_{36}$ | $S_6$ | 0.0 | 0.0 | 0.0 |
| $S_{36}$ | $S_7$ | 0.0 | 0.0 | 0.0 |
| $S_{36}$ | $S_8$ | 0.0 | 0.0 | 0.0 |
| $S_{36}$ | $S_9$ | 0.0 | 0.09332107 | 0.0 |
| $S_{36}$ | $S_{10}$ | 0.0 | 3e-08 | 0.0 |
| $S_{36}$ | $S_{11}$ | 0.0 | 0.0 | 0.0 |
| $S_{36}$ | $S_{12}$ | 0.0 | 0.0 | 0.0 |
| $S_{36}$ | $S_{13}$ | 0.0 | -0.0966466 | 0.0 |
| $S_{36}$ | $S_{14}$ | 0.0 | 0.05606147 | 0.0 |
| $S_{36}$ | $S_{15}$ | -0.16202175 | 0.0 | 0.0 |
| $S_{36}$ | $S_{16}$ | 0.0 | 0.0 | -0.3396049 |
| $S_{36}$ | $S_{17}$ | 0.0 | 0.0 | 0.0 |
| $S_{36}$ | $S_{18}$ | 0.0 | 0.0 | 0.0 |
| $S_{36}$ | $S_{19}$ | 0.0 | 0.0 | 0.0 |
| $S_{36}$ | $S_{20}$ | 0.0 | 0.0 | -0.18416303 |
| $S_{36}$ | $S_{21}$ | 0.0 | 0.0 | 0.0 |
| $S_{36}$ | $S_{22}$ | 0.0 | -0.02640432 | 0.0 |
| $S_{36}$ | $S_{23}$ | 0.32625869 | 0.0 | 0.0 |

| $S_{\text{init}}$ | $S_{\text{final}}$ | $\mu_x$ | $\mu_y$ | $\mu_z$ |
|---|---|---|---|---|
| $S_{36}$ | $S_{24}$ | 0.0 | 0.0 | 0.78694926 |
| $S_{36}$ | $S_{25}$ | 0.02857661 | 0.0 | 0.0 |
| $S_{36}$ | $S_{26}$ | 0.0 | 0.04690854 | 0.0 |
| $S_{36}$ | $S_{27}$ | 0.02101643 | 0.0 | 0.0 |
| $S_{36}$ | $S_{28}$ | 0.0 | 2.15e-05 | 0.0 |
| $S_{36}$ | $S_{29}$ | 0.0 | 0.0 | 0.0 |
| $S_{36}$ | $S_{30}$ | 0.0 | 0.0 | -0.19388086 |
| $S_{36}$ | $S_{31}$ | 0.0 | -0.34149335 | 0.0 |
| $S_{36}$ | $S_{32}$ | -0.16379181 | 0.0 | 0.0 |
| $S_{36}$ | $S_{33}$ | 0.0 | 0.0 | 0.36034684 |
| $S_{36}$ | $S_{34}$ | 0.0 | 0.0 | 0.2806624 |
| $S_{36}$ | $S_{35}$ | 1.37834785 | 0.0 | 0.0 |
| $S_{36}$ | $S_{36}$ | 0.0 | 0.0 | -1.33913548 |
| $S_{36}$ | $S_{37}$ | 0.35601843 | 0.0 | 0.0 |
| $S_{36}$ | $S_{38}$ | 0.0 | 0.0 | -0.08549 |
| $S_{36}$ | $S_{39}$ | 0.0 | 0.18796158 | 0.0 |
| $S_{36}$ | $S_{40}$ | -0.09888126 | 0.0 | 0.0 |
| $S_{36}$ | $S_{41}$ | -0.03471872 | 0.0 | 0.0 |
| $S_{36}$ | $S_{42}$ | -0.03450205 | 0.0 | 0.0 |
| $S_{36}$ | $S_{43}$ | 0.0 | 0.0 | 0.1722626 |
| $S_{36}$ | $S_{44}$ | 0.0 | 0.0 | 0.18721309 |
| $S_{37}$ | $S_0$ | 0.0 | 0.0 | 0.0 |
| $S_{37}$ | $S_1$ | 0.0 | 0.0 | 0.0 |
| $S_{37}$ | $S_2$ | 0.0 | 0.0 | 0.0163813 |
| $S_{37}$ | $S_3$ | 0.0 | 0.01408031 | 0.0 |
| $S_{37}$ | $S_4$ | 0.0 | 2e-08 | 0.0 |
| $S_{37}$ | $S_5$ | -0.29662635 | 0.0 | 0.0 |
| $S_{37}$ | $S_6$ | 0.0 | -0.05298093 | 0.0 |
| $S_{37}$ | $S_7$ | 0.0 | -1e-08 | 0.0 |
| $S_{37}$ | $S_8$ | 0.0 | 0.0 | 0.0 |
| $S_{37}$ | $S_9$ | 0.0 | 0.0 | 0.0 |
| $S_{37}$ | $S_{10}$ | 0.0 | 0.0 | 0.0 |
| $S_{37}$ | $S_{11}$ | 0.0 | -3e-08 | 0.0 |
| $S_{37}$ | $S_{12}$ | 0.0 | -0.02977205 | 0.0 |
| $S_{37}$ | $S_{13}$ | 0.0 | 0.0 | 0.0 |
| $S_{37}$ | $S_{14}$ | 0.0 | 0.0 | 0.0 |
| $S_{37}$ | $S_{15}$ | 0.0 | 0.0 | -0.60818192 |
| $S_{37}$ | $S_{16}$ | 0.16763394 | 0.0 | 0.0 |
| $S_{37}$ | $S_{17}$ | 0.0 | 2e-08 | 0.0 |
| $S_{37}$ | $S_{18}$ | 0.0 | 0.03746665 | 0.0 |

| $S_{\text{init}}$ | $S_{\text{final}}$ | $\mu_x$ | $\mu_y$ | $\mu_z$ |
|---|---|---|---|---|
| $S_{37}$ | $S_{19}$ | 0.0 | 0.23134195 | 0.0 |
| $S_{37}$ | $S_{20}$ | -1.19670086 | 0.0 | 0.0 |
| $S_{37}$ | $S_{21}$ | 0.0 | -1e-08 | 0.0 |
| $S_{37}$ | $S_{22}$ | 0.0 | 0.0 | 0.0 |
| $S_{37}$ | $S_{23}$ | 0.0 | 0.0 | 1.50465859 |
| $S_{37}$ | $S_{24}$ | 0.67753381 | 0.0 | 0.0 |
| $S_{37}$ | $S_{25}$ | 0.0 | 0.0 | -2.74261219 |
| $S_{37}$ | $S_{26}$ | 0.0 | 0.0 | 0.0 |
| $S_{37}$ | $S_{27}$ | 0.0 | 0.0 | 1.48041238 |
| $S_{37}$ | $S_{28}$ | 0.0 | 0.0 | 0.0 |
| $S_{37}$ | $S_{29}$ | 0.0 | -0.48915476 | 0.0 |
| $S_{37}$ | $S_{30}$ | 0.95122715 | 0.0 | 0.0 |
| $S_{37}$ | $S_{31}$ | 0.0 | 0.0 | 0.0 |
| $S_{37}$ | $S_{32}$ | 0.0 | 0.0 | -0.28168723 |
| $S_{37}$ | $S_{33}$ | 2.88642652 | 0.0 | 0.0 |
| $S_{37}$ | $S_{34}$ | -0.16072222 | 0.0 | 0.0 |
| $S_{37}$ | $S_{35}$ | 0.0 | 0.0 | 0.69086742 |
| $S_{37}$ | $S_{36}$ | 0.35601843 | 0.0 | 0.0 |
| $S_{37}$ | $S_{37}$ | 0.0 | 0.0 | -2.8777204 |
| $S_{37}$ | $S_{38}$ | 0.86268367 | 0.0 | 0.0 |
| $S_{37}$ | $S_{39}$ | 0.0 | 0.0 | 0.0 |
| $S_{37}$ | $S_{40}$ | 0.0 | 0.0 | -0.00276273 |
| $S_{37}$ | $S_{41}$ | 0.0 | 0.0 | 0.17799505 |
| $S_{37}$ | $S_{42}$ | 0.0 | 0.0 | -0.75724803 |
| $S_{37}$ | $S_{43}$ | -0.35497988 | 0.0 | 0.0 |
| $S_{37}$ | $S_{44}$ | -1.14777498 | 0.0 | 0.0 |
| $S_{38}$ | $S_0$ | 0.0 | -0.099872701 | 0.0 |
| $S_{38}$ | $S_1$ | 0.0 | 5e-08 | 0.0 |
| $S_{38}$ | $S_2$ | 0.18134976 | 0.0 | 0.0 |
| $S_{38}$ | $S_3$ | 0.0 | 0.0 | 0.0 |
| $S_{38}$ | $S_4$ | 0.0 | 0.0 | 0.0 |
| $S_{38}$ | $S_5$ | 0.0 | 0.0 | 0.06806973 |
| $S_{38}$ | $S_6$ | 0.0 | 0.0 | 0.0 |
| $S_{38}$ | $S_7$ | 0.0 | 0.0 | 0.0 |
| $S_{38}$ | $S_8$ | 0.0 | -5e-08 | 0.0 |
| $S_{38}$ | $S_9$ | 0.0 | 0.10241905 | 0.0 |
| $S_{38}$ | $S_{10}$ | 0.0 | 1e-08 | 0.0 |
| $S_{38}$ | $S_{11}$ | 0.0 | 0.0 | 0.0 |
| $S_{38}$ | $S_{12}$ | 0.0 | 0.0 | 0.0 |
| $S_{38}$ | $S_{13}$ | 0.0 | -0.19623435 | 0.0 |

| $S_{\text{init}}$ | $S_{\text{final}}$ | $\mu_x$ | $\mu_y$ | $\mu_z$ |
|---|---|---|---|---|
| $S_{38}$ | $S_{14}$ | 0.0 | 0.13075132 | 0.0 |
| $S_{38}$ | $S_{15}$ | 0.04094303 | 0.0 | 0.0 |
| $S_{38}$ | $S_{16}$ | 0.0 | 0.0 | -0.39857214 |
| $S_{38}$ | $S_{17}$ | 0.0 | 0.0 | 0.0 |
| $S_{38}$ | $S_{18}$ | 0.0 | 0.0 | 0.0 |
| $S_{38}$ | $S_{19}$ | 0.0 | 0.0 | 0.0 |
| $S_{38}$ | $S_{20}$ | 0.0 | 0.0 | -0.25271534 |
| $S_{38}$ | $S_{21}$ | 0.0 | 0.0 | 0.0 |
| $S_{38}$ | $S_{22}$ | 0.0 | -0.14380123 | 0.0 |
| $S_{38}$ | $S_{23}$ | 1.3435305 | 0.0 | 0.0 |
| $S_{38}$ | $S_{24}$ | 0.0 | 0.0 | 2.45300293 |
| $S_{38}$ | $S_{25}$ | 0.88058418 | 0.0 | 0.0 |
| $S_{38}$ | $S_{26}$ | 0.0 | 0.23127148 | 0.0 |
| $S_{38}$ | $S_{27}$ | 0.26738953 | 0.0 | 0.0 |
| $S_{38}$ | $S_{28}$ | 0.0 | 4.17e-05 | 0.0 |
| $S_{38}$ | $S_{29}$ | 0.0 | 0.0 | 0.0 |
| $S_{38}$ | $S_{30}$ | 0.0 | 0.0 | -1.05444082 |
| $S_{38}$ | $S_{31}$ | 0.0 | -0.68418227 | 0.0 |
| $S_{38}$ | $S_{32}$ | -0.16453956 | 0.0 | 0.0 |
| $S_{38}$ | $S_{33}$ | 0.0 | 0.0 | 0.81623304 |
| $S_{38}$ | $S_{34}$ | 0.0 | 0.0 | -0.03338928 |
| $S_{38}$ | $S_{35}$ | 2.49062097 | 0.0 | 0.0 |
| $S_{38}$ | $S_{36}$ | 0.0 | 0.0 | -0.08549 |
| $S_{38}$ | $S_{37}$ | 0.86268367 | 0.0 | 0.0 |
| $S_{38}$ | $S_{38}$ | 0.0 | 0.0 | -1.90485474 |
| $S_{38}$ | $S_{39}$ | 0.0 | -0.13616382 | 0.0 |
| $S_{38}$ | $S_{40}$ | -0.15830419 | 0.0 | 0.0 |
| $S_{38}$ | $S_{41}$ | 0.09707873 | 0.0 | 0.0 |
| $S_{38}$ | $S_{42}$ | 0.19484324 | 0.0 | 0.0 |
| $S_{38}$ | $S_{43}$ | 0.0 | 0.0 | 0.96830195 |
| $S_{38}$ | $S_{44}$ | 0.0 | 0.0 | 0.31683771 |
| $S_{39}$ | $S_0$ | 0.0 | 0.0 | -0.014518617 |
| $S_{39}$ | $S_1$ | 0.0 | 0.0 | 1.8e-07 |
| $S_{39}$ | $S_2$ | 0.0 | 0.0 | 0.0 |
| $S_{39}$ | $S_3$ | 0.36096969 | 0.0 | 0.0 |
| $S_{39}$ | $S_4$ | -0.00030318 | 0.0 | 0.0 |
| $S_{39}$ | $S_5$ | 0.0 | -0.00073808 | 0.0 |
| $S_{39}$ | $S_6$ | 5.71798923 | 0.0 | 0.0 |
| $S_{39}$ | $S_7$ | 2.74e-05 | 0.0 | 0.0 |
| $S_{39}$ | $S_8$ | 0.0 | 0.0 | -4.6e-07 |

| $S_{\text{init}}$ | $S_{\text{final}}$ | $\mu_x$ | $\mu_y$ | $\mu_z$ |
|---|---|---|---|---|
| $S_{39}$ | $S_9$ | 0.0 | 0.0 | -0.0233868 |
| $S_{39}$ | $S_{10}$ | 0.0 | 0.0 | -4e-07 |
| $S_{39}$ | $S_{11}$ | -8.05e-06 | 0.0 | 0.0 |
| $S_{39}$ | $S_{12}$ | 0.83403812 | 0.0 | 0.0 |
| $S_{39}$ | $S_{13}$ | 0.0 | 0.0 | -0.81683341 |
| $S_{39}$ | $S_{14}$ | 0.0 | 0.0 | -0.15600373 |
| $S_{39}$ | $S_{15}$ | 0.0 | 0.0 | 0.0 |
| $S_{39}$ | $S_{16}$ | 0.0 | -0.34810622 | 0.0 |
| $S_{39}$ | $S_{17}$ | -5.18e-05 | 0.0 | 0.0 |
| $S_{39}$ | $S_{18}$ | -0.02749808 | 0.0 | 0.0 |
| $S_{39}$ | $S_{19}$ | -0.65328002 | 0.0 | 0.0 |
| $S_{39}$ | $S_{20}$ | 0.0 | 2.33334705 | 0.0 |
| $S_{39}$ | $S_{21}$ | -1.15e-05 | 0.0 | 0.0 |
| $S_{39}$ | $S_{22}$ | 0.0 | 0.0 | 0.21736769 |
| $S_{39}$ | $S_{23}$ | 0.0 | 0.0 | 0.0 |
| $S_{39}$ | $S_{24}$ | 0.0 | 0.02388821 | 0.0 |
| $S_{39}$ | $S_{25}$ | 0.0 | 0.0 | 0.0 |
| $S_{39}$ | $S_{26}$ | 0.0 | 0.0 | -0.40459768 |
| $S_{39}$ | $S_{27}$ | 0.0 | 0.0 | 0.0 |
| $S_{39}$ | $S_{28}$ | 0.0 | 0.0 | 8.45e-05 |
| $S_{39}$ | $S_{29}$ | 2.07701422 | 0.0 | 0.0 |
| $S_{39}$ | $S_{30}$ | 0.0 | 0.3028504 | 0.0 |
| $S_{39}$ | $S_{31}$ | 0.0 | 0.0 | -0.25524489 |
| $S_{39}$ | $S_{32}$ | 0.0 | 0.0 | 0.0 |
| $S_{39}$ | $S_{33}$ | 0.0 | 0.29206351 | 0.0 |
| $S_{39}$ | $S_{34}$ | 0.0 | -0.20744199 | 0.0 |
| $S_{39}$ | $S_{35}$ | 0.0 | 0.0 | 0.0 |
| $S_{39}$ | $S_{36}$ | 0.0 | 0.18796158 | 0.0 |
| $S_{39}$ | $S_{37}$ | 0.0 | 0.0 | 0.0 |
| $S_{39}$ | $S_{38}$ | 0.0 | -0.13616382 | 0.0 |
| $S_{39}$ | $S_{39}$ | 0.0 | 0.0 | -2.09028161 |
| $S_{39}$ | $S_{40}$ | 0.0 | 0.0 | 0.0 |
| $S_{39}$ | $S_{41}$ | 0.0 | 0.0 | 0.0 |
| $S_{39}$ | $S_{42}$ | 0.0 | 0.0 | 0.0 |
| $S_{39}$ | $S_{43}$ | 0.0 | -1.02379219 | 0.0 |
| $S_{39}$ | $S_{44}$ | 0.0 | -0.51907338 | 0.0 |
| $S_{40}$ | $S_0$ | 0.0 | 0.0 | 0.0 |
| $S_{40}$ | $S_1$ | 0.0 | 0.0 | 0.0 |
| $S_{40}$ | $S_2$ | 0.0 | 0.0 | 0.12977326 |
| $S_{40}$ | $S_3$ | 0.0 | 0.00687869 | 0.0 |

| $S_{\text{init}}$ | $S_{\text{final}}$ | $\mu_x$ | $\mu_y$ | $\mu_z$ |
|---|---|---|---|---|
| $S_{40}$ | $S_4$ | 0.0 | -3e-08 | 0.0 |
| $S_{40}$ | $S_5$ | -0.5216897 | 0.0 | 0.0 |
| $S_{40}$ | $S_6$ | 0.0 | -0.0406418 | 0.0 |
| $S_{40}$ | $S_7$ | 0.0 | -2.8e-07 | 0.0 |
| $S_{40}$ | $S_8$ | 0.0 | 0.0 | 0.0 |
| $S_{40}$ | $S_9$ | 0.0 | 0.0 | 0.0 |
| $S_{40}$ | $S_{10}$ | 0.0 | 0.0 | 0.0 |
| $S_{40}$ | $S_{11}$ | 0.0 | 1e-08 | 0.0 |
| $S_{40}$ | $S_{12}$ | 0.0 | -0.02463636 | 0.0 |
| $S_{40}$ | $S_{13}$ | 0.0 | 0.0 | 0.0 |
| $S_{40}$ | $S_{14}$ | 0.0 | 0.0 | 0.0 |
| $S_{40}$ | $S_{15}$ | 0.0 | 0.0 | 0.15983938 |
| $S_{40}$ | $S_{16}$ | -0.13258434 | 0.0 | 0.0 |
| $S_{40}$ | $S_{17}$ | 0.0 | -3e-08 | 0.0 |
| $S_{40}$ | $S_{18}$ | 0.0 | -0.01026132 | 0.0 |
| $S_{40}$ | $S_{19}$ | 0.0 | 0.02226051 | 0.0 |
| $S_{40}$ | $S_{20}$ | 0.25686337 | 0.0 | 0.0 |
| $S_{40}$ | $S_{21}$ | 0.0 | 2e-08 | 0.0 |
| $S_{40}$ | $S_{22}$ | 0.0 | 0.0 | 0.0 |
| $S_{40}$ | $S_{23}$ | 0.0 | 0.0 | -0.17458642 |
| $S_{40}$ | $S_{24}$ | 0.02933747 | 0.0 | 0.0 |
| $S_{40}$ | $S_{25}$ | 0.0 | 0.0 | 0.33106317 |
| $S_{40}$ | $S_{26}$ | 0.0 | 0.0 | 0.0 |
| $S_{40}$ | $S_{27}$ | 0.0 | 0.0 | 0.13646126 |
| $S_{40}$ | $S_{28}$ | 0.0 | 0.0 | 0.0 |
| $S_{40}$ | $S_{29}$ | 0.0 | 0.10858511 | 0.0 |
| $S_{40}$ | $S_{30}$ | 0.02665194 | 0.0 | 0.0 |
| $S_{40}$ | $S_{31}$ | 0.0 | 0.0 | 0.0 |
| $S_{40}$ | $S_{32}$ | 0.0 | 0.0 | 0.0314753 |
| $S_{40}$ | $S_{33}$ | -0.04005131 | 0.0 | 0.0 |
| $S_{40}$ | $S_{34}$ | 0.02255223 | 0.0 | 0.0 |
| $S_{40}$ | $S_{35}$ | 0.0 | 0.0 | 0.14380874 |
| $S_{40}$ | $S_{36}$ | -0.09888126 | 0.0 | 0.0 |
| $S_{40}$ | $S_{37}$ | 0.0 | 0.0 | -0.00276273 |
| $S_{40}$ | $S_{38}$ | -0.15830419 | 0.0 | 0.0 |
| $S_{40}$ | $S_{39}$ | 0.0 | 0.0 | 0.0 |
| $S_{40}$ | $S_{40}$ | 0.0 | 0.0 | -1.63301329 |
| $S_{40}$ | $S_{41}$ | 0.0 | 0.0 | 0.14232114 |
| $S_{40}$ | $S_{42}$ | 0.0 | 0.0 | 0.25973309 |
| $S_{40}$ | $S_{43}$ | 0.02551873 | 0.0 | 0.0 |

| $S_{\text{init}}$ | $S_{\text{final}}$ | $\mu_x$ | $\mu_y$ | $\mu_z$ |
|---|---|---|---|---|
| $S_{40}$ | $S_{44}$ | 0.42868041 | 0.0 | 0.0 |
| $S_{41}$ | $S_0$ | 0.0 | 0.0 | 0.0 |
| $S_{41}$ | $S_1$ | 0.0 | 0.0 | 0.0 |
| $S_{41}$ | $S_2$ | 0.0 | 0.0 | -0.45434527 |
| $S_{41}$ | $S_3$ | 0.0 | -0.00328068 | 0.0 |
| $S_{41}$ | $S_4$ | 0.0 | 1.1e-07 | 0.0 |
| $S_{41}$ | $S_5$ | 0.11998352 | 0.0 | 0.0 |
| $S_{41}$ | $S_6$ | 0.0 | 0.08012559 | 0.0 |
| $S_{41}$ | $S_7$ | 0.0 | -1e-08 | 0.0 |
| $S_{41}$ | $S_8$ | 0.0 | 0.0 | 0.0 |
| $S_{41}$ | $S_9$ | 0.0 | 0.0 | 0.0 |
| $S_{41}$ | $S_{10}$ | 0.0 | 0.0 | 0.0 |
| $S_{41}$ | $S_{11}$ | 0.0 | -4e-08 | 0.0 |
| $S_{41}$ | $S_{12}$ | 0.0 | -0.01920126 | 0.0 |
| $S_{41}$ | $S_{13}$ | 0.0 | 0.0 | 0.0 |
| $S_{41}$ | $S_{14}$ | 0.0 | 0.0 | 0.0 |
| $S_{41}$ | $S_{15}$ | 0.0 | 0.0 | 0.06666785 |
| $S_{41}$ | $S_{16}$ | -0.0310257 | 0.0 | 0.0 |
| $S_{41}$ | $S_{17}$ | 0.0 | 8e-08 | 0.0 |
| $S_{41}$ | $S_{18}$ | 0.0 | 0.02084872 | 0.0 |
| $S_{41}$ | $S_{19}$ | 0.0 | 0.00239209 | 0.0 |
| $S_{41}$ | $S_{20}$ | -0.00597277 | 0.0 | 0.0 |
| $S_{41}$ | $S_{21}$ | 0.0 | -6e-08 | 0.0 |
| $S_{41}$ | $S_{22}$ | 0.0 | 0.0 | 0.0 |
| $S_{41}$ | $S_{23}$ | 0.0 | 0.0 | -0.13969005 |
| $S_{41}$ | $S_{24}$ | 0.14040019 | 0.0 | 0.0 |
| $S_{41}$ | $S_{25}$ | 0.0 | 0.0 | 0.01053986 |
| $S_{41}$ | $S_{26}$ | 0.0 | 0.0 | 0.0 |
| $S_{41}$ | $S_{27}$ | 0.0 | 0.0 | -0.20383087 |
| $S_{41}$ | $S_{28}$ | 0.0 | 0.0 | 0.0 |
| $S_{41}$ | $S_{29}$ | 0.0 | -0.0082569 | 0.0 |
| $S_{41}$ | $S_{30}$ | -0.28551412 | 0.0 | 0.0 |
| $S_{41}$ | $S_{31}$ | 0.0 | 0.0 | 0.0 |
| $S_{41}$ | $S_{32}$ | 0.0 | 0.0 | -0.1672382 |
| $S_{41}$ | $S_{33}$ | -0.26773563 | 0.0 | 0.0 |
| $S_{41}$ | $S_{34}$ | -0.01666352 | 0.0 | 0.0 |
| $S_{41}$ | $S_{35}$ | 0.0 | 0.0 | -0.16779504 |
| $S_{41}$ | $S_{36}$ | -0.03471872 | 0.0 | 0.0 |
| $S_{41}$ | $S_{37}$ | 0.0 | 0.0 | 0.17799505 |
| $S_{41}$ | $S_{38}$ | 0.09707873 | 0.0 | 0.0 |

| $S_{\text{init}}$ | $S_{\text{final}}$ | $\mu_x$ | $\mu_y$ | $\mu_z$ |
|---|---|---|---|---|
| $S_{41}$ | $S_{39}$ | 0.0 | 0.0 | 0.0 |
| $S_{41}$ | $S_{40}$ | 0.0 | 0.0 | 0.14232114 |
| $S_{41}$ | $S_{41}$ | 0.0 | 0.0 | -2.06923492 |
| $S_{41}$ | $S_{42}$ | 0.0 | 0.0 | -0.37811686 |
| $S_{41}$ | $S_{43}$ | -0.15559292 | 0.0 | 0.0 |
| $S_{41}$ | $S_{44}$ | -0.11134196 | 0.0 | 0.0 |
| $S_{42}$ | $S_0$ | 0.0 | 0.0 | 0.0 |
| $S_{42}$ | $S_1$ | 0.0 | 0.0 | 0.0 |
| $S_{42}$ | $S_2$ | 0.0 | 0.0 | -0.27125127 |
| $S_{42}$ | $S_3$ | 0.0 | -0.06112969 | 0.0 |
| $S_{42}$ | $S_4$ | 0.0 | -8e-08 | 0.0 |
| $S_{42}$ | $S_5$ | 0.01663566 | 0.0 | 0.0 |
| $S_{42}$ | $S_6$ | 0.0 | 0.46330796 | 0.0 |
| $S_{42}$ | $S_7$ | 0.0 | 3e-08 | 0.0 |
| $S_{42}$ | $S_8$ | 0.0 | 0.0 | 0.0 |
| $S_{42}$ | $S_9$ | 0.0 | 0.0 | 0.0 |
| $S_{42}$ | $S_{10}$ | 0.0 | 0.0 | 0.0 |
| $S_{42}$ | $S_{11}$ | 0.0 | 0.0 | 0.0 |
| $S_{42}$ | $S_{12}$ | 0.0 | 0.05821775 | 0.0 |
| $S_{42}$ | $S_{13}$ | 0.0 | 0.0 | 0.0 |
| $S_{42}$ | $S_{14}$ | 0.0 | 0.0 | 0.0 |
| $S_{42}$ | $S_{15}$ | 0.0 | 0.0 | -0.17655561 |
| $S_{42}$ | $S_{16}$ | 0.25439561 | 0.0 | 0.0 |
| $S_{42}$ | $S_{17}$ | 0.0 | 1e-08 | 0.0 |
| $S_{42}$ | $S_{18}$ | 0.0 | -0.19969176 | 0.0 |
| $S_{42}$ | $S_{19}$ | 0.0 | 0.00999551 | 0.0 |
| $S_{42}$ | $S_{20}$ | -0.42895554 | 0.0 | 0.0 |
| $S_{42}$ | $S_{21}$ | 0.0 | -2e-08 | 0.0 |
| $S_{42}$ | $S_{22}$ | 0.0 | 0.0 | 0.0 |
| $S_{42}$ | $S_{23}$ | 0.0 | 0.0 | -0.28541972 |
| $S_{42}$ | $S_{24}$ | -0.36480875 | 0.0 | 0.0 |
| $S_{42}$ | $S_{25}$ | 0.0 | 0.0 | 0.22486905 |
| $S_{42}$ | $S_{26}$ | 0.0 | 0.0 | 0.0 |
| $S_{42}$ | $S_{27}$ | 0.0 | 0.0 | 0.65779117 |
| $S_{42}$ | $S_{28}$ | 0.0 | 0.0 | 0.0 |
| $S_{42}$ | $S_{29}$ | 0.0 | 0.11554395 | 0.0 |
| $S_{42}$ | $S_{30}$ | 0.77476974 | 0.0 | 0.0 |
| $S_{42}$ | $S_{31}$ | 0.0 | 0.0 | 0.0 |
| $S_{42}$ | $S_{32}$ | 0.0 | 0.0 | -0.17908045 |
| $S_{42}$ | $S_{33}$ | 0.81616565 | 0.0 | 0.0 |

| $S_{\text{init}}$ | $S_{\text{final}}$ | $\mu_x$ | $\mu_y$ | $\mu_z$ |
|---|---|---|---|---|
| $S_{42}$ | $S_{34}$ | -0.10882037 | 0.0 | 0.0 |
| $S_{42}$ | $S_{35}$ | 0.0 | 0.0 | 0.57913384 |
| $S_{42}$ | $S_{36}$ | -0.03450205 | 0.0 | 0.0 |
| $S_{42}$ | $S_{37}$ | 0.0 | 0.0 | -0.75724803 |
| $S_{42}$ | $S_{38}$ | 0.19484324 | 0.0 | 0.0 |
| $S_{42}$ | $S_{39}$ | 0.0 | 0.0 | 0.0 |
| $S_{42}$ | $S_{40}$ | 0.0 | 0.0 | 0.25973309 |
| $S_{42}$ | $S_{41}$ | 0.0 | 0.0 | -0.37811686 |
| $S_{42}$ | $S_{42}$ | 0.0 | 0.0 | -1.2572146 |
| $S_{42}$ | $S_{43}$ | 0.5155542 | 0.0 | 0.0 |
| $S_{42}$ | $S_{44}$ | -0.6285367 | 0.0 | 0.0 |
| $S_{43}$ | $S_0$ | 0.0 | 0.48888005 | 0.0 |
| $S_{43}$ | $S_1$ | 0.0 | -2e-08 | 0.0 |
| $S_{43}$ | $S_2$ | 0.00453275 | 0.0 | 0.0 |
| $S_{43}$ | $S_3$ | 0.0 | 0.0 | 0.0 |
| $S_{43}$ | $S_4$ | 0.0 | 0.0 | 0.0 |
| $S_{43}$ | $S_5$ | 0.0 | 0.0 | 0.01683917 |
| $S_{43}$ | $S_6$ | 0.0 | 0.0 | 0.0 |
| $S_{43}$ | $S_7$ | 0.0 | 0.0 | 0.0 |
| $S_{43}$ | $S_8$ | 0.0 | 1e-08 | 0.0 |
| $S_{43}$ | $S_9$ | 0.0 | 0.11717236 | 0.0 |
| $S_{43}$ | $S_{10}$ | 0.0 | 0.0 | 0.0 |
| $S_{43}$ | $S_{11}$ | 0.0 | 0.0 | 0.0 |
| $S_{43}$ | $S_{12}$ | 0.0 | 0.0 | 0.0 |
| $S_{43}$ | $S_{13}$ | 0.0 | -0.12668579 | 0.0 |
| $S_{43}$ | $S_{14}$ | 0.0 | 0.02188728 | 0.0 |
| $S_{43}$ | $S_{15}$ | 0.28186078 | 0.0 | 0.0 |
| $S_{43}$ | $S_{16}$ | 0.0 | 0.0 | -0.25302563 |
| $S_{43}$ | $S_{17}$ | 0.0 | 0.0 | 0.0 |
| $S_{43}$ | $S_{18}$ | 0.0 | 0.0 | 0.0 |
| $S_{43}$ | $S_{19}$ | 0.0 | 0.0 | 0.0 |
| $S_{43}$ | $S_{20}$ | 0.0 | 0.0 | -0.04338927 |
| $S_{43}$ | $S_{21}$ | 0.0 | 0.0 | 0.0 |
| $S_{43}$ | $S_{22}$ | 0.0 | -0.05445384 | 0.0 |
| $S_{43}$ | $S_{23}$ | -0.40796856 | 0.0 | 0.0 |
| $S_{43}$ | $S_{24}$ | 0.0 | 0.0 | 0.25675728 |
| $S_{43}$ | $S_{25}$ | -0.33105435 | 0.0 | 0.0 |
| $S_{43}$ | $S_{26}$ | 0.0 | 0.1066169 | 0.0 |
| $S_{43}$ | $S_{27}$ | 0.40273576 | 0.0 | 0.0 |
| $S_{43}$ | $S_{28}$ | 0.0 | -8.96e-06 | 0.0 |

| $S_{\text{init}}$ | $S_{\text{final}}$ | $\mu_x$ | $\mu_y$ | $\mu_z$ |
|---|---|---|---|---|
| $S_{43}$ | $S_{29}$ | 0.0 | 0.0 | 0.0 |
| $S_{43}$ | $S_{30}$ | 0.0 | 0.0 | 1.23339905 |
| $S_{43}$ | $S_{31}$ | 0.0 | -0.67348906 | 0.0 |
| $S_{43}$ | $S_{32}$ | 0.17099422 | 0.0 | 0.0 |
| $S_{43}$ | $S_{33}$ | 0.0 | 0.0 | -1.89146496 |
| $S_{43}$ | $S_{34}$ | 0.0 | 0.0 | 0.03897392 |
| $S_{43}$ | $S_{35}$ | -2.89674572 | 0.0 | 0.0 |
| $S_{43}$ | $S_{36}$ | 0.0 | 0.0 | 0.1722626 |
| $S_{43}$ | $S_{37}$ | -0.35497988 | 0.0 | 0.0 |
| $S_{43}$ | $S_{38}$ | 0.0 | 0.0 | 0.96830195 |
| $S_{43}$ | $S_{39}$ | 0.0 | -1.02379219 | 0.0 |
| $S_{43}$ | $S_{40}$ | 0.02551873 | 0.0 | 0.0 |
| $S_{43}$ | $S_{41}$ | -0.15559292 | 0.0 | 0.0 |
| $S_{43}$ | $S_{42}$ | 0.5155542 | 0.0 | 0.0 |
| $S_{43}$ | $S_{43}$ | 0.0 | 0.0 | -2.02769353 |
| $S_{43}$ | $S_{44}$ | 0.0 | 0.0 | 0.97809453 |
| $S_{44}$ | $S_0$ | 0.0 | 0.6128152 | 0.0 |
| $S_{44}$ | $S_1$ | 0.0 | -1.1e-07 | 0.0 |
| $S_{44}$ | $S_2$ | -0.03161371 | 0.0 | 0.0 |
| $S_{44}$ | $S_3$ | 0.0 | 0.0 | 0.0 |
| $S_{44}$ | $S_4$ | 0.0 | 0.0 | 0.0 |
| $S_{44}$ | $S_5$ | 0.0 | 0.0 | -0.36756218 |
| $S_{44}$ | $S_6$ | 0.0 | 0.0 | 0.0 |
| $S_{44}$ | $S_7$ | 0.0 | 0.0 | 0.0 |
| $S_{44}$ | $S_8$ | 0.0 | -4e-08 | 0.0 |
| $S_{44}$ | $S_9$ | 0.0 | 0.07798317 | 0.0 |
| $S_{44}$ | $S_{10}$ | 0.0 | 2e-08 | 0.0 |
| $S_{44}$ | $S_{11}$ | 0.0 | 0.0 | 0.0 |
| $S_{44}$ | $S_{12}$ | 0.0 | 0.0 | 0.0 |
| $S_{44}$ | $S_{13}$ | 0.0 | -0.03527538 | 0.0 |
| $S_{44}$ | $S_{14}$ | 0.0 | -0.00529488 | 0.0 |
| $S_{44}$ | $S_{15}$ | -0.79247351 | 0.0 | 0.0 |
| $S_{44}$ | $S_{16}$ | 0.0 | 0.0 | 1.28976177 |
| $S_{44}$ | $S_{17}$ | 0.0 | 0.0 | 0.0 |
| $S_{44}$ | $S_{18}$ | 0.0 | 0.0 | 0.0 |
| $S_{44}$ | $S_{19}$ | 0.0 | 0.0 | 0.0 |
| $S_{44}$ | $S_{20}$ | 0.0 | 0.0 | -0.39380595 |
| $S_{44}$ | $S_{21}$ | 0.0 | 0.0 | 0.0 |
| $S_{44}$ | $S_{22}$ | 0.0 | -0.05063163 | 0.0 |
| $S_{44}$ | $S_{23}$ | -1.12878757 | 0.0 | 0.0 |

| $S_{\text{init}}$ | $S_{\text{final}}$ | $\mu_x$ | $\mu_y$ | $\mu_z$ |
|---|---|---|---|---|
| $S_{44}$ | $S_{24}$ | 0.0 | 0.0 | 1.53792337 |
| $S_{44}$ | $S_{25}$ | -1.27526208 | 0.0 | 0.0 |
| $S_{44}$ | $S_{26}$ | 0.0 | 0.1428613 | 0.0 |
| $S_{44}$ | $S_{27}$ | 0.41284317 | 0.0 | 0.0 |
| $S_{44}$ | $S_{28}$ | 0.0 | 3.51e-06 | 0.0 |
| $S_{44}$ | $S_{29}$ | 0.0 | 0.0 | 0.0 |
| $S_{44}$ | $S_{30}$ | 0.0 | 0.0 | -0.42025641 |
| $S_{44}$ | $S_{31}$ | 0.0 | 0.0478078 | 0.0 |
| $S_{44}$ | $S_{32}$ | -0.00491693 | 0.0 | 0.0 |
| $S_{44}$ | $S_{33}$ | 0.0 | 0.0 | 0.47228967 |
| $S_{44}$ | $S_{34}$ | 0.0 | 0.0 | 0.00529624 |
| $S_{44}$ | $S_{35}$ | 0.0458868 | 0.0 | 0.0 |
| $S_{44}$ | $S_{36}$ | 0.0 | 0.0 | 0.18721309 |
| $S_{44}$ | $S_{37}$ | -1.14777498 | 0.0 | 0.0 |
| $S_{44}$ | $S_{38}$ | 0.0 | 0.0 | 0.31683771 |
| $S_{44}$ | $S_{39}$ | 0.0 | -0.51907338 | 0.0 |
| $S_{44}$ | $S_{40}$ | 0.42868041 | 0.0 | 0.0 |
| $S_{44}$ | $S_{41}$ | -0.11134196 | 0.0 | 0.0 |
| $S_{44}$ | $S_{42}$ | -0.6285367 | 0.0 | 0.0 |
| $S_{44}$ | $S_{43}$ | 0.0 | 0.0 | 0.97809453 |
| $S_{44}$ | $S_{44}$ | 0.0 | 0.0 | -5.18552102 |

## A.2 Nitrobenzene with 13° Rotated Dihedral angle off from Ground State Geometry

Table A.3: Calculated singlet energy levels of nitrobenzene with the $NO_2$ group rotated to form a 13° dihedral angle between the plane of the ring and the plane defined by the members of the functional group. The bond angles and bond distances are the same as those for the ground state optimized geometry.

| State | Symmetry | Energy (eV) |
|---|---|---|
| $S_0$ | $A_1$ | 0.0 |
| $S_1$ | $A_1$ | 4.173256832 |
| $S_2$ | $A_1$ | 4.563929072 |
| $S_3$ | $A_1$ | 4.582596704 |
| $S_4$ | $A_1$ | 4.957134992 |
| $S_5$ | $A_1$ | 5.8771388159999995 |
| $S_6$ | $A_1$ | 5.9669091519999995 |
| $S_7$ | $A_1$ | 5.975402895999999 |
| $S_8$ | $A_1$ | 6.29511632 |
| $S_9$ | $A_1$ | 6.370814192 |
| $S_{10}$ | $A_1$ | 7.339029472 |
| $S_{11}$ | $A_1$ | 7.54705616 |
| $S_{12}$ | $A_1$ | 7.581602063999999 |
| $S_{13}$ | $A_1$ | 8.6292136 |
| $S_{14}$ | $A_1$ | 8.84774656 |
| $S_{15}$ | $A_1$ | 8.913710367999998 |
| $S_{16}$ | $A_1$ | 9.222676256 |
| $S_{17}$ | $A_1$ | 9.251906192 |
| $S_{18}$ | $A_1$ | 9.275512527999998 |
| $S_{19}$ | $A_1$ | 9.360694768 |
| $S_{20}$ | $A_1$ | 9.43681424 |

Table A.4: Calculated Singlet to Singlet dipole transitions of nitrobenzene with the $NO_2$ group rotated to form a 13° dihedral angle between the plane of the ring and the plane defined by the members of the functional group. The bond angles and bond distances are the same as those for the ground state optimized geometry. Dipole matrix elements were calculated though 1st and 2nd order response theory calculations as implemented in the Dalton quantum chemistry software package. Here $S_{\text{init}}$ and $S_{\text{final}}$ are used to represent the initial and final states of a dipole mediated transition, and $\mu_x$, $\mu_y$, $\mu_z$ represent the strength of the dipole transition in atomic units.

| $S_{\text{init}}$ | $S_{\text{final}}$ | $\mu_x$ | $\mu_y$ | $\mu_z$ |
|---|---|---|---|---|
| $S_0$ | $S_0$ | 0.0 | 0.0 | -1.71817202 |
| $S_0$ | $S_1$ | 2.68e-10 | -9.03e-11 | 0.074331482 |
| $S_0$ | $S_2$ | 0.009971888 | -0.033220861 | -5.96e-10 |
| $S_0$ | $S_3$ | -1.07e-13 | -2.68e-14 | -3.43e-12 |
| $S_0$ | $S_4$ | -1.08e-12 | -4e-13 | -2.42e-14 |
| $S_0$ | $S_5$ | -6.25e-14 | -1.89e-14 | 2.98e-12 |
| $S_0$ | $S_6$ | 6.56e-12 | -1.03e-12 | 3.89e-14 |
| $S_0$ | $S_7$ | 0.022007786 | -0.018304187 | -2.33e-10 |
| $S_0$ | $S_8$ | 0.63082808 | 0.21451413 | -3.18e-09 |
| $S_0$ | $S_9$ | -1.47e-09 | -6.47e-10 | -0.89123235 |
| $S_0$ | $S_{10}$ | -3.69e-13 | -8.62e-15 | -3.74e-11 |
| $S_0$ | $S_{11}$ | -3.47e-09 | -1.51e-10 | -1.8793054 |
| $S_0$ | $S_{12}$ | 1.8183346 | 0.026092185 | -3.26e-09 |
| $S_0$ | $S_{13}$ | -5.07e-10 | -9.16e-11 | -0.32764627 |
| $S_0$ | $S_{14}$ | -0.34033054 | -0.1023732 | -1.24e-10 |
| $S_0$ | $S_{15}$ | -1.89e-09 | -4.08e-10 | 0.13185306 |
| $S_0$ | $S_{16}$ | -2.08e-11 | -1.23e-10 | -0.065582947 |
| $S_0$ | $S_{17}$ | 5.25e-10 | -2.23e-09 | 0.032353253 |
| $S_0$ | $S_{18}$ | 0.003066984 | 0.25188953 | 4.18e-11 |
| $S_0$ | $S_{19}$ | 1.74e-14 | 8.51e-15 | 1.39e-12 |
| $S_0$ | $S_{20}$ | -9.94e-10 | 3.41e-10 | 0.2229964 |
| $S_1$ | $S_0$ | 2.68e-10 | -9.03e-11 | 0.074331482 |
| $S_1$ | $S_1$ | 4.9e-05 | 2.05e-06 | -2.25491472 |
| $S_1$ | $S_2$ | 0.58018571 | 0.14445982 | 5.28e-06 |
| $S_1$ | $S_3$ | 7.6e-07 | -1e-07 | 1e-08 |
| $S_1$ | $S_4$ | -2.2e-07 | -1e-08 | -1e-08 |
| $S_1$ | $S_5$ | -2.93e-06 | 5.7e-07 | 0.0 |
| $S_1$ | $S_6$ | 3.3e-07 | 1e-08 | 7e-08 |
| $S_1$ | $S_7$ | 0.01304391 | 0.00503539 | -4e-08 |
| $S_1$ | $S_8$ | 0.01614673 | -0.00703524 | 1.08e-06 |
| $S_1$ | $S_9$ | 3.51e-06 | -2e-06 | 0.09618598 |
| $S_1$ | $S_{10}$ | -2.87e-06 | 7e-08 | -1e-08 |

| $S_{\text{init}}$ | $S_{\text{final}}$ | $\mu_x$ | $\mu_y$ | $\mu_z$ |
|---|---|---|---|---|
| $S_1$ | $S_{11}$ | -1.18e-05 | 1.96e-06 | -0.0705982 |
| $S_1$ | $S_{12}$ | 0.00100806 | -0.00214225 | 1.04e-06 |
| $S_1$ | $S_{13}$ | 5.01e-06 | -4.88e-06 | 0.04281955 |
| $S_1$ | $S_{14}$ | -0.03611781 | 0.00277616 | -2e-08 |
| $S_1$ | $S_{15}$ | -5.7e-06 | -7.93e-06 | 0.07781391 |
| $S_1$ | $S_{16}$ | -4e-06 | -8.32e-06 | 0.08085548 |
| $S_1$ | $S_{17}$ | 2.03e-06 | -2e-07 | -0.01157782 |
| $S_1$ | $S_{18}$ | 0.00800434 | 0.0040038 | -8.2e-07 |
| $S_1$ | $S_{19}$ | -8.6e-07 | -1.6e-06 | 6e-08 |
| $S_1$ | $S_{20}$ | 1.34e-05 | -3.79e-06 | 0.12394873 |
| $S_2$ | $S_0$ | 0.009971888 | -0.033220861 | -5.96e-10 |
| $S_2$ | $S_1$ | 0.58018571 | 0.14445982 | 5.28e-06 |
| $S_2$ | $S_2$ | 8.01e-05 | 6.35e-06 | -2.18217425 |
| $S_2$ | $S_3$ | -1.9e-07 | -1e-08 | -4e-08 |
| $S_2$ | $S_4$ | 4.03e-06 | -7.2e-07 | 0.0 |
| $S_2$ | $S_5$ | 5.3e-07 | 6e-08 | -1.1e-07 |
| $S_2$ | $S_6$ | -2.82e-06 | 7.3e-07 | -1e-08 |
| $S_2$ | $S_7$ | -2.06e-05 | 1.5e-06 | -0.02320817 |
| $S_2$ | $S_8$ | -1e-08 | -4.77e-06 | -0.02125772 |
| $S_2$ | $S_9$ | -0.05506959 | -0.00231793 | 2.9e-07 |
| $S_2$ | $S_{10}$ | -7e-08 | 0.0 | 1.7e-07 |
| $S_2$ | $S_{11}$ | 0.00077239 | 0.00273981 | 1.07e-06 |
| $S_2$ | $S_{12}$ | -1.29e-06 | 2.25e-06 | 0.02803274 |
| $S_2$ | $S_{13}$ | -0.02575671 | -0.00063014 | -9e-06 |
| $S_2$ | $S_{14}$ | -6.68e-05 | 1.53e-05 | -0.00844464 |
| $S_2$ | $S_{15}$ | -0.01400232 | 0.00595011 | 1.47e-05 |
| $S_2$ | $S_{16}$ | -0.02107763 | -0.00298707 | -1.34e-05 |
| $S_2$ | $S_{17}$ | 0.01714932 | 0.00277432 | -6.3e-07 |
| $S_2$ | $S_{18}$ | -4.62e-06 | 1.86e-06 | -0.00584934 |
| $S_2$ | $S_{19}$ | -6.1e-07 | 2e-08 | 1.67e-06 |
| $S_2$ | $S_{20}$ | -0.02936287 | 0.00241162 | 2.95e-06 |
| $S_3$ | $S_0$ | -1.07e-13 | -2.68e-14 | -3.43e-12 |
| $S_3$ | $S_1$ | 7.6e-07 | -1e-07 | 1e-08 |
| $S_3$ | $S_2$ | -1.9e-07 | -1e-08 | -4e-08 |
| $S_3$ | $S_3$ | -8.02e-05 | 8.91e-06 | -2.82622299 |
| $S_3$ | $S_4$ | 0.0667962 | 0.02217062 | 1.64e-06 |
| $S_3$ | $S_5$ | -1.11e-05 | 1.89e-06 | -0.06286559 |
| $S_3$ | $S_6$ | -0.16864158 | -0.03703783 | -3.3e-07 |
| $S_3$ | $S_7$ | 1.8e-07 | 2e-08 | -4.3e-07 |
| $S_3$ | $S_8$ | 1.7e-07 | 2e-08 | -1e-08 |

| $S_{\text{init}}$ | $S_{\text{final}}$ | $\mu_x$ | $\mu_y$ | $\mu_z$ |
|---|---|---|---|---|
| $S_3$ | $S_9$ | -1.55e-06 | 6.2e-07 | 0.0 |
| $S_3$ | $S_{10}$ | 6.3e-06 | 1.64e-06 | -0.06868482 |
| $S_3$ | $S_{11}$ | -4.6e-07 | 6e-07 | 0.0 |
| $S_3$ | $S_{12}$ | -2.5e-07 | 0.0 | -7e-08 |
| $S_3$ | $S_{13}$ | -1.52e-06 | -2.8e-07 | -2.4e-07 |
| $S_3$ | $S_{14}$ | -4.3e-07 | -1e-08 | 3.92e-06 |
| $S_3$ | $S_{15}$ | -9.3e-07 | -3.1e-07 | 6.2e-07 |
| $S_3$ | $S_{16}$ | 1.29e-06 | 4e-08 | 1e-08 |
| $S_3$ | $S_{17}$ | 3.7e-07 | 6e-08 | 1e-08 |
| $S_3$ | $S_{18}$ | -5e-08 | -1e-08 | -1.2e-07 |
| $S_3$ | $S_{19}$ | 0.00013443 | -2.56e-05 | -0.06980402 |
| $S_3$ | $S_{20}$ | -6e-07 | -2.09e-06 | -3e-07 |
| $S_4$ | $S_0$ | -1.08e-12 | -4e-13 | -2.42e-14 |
| $S_4$ | $S_1$ | -2.2e-07 | -1e-08 | -1e-08 |
| $S_4$ | $S_2$ | 4.03e-06 | -7.2e-07 | 0.0 |
| $S_4$ | $S_3$ | 0.0667962 | 0.02217062 | 1.64e-06 |
| $S_4$ | $S_4$ | 8.58e-05 | -2.59e-06 | -1.93446185 |
| $S_4$ | $S_5$ | 1.39513376 | -0.01281112 | -6.02e-05 |
| $S_4$ | $S_6$ | -0.00021359 | 1.27e-05 | 0.02627293 |
| $S_4$ | $S_7$ | -3.54e-05 | 7.67e-06 | 1.4e-07 |
| $S_4$ | $S_8$ | 6.3e-07 | 2.55e-06 | -1e-08 |
| $S_4$ | $S_9$ | -2.8e-07 | 0.0 | 0.0 |
| $S_4$ | $S_{10}$ | -1.17147022 | 0.0112284 | 3.01e-05 |
| $S_4$ | $S_{11}$ | -4.9e-07 | 5e-08 | -4e-08 |
| $S_4$ | $S_{12}$ | -3.69e-06 | 2.93e-06 | -2e-08 |
| $S_4$ | $S_{13}$ | -1e-06 | 1e-08 | -1.8e-07 |
| $S_4$ | $S_{14}$ | -5.9e-06 | 2.38e-06 | -1.3e-07 |
| $S_4$ | $S_{15}$ | -1.4e-06 | 2e-08 | -1.2e-07 |
| $S_4$ | $S_{16}$ | 1.6e-07 | 0.0 | -9e-08 |
| $S_4$ | $S_{17}$ | 1.6e-07 | 0.0 | 1.1e-07 |
| $S_4$ | $S_{18}$ | 8e-08 | -7e-08 | 1e-08 |
| $S_4$ | $S_{19}$ | 0.24657757 | 0.0350243 | -3.19e-05 |
| $S_4$ | $S_{20}$ | -2.35e-06 | 7e-08 | -7.9e-07 |
| $S_5$ | $S_0$ | -6.25e-14 | -1.89e-14 | 2.98e-12 |
| $S_5$ | $S_1$ | -2.93e-06 | 5.7e-07 | 0.0 |
| $S_5$ | $S_2$ | 5.3e-07 | 6e-08 | -1.1e-07 |
| $S_5$ | $S_3$ | -1.11e-05 | 1.89e-06 | -0.06286559 |
| $S_5$ | $S_4$ | 1.39513376 | -0.01281112 | -6.02e-05 |
| $S_5$ | $S_5$ | 0.00017859 | -1.23e-05 | -1.70813894 |
| $S_5$ | $S_6$ | -0.32935515 | 0.00133433 | 1.57e-05 |

| $S_{\text{init}}$ | $S_{\text{final}}$ | $\mu_x$ | $\mu_y$ | $\mu_z$ |
|---|---|---|---|---|
| $S_5$ | $S_7$ | -9.47e-06 | -1.05e-06 | 3.2e-07 |
| $S_5$ | $S_8$ | 6.7e-07 | 1e-07 | 2.3e-07 |
| $S_5$ | $S_9$ | 2.82e-06 | -6.2e-07 | 2e-08 |
| $S_5$ | $S_{10}$ | 0.00019943 | -1.47e-05 | 0.40795097 |
| $S_5$ | $S_{11}$ | -1.87e-06 | -2.1e-07 | -1e-08 |
| $S_5$ | $S_{12}$ | -3e-07 | -2.4e-07 | -7e-08 |
| $S_5$ | $S_{13}$ | -6.3e-07 | -1.9e-07 | -1e-08 |
| $S_5$ | $S_{14}$ | -6e-08 | -1e-08 | 9e-08 |
| $S_5$ | $S_{15}$ | 1.69e-06 | 6e-07 | 0.0 |
| $S_5$ | $S_{16}$ | 1.7e-07 | -2e-08 | -1e-08 |
| $S_5$ | $S_{17}$ | 2.8e-07 | 3e-08 | 0.0 |
| $S_5$ | $S_{18}$ | 1e-08 | 0.0 | -1e-08 |
| $S_5$ | $S_{19}$ | 4.62e-06 | -7.7e-07 | 0.08130132 |
| $S_5$ | $S_{20}$ | -6.44e-06 | 2.3e-07 | 1.7e-07 |
| $S_6$ | $S_0$ | 6.56e-12 | -1.03e-12 | 3.89e-14 |
| $S_6$ | $S_1$ | 3.3e-07 | 1e-08 | 7e-08 |
| $S_6$ | $S_2$ | -2.82e-06 | 7.3e-07 | -1e-08 |
| $S_6$ | $S_3$ | -0.16864158 | -0.03703783 | -3.3e-07 |
| $S_6$ | $S_4$ | -0.00021359 | 1.27e-05 | 0.02627293 |
| $S_6$ | $S_5$ | -0.32935515 | 0.00133433 | 1.57e-05 |
| $S_6$ | $S_6$ | 0.00032037 | -1.57e-05 | -1.59442702 |
| $S_6$ | $S_7$ | 3.01e-05 | -1.46e-05 | 1.2e-07 |
| $S_6$ | $S_8$ | 9.1e-06 | -9.6e-07 | 0.0 |
| $S_6$ | $S_9$ | 1.33e-06 | 1.3e-07 | 0.0 |
| $S_6$ | $S_{10}$ | 0.44646315 | -0.01226407 | -1.59e-05 |
| $S_6$ | $S_{11}$ | 6e-08 | -2e-08 | -2e-08 |
| $S_6$ | $S_{12}$ | 7.41e-06 | -3.16e-06 | -2e-08 |
| $S_6$ | $S_{13}$ | 8.5e-07 | -4e-08 | 4e-08 |
| $S_6$ | $S_{14}$ | 3.25e-06 | -1.97e-06 | 0.0 |
| $S_6$ | $S_{15}$ | 4.5e-07 | -2e-08 | 4e-08 |
| $S_6$ | $S_{16}$ | -3.2e-07 | 1e-08 | 0.0 |
| $S_6$ | $S_{17}$ | -3.2e-07 | 1e-08 | 0.0 |
| $S_6$ | $S_{18}$ | -6e-08 | 2e-08 | 0.0 |
| $S_6$ | $S_{19}$ | -0.18811072 | -0.05488063 | -7.72e-06 |
| $S_6$ | $S_{20}$ | 7.97e-06 | -1.7e-07 | -2.4e-07 |
| $S_7$ | $S_0$ | 0.022007786 | -0.018304187 | -2.33e-10 |
| $S_7$ | $S_1$ | 0.01304391 | 0.00503539 | -4e-08 |
| $S_7$ | $S_2$ | -2.06e-05 | 1.5e-06 | -0.02320817 |
| $S_7$ | $S_3$ | 1.8e-07 | 2e-08 | -4.3e-07 |
| $S_7$ | $S_4$ | -3.54e-05 | 7.67e-06 | 1.4e-07 |

| $S_{\text{init}}$ | $S_{\text{final}}$ | $\mu_x$ | $\mu_y$ | $\mu_z$ |
|---|---|---|---|---|
| $S_7$ | $S_5$ | -9.47e-06 | -1.05e-06 | 3.2e-07 |
| $S_7$ | $S_6$ | 3.01e-05 | -1.46e-05 | 1.2e-07 |
| $S_7$ | $S_7$ | 0.0006677 | -4.81e-05 | -1.68433501 |
| $S_7$ | $S_8$ | -2.69e-05 | 7.1e-07 | 0.136212 |
| $S_7$ | $S_9$ | 0.87734821 | -0.00598172 | -3.14e-05 |
| $S_7$ | $S_{10}$ | 1.02e-05 | 7.7e-07 | -2.4e-07 |
| $S_7$ | $S_{11}$ | 0.54175161 | -0.01574501 | -8.91e-06 |
| $S_7$ | $S_{12}$ | -0.00015491 | 8.1e-07 | -0.7641581 |
| $S_7$ | $S_{13}$ | -0.03393907 | 0.0381633 | 6.09e-06 |
| $S_7$ | $S_{14}$ | 2.43e-05 | 1.91e-06 | 0.09079493 |
| $S_7$ | $S_{15}$ | -0.35157369 | -0.01900341 | 3.96e-06 |
| $S_7$ | $S_{16}$ | 0.03324073 | -0.01015755 | -1.05e-06 |
| $S_7$ | $S_{17}$ | 0.03283784 | -0.05573303 | -1.88e-06 |
| $S_7$ | $S_{18}$ | -2.67e-06 | -5.86e-06 | -0.0666113 |
| $S_7$ | $S_{19}$ | -3.5e-07 | -1.3e-07 | -2.2e-07 |
| $S_7$ | $S_{20}$ | -0.38698502 | 0.00076337 | 4.72e-05 |
| $S_8$ | $S_0$ | 0.63082808 | 0.21451413 | -3.18e-09 |
| $S_8$ | $S_1$ | 0.01614673 | -0.00703524 | 1.08e-06 |
| $S_8$ | $S_2$ | -1e-08 | -4.77e-06 | -0.02125772 |
| $S_8$ | $S_3$ | 1.7e-07 | 2e-08 | -1e-08 |
| $S_8$ | $S_4$ | 6.3e-07 | 2.55e-06 | -1e-08 |
| $S_8$ | $S_5$ | 6.7e-07 | 1e-07 | 2.3e-07 |
| $S_8$ | $S_6$ | 9.1e-06 | -9.6e-07 | 0.0 |
| $S_8$ | $S_7$ | -2.69e-05 | 7.1e-07 | 0.136212 |
| $S_8$ | $S_8$ | -0.00017909 | -2.15e-05 | -2.18866342 |
| $S_8$ | $S_9$ | 0.02205881 | 0.00956621 | 2.06e-06 |
| $S_8$ | $S_{10}$ | 2.2e-07 | 1e-08 | -3.3e-07 |
| $S_8$ | $S_{11}$ | -0.0810751 | -0.01171733 | -1.66e-06 |
| $S_8$ | $S_{12}$ | -2.91e-05 | -4.86e-06 | -0.12316439 |
| $S_8$ | $S_{13}$ | 0.37656406 | 0.01179711 | -7.45e-06 |
| $S_8$ | $S_{14}$ | 9.82e-05 | 1.65e-05 | 0.54136118 |
| $S_8$ | $S_{15}$ | 0.05962157 | 0.04297644 | 1.81e-05 |
| $S_8$ | $S_{16}$ | 0.00326796 | -0.0521216 | 1.36e-06 |
| $S_8$ | $S_{17}$ | -0.00999954 | -0.00630062 | -4e-07 |
| $S_8$ | $S_{18}$ | 1.44e-05 | 1.25e-06 | 0.00154715 |
| $S_8$ | $S_{19}$ | 3.96e-06 | 2.1e-07 | 2.11e-06 |
| $S_8$ | $S_{20}$ | 0.18840992 | 0.01990897 | 4.4e-07 |
| $S_9$ | $S_0$ | -1.47e-09 | -6.47e-10 | -0.89123235 |
| $S_9$ | $S_1$ | 3.51e-06 | -2e-06 | 0.09618598 |
| $S_9$ | $S_2$ | -0.05506959 | -0.00231793 | 2.9e-07 |

| $S_{\text{init}}$ | $S_{\text{final}}$ | $\mu_x$ | $\mu_y$ | $\mu_z$ |
|---|---|---|---|---|
| $S_9$ | $S_3$ | -1.55e-06 | 6.2e-07 | 0.0 |
| $S_9$ | $S_4$ | -2.8e-07 | 0.0 | 0.0 |
| $S_9$ | $S_5$ | 2.82e-06 | -6.2e-07 | 2e-08 |
| $S_9$ | $S_6$ | 1.33e-06 | 1.3e-07 | 0.0 |
| $S_9$ | $S_7$ | 0.87734821 | -0.00598172 | -3.14e-05 |
| $S_9$ | $S_8$ | 0.02205881 | 0.00956621 | 2.06e-06 |
| $S_9$ | $S_9$ | 0.00010439 | -1.9e-06 | -0.67203806 |
| $S_9$ | $S_{10}$ | -4.32e-06 | 7.9e-07 | 0.0 |
| $S_9$ | $S_{11}$ | -1.25e-05 | -8.4e-07 | -0.52186923 |
| $S_9$ | $S_{12}$ | 0.09906098 | 0.00029757 | -6.96e-06 |
| $S_9$ | $S_{13}$ | -4.14e-05 | -3.07e-06 | -0.05183272 |
| $S_9$ | $S_{14}$ | -0.11272911 | -0.01434768 | 4.95e-06 |
| $S_9$ | $S_{15}$ | 6.28e-05 | -4.88e-06 | 0.17821949 |
| $S_9$ | $S_{16}$ | -7.67e-06 | 7.67e-06 | -0.11525705 |
| $S_9$ | $S_{17}$ | 1.57e-06 | -4.81e-06 | -0.03738266 |
| $S_9$ | $S_{18}$ | 0.02474744 | -0.02401284 | 2.6e-07 |
| $S_9$ | $S_{19}$ | 7.58e-06 | -2.92e-06 | -2e-08 |
| $S_9$ | $S_{20}$ | 7.47e-05 | 4.75e-06 | 1.14806488 |
| $S_{10}$ | $S_0$ | -3.69e-13 | -8.62e-15 | -3.74e-11 |
| $S_{10}$ | $S_1$ | -2.87e-06 | 7e-08 | -1e-08 |
| $S_{10}$ | $S_2$ | -7e-08 | 0.0 | 1.7e-07 |
| $S_{10}$ | $S_3$ | 6.3e-06 | 1.64e-06 | -0.06868482 |
| $S_{10}$ | $S_4$ | -1.17147022 | 0.0112284 | 3.01e-05 |
| $S_{10}$ | $S_5$ | 0.00019943 | -1.47e-05 | 0.40795097 |
| $S_{10}$ | $S_6$ | 0.44646315 | -0.01226407 | -1.59e-05 |
| $S_{10}$ | $S_7$ | 1.02e-05 | 7.7e-07 | -2.4e-07 |
| $S_{10}$ | $S_8$ | 2.2e-07 | 1e-08 | -3.3e-07 |
| $S_{10}$ | $S_9$ | -4.32e-06 | 7.9e-07 | 0.0 |
| $S_{10}$ | $S_{10}$ | 1.09e-06 | -6.6e-07 | -0.7198112 |
| $S_{10}$ | $S_{11}$ | 3.04e-06 | 5e-07 | 4e-08 |
| $S_{10}$ | $S_{12}$ | -3.42e-06 | -3.3e-07 | -1e-07 |
| $S_{10}$ | $S_{13}$ | 3.05e-06 | -3.9e-07 | -2e-08 |
| $S_{10}$ | $S_{14}$ | 5e-08 | 2e-08 | -1.9e-07 |
| $S_{10}$ | $S_{15}$ | -1.15e-06 | -1.35e-06 | -2e-08 |
| $S_{10}$ | $S_{16}$ | -1.9e-07 | -6e-08 | 1e-08 |
| $S_{10}$ | $S_{17}$ | -1e-08 | 1.1e-07 | 0.0 |
| $S_{10}$ | $S_{18}$ | 1e-08 | 0.0 | 0.0 |
| $S_{10}$ | $S_{19}$ | 1.6e-06 | -3.5e-07 | -0.02490173 |
| $S_{10}$ | $S_{20}$ | -1.01e-06 | -8e-07 | -5e-08 |
| $S_{11}$ | $S_0$ | -3.47e-09 | -1.51e-10 | -1.8793054 |

| $S_{\text{init}}$ | $S_{\text{final}}$ | $\mu_x$ | $\mu_y$ | $\mu_z$ |
|---|---|---|---|---|
| $S_{11}$ | $S_1$ | -1.18e-05 | 1.96e-06 | -0.0705982 |
| $S_{11}$ | $S_2$ | 0.00077239 | 0.00273981 | 1.07e-06 |
| $S_{11}$ | $S_3$ | -4.6e-07 | 6e-07 | 0.0 |
| $S_{11}$ | $S_4$ | -4.9e-07 | 5e-08 | -4e-08 |
| $S_{11}$ | $S_5$ | -1.87e-06 | -2.1e-07 | -1e-08 |
| $S_{11}$ | $S_6$ | 6e-08 | -2e-08 | -2e-08 |
| $S_{11}$ | $S_7$ | 0.54175161 | -0.01574501 | -8.91e-06 |
| $S_{11}$ | $S_8$ | -0.0810751 | -0.01171733 | -1.66e-06 |
| $S_{11}$ | $S_9$ | -1.25e-05 | -8.4e-07 | -0.52186923 |
| $S_{11}$ | $S_{10}$ | 3.04e-06 | 5e-07 | 4e-08 |
| $S_{11}$ | $S_{11}$ | 0.00010719 | -7e-06 | -1.17995072 |
| $S_{11}$ | $S_{12}$ | -0.26323495 | -0.00011841 | 4.32e-06 |
| $S_{11}$ | $S_{13}$ | -1.87e-05 | 2.88e-06 | -0.17196151 |
| $S_{11}$ | $S_{14}$ | 0.11706717 | 0.01089557 | -3.79e-06 |
| $S_{11}$ | $S_{15}$ | -2.15e-05 | 4.81e-06 | -0.20171318 |
| $S_{11}$ | $S_{16}$ | 2.86e-06 | 5.7e-07 | 0.07550888 |
| $S_{11}$ | $S_{17}$ | 3.45e-06 | 3.9e-07 | 0.02226655 |
| $S_{11}$ | $S_{18}$ | -0.03271045 | -0.01290471 | 8e-08 |
| $S_{11}$ | $S_{19}$ | -1.22e-05 | 1.96e-06 | 0.0 |
| $S_{11}$ | $S_{20}$ | -2.9e-07 | -5.49e-06 | -0.60895491 |
| $S_{12}$ | $S_0$ | 1.8183346 | 0.026092185 | -3.26e-09 |
| $S_{12}$ | $S_1$ | 0.00100806 | -0.00214225 | 1.04e-06 |
| $S_{12}$ | $S_2$ | -1.29e-06 | 2.25e-06 | 0.02803274 |
| $S_{12}$ | $S_3$ | -2.5e-07 | 0.0 | -7e-08 |
| $S_{12}$ | $S_4$ | -3.69e-06 | 2.93e-06 | -2e-08 |
| $S_{12}$ | $S_5$ | -3e-07 | -2.4e-07 | -7e-08 |
| $S_{12}$ | $S_6$ | 7.41e-06 | -3.16e-06 | -2e-08 |
| $S_{12}$ | $S_7$ | -0.00015491 | 8.1e-07 | -0.7641581 |
| $S_{12}$ | $S_8$ | -2.91e-05 | -4.86e-06 | -0.12316439 |
| $S_{12}$ | $S_9$ | 0.09906098 | 0.00029757 | -6.96e-06 |
| $S_{12}$ | $S_{10}$ | -3.42e-06 | -3.3e-07 | -1e-07 |
| $S_{12}$ | $S_{11}$ | -0.26323495 | -0.00011841 | 4.32e-06 |
| $S_{12}$ | $S_{12}$ | 0.00010758 | -2.82e-06 | -1.34467896 |
| $S_{12}$ | $S_{13}$ | -0.12778716 | 0.00952816 | 8.31e-06 |
| $S_{12}$ | $S_{14}$ | -6.84e-06 | 5.75e-06 | 0.12526801 |
| $S_{12}$ | $S_{15}$ | -0.24303732 | 0.00425744 | 1.15e-05 |
| $S_{12}$ | $S_{16}$ | 0.03930251 | -0.00206084 | -7.9e-07 |
| $S_{12}$ | $S_{17}$ | 0.00836749 | 0.04285395 | -8e-07 |
| $S_{12}$ | $S_{18}$ | -1.91e-06 | -5.15e-06 | 0.03888172 |
| $S_{12}$ | $S_{19}$ | 7.2e-07 | 6e-08 | -3.5e-07 |

| $S_{\text{init}}$ | $S_{\text{final}}$ | $\mu_x$ | $\mu_y$ | $\mu_z$ |
|---|---|---|---|---|
| $S_{12}$ | $S_{20}$ | -0.6607976 | 0.01326818 | 1.09e-05 |
| $S_{13}$ | $S_0$ | -5.07e-10 | -9.16e-11 | -0.32764627 |
| $S_{13}$ | $S_1$ | 5.01e-06 | -4.88e-06 | 0.04281955 |
| $S_{13}$ | $S_2$ | -0.02575671 | -0.00063014 | -9e-06 |
| $S_{13}$ | $S_3$ | -1.52e-06 | -2.8e-07 | -2.4e-07 |
| $S_{13}$ | $S_4$ | -1e-06 | 1e-08 | -1.8e-07 |
| $S_{13}$ | $S_5$ | -6.3e-07 | -1.9e-07 | -1e-08 |
| $S_{13}$ | $S_6$ | 8.5e-07 | -4e-08 | 4e-08 |
| $S_{13}$ | $S_7$ | -0.03393907 | 0.0381633 | 6.09e-06 |
| $S_{13}$ | $S_8$ | 0.37656406 | 0.01179711 | -7.45e-06 |
| $S_{13}$ | $S_9$ | -4.14e-05 | -3.07e-06 | -0.05183272 |
| $S_{13}$ | $S_{10}$ | 3.05e-06 | -3.9e-07 | -2e-08 |
| $S_{13}$ | $S_{11}$ | -1.87e-05 | 2.88e-06 | -0.17196151 |
| $S_{13}$ | $S_{12}$ | -0.12778716 | 0.00952816 | 8.31e-06 |
| $S_{13}$ | $S_{13}$ | -0.00042582 | -2.04e-05 | -3.13021741 |
| $S_{13}$ | $S_{14}$ | -0.85889608 | -0.00587774 | 4.08e-05 |
| $S_{13}$ | $S_{15}$ | 0.00032908 | 1.1e-05 | 1.48099344 |
| $S_{13}$ | $S_{16}$ | -1.92e-05 | -9.3e-07 | -0.07583746 |
| $S_{13}$ | $S_{17}$ | 1.5e-05 | 9.3e-07 | -0.01994969 |
| $S_{13}$ | $S_{18}$ | 0.01922809 | 0.00119296 | 4.9e-07 |
| $S_{13}$ | $S_{19}$ | 8.61e-06 | -1.3e-07 | -3e-08 |
| $S_{13}$ | $S_{20}$ | 1.61e-05 | 1.78e-06 | 0.26275133 |
| $S_{14}$ | $S_0$ | -0.34033054 | -0.1023732 | -1.24e-10 |
| $S_{14}$ | $S_1$ | -0.03611781 | 0.00277616 | -2e-08 |
| $S_{14}$ | $S_2$ | -6.68e-05 | 1.53e-05 | -0.00844464 |
| $S_{14}$ | $S_3$ | -4.3e-07 | -1e-08 | 3.92e-06 |
| $S_{14}$ | $S_4$ | -5.9e-06 | 2.38e-06 | -1.3e-07 |
| $S_{14}$ | $S_5$ | -6e-08 | -1e-08 | 9e-08 |
| $S_{14}$ | $S_6$ | 3.25e-06 | -1.97e-06 | 0.0 |
| $S_{14}$ | $S_7$ | 2.43e-05 | 1.91e-06 | 0.09079493 |
| $S_{14}$ | $S_8$ | 9.82e-05 | 1.65e-05 | 0.54136118 |
| $S_{14}$ | $S_9$ | -0.11272911 | -0.01434768 | 4.95e-06 |
| $S_{14}$ | $S_{10}$ | 5e-08 | 2e-08 | -1.9e-07 |
| $S_{14}$ | $S_{11}$ | 0.11706717 | 0.01089557 | -3.79e-06 |
| $S_{14}$ | $S_{12}$ | -6.84e-06 | 5.75e-06 | 0.12526801 |
| $S_{14}$ | $S_{13}$ | -0.85889608 | -0.00587774 | 4.08e-05 |
| $S_{14}$ | $S_{14}$ | -0.00023132 | -2.48e-05 | -3.15305014 |
| $S_{14}$ | $S_{15}$ | 0.48928467 | -0.02428975 | -2.83e-05 |
| $S_{14}$ | $S_{16}$ | 0.02351243 | 0.00240948 | 3.2e-07 |
| $S_{14}$ | $S_{17}$ | 0.00484549 | -0.00014411 | -2e-08 |

| $S_{\text{init}}$ | $S_{\text{final}}$ | $\mu_x$ | $\mu_y$ | $\mu_z$ |
|---|---|---|---|---|
| $S_{14}$ | $S_{18}$ | -7.39e-06 | 9.4e-07 | 0.00841371 |
| $S_{14}$ | $S_{19}$ | -1.46e-06 | -3e-08 | 6e-08 |
| $S_{14}$ | $S_{20}$ | -0.24713147 | -0.0385675 | 1.96e-06 |
| $S_{15}$ | $S_0$ | -1.89e-09 | -4.08e-10 | 0.13185306 |
| $S_{15}$ | $S_1$ | -5.7e-06 | -7.93e-06 | 0.07781391 |
| $S_{15}$ | $S_2$ | -0.01400232 | 0.00595011 | 1.47e-05 |
| $S_{15}$ | $S_3$ | -9.3e-07 | -3.1e-07 | 6.2e-07 |
| $S_{15}$ | $S_4$ | -1.4e-06 | 2e-08 | -1.2e-07 |
| $S_{15}$ | $S_5$ | 1.69e-06 | 6e-07 | 0.0 |
| $S_{15}$ | $S_6$ | 4.5e-07 | -2e-08 | 4e-08 |
| $S_{15}$ | $S_7$ | -0.35157369 | -0.01900341 | 3.96e-06 |
| $S_{15}$ | $S_8$ | 0.05962157 | 0.04297644 | 1.81e-05 |
| $S_{15}$ | $S_9$ | 6.28e-05 | -4.88e-06 | 0.17821949 |
| $S_{15}$ | $S_{10}$ | -1.15e-06 | -1.35e-06 | -2e-08 |
| $S_{15}$ | $S_{11}$ | -2.15e-05 | 4.81e-06 | -0.20171318 |
| $S_{15}$ | $S_{12}$ | -0.24303732 | 0.00425744 | 1.15e-05 |
| $S_{15}$ | $S_{13}$ | 0.00032908 | 1.1e-05 | 1.48099344 |
| $S_{15}$ | $S_{14}$ | 0.48928467 | -0.02428975 | -2.83e-05 |
| $S_{15}$ | $S_{15}$ | -4.93e-05 | -1.35e-05 | -1.74674711 |
| $S_{15}$ | $S_{16}$ | 1.41e-05 | 6.63e-06 | -0.04394848 |
| $S_{15}$ | $S_{17}$ | 1.25e-05 | -3.08e-06 | -0.02119869 |
| $S_{15}$ | $S_{18}$ | 0.03167193 | 0.00185779 | 4e-07 |
| $S_{15}$ | $S_{19}$ | 1.02e-05 | -1.55e-06 | 2e-08 |
| $S_{15}$ | $S_{20}$ | -0.00016372 | 4.99e-06 | -0.02092554 |
| $S_{16}$ | $S_0$ | -2.08e-11 | -1.23e-10 | -0.065582947 |
| $S_{16}$ | $S_1$ | -4e-06 | -8.32e-06 | 0.08085548 |
| $S_{16}$ | $S_2$ | -0.02107763 | -0.00298707 | -1.34e-05 |
| $S_{16}$ | $S_3$ | 1.29e-06 | 4e-08 | 1e-08 |
| $S_{16}$ | $S_4$ | 1.6e-07 | 0.0 | -9e-08 |
| $S_{16}$ | $S_5$ | 1.7e-07 | -2e-08 | -1e-08 |
| $S_{16}$ | $S_6$ | -3.2e-07 | 1e-08 | 0.0 |
| $S_{16}$ | $S_7$ | 0.03324073 | -0.01015755 | -1.05e-06 |
| $S_{16}$ | $S_8$ | 0.00326796 | -0.0521216 | 1.36e-06 |
| $S_{16}$ | $S_9$ | -7.67e-06 | 7.67e-06 | -0.11525705 |
| $S_{16}$ | $S_{10}$ | -1.9e-07 | -6e-08 | 1e-08 |
| $S_{16}$ | $S_{11}$ | 2.86e-06 | 5.7e-07 | 0.07550888 |
| $S_{16}$ | $S_{12}$ | 0.03930251 | -0.00206084 | -7.9e-07 |
| $S_{16}$ | $S_{13}$ | -1.92e-05 | -9.3e-07 | -0.07583746 |
| $S_{16}$ | $S_{14}$ | 0.02351243 | 0.00240948 | 3.2e-07 |
| $S_{16}$ | $S_{15}$ | 1.41e-05 | 6.63e-06 | -0.04394848 |

| $S_{\text{init}}$ | $S_{\text{final}}$ | $\mu_x$ | $\mu_y$ | $\mu_z$ |
|---|---|---|---|---|
| $S_{16}$ | $S_{16}$ | 0.00015216 | -4.45e-06 | -1.36125514 |
| $S_{16}$ | $S_{17}$ | 7.67e-06 | -7.2e-07 | -0.05851604 |
| $S_{16}$ | $S_{18}$ | -0.07461609 | -0.00060767 | 6.4e-07 |
| $S_{16}$ | $S_{19}$ | 2.96e-06 | -3.2e-07 | 0.0 |
| $S_{16}$ | $S_{20}$ | -5.74e-06 | -1.05e-05 | -0.00591966 |
| $S_{17}$ | $S_0$ | 5.25e-10 | -2.23e-09 | 0.032353253 |
| $S_{17}$ | $S_1$ | 2.03e-06 | -2e-07 | -0.01157782 |
| $S_{17}$ | $S_2$ | 0.01714932 | 0.00277432 | -6.3e-07 |
| $S_{17}$ | $S_3$ | 3.7e-07 | 6e-08 | 1e-08 |
| $S_{17}$ | $S_4$ | 1.6e-07 | 0.0 | 1.1e-07 |
| $S_{17}$ | $S_5$ | 2.8e-07 | 3e-08 | 0.0 |
| $S_{17}$ | $S_6$ | -3.2e-07 | 1e-08 | 0.0 |
| $S_{17}$ | $S_7$ | 0.03283784 | -0.05573303 | -1.88e-06 |
| $S_{17}$ | $S_8$ | -0.00999954 | -0.00630062 | -4e-07 |
| $S_{17}$ | $S_9$ | 1.57e-06 | -4.81e-06 | -0.03738266 |
| $S_{17}$ | $S_{10}$ | -1e-08 | 1.1e-07 | 0.0 |
| $S_{17}$ | $S_{11}$ | 3.45e-06 | 3.9e-07 | 0.02226655 |
| $S_{17}$ | $S_{12}$ | 0.00836749 | 0.04285395 | -8e-07 |
| $S_{17}$ | $S_{13}$ | 1.5e-05 | 9.3e-07 | -0.01994969 |
| $S_{17}$ | $S_{14}$ | 0.00484549 | -0.00014411 | -2e-08 |
| $S_{17}$ | $S_{15}$ | 1.25e-05 | -3.08e-06 | -0.02119869 |
| $S_{17}$ | $S_{16}$ | 7.67e-06 | -7.2e-07 | -0.05851604 |
| $S_{17}$ | $S_{17}$ | 0.00031003 | -1.71e-05 | -2.9117312 |
| $S_{17}$ | $S_{18}$ | -1.03302305 | 0.00512715 | 1.5e-05 |
| $S_{17}$ | $S_{19}$ | 4.8e-07 | -2e-08 | 0.0 |
| $S_{17}$ | $S_{20}$ | -9.49e-06 | 1.43e-05 | -0.07000691 |
| $S_{18}$ | $S_0$ | 0.003066984 | 0.25188953 | 4.18e-11 |
| $S_{18}$ | $S_1$ | 0.00800434 | 0.0040038 | -8.2e-07 |
| $S_{18}$ | $S_2$ | -4.62e-06 | 1.86e-06 | -0.00584934 |
| $S_{18}$ | $S_3$ | -5e-08 | -1e-08 | -1.2e-07 |
| $S_{18}$ | $S_4$ | 8e-08 | -7e-08 | 1e-08 |
| $S_{18}$ | $S_5$ | 1e-08 | 0.0 | -1e-08 |
| $S_{18}$ | $S_6$ | -6e-08 | 2e-08 | 0.0 |
| $S_{18}$ | $S_7$ | -2.67e-06 | -5.86e-06 | -0.0666113 |
| $S_{18}$ | $S_8$ | 1.44e-05 | 1.25e-06 | 0.00154715 |
| $S_{18}$ | $S_9$ | 0.02474744 | -0.02401284 | 2.6e-07 |
| $S_{18}$ | $S_{10}$ | 1e-08 | 0.0 | 0.0 |
| $S_{18}$ | $S_{11}$ | -0.03271045 | -0.01290471 | 8e-08 |
| $S_{18}$ | $S_{12}$ | -1.91e-06 | -5.15e-06 | 0.03888172 |
| $S_{18}$ | $S_{13}$ | 0.01922809 | 0.00119296 | 4.9e-07 |

| $S_{\text{init}}$ | $S_{\text{final}}$ | $\mu_x$ | $\mu_y$ | $\mu_z$ |
|---|---|---|---|---|
| $S_{18}$ | $S_{14}$ | -7.39e-06 | 9.4e-07 | 0.00841371 |
| $S_{18}$ | $S_{15}$ | 0.03167193 | 0.00185779 | 4e-07 |
| $S_{18}$ | $S_{16}$ | -0.07461609 | -0.00060767 | 6.4e-07 |
| $S_{18}$ | $S_{17}$ | -1.03302305 | 0.00512715 | 1.5e-05 |
| $S_{18}$ | $S_{18}$ | 0.00021871 | -6.23e-06 | -3.52528009 |
| $S_{18}$ | $S_{19}$ | 1e-08 | 0.0 | 0.0 |
| $S_{18}$ | $S_{20}$ | 0.06754775 | 0.00911442 | -1.15e-06 |
| $S_{19}$ | $S_0$ | 1.74e-14 | 8.51e-15 | 1.39e-12 |
| $S_{19}$ | $S_1$ | -8.6e-07 | -1.6e-06 | 6e-08 |
| $S_{19}$ | $S_2$ | -6.1e-07 | 2e-08 | 1.67e-06 |
| $S_{19}$ | $S_3$ | 0.00013443 | -2.56e-05 | -0.06980402 |
| $S_{19}$ | $S_4$ | 0.24657757 | 0.0350243 | -3.19e-05 |
| $S_{19}$ | $S_5$ | 4.62e-06 | -7.7e-07 | 0.08130132 |
| $S_{19}$ | $S_6$ | -0.18811072 | -0.05488063 | -7.72e-06 |
| $S_{19}$ | $S_7$ | -3.5e-07 | -1.3e-07 | -2.2e-07 |
| $S_{19}$ | $S_8$ | 3.96e-06 | 2.1e-07 | 2.11e-06 |
| $S_{19}$ | $S_9$ | 7.58e-06 | -2.92e-06 | -2e-08 |
| $S_{19}$ | $S_{10}$ | 1.6e-06 | -3.5e-07 | -0.02490173 |
| $S_{19}$ | $S_{11}$ | -1.22e-05 | 1.96e-06 | 0.0 |
| $S_{19}$ | $S_{12}$ | 7.2e-07 | 6e-08 | -3.5e-07 |
| $S_{19}$ | $S_{13}$ | 8.61e-06 | -1.3e-07 | -3e-08 |
| $S_{19}$ | $S_{14}$ | -1.46e-06 | -3e-08 | 6e-08 |
| $S_{19}$ | $S_{15}$ | 1.02e-05 | -1.55e-06 | 2e-08 |
| $S_{19}$ | $S_{16}$ | 2.96e-06 | -3.2e-07 | 0.0 |
| $S_{19}$ | $S_{17}$ | 4.8e-07 | -2e-08 | 0.0 |
| $S_{19}$ | $S_{18}$ | 1e-08 | 0.0 | 0.0 |
| $S_{19}$ | $S_{19}$ | 2.2e-05 | -2.66e-06 | -3.05111504 |
| $S_{19}$ | $S_{20}$ | -2.14e-05 | 9.3e-07 | 0.0 |
| $S_{20}$ | $S_0$ | -9.94e-10 | 3.41e-10 | 0.2229964 |
| $S_{20}$ | $S_1$ | 1.34e-05 | -3.79e-06 | 0.12394873 |
| $S_{20}$ | $S_2$ | -0.02936287 | 0.00241162 | 2.95e-06 |
| $S_{20}$ | $S_3$ | -6e-07 | -2.09e-06 | -3e-07 |
| $S_{20}$ | $S_4$ | -2.35e-06 | 7e-08 | -7.9e-07 |
| $S_{20}$ | $S_5$ | -6.44e-06 | 2.3e-07 | 1.7e-07 |
| $S_{20}$ | $S_6$ | 7.97e-06 | -1.7e-07 | -2.4e-07 |
| $S_{20}$ | $S_7$ | -0.38698502 | 0.00076337 | 4.72e-05 |
| $S_{20}$ | $S_8$ | 0.18840992 | 0.01990897 | 4.4e-07 |
| $S_{20}$ | $S_9$ | 7.47e-05 | 4.75e-06 | 1.14806488 |
| $S_{20}$ | $S_{10}$ | -1.01e-06 | -8e-07 | -5e-08 |
| $S_{20}$ | $S_{11}$ | -2.9e-07 | -5.49e-06 | -0.60895491 |

| $S_{\text{init}}$ | $S_{\text{final}}$ | $\mu_x$ | $\mu_y$ | $\mu_z$ |
|---|---|---|---|---|
| $S_{20}$ | $S_{12}$ | -0.6607976 | 0.01326818 | 1.09e-05 |
| $S_{20}$ | $S_{13}$ | 1.61e-05 | 1.78e-06 | 0.26275133 |
| $S_{20}$ | $S_{14}$ | -0.24713147 | -0.0385675 | 1.96e-06 |
| $S_{20}$ | $S_{15}$ | -0.00016372 | 4.99e-06 | -0.02092554 |
| $S_{20}$ | $S_{16}$ | -5.74e-06 | -1.05e-05 | -0.00591966 |
| $S_{20}$ | $S_{17}$ | -9.49e-06 | 1.43e-05 | -0.07000691 |
| $S_{20}$ | $S_{18}$ | 0.06754775 | 0.00911442 | -1.15e-06 |
| $S_{20}$ | $S_{19}$ | -2.14e-05 | 9.3e-07 | 0.0 |
| $S_{20}$ | $S_{20}$ | 0.00065806 | -4.47e-05 | -1.2216931 |

# Bibliography


[1] Margherita Maiuri, Marco Garavelli, and Giulio Cerullo. “Ultrafast Spectroscopy: State of the Art and Open Challenges”. In: *Journal of the American Chemical Society* 142.1 (Jan. 2020). Publisher: American Chemical Society, pp. 3–15. ISSN: 0002-7863. DOI: 10.1021/jacs.9b10533. URL: https://doi.org/10.1021/jacs.9b10533 (visited on 07/08/2023).

[2] Dóra Vörös and Sebastian Mai. “Role of Ultrafast Internal Conversion and Intersystem Crossing in the Nonadiabatic Relaxation Dynamics of ortho-Nitrobenzaldehyde”. In: *The Journal of Physical Chemistry A* (July 2023). Publisher: American Chemical Society. ISSN: 1089-5639. DOI: 10.1021/acs.jpca.3c02899. URL: https://doi.org/10.1021/acs.jpca.3c02899 (visited on 07/11/2023).

[3] Michael S. Schuurman and Albert Stolow. “Dynamics at Conical Intersections”. en. In: *Annual Review of Physical Chemistry* 69.1 (Apr. 2018), pp. 427–450. ISSN: 0066-426X, 1545-1593. DOI: 10.1146/annurev-physchem-052516-050721. URL: https://www.annualreviews.org/doi/10.1146/annurev-physchem-052516-050721 (visited on 07/10/2023).

[4] Markus Kowalewski et al. “Simulating Coherent Multidimensional Spectroscopy of Nonadiabatic Molecular Processes: From the Infrared to the X-ray Regime”. In: *Chemical Reviews* 117.19 (Oct. 2017). Publisher: American Chemical Society, pp. 12165–12226. ISSN: 0009-2665. DOI: 10.1021/acs.chemrev.7b00081. URL: https://doi.org/10.1021/acs.chemrev.7b00081 (visited on 07/12/2023).

[5] Susanne Ullrich et al. “Electronic relaxation dynamics in DNA and RNA bases studied by time-resolved photoelectron spectroscopy”. en. In: *Physical Chemistry Chemical Physics* 6.10 (2004). Publisher: Royal Society of Chemistry, pp. 2796–2801. DOI: 10.1039/B316324E. URL: https://pubs.rsc.org/en/content/articlelanding/2004/cp/b316324e (visited on 07/10/2023).

[6] Clélia Canuel et al. “Excited states dynamics of DNA and RNA bases: Characterization of a stepwise deactivation pathway in the gas phase”. In: *The Journal of Chemical Physics* 122.7 (Feb. 2005), p. 074316. ISSN: 0021-9606. DOI: 10.1063/1.1850469. URL: https://doi.org/10.1063/1.1850469 (visited on 07/10/2023).

[7] Mario Barbatti et al. “Relaxation mechanisms of UV-photoexcited DNA and RNA nucleobases”. In: *Proceedings of the National Academy of Sciences* 107.50 (Dec. 2010). Publisher: Proceedings of the National Academy of Sciences, pp. 21453–21458. DOI: 10.1073/pnas.1014982107. URL: https://www.pnas.org/doi/full/10.1073/pnas.1014982107 (visited on 07/10/2023).

[8] Weijie Hua, Shaul Mukamel, and Yi Luo. “Transient X-ray Absorption Spectral Fingerprints of the S1 Dark State in Uracil”. In: *The Journal of Physical Chemistry Letters* 10.22 (Nov. 2019). Publisher: American Chemical Society, pp. 7172–7178. DOI: 10.1021/acs.jpclett.9b02692. URL: https://doi.org/10.1021/acs.jpclett.9b02692 (visited on 07/10/2023).

[9] Benjamin P. Fingerhut, Konstantin E. Dorfman, and Shaul Mukamel. “Probing the Conical Intersection Dynamics of the RNA Base Uracil by UV-Pump Stimulated-Raman-Probe Signals; Ab Initio Simulations”. In: *Journal of Chemical Theory and Computation* 10.3 (Mar. 2014). Publisher: American Chemical Society, pp. 1172–1188. ISSN: 1549-9618. DOI: 10.1021/ct401012u. URL: https://doi.org/10.1021/ct401012u (visited on 07/10/2023).

[10] Ryan N. Coffee et al. “Development of ultrafast capabilities for X-ray free-electron lasers at the linac coherent light source”. In: *Philosophical Transactions of the Royal Society A: Mathematical, Physical and Engineering Sciences* 377.2145 (Apr. 2019). Publisher: Royal Society, p. 20180386. DOI: 10.1098/rsta.2018.0386. URL: https://royalsocietypublishing.org/doi/10.1098/rsta.2018.0386 (visited on 07/16/2023).

[11] Graham A. Worth and Lorenz S. Cederbaum. “BEYOND BORN-OPPENHEIMER: Molecular Dynamics Through a Conical Intersection”. en. In: *Annual Review of Physical Chemistry* 55.1 (June 2004), pp. 127–158. ISSN: 0066-426X, 1545-1593. DOI: 10.1146/annurev.physchem.55.091602.094335. URL: https://www.annualreviews.org/doi/10.1146/annurev.physchem.55.091602.094335 (visited on 07/04/2023).

[12] Satoshi Takahashi and Kazuo Takatsuka. “On the validity range of the Born-Oppenheimer approximation: A semiclassical study for all-particle quantization of three-body Coulomb systems”. In: *The Journal of Chemical Physics* 124.14 (Apr. 2006), p. 144101. ISSN: 0021-9606. DOI: 10.1063/1.2173997. URL: https://aip-scitation-org.libproxy.berkeley.edu/doi/10.1063/1.2173997 (visited on 03/20/2023).

[13] Basile F. E. Curchod and Todd J. Martínez. “Ab Initio Nonadiabatic Quantum Molecular Dynamics”. In: *Chemical Reviews* 118.7 (Apr. 2018). Publisher: American Chemical Society, pp. 3305–3336. ISSN: 0009-2665. DOI: 10.1021/acs.chemrev.7b00423. URL: https://doi.org/10.1021/acs.chemrev.7b00423 (visited on 07/18/2023).

[14] Dmitrii V. Shalashilin. "Multiconfigurational Ehrenfest approach to quantum coherent dynamics in large molecular systems". en. In: *Faraday Discussions* 153.0 (Oct. 2011). Publisher: The Royal Society of Chemistry, pp. 105–116. ISSN: 1364-5498. DOI: 10.1039/C1FD00034A. URL: https://pubs.rsc.org/en/content/articlelanding/2011/fd/c1fd00034a (visited on 07/18/2023).

[15] Andrew M. Weiner. *Ultrafast Optics*. English. John Wiley & Sons Inc., 2009. ISBN: 978-0-471-41539-8.

[16] Romain Geneaux et al. "Transient absorption spectroscopy using high harmonic generation: a review of ultrafast X-ray dynamics in molecules and solids". In: *Philosophical Transactions of the Royal Society A: Mathematical, Physical and Engineering Sciences* 377.2145 (Apr. 2019). Publisher: Royal Society, p. 20170463. DOI: 10.1098/rsta.2017.0463. URL: https://royalsocietypublishing.org/doi/10.1098/rsta.2017.0463 (visited on 08/22/2023).

[17] Somnath Biswas et al. "Coherent Two-Dimensional and Broadband Electronic Spectroscopies". In: *Chemical Reviews* 122.3 (Feb. 2022). Publisher: American Chemical Society, pp. 4257–4321. ISSN: 0009-2665. DOI: 10.1021/acs.chemrev.1c00623. URL: https://doi.org/10.1021/acs.chemrev.1c00623 (visited on 08/29/2023).

[18] Thomas Ding et al. "Time-resolved four-wave-mixing spectroscopy for inner-valence transitions". en. In: *Optics Letters* 41.4 (Feb. 2016), p. 709. ISSN: 0146-9592, 1539-4794. DOI: 10.1364/OL.41.000709. URL: https://www.osapublishing.org/abstract.cfm?URI=ol-41-4-709 (visited on 10/24/2019).

[19] Pavel V. Kolesnichenko, Jonathan O. Tollerud, and Jeffrey A. Davis. "Background-free time-resolved coherent Raman spectroscopy (CSRS and CARS): Heterodyne detection of low-energy vibrations and identification of excited-state contributions". In: *APL Photonics* 4.5 (May 2019), p. 056102. ISSN: 2378-0967. DOI: 10.1063/1.5090585. URL: https://doi.org/10.1063/1.5090585 (visited on 08/29/2023).

[20] Peter Ljungberg and Ove Axner. "Degenerate four-wave mixing from laser-populated excited states". EN. In: *Applied Optics* 34.3 (Jan. 1995), pp. 527–536. ISSN: 2155-3165. DOI: 10.1364/AO.34.000527. URL: http://www.osapublishing.org/ao/abstract.cfm?uri=ao-34-3-527 (visited on 12/04/2019).

[21] F. Bencivenga et al. "Four-wave mixing experiments with extreme ultraviolet transient gratings". en. In: *Nature* 520.7546 (Apr. 2015), pp. 205–208. ISSN: 0028-0836, 1476-4687. DOI: 10.1038/nature14341. URL: http://www.nature.com/articles/nature14341 (visited on 10/24/2019).

[22] Jaeyoung Sung and Robert J. Silbey. “Four wave mixing spectroscopy for a multilevel system”. In: *The Journal of Chemical Physics* 115.20 (Nov. 2001), pp. 9266–9287. ISSN: 0021-9606. DOI: 10.1063/1.1413979. URL: https://doi.org/10.1063/1.1413979 (visited on 08/22/2023).

[23] Gregory D. Scholes et al. “Using coherence to enhance function in chemical and biophysical systems”. en. In: *Nature* 543.7647 (Mar. 2017). Number: 7647 Publisher: Nature Publishing Group, pp. 647–656. ISSN: 1476-4687. DOI: 10.1038/nature21425. URL: https://www.nature.com/articles/nature21425 (visited on 08/29/2023).

[24] Erika R. Warrick et al. “Multiple pulse coherent dynamics and wave packet control of the N2 a 1+g dark state by attosecond four-wave mixing”. en. In: *Faraday Discussions* 212.0 (Dec. 2018). Publisher: The Royal Society of Chemistry, pp. 157–174. ISSN: 1364-5498. DOI: 10.1039/C8FD00074C. URL: https://pubs.rsc.org/en/content/articlelanding/2018/fd/c8fd00074c (visited on 08/29/2023).

[25] Daniel M Neumark. “Time-Resolved Photoelectron Spectroscopy Of Molecules And Clusters”. en. In: *Annual Review of Physical Chemistry* 52.1 (Oct. 2001), pp. 255–277. ISSN: 0066-426X, 1545-1593. DOI: 10.1146/annurev.physchem.52.1.255. URL: https://www.annualreviews.org/doi/10.1146/annurev.physchem.52.1.255 (visited on 08/22/2023).

[26] Albert Stolow, Arthur E. Bragg, and Daniel M. Neumark. “Femtosecond Time-Resolved Photoelectron Spectroscopy”. In: *Chemical Reviews* 104.4 (Apr. 2004). Publisher: American Chemical Society, pp. 1719–1758. ISSN: 0009-2665. DOI: 10.1021/cr020683w. URL: https://doi.org/10.1021/cr020683w (visited on 08/22/2023).

[27] James D. Gaynor, Robert B. Weakly, and Munira Khalil. “Multimode two-dimensional vibronic spectroscopy. I. Orientational response and polarization-selectivity”. In: *The Journal of Chemical Physics* 154.18 (May 2021). Publisher: American Institute of Physics, p. 184201. ISSN: 0021-9606. DOI: 10.1063/5.0047724. URL: https://aip.scitation.org/doi/10.1063/5.0047724 (visited on 07/21/2021).

[28] Robert B. Weakly, James D. Gaynor, and Munira Khalil. “Multimode two-dimensional vibronic spectroscopy. II. Simulating and extracting vibronic coupling parameters from polarization-selective spectra”. In: *The Journal of Chemical Physics* 154.18 (May 2021). Publisher: American Institute of Physics, p. 184202. ISSN: 0021-9606. DOI: 10.1063/5.0047727. URL: https://aip.scitation.org/doi/10.1063/5.0047727 (visited on 07/21/2021).

[29] A. Tokmakoff. “Orientational correlation functions and polarization selectivity for nonlinear spectroscopy of isotropic media. I. Third order”. In: *The Journal of Chemical Physics* 105.1 (July 1996), pp. 1–12. ISSN: 0021-9606. DOI: 10.1063/1.471856. URL: https://doi.org/10.1063/1.471856 (visited on 08/26/2023).

[30] Elizabeth L. Read et al. “Cross-peak-specific two-dimensional electronic spectroscopy”. In: *Proceedings of the National Academy of Sciences* 104.36 (Sept. 2007). Publisher: Proceedings of the National Academy of Sciences, pp. 14203–14208. DOI: 10.1073/pnas.0701201104. URL: https://www.pnas.org/doi/full/10.1073/pnas.0701201104 (visited on 08/29/2023).

[31] S. Woutersen and P. Hamm. “Structure Determination of Trialanine in Water Using Polarization Sensitive Two-Dimensional Vibrational Spectroscopy”. In: *The Journal of Physical Chemistry B* 104.47 (Nov. 2000). Publisher: American Chemical Society, pp. 11316–11320. ISSN: 1520-6106. DOI: 10.1021/jp001546a. URL: https://doi.org/10.1021/jp001546a (visited on 08/29/2023).

[32] Patrick L. Kramer et al. “Observation and theory of reorientation-induced spectral diffusion in polarization-selective 2D IR spectroscopy”. In: *The Journal of Chemical Physics* 142.18 (May 2015), p. 184505. ISSN: 0021-9606. DOI: 10.1063/1.4920949. URL: https://doi.org/10.1063/1.4920949 (visited on 08/29/2023).

[33] David M. Jonas. “Vibrational and Nonadiabatic Coherence in 2D Electronic Spectroscopy, the Jahn–Teller Effect, and Energy Transfer”. In: *Annual Review of Physical Chemistry* 69.1 (2018). _eprint: https://doi.org/10.1146/annurev-physchem-052516-050602, pp. 327–352. DOI: 10.1146/annurev-physchem-052516-050602. URL: https://doi.org/10.1146/annurev-physchem-052516-050602 (visited on 08/29/2023).

[34] Richard Thurston et al. “Ultrafast Dynamics of Excited Electronic States in Nitrobenzene Measured by Ultrafast Transient Polarization Spectroscopy”. In: *The Journal of Physical Chemistry A* 124.13 (Apr. 2020). Publisher: American Chemical Society, pp. 2573–2579. ISSN: 1089-5639. DOI: 10.1021/acs.jpca.0c01943. URL: https://doi.org/10.1021/acs.jpca.0c01943 (visited on 09/01/2023).

[35] Maxim F. Gelin, Lipeng Chen, and Wolfgang Domcke. “Equation-of-Motion Methods for the Calculation of Femtosecond Time-Resolved 4-Wave-Mixing and N-Wave-Mixing Signals”. In: *Chemical Reviews* 122.24 (Dec. 2022). Publisher: American Chemical Society, pp. 17339–17396. ISSN: 0009-2665. DOI: 10.1021/acs.chemrev.2c00329. URL: https://doi.org/10.1021/acs.chemrev.2c00329 (visited on 05/25/2023).

[36] Robert W. Boyd. *Non-Linear Optics*. 3rd. Academic Press, 2008. ISBN: 978-0-12-369470-6.

[37] Shaul Mukamel. *Principles of Nonlinear Optical Spectroscopy*. Oxford University Press, Inc, 1995. ISBN: 978-0-19-513291-5.

[38] Peter Hamm and Martin Zanni. *Concepts and Methods of 2D Infrared Spectroscopy*. Cambridge: Cambridge University Press, 2011. ISBN: 978-1-107-00005-6. DOI: 10.1017/CBO9780511675935. URL: https://www.cambridge.org/core/books/concepts-and-methods-of-2d-infrared-spectroscopy/8D35AA43C878AF1812CDCAF8890C9FE6 (visited on 09/25/2023).

[39] Timothy Russell Dickson. "Time-Resolved Optical Kerr Effect Spectroscopy by Four-Wave Mixing". en_ca. Thesis. University of Toronto, 1991. URL: http://hdl.handle.net/1807/81339 (visited on 10/22/2019).

[40] D. McMorrow, W.T. Lotshaw, and G.A. Kenney-Wallace. "Femtosecond optical Kerr studies on the origin of the nonlinear responses in simple liquids". en. In: *IEEE Journal of Quantum Electronics* 24.2 (Feb. 1988), pp. 443–454. ISSN: 00189197. DOI: 10.1109/3.144. URL: http://ieeexplore.ieee.org/document/144/ (visited on 10/22/2019).

[41] Q. L. Zhou et al. "Enhanced nonresonant nonlinear optical processes from populated electronic excited states". en. In: *Physical Review A* 43.3 (Feb. 1991), pp. 1673–1676. ISSN: 1050-2947, 1094-1622. DOI: 10.1103/PhysRevA.43.1673. URL: https://link.aps.org/doi/10.1103/PhysRevA.43.1673 (visited on 10/22/2019).

[42] W.-D. Cheng et al. "Enhancements of third-order nonlinear optical response in excited state of the fullerenes C 60 and C 70". en. In: *Physical Review B* 66.11 (Sept. 2002), p. 113401. ISSN: 0163-1829, 1095-3795. DOI: 10.1103/PhysRevB.66.113401. URL: https://link.aps.org/doi/10.1103/PhysRevB.66.113401 (visited on 10/22/2019).

[43] Tiago Buckup and Jérémie Léonard. "Multidimensional Vibrational Coherence Spectroscopy". en. In: *Multidimensional Time-Resolved Spectroscopy*. Ed. by Tiago Buckup and Jérémie Léonard. Topics in Current Chemistry Collections. Cham: Springer International Publishing, 2019, pp. 207–245. ISBN: 978-3-030-02478-9. DOI: 10.1007/978-3-030-02478-9_5. URL: https://doi.org/10.1007/978-3-030-02478-9_5 (visited on 05/19/2021).

[44] Jürgen Hauer, Tiago Buckup, and Marcus Motzkus. "Pump-Degenerate Four Wave Mixing as a Technique for Analyzing Structural and Electronic Evolution: Multidimensional Time-Resolved Dynamics near a Conical Intersection". In: *The Journal of Physical Chemistry A* 111.42 (Oct. 2007). Publisher: American Chemical Society, pp. 10517–10529. ISSN: 1089-5639. DOI: 10.1021/jp073727j. URL: https://doi.org/10.1021/jp073727j (visited on 08/22/2023).

[45] Jan Philip Kraack, Marcus Motzkus, and Tiago Buckup. "Excited State Vibrational Spectra of All-trans Retinal Derivatives in Solution Revealed By Pump-DFWM Experiments". In: *The Journal of Physical Chemistry B* 122.51 (Dec. 2018). Publisher: American Chemical Society, pp. 12271–12281. ISSN: 1520-6106. DOI:

10.1021/acs.jpcb.8b08495. URL: https://doi.org/10.1021/acs.jpcb.8b08495 (visited on 06/07/2023).

[46] Marie S. Marek et al. "Highlighting short-lived excited electronic states with pump-degenerate-four-wave-mixing". In: *The Journal of Chemical Physics* 139.7 (Aug. 2013), p. 074202. ISSN: 0021-9606. DOI: 10.1063/1.4818164. URL: https://doi.org/10.1063/1.4818164 (visited on 09/26/2023).

[47] Chong Hoon Kwak and Gun Yeup Kim. "Rigorous theory of molecular orientational nonlinear optics". en. In: *AIP Advances* 5.1 (Jan. 2015), p. 017124. ISSN: 2158-3226. DOI: 10.1063/1.4906521. URL: http://aip.scitation.org/doi/10.1063/1.4906521 (visited on 10/22/2019).

[48] D. C. Rodenberger, J. R. Heflin, and A. F. Garrto. "Excited-state enhancement of optical nonlinearities in linear conjugated molecules". en. In: *Nature* 359.6393 (Sept. 1992), pp. 309–311. ISSN: 1476-4687. DOI: 10.1038/359309a0. URL: https://www-nature-com.libproxy.berkeley.edu/articles/359309a0 (visited on 10/22/2019).

[49] D. C. Rodenberger, J. R. Heflin, and A. F. Garito. "Excited-state enhancement of third-order nonlinear optical responses in conjugated organic chains". In: *Physical Review A* 51.4 (Apr. 1995), pp. 3234–3245. DOI: 10.1103/PhysRevA.51.3234. URL: https://link.aps.org/doi/10.1103/PhysRevA.51.3234 (visited on 12/04/2019).

[50] Kazuo Kasatani. "Subpicosecond degenerate four-wave mixing and optical Kerr effect of organic dyes in excited states". en. In: *Journal of Luminescence* 87-89 (May 2000), pp. 889–891. ISSN: 0022-2313. DOI: 10.1016/S0022-2313(99)00459-7. URL: https://www.sciencedirect.com/science/article/pii/S0022231399004597 (visited on 10/17/2022).

[51] Jan Philip Kraack et al. "Mapping multidimensional excited state dynamics using pump-impulsive-vibrational-spectroscopy and pump-degenerate-four-wave-mixing". en. In: *Physical Chemistry Chemical Physics* 15.34 (Aug. 2013). Publisher: The Royal Society of Chemistry, pp. 14487–14501. ISSN: 1463-9084. DOI: 10.1039/C3CP50871D. URL: https://pubs.rsc.org/en/content/articlelanding/2013/cp/c3cp50871d (visited on 06/13/2023).

[52] Stephen Palese et al. "Femtosecond optical Kerr effect studies of water". en. In: (), p. 9.

[53] Xiang Zhu et al. "Mode-Selective Optical Kerr Effect Spectroscopy". In: *The Journal of Physical Chemistry B* 108.11 (Mar. 2004). Publisher: American Chemical Society, pp. 3384–3386. ISSN: 1520-6106. DOI: 10.1021/jp037286p. URL: https://doi.org/10.1021/jp037286p (visited on 03/10/2020).

[54] Xiang Zhu, Richard A. Farrer, and John T. Fourkas. "Optical Kerr Effect Spectroscopy Using Time-Delayed Pairs of Pump Pulses with Orthogonal Polarizations". In: *The Journal of Physical Chemistry B* 109.17 (May 2005). Publisher: American Chemical Society, pp. 8481–8488. ISSN: 1520-6106. DOI: 10.1021/jp046761w. URL: https://doi.org/10.1021/jp046761w (visited on 10/17/2022).

[55] Alexander S. Shorokhov et al. "Ultrafast control of third-order optical nonlinearities in fishnet metamaterials". en. In: *Scientific Reports* 6.1 (Sept. 2016), p. 28440. ISSN: 2045-2322. DOI: 10.1038/srep28440. URL: http://www.nature.com/articles/srep28440 (visited on 10/22/2019).

[56] A. B Fedotov et al. "Third-harmonic generation in a laser-pre-excited gas: the role of excited-state neutrals". en. In: *Physics Letters A* 271.5 (July 2000), pp. 407–412. ISSN: 0375-9601. DOI: 10.1016/S0375-9601(00)00390-X. URL: http://www.sciencedirect.com/science/article/pii/S037596010000390X (visited on 12/04/2019).

[57] Dale McMorrow and William T. Lotshaw. "Intermolecular dynamics in acetonitrile probed with femtosecond Fourier-transform Raman spectroscopy". en. In: *The Journal of Physical Chemistry* 95.25 (Dec. 1991), pp. 10395–10406. ISSN: 0022-3654, 1541-5740. DOI: 10.1021/j100178a029. URL: https://pubs.acs.org/doi/abs/10.1021/j100178a029 (visited on 10/22/2019).

[58] Dale McMorrow and William T. Lotshaw. "The frequency response of condensed-phase media to femtosecond optical pulses: spectral-filter effects". en. In: *Chemical Physics Letters* 174.1 (Nov. 1990), pp. 85–94. ISSN: 00092614. DOI: 10.1016/0009-2614(90)85331-6. URL: https://linkinghub.elsevier.com/retrieve/pii/0009261490853316 (visited on 10/22/2019).

[59] Soh Kushida et al. "Ultrafast Dynamics of Solute Molecules Probed by Resonant Optical Kerr Effect Spectroscopy". In: *The Journal of Physical Chemistry Letters* 13.40 (Oct. 2022). Publisher: American Chemical Society, pp. 9309–9315. DOI: 10.1021/acs.jpclett.2c02461. URL: https://doi.org/10.1021/acs.jpclett.2c02461 (visited on 10/17/2022).

[60] Bijay Kumar Agarwalla, Konstantin E. Dorfman, and Shaul Mukamel. "Evaluation of optical probe signals from nonequilibrium systems". In: *Physical Review A* 91.5 (May 2015). Publisher: American Physical Society, p. 052501. DOI: 10.1103/PhysRevA.91.052501. URL: https://link.aps.org/doi/10.1103/PhysRevA.91.052501 (visited on 10/17/2022).

[61] Richard Thurston et al. "Time-resolved ultrafast transient polarization spectroscopy to investigate nonlinear processes and dynamics in electronically excited molecules on the femtosecond time scale". In: *Review of Scientific Instruments* 91.5 (May 2020). Publisher:

American Institute of Physics, p. 053101. ISSN: 0034-6748. DOI: 10.1063/1.5144482. URL: https://aip-scitation-org.libproxy.berkeley.edu/doi/full/10.1063/1.5144482 (visited on 05/10/2021).

[62] D. A. Van Baak and George Herold. "Response of a lock-in amplifier to noise". In: *American Journal of Physics* 82.8 (Aug. 2014). Publisher: American Association of Physics Teachers, pp. 785–797. ISSN: 0002-9505. DOI: 10.1119/1.4873915. URL: https://aapt.scitation.org/doi/full/10.1119/1.4873915 (visited on 02/08/2023).

[63] T. C. O'Haver. "Lock-in amplifiers - Part I". In: *Journal of Chemical Education* 49.3 (Mar. 1972). Publisher: American Chemical Society, A131. ISSN: 0021-9584. DOI: 10.1021/ed049pA131. URL: https://doi.org/10.1021/ed049pA131 (visited on 02/08/2023).

[64] Neil A. Smith and Stephen R. Meech. "Ultrafast Dynamics of Polar Monosubstituted Benzene Liquids Studied by the Femtosecond Optical Kerr Effect". en. In: *The Journal of Physical Chemistry A* 104.18 (May 2000), pp. 4223–4235. ISSN: 1089-5639, 1520-5215. DOI: 10.1021/jp993170a. URL: https://pubs.acs.org/doi/10.1021/jp993170a (visited on 10/22/2019).

[65] William T. Lotshaw et al. "Femtosecond dynamics of the optical kerr effect in liquid nitrobenzene and chlorobenzene". en. In: *Chemical Physics Letters* 136.3 (May 1987), pp. 323–328. ISSN: 0009-2614. DOI: 10.1016/0009-2614(87)80260-9. URL: https://www.sciencedirect.com/science/article/pii/0009261487802609 (visited on 02/05/2023).

[66] V. G. Nikiforov et al. "Analyzing the Signal of the Ultrafast Optical Kerr Effect by Considering the Correlation between the Rotational Responses of Molecules in a Liquid". en. In: *Bulletin of the Russian Academy of Sciences: Physics* 83.3 (Mar. 2019), pp. 370–373. ISSN: 1934-9432. DOI: 10.3103/S1062873819030353. URL: https://doi.org/10.3103/S1062873819030353 (visited on 02/08/2023).

[67] Eugene Hecht. *Optics*. 5th ed. Pearson Education, Incorporated, 2017. ISBN: 978-0-13-397722-6.

[68] Manickam Neelakandan, Debi Pant, and Edward L. Quitevis. "Structure and Intermolecular Dynamics of Liquids: Femtosecond Optical Kerr Effect Measurements in Nonpolar Fluorinated Benzenes". en. In: *The Journal of Physical Chemistry A* 101.16 (Apr. 1997), pp. 2936–2945. ISSN: 1089-5639, 1520-5215. DOI: 10.1021/jp964047b. URL: https://pubs.acs.org/doi/10.1021/jp964047b (visited on 10/22/2019).

[69] C Kalpouzos et al. "Femtosecond Laser- Induced Kerr Responses in Liquid CS," en. In: (), p. 3.

[70] William T. Lotshaw et al. “Intermolecular vibrational coherence in molecular liquids”. en. In: *Journal of Raman Spectroscopy* 26.7 (July 1995), pp. 571–583. ISSN: 03770486. DOI: 10.1002/jrs.1250260712. URL: http://doi.wiley.com/10.1002/jrs.1250260712 (visited on 10/22/2019).

[71] Angelo Giussani and Graham A. Worth. “Insights into the Complex Photophysics and Photochemistry of the Simplest Nitroaromatic Compound: A CASPT2//CASSCF Study on Nitrobenzene”. In: *Journal of Chemical Theory and Computation* 13.6 (June 2017), pp. 2777–2788. ISSN: 1549-9618. DOI: 10.1021/acs.jctc.6b01149. URL: https://doi.org/10.1021/acs.jctc.6b01149 (visited on 12/13/2019).

[72] Sunanda Krishnakumar et al. “Experimental and computational studies on the electronic excited states of nitrobenzene”. en. In: *Journal of Quantitative Spectroscopy and Radiative Transfer* 184 (Nov. 2016), pp. 89–99. ISSN: 00224073. DOI: 10.1016/j.jqsrt.2016.06.005. URL: https://linkinghub.elsevier.com/retrieve/pii/S0022407316301947 (visited on 10/22/2019).

[73] Juan Soto and Manuel Algarra. “Electronic Structure of Nitrobenzene: A Benchmark Example of the Accuracy of the Multi-State CASPT2 Theory”. In: *The Journal of Physical Chemistry A* 125.43 (Nov. 2021). Publisher: American Chemical Society, pp. 9431–9437. ISSN: 1089-5639. DOI: 10.1021/acs.jpca.1c04595. URL: https://doi.org/10.1021/acs.jpca.1c04595 (visited on 06/14/2023).

[74] Bernard Vidal and John N. Murrell. “The effect of solvent on the position of the first absorption band of nitrobenzene”. en. In: *Chemical Physics Letters* 31.1 (Feb. 1975), pp. 46–47. ISSN: 0009-2614. DOI: 10.1016/0009-2614(75)80054-6. URL: https://www.sciencedirect.com/science/article/pii/0009261475800546 (visited on 02/22/2023).

[75] Neil A. Smith and Stephen R. Meech. “Optically-heterodyne-detected optical Kerr effect (OHD-OKE): Applications in condensed phase dynamics”. In: *International Reviews in Physical Chemistry* 21.1 (Jan. 2002). Publisher: Taylor & Francis _eprint: https://doi.org/10.1080/01442350110092701, pp. 75–100. ISSN: 0144-235X. DOI: 10.1080/01442350110092701. URL: https://doi.org/10.1080/01442350110092701 (visited on 01/10/2023).

[76] Neil T. Hunt, Andrew A. Jaye, and Stephen R. Meech. “Ultrafast dynamics in complex fluids observed through the ultrafast optically-heterodyne-detected optical-Kerr-effect (OHD-OKE)”. en. In: *Physical Chemistry Chemical Physics* 9.18 (May 2007). Publisher: The Royal Society of Chemistry, pp. 2167–2180. ISSN: 1463-9084. DOI: 10.1039/B616078F. URL: https://pubs.rsc.org/en/content/articlelanding/2007/cp/b616078f (visited on 01/23/2023).

[77] Gui-hua Zhang and Ya-min Wang. "Study of Jones Matrix of The Birefringent Crystal". In: *2009 Symposium on Photonics and Optoelectronics*. ISSN: 2156-8480. Aug. 2009, pp. 1–4. DOI: 10.1109/SOPO.2009.5230257.

[78] I. Santa et al. "Time-Resolved Optical Kerr Effect Measurements in Aqueous Ionic Solutions". In: *The Journal of Physical Chemistry* 98.31 (Aug. 1994). Publisher: American Chemical Society, pp. 7692–7701. ISSN: 0022-3654. DOI: 10.1021/j100082a047. URL: https://doi.org/10.1021/j100082a047 (visited on 11/17/2022).

[79] E. P. Ippen and C. V. Shank. "Picosecond response of a highrepetitionrate CS2 optical Kerr gate". In: *Applied Physics Letters* 26.3 (Feb. 1975). Publisher: American Institute of Physics, pp. 92–93. ISSN: 0003-6951. DOI: 10.1063/1.88092. URL: https://aip-scitation-org.libproxy.berkeley.edu/doi/abs/10.1063/1.88092 (visited on 11/15/2022).

[80] M. A. Duguay and J. W. Hansen. "An ultrafast light gate". In: *Applied Physics Letters* 15.6 (Sept. 1969). Publisher: American Institute of Physics, pp. 192–194. ISSN: 0003-6951. DOI: 10.1063/1.1652962. URL: https://aip-scitation-org.libproxy.berkeley.edu/doi/10.1063/1.1652962 (visited on 11/21/2022).

[81] E. W. Castner et al. "Femtosecond Fourier-transform spectroscopy of low-frequency intermolecular motions in weakly interacting liquids". en. In: *Journal of Luminescence* 60-61 (Apr. 1994), pp. 723–726. ISSN: 0022-2313. DOI: 10.1016/0022-2313(94)90261-5. URL: https://www.sciencedirect.com/science/article/pii/0022231394902615 (visited on 11/17/2022).

[82] R. Trebino et al. "Highly reliable measurement of ultrashort laser pulses". In: *Journal of Applied Physics* 128.17 (Nov. 2020). Publisher: American Institute of Physics, p. 171103. ISSN: 0021-8979. DOI: 10.1063/5.0022552. URL: https://aip.scitation.org/doi/10.1063/5.0022552 (visited on 01/23/2023).

[83] Yi Cai et al. "The Development of the Temporal Measurements for Ultrashort Laser Pulses". en. In: *Applied Sciences* 10.21 (Jan. 2020). Number: 21 Publisher: Multidisciplinary Digital Publishing Institute, p. 7401. ISSN: 2076-3417. DOI: 10.3390/app10217401. URL: https://www.mdpi.com/2076-3417/10/21/7401 (visited on 01/23/2023).

[84] Jiapeng Zhao et al. "Compressive ultrafast pulse measurement via time-domain single-pixel imaging". EN. In: *Optica* 8.9 (Sept. 2021). Publisher: Optica Publishing Group, pp. 1176–1185. ISSN: 2334-2536. DOI: 10.1364/OPTICA.431455. URL: https://opg.optica.org/optica/abstract.cfm?uri=optica-8-9-1176 (visited on 01/23/2023).

[85] Daniel J. Kane and Andrei B. Vakhtin. “A review of ptychographic techniques for ultrashort pulse measurement”. en. In: *Progress in Quantum Electronics*. Special issue in honor of Professor J. Gary Eden on the occasion of his 60th birthday 81 (Jan. 2022), p. 100364. ISSN: 0079-6727. DOI: 10.1016/j.pquantelec.2021.100364. URL: https://www.sciencedirect.com/science/article/pii/S0079672721000495 (visited on 01/23/2023).

[86] Francis Walz et al. “Electric field measurement of femtosecond time-resolved four-wave mixing signals in molecules”. EN. In: *Optics Express* 30.20 (Sept. 2022). Publisher: Optica Publishing Group, pp. 36065–36072. ISSN: 1094-4087. DOI: 10.1364/OE.470925. URL: https://opg.optica.org/oe/abstract.cfm?uri=oe-30-20-36065 (visited on 11/17/2022).

[87] J. A. Giordmaine. “Nonlinear Optical Properties of Liquids”. In: *Physical Review* 138.6A (June 1965). Publisher: American Physical Society, A1599–A1606. DOI: 10.1103/PhysRev.138.A1599. URL: https://link.aps.org/doi/10.1103/PhysRev.138.A1599 (visited on 04/29/2022).

[88] Steven R. Vigil and Mark G. Kuzyk. “Absolute molecular optical Kerr effect spectroscopy of dilute organic solutions and neat organic liquids”. EN. In: *JOSA B* 18.5 (May 2001). Publisher: Optical Society of America, pp. 679–691. ISSN: 1520-8540. DOI: 10.1364/JOSAB.18.000679. URL: https://www-osapublishing-org.libproxy.berkeley.edu/josab/abstract.cfm?uri=josab-18-5-679 (visited on 10/18/2021).

[89] P. P. Ho and R. R. Alfano. “Optical Kerr effect in liquids”. In: *Physical Review A* 20.5 (Nov. 1979). Publisher: American Physical Society, pp. 2170–2187. DOI: 10.1103/PhysRevA.20.2170. URL: https://link.aps.org/doi/10.1103/PhysRevA.20.2170 (visited on 10/18/2021).

[90] P. P. Ho, P. Y. Lu, and R. R. Alfano. “Oscillatory optically induced Kerr kinetics in nitrobenzene”. en. In: *Optics Communications* 30.3 (Sept. 1979), pp. 426–428. ISSN: 0030-4018. DOI: 10.1016/0030-4018(79)90386-9. URL: https://www.sciencedirect.com/science/article/pii/0030401879903869 (visited on 05/03/2023).

[91] Ming-Fu Lin et al. “Photodissociation dynamics of nitrobenzene and o-nitrotoluene”. In: *The Journal of Chemical Physics* 126.6 (Feb. 2007), p. 064310. ISSN: 0021-9606. DOI: 10.1063/1.2435351. URL: https://doi.org/10.1063/1.2435351 (visited on 06/14/2023).

[92] Douglas B. Galloway et al. “Pathways and kinetic energy disposal in the photodissociation of nitrobenzene”. In: *The Journal of Chemical Physics* 98.3 (Feb. 1993), pp. 2107–2114. ISSN: 0021-9606. DOI: 10.1063/1.464188. URL: https://doi.org/10.1063/1.464188 (visited on 06/14/2023).

[93] M. Takezaki, N. Hirota, and M. Terazima. "Relaxation of nitrobenzene from the excited singlet state". In: *The Journal of Chemical Physics* 108.11 (Mar. 1998), pp. 4685–4686. ISSN: 0021-9606. DOI: 10.1063/1.475883. URL: https://doi.org/10.1063/1.475883 (visited on 05/30/2023).

[94] R. Hurley and A. C. Testa. "Triplet-state yield of aromatic nitro compounds". In: *Journal of the American Chemical Society* 90.8 (Apr. 1968). Publisher: American Chemical Society, pp. 1949–1952. ISSN: 0002-7863. DOI: 10.1021/ja01010a004. URL: https://doi.org/10.1021/ja01010a004 (visited on 05/30/2023).

[95] Leonid S. Khaikin et al. "IR spectra of nitrobenzene and nitrobenzene-15N in the gas phase, ab initio analysis of vibrational spectra and reliable force fields of nitrobenzene and 1,3,5-trinitrobenzene. Investigation of equilibrium geometry and internal rotation in these simplest aromatic nitro compounds with one and three rotors by means of electron diffraction, spectroscopic, and quantum chemistry data". en. In: *Structural Chemistry* 26.5 (Dec. 2015), pp. 1651–1687. ISSN: 1572-9001. DOI: 10.1007/s11224-015-0613-9. URL: https://doi.org/10.1007/s11224-015-0613-9 (visited on 07/03/2023).

[96] Jan-M. Mewes et al. "On the molecular mechanism of non-radiative decay of nitrobenzene and the unforeseen challenges this simple molecule holds for electronic structure theory". en. In: *Physical Chemistry Chemical Physics* 16.24 (May 2014). Publisher: The Royal Society of Chemistry, pp. 12393–12406. ISSN: 1463-9084. DOI: 10.1039/C4CP01232A. URL: https://pubs.rsc.org/en/content/articlelanding/2014/cp/c4cp01232a (visited on 07/04/2023).

[97] Rick Trebino et al. "Measuring ultrashort laser pulses in the time-frequency domain using frequency-resolved optical gating". In: *Review of Scientific Instruments* 68.9 (Sept. 1997), pp. 3277–3295. ISSN: 0034-6748. DOI: 10.1063/1.1148286. URL: https://doi.org/10.1063/1.1148286 (visited on 07/04/2023).

[98] I. Orfanos et al. "Attosecond pulse metrology". In: *APL Photonics* 4.8 (Aug. 2019), p. 080901. ISSN: 2378-0967. DOI: 10.1063/1.5086773. URL: https://doi.org/10.1063/1.5086773 (visited on 07/04/2023).

[99] Václav Perlík, Jürgen Hauer, and František Šanda. "Finite pulse effects in single and double quantum spectroscopies". EN. In: *JOSA B* 34.2 (Feb. 2017). Publisher: Optica Publishing Group, pp. 430–439. ISSN: 1520-8540. DOI: 10.1364/JOSAB.34.000430. URL: https://opg.optica.org/josab/abstract.cfm?uri=josab-34-2-430 (visited on 02/28/2022).

[100] Christopher L. Smallwood, Travis M. Autry, and Steven T. Cundiff. "Analytical solutions to the finite-pulse Bloch model for multidimensional coherent spectroscopy". EN. In: *JOSA B* 34.2 (Feb. 2017). Publisher: Optica Publishing Group, pp. 419–429. ISSN: 1520-8540. DOI: 10.1364/JOSAB.34.000419. URL: https://opg.optica.org/josab/abstract.cfm?uri=josab-34-2-419 (visited on 02/24/2022).

[101] André Anda and Jared H. Cole. "Two-dimensional spectroscopy beyond the perturbative limit: The influence of finite pulses and detection modes". In: *The Journal of Chemical Physics* 154.11 (Mar. 2021), p. 114113. ISSN: 0021-9606. DOI: 10.1063/5.0038550. URL: https://doi.org/10.1063/5.0038550 (visited on 08/29/2023).

[102] Peter A. Rose and Jacob J. Krich. "Numerical method for nonlinear optical spectroscopies: Ultrafast ultrafast spectroscopy". In: *The Journal of Chemical Physics* 150.21 (June 2019), p. 214105. ISSN: 0021-9606. DOI: 10.1063/1.5094062. URL: https://doi.org/10.1063/1.5094062 (visited on 08/28/2023).

[103] Peter A. Rose and Jacob J. Krich. "Automatic Feynman diagram generation for nonlinear optical spectroscopies and application to fifth-order spectroscopy with pulse overlaps". In: *The Journal of Chemical Physics* 154.3 (Jan. 2021), p. 034109. ISSN: 0021-9606. DOI: 10.1063/5.0024105. URL: https://doi.org/10.1063/5.0024105 (visited on 09/05/2023).

[104] Peter A. Rose and Jacob J. Krich. "Efficient numerical method for predicting nonlinear optical spectroscopies of open systems". In: *The Journal of Chemical Physics* 154.3 (Jan. 2021), p. 034108. ISSN: 0021-9606. DOI: 10.1063/5.0024104. URL: https://doi.org/10.1063/5.0024104 (visited on 09/05/2023).

[105] Attila Szabo and Neil S. Ostlund. *Modern Quantum Chemistry - Introduction to Advanced Electronic Structure Theory*. revised 1st. New York: McGraw-Hill, Inc., 1989. ISBN: 978-0-486-69186-2.

[106] S. Bludman and P. B. Daitch. "Validity of the Born-Oppenheimer Approximation". In: *Physical Review* 95.3 (Aug. 1954), pp. 823–830. DOI: 10.1103/PhysRev.95.823. URL: https://link.aps.org/doi/10.1103/PhysRev.95.823 (visited on 03/20/2023).

[107] Michael A. Robb et al. "A Computational Strategy for Organic Photochemistry". en. In: *Reviews in Computational Chemistry*. John Wiley & Sons, Ltd, 2000, pp. 87–146. ISBN: 9780470125922. DOI: 10.1002/9780470125922.ch2. URL: https://onlinelibrary.wiley.com/doi/abs/10.1002/9780470125922.ch2 (visited on 03/20/2023).

[108] Michael W. Schmidt and Mark S. Gordon. "THE CONSTRUCTION AND INTERPRETATION OF MCSCF WAVEFUNCTIONS". en. In: *Annual Review of Physical Chemistry* 49.1 (Oct. 1998), pp. 233–266. ISSN: 0066-426X, 1545-1593. DOI: 10.1146/annurev.physchem.49.1.233. URL: https://www.annualreviews.org/doi/10.1146/annurev.physchem.49.1.233 (visited on 07/07/2023).

[109] Trygve U. Helgaker et al. "Molecular Hessians for large-scale MCSCF wave functions". In: *The Journal of Chemical Physics* 84.11 (June 1986). Publisher: American Institute of Physics, pp. 6266–6279. ISSN: 0021-9606. DOI: 10.1063/1.450771. URL: https://aip-scitation-org.libproxy.berkeley.edu/doi/10.1063/1.450771 (visited on 08/02/2021).

[110] Ilya G. Kaplan. “The Pauli Exclusion Principle and the Problems of Its Experimental Verification”. en. In: *Symmetry* 12.2 (Feb. 2020). Number: 2 Publisher: Multidisciplinary Digital Publishing Institute, p. 320. ISSN: 2073-8994. DOI: 10.3390/sym12020320. URL: https://www.mdpi.com/2073-8994/12/2/320 (visited on 07/07/2023).

[111] Hans- Jo/rgen Aa. Jensen and Poul Jo/rgensen. “A direct approach to second-order MCSCF calculations using a norm extended optimization scheme”. In: *The Journal of Chemical Physics* 80.3 (Feb. 1984), pp. 1204–1214. ISSN: 0021-9606. DOI: 10.1063/1.446797. URL: https://doi.org/10.1063/1.446797 (visited on 07/08/2023).

[112] Hans Jørgen Aa. Jensen and Hans Ågren. “A direct, restricted-step, second-order MC SCF program for large scale ab initio calculations”. en. In: *Chemical Physics* 104.2 (May 1986), pp. 229–250. ISSN: 0301-0104. DOI: 10.1016/0301-0104(86)80169-0. URL: https://www.sciencedirect.com/science/article/pii/0301010486801690 (visited on 05/18/2022).

[113] Immanuel M. Bomze. “On Standard Quadratic Optimization Problems”. en. In: *Journal of Global Optimization* 13.4 (Dec. 1998), pp. 369–387. ISSN: 1573-2916. DOI: 10.1023/A:1008369322970. URL: https://doi.org/10.1023/A:1008369322970 (visited on 07/08/2023).

[114] Kestutis Aidas et al. “The Dalton quantum chemistry program system: The Dalton program”. en. In: *Wiley Interdisciplinary Reviews: Computational Molecular Science* 4.3 (May 2014), pp. 269–284. ISSN: 17590876. DOI: 10.1002/wcms.1172. URL: http://doi.wiley.com/10.1002/wcms.1172 (visited on 03/08/2019).

[115] Jeppe Olsen and Poul Jo/rgensen. “Linear and nonlinear response functions for an exact state and for an MCSCF state”. In: *The Journal of Chemical Physics* 82.7 (Apr. 1985). Publisher: American Institute of Physics, pp. 3235–3264. ISSN: 0021-9606. DOI: 10.1063/1.448223. URL: https://aip-scitation-org.libproxy.berkeley.edu/doi/10.1063/1.448223 (visited on 04/13/2020).

[116] Thomas Bondo Pedersen. “Introduction to Response Theory”. en. In: *Handbook of Computational Chemistry*. Ed. by Jerzy Leszczynski. Dordrecht: Springer Netherlands, 2016, pp. 1–26. ISBN: 978-94-007-6169-8. DOI: 10.1007/978-94-007-6169-8_5-2. URL: https://doi.org/10.1007/978-94-007-6169-8_5-2 (visited on 08/02/2023).

[117] J. J. Sakurai. *Modern quantum mechanics*. eng. 2nd ed. Wu li xue jing dian jiao cai (ying yin ban). Boston: Addison-Wesley, 2011. ISBN: 978-0-8053-8291-4.

[118] Dan Jonsson et al. “Response theory for static and dynamic polarizabilities of excited states”. In: *The Journal of Chemical Physics* 105.2 (July 1996), pp. 581–587. ISSN: 0021-9606. DOI: 10.1063/1.471911. URL: https://aip-scitation-org.libproxy.berkeley.edu/doi/abs/10.1063/1.471911 (visited on 12/04/2019).

[119] Mark G. Kuzyk, Kenneth D. Singer, and George I. Stegeman. "Theory of Molecular Nonlinear Optics". en. In: *Advances in Optics and Photonics* 5.1 (Mar. 2013), p. 4. ISSN: 1943-8206. DOI: 10.1364/AOP.5.000004. URL: https://www.osapublishing.org/aop/abstract.cfm?uri=aop-5-1-4 (visited on 10/22/2019).

[120] Steven S. Andrews. "Using Rotational Averaging To Calculate the Bulk Response of Isotropic and Anisotropic Samples from Molecular Parameters". en. In: *Journal of Chemical Education* 81.6 (June 2004), p. 877. ISSN: 0021-9584, 1938-1328. DOI: 10.1021/ed081p877. URL: https://pubs.acs.org/doi/abs/10.1021/ed081p877 (visited on 10/22/2019).

[121] Garth J. Simpson. "Connection of Jones and Mueller Tensors in Second Harmonic Generation and Multi-Photon Fluorescence Measurements". In: *The Journal of Physical Chemistry B* 120.13 (Apr. 2016). Publisher: American Chemical Society, pp. 3281–3302. ISSN: 1520-6106. DOI: 10.1021/acs.jpcb.5b11841. URL: https://doi.org/10.1021/acs.jpcb.5b11841 (visited on 08/04/2023).

[122] X.-C. Zhang et al. "Difference-frequency generation and sum-frequency generation near the band gap of zincblende crystals". In: *Applied Physics Letters* 64.5 (Jan. 1994), pp. 622–624. ISSN: 0003-6951. DOI: 10.1063/1.111069. URL: https://doi.org/10.1063/1.111069 (visited on 08/04/2023).

[123] Garth J. Simpson, Sarah G. Westerbuhr, and Kathy L. Rowlen. "Molecular Orientation and Angular Distribution Probed by Angle-Resolved Absorbance and Second Harmonic Generation". In: *Analytical Chemistry* 72.5 (Mar. 2000). Publisher: American Chemical Society, pp. 887–898. ISSN: 0003-2700. DOI: 10.1021/ac9912956. URL: https://doi.org/10.1021/ac9912956 (visited on 08/04/2023).

[124] Yixing Chen, Kailash C. Jena, and Sylvie Roke. "From Hydrophobic to Hydrophilic: The Structure and Density of the Hexadecane Droplet/Alkanol/Water Interface". In: *The Journal of Physical Chemistry C* 119.31 (Aug. 2015). Publisher: American Chemical Society, pp. 17725–17734. ISSN: 1932-7447. DOI: 10.1021/acs.jpcc.5b04904. URL: https://doi.org/10.1021/acs.jpcc.5b04904 (visited on 08/04/2023).

[125] Nanna Holmgaard List et al. "Relation between Nonlinear Optical Properties of Push–Pull Molecules and Metric of Charge Transfer Excitations". In: *Journal of Chemical Theory and Computation* 11.9 (Sept. 2015). Publisher: American Chemical Society, pp. 4182–4188. ISSN: 1549-9618. DOI: 10.1021/acs.jctc.5b00538. URL: https://doi.org/10.1021/acs.jctc.5b00538 (visited on 11/01/2023).

[126] Pierre Beaujean and Benoît Champagne. "Coupled cluster investigation of the vibrational and electronic second and third harmonic scattering hyperpolarizabilities of the water molecule". In: *The Journal of Chemical Physics* 151.6 (Aug. 2019), p. 064303. ISSN: 0021-9606. DOI: 10.1063/1.5110375. URL: https://doi.org/10.1063/1.5110375 (visited on 10/23/2023).

[127] L. Klasinc, B. Kovac, and H. Gusten. “Photoelectron spectra of acenes. Electronic structure and substituent effects”. en. In: *Pure and Applied Chemistry* 55.2 (Jan. 1983). Publisher: De Gruyter, pp. 289–298. ISSN: 1365-3075. DOI: 10.1351/pac198855020289. URL: https://www.degruyter.com/document/doi/10.1351/pac198855020289/html (visited on 08/08/2023).

[128] Aldo Domenicano et al. “Molecular structure of nitrobenzene in the planar and orthogonal conformations”. en. In: *Structural Chemistry* 1.1 (Jan. 1990), pp. 107–122. ISSN: 1572-9001. DOI: 10.1007/BF00675790. URL: https://doi.org/10.1007/BF00675790 (visited on 04/14/2022).

[129] William E. Boyce and Richard C. DiPrima. *Elementary Differential Equations*. English. 9th ed. Hoboken, NJ: Wiley: Rosatone, Laurie, 2009. ISBN: 978-0-470-03940-3.

[130] Aijun Ye, Serguei Patchkovskii, and Jochen Autschbach. “Static and dynamic second hyperpolarizability calculated by time-dependent density functional cubic response theory with local contribution and natural bond orbital analysis”. en. In: *The Journal of Chemical Physics* 127.7 (Aug. 2007), p. 074104. ISSN: 0021-9606, 1089-7690. DOI: 10.1063/1.2749505. URL: http://aip.scitation.org/doi/10.1063/1.2749505 (visited on 03/07/2019).

[131] Diptarka Hait and Martin Head-Gordon. “How Accurate Is Density Functional Theory at Predicting Dipole Moments? An Assessment Using a New Database of 200 Benchmark Values”. en. In: *Journal of Chemical Theory and Computation* 14.4 (Apr. 2018), pp. 1969–1981. ISSN: 1549-9618, 1549-9626. DOI: 10.1021/acs.jctc.7b01252. URL: https://pubs.acs.org/doi/10.1021/acs.jctc.7b01252 (visited on 10/22/2019).

[132] Kaushik D. Nanda and Anna I. Krylov. “The orbital picture of the first dipole hyperpolarizability from many-body response theory”. In: *The Journal of Chemical Physics* 154.18 (May 2021). Publisher: American Institute of Physics, p. 184109. ISSN: 0021-9606. DOI: 10.1063/5.0049184. URL: https://aip.scitation.org/doi/10.1063/5.0049184 (visited on 03/13/2023).

[133] Julian Schwinger et al. *Classical Electrodynamics*. Westview Press, 1998. ISBN: 978-0-7382-0056-9.

[134] John David Jackson. *Classical Electrodynamics*. 3rd. John Wiley & Sons Inc., 1999. ISBN: 978-0-471-30932-1.

[135] Zaiyong Feng, Linghua Ye, and Yi Zhang. “On the Fractional Derivative of Dirac Delta Function and Its Application”. en. In: *Advances in Mathematical Physics* 2020 (Oct. 2020). Publisher: Hindawi, e1842945. ISSN: 1687-9120. DOI: 10.1155/2020/1842945. URL: https://www.hindawi.com/journals/amp/2020/1842945/ (visited on 07/05/2023).

[136] Timothy B. Boykin. "Derivatives of the Dirac delta function by explicit construction of sequences". In: *American Journal of Physics* 71.5 (May 2003), pp. 462–468. ISSN: 0002-9505. DOI: 10.1119/1.1557302. URL: https://doi.org/10.1119/1.1557302 (visited on 07/05/2023).

[137] David L. Andrews and Philip Allcock. *Optical Harmonics in Molecular Systems*. en. Weinheim, FRG: Wiley-VCH Verlag GmbH & Co. KGaA, June 2002. ISBN: 978-3-527-60274-2 978-3-527-40317-2. DOI: 10.1002/3527602747. URL: http://doi.wiley.com/10.1002/3527602747 (visited on 10/22/2019).

[138] Varun Makhija. "Laser-induced rotational dynamics as a route to molecular frame measurements". en_US. In: (2014). Accepted: 2014-11-03T15:29:40Z Publisher: Kansas State University. URL: https://krex.k-state.edu/handle/2097/18522 (visited on 08/21/2023).

[139] Liang Z. Tan. *mf-photophysics / utps · GitLab*. en. Aug. 2023. URL: https://gitlab.com/mf-photophysics/utps (visited on 08/12/2023).

[140] Peer Fischer, A. D. Buckingham, and A. C. Albrecht. "Isotropic second-order nonlinear optical susceptibilities". In: *Physical Review A* 64.5 (Oct. 2001). Publisher: American Physical Society, p. 053816. DOI: 10.1103/PhysRevA.64.053816. URL: https://link.aps.org/doi/10.1103/PhysRevA.64.053816 (visited on 08/15/2023).

[141] C. F. Roos et al. "Precision Spectroscopy with Entangled States: Measurement of Electric Quadrupole Moments". In: *AIP Conference Proceedings* 869.1 (Nov. 2006), pp. 111–118. ISSN: 0094-243X. DOI: 10.1063/1.2400640. URL: https://doi.org/10.1063/1.2400640 (visited on 08/30/2023).

[142] Naven Chetty and Vincent W. Couling. "Measurement of the electric quadrupole moment of CO". In: *The Journal of Chemical Physics* 134.16 (Apr. 2011), p. 164307. ISSN: 0021-9606. DOI: 10.1063/1.3585605. URL: https://doi.org/10.1063/1.3585605 (visited on 08/30/2023).

[143] Jun-Ho Choi and Minhaeng Cho. "Quadrupole contribution to the third-order optical activity spectroscopy". In: *The Journal of Chemical Physics* 127.2 (July 2007), p. 024507. ISSN: 0021-9606. DOI: 10.1063/1.2750342. URL: https://doi.org/10.1063/1.2750342 (visited on 08/30/2023).

[144] C. J. Ho et al. "Measuring the nuclear magnetic quadrupole moment in heavy polar molecules". In: *Frontiers in Physics* 11 (2023). ISSN: 2296-424X. URL: https://www.frontiersin.org/articles/10.3389/fphy.2023.1086980 (visited on 09/09/2023).

[145] P. Winkler et al. “How the anisotropy of surface oxide formation influences the transient activity of a surface reaction”. en. In: *Nature Communications* 12.1 (Jan. 2021). Number: 1 Publisher: Nature Publishing Group, p. 69. ISSN: 2041-1723. DOI: 10.1038/s41467-020-20377-9. URL: https://www.nature.com/articles/s41467-020-20377-9 (visited on 09/09/2023).

[146] Fabio Novelli et al. “Strong Anisotropy in Liquid Water upon Librational Excitation Using Terahertz Laser Fields”. In: *The Journal of Physical Chemistry B* 124.24 (June 2020). Publisher: American Chemical Society, pp. 4989–5001. ISSN: 1520-6106. DOI: 10.1021/acs.jpcb.0c02448. URL: https://doi.org/10.1021/acs.jpcb.0c02448 (visited on 09/09/2023).

[147] Takuma Yagasaki, Junichi Ono, and Shinji Saito. “Ultrafast energy relaxation and anisotropy decay of the librational motion in liquid water: A molecular dynamics study”. In: *The Journal of Chemical Physics* 131.16 (Oct. 2009), p. 164511. ISSN: 0021-9606. DOI: 10.1063/1.3254518. URL: https://doi.org/10.1063/1.3254518 (visited on 09/09/2023).

[148] Tomasz M. Kardaś et al. “Full 3D modelling of pulse propagation enables efficient nonlinear frequency conversion with low energy laser pulses in a single-element tripler”. en. In: *Scientific Reports* 7.1 (Feb. 2017). Number: 1 Publisher: Nature Publishing Group, p. 42889. ISSN: 2045-2322. DOI: 10.1038/srep42889. URL: https://www.nature.com/articles/srep42889 (visited on 09/09/2023).

[149] Jonathan Segal, Dan Huppert, and Boris Fainberg. “Resonance heterodyne optical Kerr effect spectroscopy of population wave packets with intense chirped pulses”. en. In: *Journal of Luminescence*. Proceedings of the 2002 International Conference on Luminescence and Optical Spectroscopy of Condensed Matter 102-103 (May 2003), pp. 669–675. ISSN: 0022-2313. DOI: 10.1016/S0022-2313(02)00621-X. URL: https://www.sciencedirect.com/science/article/pii/S002223130200621X (visited on 01/10/2023).

[150] T. J. Dunn, I. A. Walmsley, and S. Mukamel. “Experimental Determination of the Quantum-Mechanical State of a Molecular Vibrational Mode Using Fluorescence Tomography”. In: *Physical Review Letters* 74.6 (Feb. 1995). Publisher: American Physical Society, pp. 884–887. DOI: 10.1103/PhysRevLett.74.884. URL: https://link.aps.org/doi/10.1103/PhysRevLett.74.884 (visited on 06/28/2023).

[151] A. A. Ischenko. “Molecular Tomography of the Quantum State by Time-Resolved Electron Diffraction”. en. In: *Physics Research International* 2013 (Dec. 2013). Publisher: Hindawi, e236743. ISSN: 2090-2220. DOI: 10.1155/2013/236743. URL: https://www.hindawi.com/journals/physri/2013/236743/ (visited on 06/28/2023).

[152] Ming Zhang et al. “Quantum state tomography of molecules by ultrafast diffraction”. en. In: *Nature Communications* 12.1 (Sept. 2021). Number: 1 Publisher: Nature Publishing Group, p. 5441. ISSN: 2041-1723. DOI: 10.1038/s41467-021-25770-6. URL: https://www.nature.com/articles/s41467-021-25770-6 (visited on 07/07/2022).

[153] D. T. Smithey et al. “Measurement of the Wigner distribution and the density matrix of a light mode using optical homodyne tomography: Application to squeezed states and the vacuum”. In: *Physical Review Letters* 70.9 (Mar. 1993). Publisher: American Physical Society, pp. 1244–1247. DOI: 10.1103/PhysRevLett.70.1244. URL: https://link.aps.org/doi/10.1103/PhysRevLett.70.1244 (visited on 06/28/2023).

[154] Ermes Toninelli et al. “Concepts in quantum state tomography and classical implementation with intense light: a tutorial”. EN. In: *Advances in Optics and Photonics* 11.1 (Mar. 2019). Publisher: Optica Publishing Group, pp. 67–134. ISSN: 1943-8206. DOI: 10.1364/AOP.11.000067. URL: https://opg.optica.org/aop/abstract.cfm?uri=aop-11-1-67 (visited on 09/11/2023).

[155] Luna Morrigan et al. *Ultrafast Molecular Frame Quantum Tomography*. arXiv:2303.03558 [physics, physics:quant-ph]. Mar. 2023. DOI: 10.48550/arXiv.2303.03558. URL: http://arxiv.org/abs/2303.03558 (visited on 09/12/2023).

[156] Jie Li et al. “Attosecond science based on high harmonic generation from gases and solids”. en. In: *Nature Communications* 11.1 (June 2020). Number: 1 Publisher: Nature Publishing Group, p. 2748. ISSN: 2041-1723. DOI: 10.1038/s41467-020-16480-6. URL: https://www.nature.com/articles/s41467-020-16480-6 (visited on 09/14/2023).

[157] Brian W. J. McNeil and Neil R. Thompson. “X-ray free-electron lasers”. en. In: *Nature Photonics* 4.12 (Dec. 2010). Number: 12 Publisher: Nature Publishing Group, pp. 814–821. ISSN: 1749-4893. DOI: 10.1038/nphoton.2010.239. URL: https://www.nature.com/articles/nphoton.2010.239 (visited on 09/14/2023).

[158] Francesca Calegari et al. “Advances in attosecond science”. en. In: *Journal of Physics B: Atomic, Molecular and Optical Physics* 49.6 (Feb. 2016). Publisher: IOP Publishing, p. 062001. ISSN: 0953-4075. DOI: 10.1088/0953-4075/49/6/062001. URL: https://dx.doi.org/10.1088/0953-4075/49/6/062001 (visited on 09/14/2023).

[159] Stefano M. Cavaletto, Daniel Keefer, and Shaul Mukamel. “High Temporal and Spectral Resolution of Stimulated X-Ray Raman Signals with Stochastic Free-Electron-Laser Pulses”. In: *Physical Review X* 11.1 (Feb. 2021). Publisher: American Physical Society, p. 011029. DOI: 10.1103/PhysRevX.11.011029. URL: https://link.aps.org/doi/10.1103/PhysRevX.11.011029 (visited on 09/14/2023).

[160] Deependra Jadoun and Markus Kowalewski. "Tracking Conical Intersections with Nonlinear X-ray Raman Spectroscopy". In: *Ultrafast Science* 2022 (Dec. 2022). Publisher: American Association for the Advancement of Science, p. 0003. DOI: 10.34133/ultrafastscience.0003. URL: https://spj.science.org/doi/10.34133/ultrafastscience.0003 (visited on 09/14/2023).

[161] Yves Kayser et al. "Core-level nonlinear spectroscopy triggered by stochastic X-ray pulses". en. In: *Nature Communications* 10.1 (Oct. 2019). Number: 1 Publisher: Nature Publishing Group, p. 4761. ISSN: 2041-1723. DOI: 10.1038/s41467-019-12717-1. URL: https://www.nature.com/articles/s41467-019-12717-1 (visited on 09/14/2023).

[162] Artur Nenov et al. "X-ray linear and non-linear spectroscopy of the ESCA molecule". In: *The Journal of Chemical Physics* 151.11 (Sept. 2019), p. 114110. ISSN: 0021-9606. DOI: 10.1063/1.5116699. URL: https://doi.org/10.1063/1.5116699 (visited on 09/14/2023).

[163] K. S. Schulze et al. "Determination of the polarization state of x rays with the help of anomalous transmission". In: *Applied Physics Letters* 104.15 (Apr. 2014), p. 151110. ISSN: 0003-6951. DOI: 10.1063/1.4872180. URL: https://doi.org/10.1063/1.4872180 (visited on 09/15/2023).

[164] Jia-Min Yang et al. "X-ray polarization measurement of the Beamline 4B7 of Beijing synchrotron radiation facility using a PET crystal". In: *Nuclear Instruments and Methods in Physics Research Section A: Accelerators, Spectrometers, Detectors and Associated Equipment* 615.1 (Mar. 2010), pp. 100–104. ISSN: 0168-9002. DOI: 10.1016/j.nima.2009.12.076. URL: https://www.sciencedirect.com/science/article/pii/S0168900209024139 (visited on 08/30/2023).

[165] Robert Schoenlein et al. "Recent advances in ultrafast X-ray sources". In: *Philosophical Transactions of the Royal Society A: Mathematical, Physical and Engineering Sciences* 377.2145 (Apr. 2019). Publisher: Royal Society, p. 20180384. DOI: 10.1098/rsta.2018.0384. URL: https://royalsocietypublishing.org/doi/10.1098/rsta.2018.0384 (visited on 09/15/2023).

[166] H. P. Freund and P. J. M. van der Slot. "Variable polarization states in free-electron lasers". en. In: *Journal of Physics Communications* 5.8 (Aug. 2021). Publisher: IOP Publishing, p. 085011. ISSN: 2399-6528. DOI: 10.1088/2399-6528/ac1c89. URL: https://dx.doi.org/10.1088/2399-6528/ac1c89 (visited on 08/30/2023).

[167] Angelica Moise, Kevin C. Prince, and Robert Richter. "Time-resolved study of excited states of N2 near its first ionization threshold". In: *The Journal of Chemical Physics* 134.11 (Mar. 2011), p. 114312. ISSN: 0021-9606. DOI: 10.1063/1.3560909. URL: https://doi.org/10.1063/1.3560909 (visited on 09/15/2023).

[168] R. F. Wuerker et al. “Lifetime measurements of the excited states of N2 AND N2+ by laser-induced fluorescence”. In: *Chemical Physics Letters* 150.6 (Sept. 1988), pp. 443–446. ISSN: 0009-2614. DOI: 10.1016/0009-2614(88)80434-2. URL: https://www.sciencedirect.com/science/article/pii/0009261488804342 (visited on 09/15/2023).

[169] F. Frank et al. “Invited Review Article: Technology for Attosecond Science”. In: *Review of Scientific Instruments* 83.7 (July 2012), p. 071101. ISSN: 0034-6748. DOI: 10.1063/1.4731658. URL: https://doi.org/10.1063/1.4731658 (visited on 08/30/2023).

[170] V. Anand et al. “All femtosecond optical pump and x-ray probe: holey-axicon for free electron lasers”. en. In: *Journal of Physics: Photonics* 3.2 (Feb. 2021). Publisher: IOP Publishing, p. 024002. ISSN: 2515-7647. DOI: 10.1088/2515-7647/abd4ef. URL: https://dx.doi.org/10.1088/2515-7647/abd4ef (visited on 08/30/2023).

[171] A.-L. Viotti et al. “FLASH free electron laser pump-probe laser concept based on spectral broadening of high-power ytterbium picosecond systems in multi-pass cells”. In: *Review of Scientific Instruments* 94.2 (Feb. 2023), p. 023002. ISSN: 0034-6748. DOI: 10.1063/5.0131717. URL: https://doi.org/10.1063/5.0131717 (visited on 08/30/2023).

[172] Hong-Guang Duan et al. “Primary Charge Separation in the Photosystem II Reaction Center Revealed by a Global Analysis of the Two-dimensional Electronic Spectra”. en. In: *Scientific Reports* 7.1 (Sept. 2017). Number: 1 Publisher: Nature Publishing Group, p. 12347. ISSN: 2045-2322. DOI: 10.1038/s41598-017-12564-4. URL: https://www.nature.com/articles/s41598-017-12564-4 (visited on 09/17/2023).

[173] Manoj Mandal, Keisuke Saito, and Hiroshi Ishikita. “Two Distinct Oxygen-Radical Conformations in the X-ray Free Electron Laser Structures of Photosystem II”. In: *The Journal of Physical Chemistry Letters* 12.16 (Apr. 2021). Publisher: American Chemical Society, pp. 4032–4037. DOI: 10.1021/acs.jpclett.1c00814. URL: https://doi.org/10.1021/acs.jpclett.1c00814 (visited on 09/17/2023).

[174] Jordan T. O’Neal et al. “Electronic Population Transfer via Impulsive Stimulated X-Ray Raman Scattering with Attosecond Soft-X-Ray Pulses”. In: *Physical Review Letters* 125.7 (Aug. 2020). Publisher: American Physical Society, p. 073203. DOI: 10.1103/PhysRevLett.125.073203. URL: https://link.aps.org/doi/10.1103/PhysRevLett.125.073203 (visited on 09/16/2023).